technische universität dortmund

Supramolecular Chemistry of Metal Ions and Nitrogen Based Ligands including Pyrimidine Nucleobases

Self-assembly, Metallacalix[n]arenes, Host-Guest Chemistry, Hydrogen Bonding, pK_a Values

Anupam Khutia

Ph.D. Thesis submitted to the

Fakultät Chemie, Technische Universität Dortmund, Germany

for obtaining the degree of a

Doktor der Naturwissenschaften

technische universität dortmund

Supramolecular Chemistry of Metal Ions and Nitrogen Based Ligands including Pyrimidine Nucleobases

Self-assembly, Metallacalix[n]arenes, Host-Guest Chemistry, Hydrogen Bonding, pK_a Values

Anupam Khutia

Ph.D. Thesis submitted to the
Fakultät Chemie, Technische Universität Dortmund, Germany
for obtaining the degree of a
Doktor der Naturwissenschaften

Ph.D. Advisor	Prof. Dr. Bernhard Lippert
Referee	Prof. Dr. Jens Müller
Date of the oral exam and defense of the Ph.D. thesis	29.11.2010

This work was carried out between September 2007 and November 2010 at the Lehrstuhl für Bioanorganische Chemie, Fakultät Chemie, Technische Universität Dortmund, Germany.

My special thanks go to my Ph. D. Supervisor

Prof. Dr. Bernhard Lippert

for the opportunity to study in his group, for the interesting topics, for his most valuable guidance and support through my doctoral studies.

I also would like to thank Prof. Dr. Jens Müller for kindly acting as second examiner of my doctoral thesis.

I would like to express my gratitude to Prof. Dr. Martin Engelhard, Dr. Jutta Roetter, Christa Hornemann, Dr. Waltraud Hofmann-Goody and and International Max Planck Research School in Chemical Biology, Dortmund for assistance and financial support. I am indebted to Ms. Michaela Markert, Ms. Birgit Thormann and Dr. Gabriele Trötscher-Kaus for their assistance and support in a number of ways.

I would like to thank Dr. Pablo J. Sanz Miguel for carrying out all X-ray crystal structure determinations, and funny conversations outside or inside the lab. I would like to thank Sabine Siebel for translating the summary into German. I am grateful to Mr. Andreas Brockmeyer (MPI Dortmund) for recording the mass spectrum of one of the compounds and also to Markus Hüffner for carrying out the elemental analyses.

I also want to acknowledge all my colleagues of the working group, past and present, Dr. Neeladri Das, Dr. Pablo J. Sanz Miguel, Dr. Diego Montagner, Dr. Pilar Brandi, Dr. Francisca Alberti, Dr. Barbara Müller, Dr. Thea Welzel, Dr. Weizheng Shen, Dr. Deepali Gupta, Dr. Tushar van der Wijst, Dr. Susana Ibáñez, Anzhela Galstyan, Sabine Siebel, Philipp von Grebe, Lu Yin, Witold Zielinski, Agnes Kozma for the good atmosphere in the lab.

I also would like to thank all of my Indian friends, Tulika, Malay, Saonli, Souvik, Debapratim, Neeladri and Madhu, Rajorshi, Kirti, Sudhir, Raghu, Mahadeb, Krishna, Govind, Manoj for the nice time, we have spent together outside the lab.

Finally, my most sincere gratitude goes to my family. Their continuous support and encouragement made this entire effort possible.

Index

List of abbreviations

2,2'-bpy	2,2'-bipyridine
2,2'-bpz	2,2'-bipyrazine
3,3'-bpy	3,3'-bipyridine
δ	chemical shifts
d	doublet
dd	doublet-of-doublet
ddd	doublet-of-doublet-of-doublet
DMSO	dimethyl sulfoxide
DNA	deoxyribonucleic acid
en	ethylenediamine
h	hour
hh	*head-head*
ht	*head-tail*
H_2C	cytosine
HC	cytosine monoanion
C	cytosine dianion
H_2U	uracil
HU	uracil monoanion
U	uracil dianion
HRMS	high resolution mass spectroscopy
IR	infrared
NMR	nuclear magnetic resonance
pK_a	negative logarithms of the acidity constant
pH	negative logarithm of the proton concentration
ppm	parts per million
RNA	ribonucleic acid

RT	room temperature
TMA	tetramethylammonium tetrafluoroborate
TMEDA	tetramethylethylenedimine
TSP	sodium-3-(trimethylsilyl)-propanesulfonate

1. Introduction

1.1. Metal ions–nucleic acid interaction

A nucleic acid such as DNA or RNA is a macromolecule composed of nucleotides which are joined through phospho-diester linkages.[1] DNA was first discovered by Friedrich Miescher in 1870. All nucleotides are constructed from three components: a phosphate group, a pentose sugar entity and a heterocyclic ring. The heterocyclic parts of nucleic acid consist of purine bases (adenine, guanine) and pyrimidine bases (cytosine, uracil and thymine). The most common nucleic acids are ribonucleic acid (RNA) and deoxyribonucleic acid (DNA). Artificially synthesized nucleic acids are also known in the literature e.g. peptide nucleic acid (PNA)[2a-2c], glycol nucleic acid (GNA)[2d] etc. with their potential application in medicinal chemistry. DNA and RNA differ in the structure of the attached sugar entity: DNA contains 2-deoxyribose whereas RNA has a ribose entity, and also in the heterocyclic part. Although adenine, guanine and cytosine are found both in DNA and RNA, thymine occurs only in DNA and uracil occurs only in RNA. The

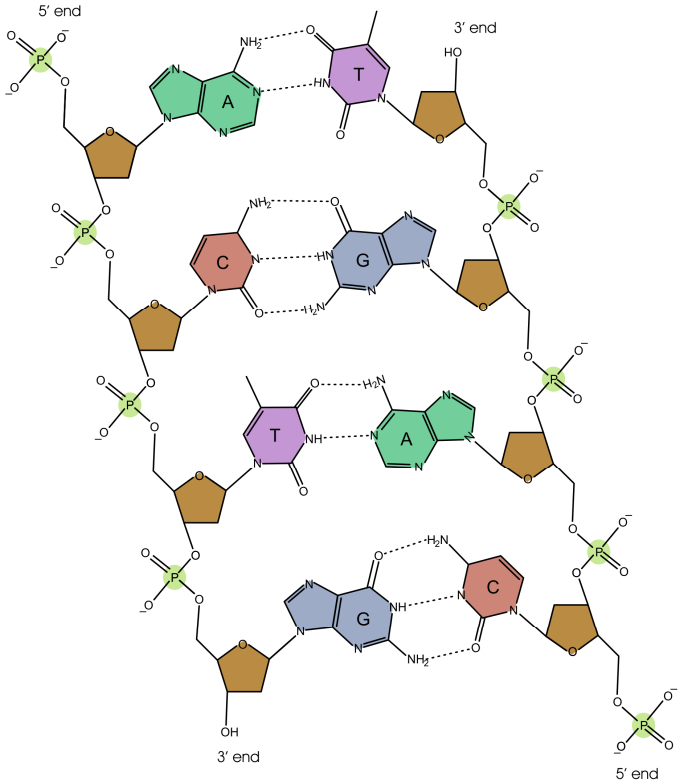

Scheme 1.1: Schematic diagram of chemical structure of DNA

antiparallel double helical structure of DNA is stabilized by the hydrogen bonds between complementary bases (Scheme 1.1). DNA is also known to exist in several other forms like triple stranded DNA, four stranded DNA etc. [1,3] Two types of base pairs, namely Watson-Crick base pairs, and rarely Hoogsteen base pairs, are observed in DNA. In Watson-Crick base pairing, adenine (A) forms a base pair with thymine (T), and guanine (G) with cytosine (C) in DNA. The GC base pair, having three intermolecular H bonds is more stable than the AT base pair which has only two intermolecular hydrogen bonds (Scheme 1.2).

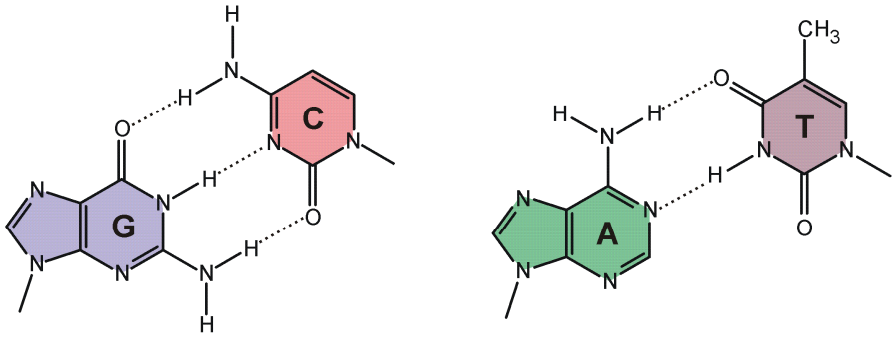

Scheme 1.2: Schematic diagram of Watson-Crick type hydrogen bonding scheme involving guanine, cytosine (left) and adenine, thymine (right).

Nucleic acids, being polyanionic in nature, require cations for charge neutralization and in most cases these are non-coordinating alkali metal ions. Interaction of metal species with nucleic acid can occur in the following two ways: weak non-covalent bonding (e.g. outer-sphere binding via aqua ligands)[4a,4b] and strong direct coordinative bonding to phosphate oxygen atoms, ribose oxygen atoms and various atoms of the heterocyclic bases.[4c] Coordinative bond formation is reversible and the metal ion can be substantially replaced by strong nucleophiles. Coordination of hard metal ions either to the oxygen atoms of phosphate groups or to the hydroxyl groups of ribose entity has been observed and structurally characterized in a number of cases.[5] The heterocyclic parts of nucleic acids show the most versatile binding patterns with metal ions.[4c,6] Both endocyclic (N, C) as well as exocyclic atoms (O, N) in purine and pyrimidine nucleobases can take part in metal ion binding. A variety of coordination modes of nucleobases with different transition metal species has been established and characterized by X-ray crystallography.[6] The parent purine (adenine, guanine) and pyrimidine nucleobases (uracil, thymine, and cytosine) in their preferred keto, amino tautomeric forms are shown in Scheme 1.3. For model studies, N9 blocked purine nucleobases (e.g. 9-methyladenine, 9-methylguanine)

and N1 blocked pyrimidine nucleobases (e.g. 1-methyluracil, 1-methylthymine, and 1-methylcytosine) are frequently employed to avoid metal coordination at N9 and N1, respectively. This situation has a close similarity to the environment of nucleic acids (in DNA or RNA), where the N9 position of purine bases and the N1 position of pyrimidine bases are connected to sugar rings.

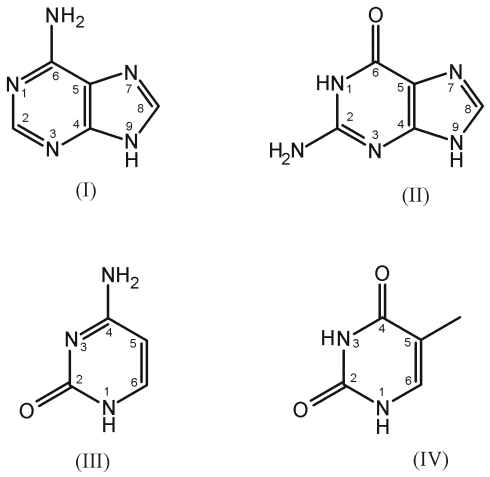

Scheme 1.3: Schematic representation of the four common parent DNA nucleobases in their favored tautomeric form (I) adenine, (II) guanine, (III) cytosine and (IV) thymine.

Metal coordination has a strong influence on acid-base equilibria of nucleobases. Metal coordination to one site of a nucleobase lowers the pK_a value of acidic protons and increases the metal binding affinity to a secondary site of a deprotonated base. The parent as well as model nucleobases can exist in neutral, cationic or anionic forms, depending on the pH of the solution. Protonation or deprotonation occurs at the heteroatoms of the bases. Various tautomeric structures are possible for nucleobases and metal coordination can also stabilize rare tautomeric structures of nucleobases, which are normally present in very low concentration only. These rare tautomeric structures can form non-Watson Crick pairs with common tautomers. Such mispairing can lead to mutations.

1.2. Platinum (II) based antitumor drug: cisplatin

The antitumor activity of cisplatin *cis*-[$PtCl_2(NH_3)_2$] was first established in Rosenberg's lab in the mid 1960's.[7] Cisplatin was approved by the FDA in 1978 and is used today to treat ovarian, cervical, head, neck and lung cancer etc. Later findings suggest that a specific Pt-DNA adduct (intrastrand cross-linking of *cis*-$(NH_3)_2Pt^{II}$ with two adjacent guanine–*N7*) is

most likely responsible for its action.[8,9] However, cisplatin has severe side effects like neurotoxicity, nephrotoxicity etc. Following the clinical success of cisplatin, thousands of platinum based compounds have been synthesized and tested for antitumor activity, but only few have entered human clinical trials. Among them, carboplatin (diammine[1,1-cyclobutanedicarboxylato]-*O*,*O*'-platinum(II)), oxaliplatin ((*trans*-L-diaminocyclohexane) oxalatoplatinum(II)), and nedaplatin (*cis*-diammine-glycoloato-*O*,*O*'-platinum(II)) showed promising results and have been approved for the treatment of cancer by various countries (Scheme 1.4).[10] Because of its lower toxicity compared to cisplatin, carboplatin has received worldwide approval and it can be given at much higher doses (up to 2000 mg/dose). In recent years, extensive research has been going on to generate potential chemotherapeutic agent based on numerous other transition metal species.[11]

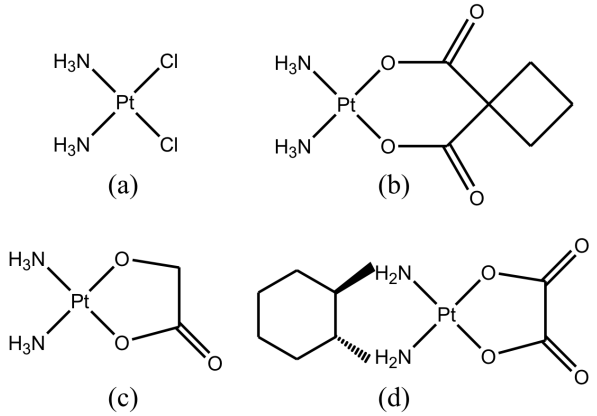

Scheme 1.4: Chemical structure of (a) cisplatin, (b) carboplatin, (c) nedaplatin and (d) oxaliplatin.

1.3. Platinum pyrimidine blues

The “platinum pyrimidine blues” are a class of intensely colored compounds, reported in the early 1970's by Rosenberg and they showed promising antitumor activity.[12] This class of compounds is derived from the reaction of diaqua species of cisplatin with pyrimidine nucleobases and related cyclic or open amides.[13] The “pyrimidine blues” have close similarity to the “platinblau” compounds, obtained upon treatment of $PtCl_2(CH_3CN)_2$ with $AgNO_3$ in water, reported by Hofmann in 1908.[13] The “blues” have attracted attention of many researchers because of their interesting structure, mixed valency and paramagnetism etc. The intense color of the compounds arises from an intervalence charge transfer between Pt centers of different oxidation states.[14] Initially “platinum pyrimidine blues” showed promising testing results and were actually introduced in clinical

trials. Problems arising from improper characterization and problems of reproducible synthesis eventually led to a clinical stop. These “blues” are also useful staining agents for nucleic acids in cells.[15] They can bind to DNA covalently in a slower reaction, with loss of the pyrimidine entities.[16]

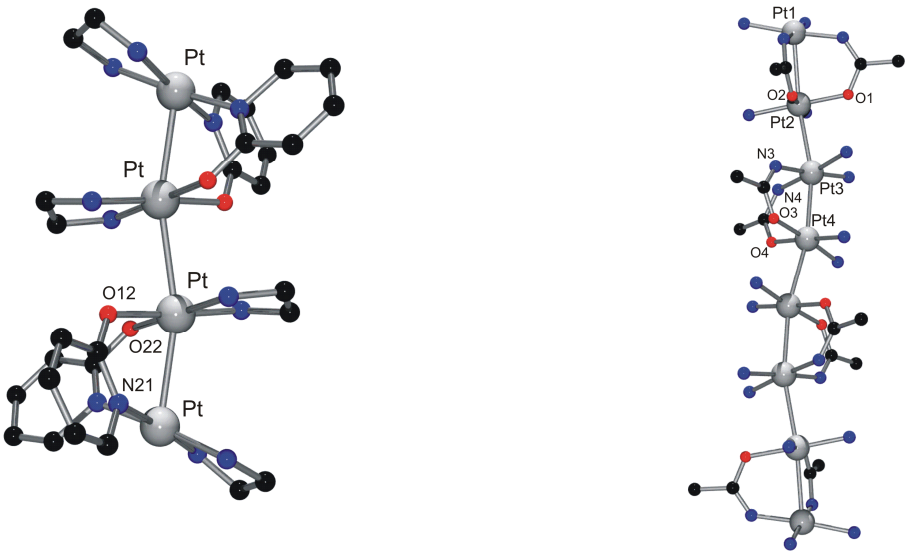

Figure 1.1: The crystal structure of ethylenediamineplatinum α-pyridone blue[22] (left) and octanuclear platinum acetamide blue[21] (right)

Lippard and coworkers reported the first X-ray structure of a “blue” in 1977. It was obtained from reaction of the diaqua species of cisplatin with the α-pyridone ligand.[17] In the solid state structure of the tetranuclear “α-pyridone blue”, two *cis*-diammineplatinum entities are bridged in *head-head* fashion by two α-pyridonate ligands to give a dimer, and two dimers are connected via H bonds to two *O*,*O*-coordinated Pt ions. A view of “ethylenediamineplatinum α-pyridone blue” is provided in Figure 1.1. This “blue” contains three Pt^{II} and one Pt^{III} entities which gives an average Pt oxidation state of +2.25. The “α-pyridone blue” was studied using several spectroscopy techniques like EPR, magnetic susceptibility measurement, visible spectroscopy etc.[18] An analogous “blue” was also reported from the same research group in 1984 with the 1-methyluracil ligand.[19] In case of cyclic amides, *head-head* orientation within dinuclear entity is necessary to permit dimer-of-dimer formation to avoid steric hindrance. Likewise the *head-tail* arranged dinuclear complex *cis*-[{$(NH_3)_2$Pt(μ-1-metylthyminato-*N3*,*O4*}$_2$]$(NO_3)_2$ does not allow dimer-of-dimer formation to give a tetranuclear complex.[20] Another octanuclear compound (related to the “blue”) has also been reported with linear acetamide ligand. It consists of four stacked

dinuclear *cis*-$(NH_3)_2Pt$ entities and *head-head* arranged acetamidato ligands (Figure 1.1).[21]

The pyrimidine nucleobases are more versatile ligands compared to either open or cyclic amides for the formation of “blues”, as more metal coordination sites via N, O are available. A series of heterometallic complexes has been reported with 1-substituted pyrimidine nucleobases, which have close resemblance with the “Pt pyrimidine blue”. A heteronuclear complex derived from *cis*-$(NH_3)_2Pt^{II}$ and Ag^+ ion with 1-methyluracil has been prepared and its conversion to a “blue” has likewise been studied.[23] Another blue with 1-methyluracil containing two Pt^{II} and one Pd^{III} has been reported and the distinct feature of this blue is that it can be reversibly oxidized to $Pt^{II}Pd^{III}Pt^{II}$ and $Pt^{II}Pd^{IV}Pt^{II}$, or reduced to $Pt^{II}Pd^{I}Pt^{II}$.[24]

Unsubstituted pyrimidine nucleobases like uracil, thymine also yield “blues”, but the nature of these species is not clear yet. It has been suggested[13a] that the “blues” derived from unsubstituted pyrimidine bases may have many possible structures because of their versatile metal coordination sites and can have cyclic and/or open oligomeric species, along with a mixed valence character. In 1994, Lippert and coworkers reported the formation of a cyclic tetranuclear species from the reaction of $(en)Pt^{II}$ with unsubstituted Uracil.[25] This cyclic complex has spurred particular interest because of its close structural similarity with organic calix[n]arenes, and can therefore be considered a metal analogue of a classical calix[4]arene. Cyclic complexes of this type are consequently termed as “metallacalix[n]arene” and their relationship with classical calix[n]arenes is described below.

1.4. Relationship between calix[n]arenes and metallacalix[n]arenes

Classical calix[n]arenes are cyclic oligomers of *para* substituted phenols linked through methylene bridges where the number “n” specifies the number of phenols and therefore the size of macrocycle.[26] Owing to their bowl-shaped structure, they are useful building blocks in the design of novel host molecules. The most useful property of calixarenes and their derivatives is their ability to function as molecular baskets and to bind neutral and/or ionic guests either in their cavity or at the periphery.[27] Synthetic calixarene derivatives having nanocavities can be used for the encapsulation of drugs and their active transport through cell membranes.[28a] When attached to appropriate functional groups, calixarenes

could yield biomimetic model systems.[28b,28c] Simple calixarenes have many conformational isomers because of two different rotational modes of the phenol units. Calix[4]arene shows four conformers - "cone" (C_{4v}), "partial cone" (C_s), "1,2-alternate" (C_{2h}), and "1,3-alternate" (D_{2d}), as designated by Gutsche and coworkers (Scheme 1.5).[26] In the cone conformation all the four phenolic-OH groups are involved in circular hydrogen bonding. Functionalization of calixarenes either at the lower rim (phenolic OH groups) or at the upper rim (*para* position of the aromatic moiety) often produces derivatives with reduced conformational mobility.

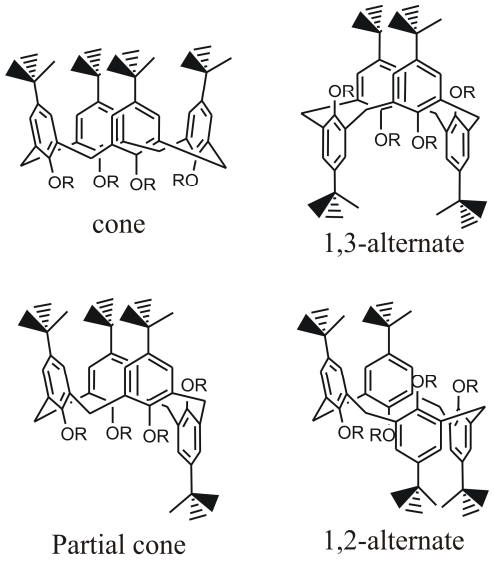

Scheme 1.5: Four different conformations of calix[4]arene.

Several successful attempts have been made so far to obtain molecules which are structurally analogous to organic calix[n]arenes. In these modified calixarenes, the original phenol groups are replaced by numerous other aromatic rings including heterocycles. Representative examples include calix[n]resorcarenes[30], calix[n]pyrroles[31], heterocalix[n]aromatics[32] etc. In many examples, methylene bridges have been substituted by other heteroatoms, e.g. NH in azacalix[n]arene.[29] The pyrimidine ligands are of particular interest in this context because they have two N donor coordination sites (which provide a 120° angle), which in combination with a *cis* blocked d^8 square planar metal entity *cis*-a_2M^{II} (which provides a 90° angle, a = NH_3, a_2 = en, 2,2'-bpy; M = Pt, Pd) could lead to the formation of metallacalix[n]arene.[25,33] So in metallacalixarenes, heterocyclic pyrimidine bases replace the phenol ring of the classical calixarene and methylene bridges are replaced by *cis*-a_2M^{II} entities (Scheme 1.6). The cyclic uracil complex [{Pt(en)(UH-*N1*,*N3*)}$_4$]$(NO_3)_4$ was the first example of a metallacalix[4]arene which

was obtained from self-assembly of [Pt(en)(UH-*N1*)(H_2O)](NO_3) (Figure 1.2). This molecule shows a rotational behavior similar to an organic calix[4]arene.[25] It adopts a 1,3-alternate conformation in the solid state, which is stabilized by short hydrogen bonds

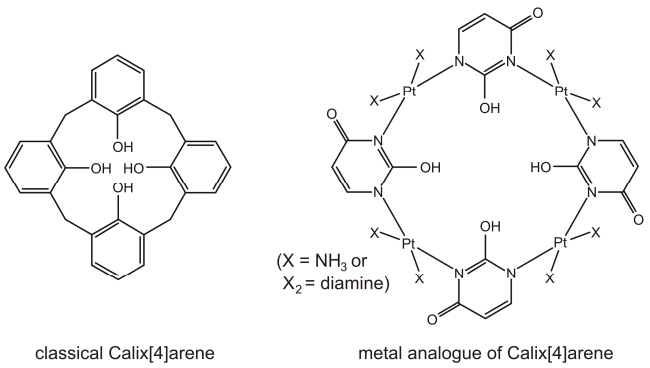

Scheme 1.6: Schematic representation of classical calix[4]arene (left) and metallacalix[4]arene (right).

between exocyclic OH2 and O4 (or O2 and OH4) sites of uracil. Hence, the uracil anion is present in a rare tautomeric structure. This cyclic complex exhibits pH–dependent conformational changes in solution.[25b] Different conformers of [{Pt(en)(UH-*N1*,*N3*)}$_4$](NO_3)$_4$ can be stabilized by additional metal binding to exocyclic group of pyrimidine nucleobases. For example, Ag^+ coordination favors the cone conformer over the 1,3 alternate conformer to yield an octanuclear species [{enPt(UH-*N1*,*N3*,*O2*)Ag}$_4$]$^{8+}$.[25b] Analogous to calix[n]arene, the metallacalix[4]arene are also capable of incorporating hard metals at the oxo surface. For example, the metallacalix[4]arene [{Pt(en)(UH-*N1*,*N3*)}$_4$](NO_3)$_4$ in its 1,3-alternate conformation can coordinate four additional divalent metal ions through its exocyclic oxo surface giving rise to the formation of octanuclear species [{enPt(UH-*N1*,*N3*,*O2*,*O4*)M}$_4$]$^{8+}$ (M = Ni^{II}, Pt^{II}, Pd^{II})

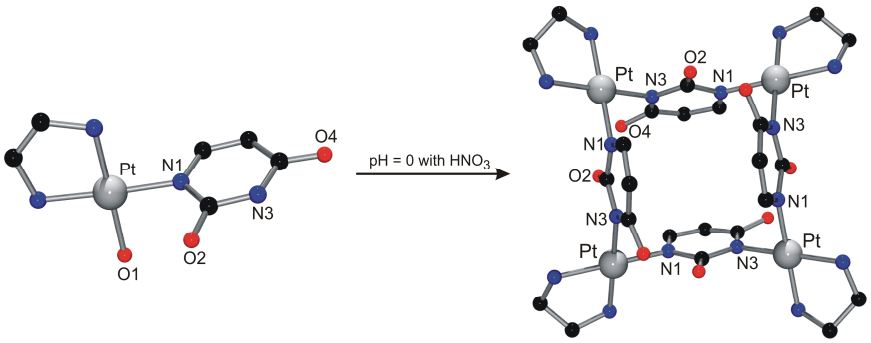

Figure 1.2: Formation of cyclic tetranuclear complex [{Pt(en)(UH-N1,N3)}$_4$]$^{4+}$ from mononuclear [Pt(en)(UH-N1)(H_2O)]$^+$.[25b]

(Figure 1.3a).[34] Like a classical calix[4]arenes, metallacalix[4]arenes or its heterometallic derivatives can act as receptor towards organic anions[35] as well as cations (Figure 1.3b).[36] Metallacalix[4]arenes derived from 2-hydroxypyrimidine show non-covalent interactions with DNA and form particular structures with DNA.[37]

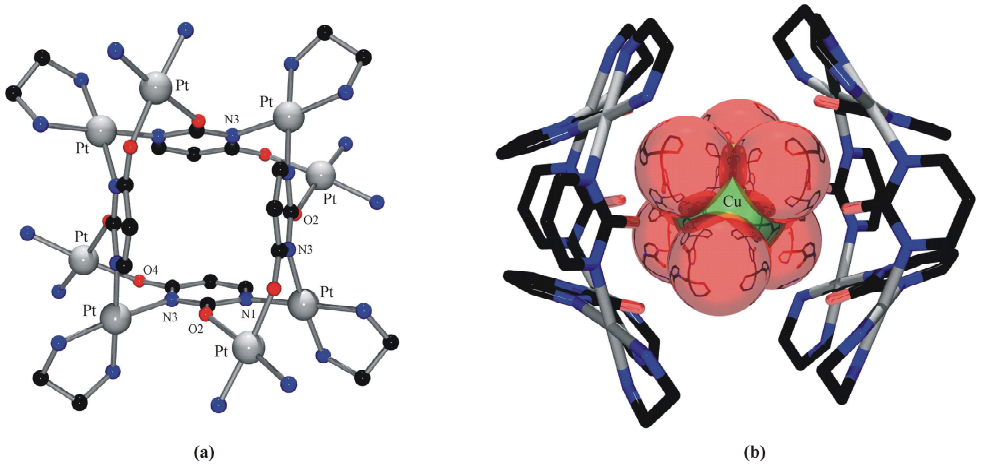

Figure 1.3: View of (a) octanuclear complex [enPt(UH-N1,N3,O2,O4){*cis*-$(NH_3)_2Pt$}]$_4^{8+}$ [34a] and (b) interaction of $[Cu(H_2O)_6]^{2+}$ with the oxo surfaces of two metallacalix[4]arenes.[36]

Metallacalix[n]arenes of different sizes are known in literature e.g. ranging from n = 3[38] to n = 4,[25,33,36] n = 6,[39] and n = 8[40]. In 2003 E. Barea et al. reported the formation of a cyclic hexanuclear metallacalix[6]arene which readily converts to the thermodynamically more stable metallacalix[4]arene on heating.[39] It is also possible to combine pyrimidine ligands with other ditopic heterocyclic ligands to give additional cyclic metallacalix[n]arenes.[41]

1.5. Supramolecular chemistry

According to J. M. Lehn, “supramolecular chemistry is a highly interdisciplinary field of science covering the chemical, physical and biological features of the chemical species of greater complexity than the molecules themselves that are held together and organized by means of intermolecular (non-covalent) interactions”.[42] It can also be defined as the “chemistry beyond the molecule”, bearing organized entities of higher complexity.[42] While “molecular chemistry” deals with structure and properties of molecular species which are connected through covalent bonding, “supramolecular chemistry” is concerned with aggregates of molecules which are held together by non-covalent interaction.[43] Various

intermolecular forces are operative in supramolecular chemistry which include hydrogen bonding, electrostatic interactions (ion-ion, ion-dipole, dipole-dipole), π–π interactions, van der Waals forces, coordination bonds etc. The non-covalent bonds are relatively weak compared to covalent bonding in molecular chemistry. Usually strong binding is only observed if multiple interactions cooperate. So most supramolecular complexes are reversibly formed and should be considered as highly dynamic units.

Studies of intermolecular forces originally started in the 1960's following Pederson's discovery of crown ethers which selectively bind different alkali cations in a host-guest manner. He synthesized a series of crown ethers of different ring size which acted as hosts and selectively incorporated different alkali metal ions.[44] Soon after, Donald Cram and J. M. Lehn independently synthesized a series of 3-dimensional organic cyclic compounds which acted as hosts and selectively bonded not only ions but also neutral molecules.[45,46] In 1987 they shared the “Nobel prize” in chemistry “for their development and use of molecules with structure-specific interactions of high selectivity”. Since then, contributions from scientists and researchers worldwide in the field of supramolecular chemistry have broadened the scope beyond simple host-guest chemistry.

Important concepts in supramolecular chemistry include self-assembly, molecular recognition, dynamic covalent synthesis etc. According to Whitesides “Self-assembly is a process in which components, either separate or linked, spontaneously form ordered aggregates”.[47] There are two types of molecular self-assembly processes, namely intramolecular self-assembly and intermolecular self-assembly. Examples of molecular self-assembly are also found in nature. Naturally occurring DNA, perhaps the best known self-assembling structure in biological systems, uses multiple hydrogen bonding interactions between complementary bases as well as π–π stacking to stabilize the double helical structure.

Since the early 1990's, interest in the design and construction of transition metal mediated self-assembled supramolecular entities has experienced extraordinary progress because of potential application as sensors, probes, photonic devices, catalysts as well as in basic host–guest chemistry.[48] Supramolecular coordination compounds bear exceptional advantages over their organic counterparts because they can be synthesized in one-pot reactions with high yields and display physical properties that are generally inaccessible with organic species.[49-54] Depending on the type of metal ions and bridging organic ligands used, metal-mediated self-assembly can lead to the formation of either

polymeric frameworks or discrete supramolecular entities of defined shape. The first classes of compounds are extended infinitely into one, two or three dimension and are commonly known as metal-organic coordination networks (MOCNs) or metal-organic frameworks (MOFs). The MOFs are generally porous and have particular applications ranging from gas storage (H_2, CH_4 etc.) to catalysis and controlled drug delivery etc.[55,56]

The coordination driven self-assembly leading to the formation of supramolecules with finite shape has received more attention since the early report of a molecular squares by Fujita and coworkers. (Scheme 1.7).[57] Since then a series of metal based macrocycles which include 2-D macrocycles and 3-D cages/capsules of different shapes and sizes, have been reported by several research groups. These cages can be utilized in unusual guest encapsulation,[58] in stabilizing unstable intermediate in a reaction[58], or in carrying out uncommon organic reactions in aqueous medium[59] etc. For example, air unstable white phosphorous can be stabilized in the presence of suitable metal cage.[58a]

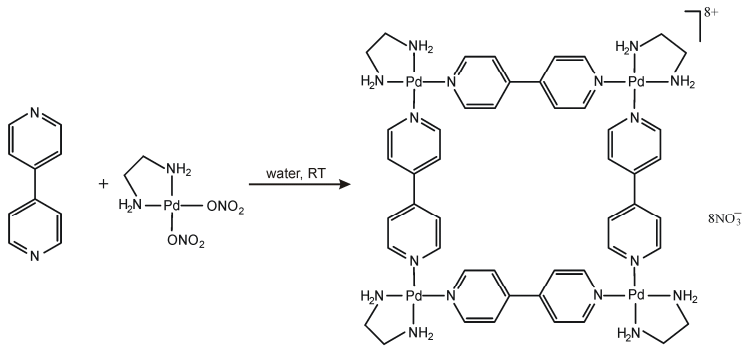

Scheme 1.7: Preparation of molecular square $[Pd(en)(4,4'\text{-bipyridine})]_4(NO_3)_8$ starting from the metal fragment $Pd(en)(NO_3)_2$ and the organic linker 4,4'-bipyridine.[57]

1.6. Aim of the thesis

Studies on the interactions of metal ions with components of nucleic acid have received increased attention following the discovery of the platinum anticancer agent cisplatin. It binds to DNA nucleobases which is responsible for its action as antitumor agent. Development of potential chemotherapeutic agents which selectively bind to DNA has been a major focus of research in recent years. Pyrimidine nucleobases, thymine (uracil in RNA) and cytosine, are among the most important components of DNA. The pyrimidine bases are considered versatile ligands because of the presence of many different coordination sites – endocyclic N1, N3; exocyclic O2, O4 (in uracil and thymine); O2, N4 (in cytosine). Even for uracil and cytosine, metal binding through C5 is also known in literature, resulting in the formation organometallic compounds. The here described work

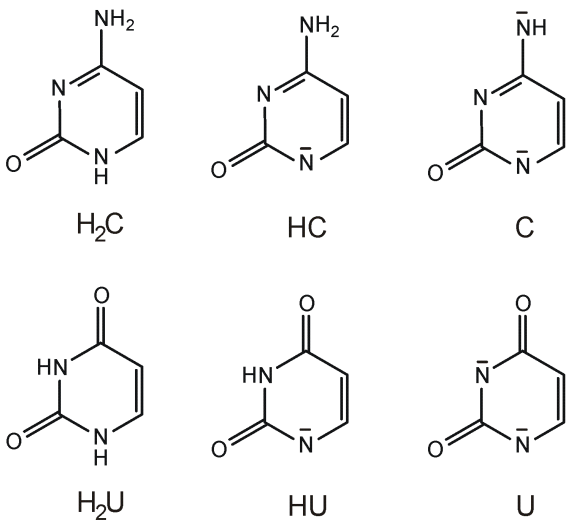

Scheme 1.8

is focused on the structural characterization of various metal complexes, in particular of Pt^{II} and of Pd^{II}, with unsubstituted pyrimidine nucleobases and related heterocyclic ligands. These complexes were studied to establish the various possible coordination modes of nucleobases, to better understand the effects of metallation on acid-base equilibria, and to stabilize rare tautomeric forms of nucleobases. The nucleobases applied have pronounced propensity to form cyclic complexes when combined with appropriate metal entities. The pyrimidine nucleobases having low symmetry (C_s) can form mixture of products which differ in the N1, N3 connectivity. However in a “directed” approach, starting with a preformed kinetically inert corner unit, the number of possible products can be reduced to a single linkage isomer. A series of cyclic complexes of defined shape has been prepared

and characterized crystallographically. These cyclic complexes have a unique structural similarity with organic calix[n]arenes and therefore are termed as metallacalix[n]arenes. They can be related to the “metal coordination driven self assembly”, a major concept in supramolecular chemistry.

The unsubstituted pyrimidine nucleobases can lead to the formation of “Pt pyrimidine blues”, the nature of which is not fully clarified as yet. Theses “blues” have attracted attention to chemists because of their interesting properties like mixed-valency, paramagnetism etc. The intense color in these complexes is due to intra-valence charge transfer between Pt centers with different oxidation states. The structural analysis of metal complexes synthesized in this work and their solution chemistry will help to understand the structural complexity of “Pt-Pyrimidine Blues”, once considered second generation platinum antitumor agents.

The main goals of here described research are outlined below:

- To develop the basic chemistry of platinacalix[4]arenes based on low symmetrical pyrimidine nucleobases (uracil, cytosine):
    - Preparation of cyclic metallacalix[n]arene with single linkage isomer and particular conformational state. It will be shown that formation of a particular linkage isomer can be achieved starting from kinetically inert corner fragments.
    - To understand the effect of metal coordination on acid-base equilibria and stabilization of rare tautomeric structure of pyrimidine nucleobases.
    - The decoration of exocyclic (O2, O4/N4) groups of pyrimidine nucleobases in metallacalix[n]arene by coordination of additional metal entities to generate high nuclearity derivatives.
    - To understand the structural complexity of “Pt-pyrimidine blues”.

- To synthesize supramolecular cages of varying ring size on the basis of related heterocyclic ligands and to understand their solution chemistry:
    - Synthesis of a new class of cyclic complexes based on biuracil ligand which can be considered as hybrids between classical calix[n]arenes and metallacalix[n]arenes.

- Synthesis of new N-heterocyclic ligands and their reaction products with different metal ions.

In particular, X-ray structure analysis of a large number of metal complexes will be presented in this thesis. The ^{1}H NMR spectra will be helpful to understand the solution behavior of these complexes. The pD dependant ^{1}H NMR spectra have also been carried out to evaluate relevant acid-base equilibria. The isolated complexes are numbered in bold face.

1.7. References

[1] G. M. Blackburn, M. J. Gait, D. Loakes, D. M. William, *Nucleic acids in chemistry and biology*, The Royal Society of Chemistry, Cambridge, **2006**.

[2] a) P. E. Nielsen, *Acc. Chem. Res.* **1999**, *32*, 624–630; b) P. E. Nielson, M. Egholm, R. H. Berg, O. Buchardt, *Science* **1991**, *254*, 1497–1500; c) V. Menchise, G. de Simone, T. Tedeschi, R. Corradini, S. Sforza, R. Marchelli, D. Capasso, M. Saviano, C. Pedone, *Proc. Natl. Acad. Sci. USA* **2003**, *100*, 12021–12026; d) E. Meggers, L. Zhang, *Acc. Chem. Res.* **2010**, *43*, 1092–1102.

[3] R. M. Roat-Malone, *Bioinorganic Chemistry: A Short Course*, John Wiley & Sons, New Jersey, **2007**.

[4] a) M. J. Hannon, *Chem. Soc. Rev.* **2007**, *36*, 280–295; b) A. Oleksi, A. G. Blanco, R. Boer, I. Usón, J. Aymami, A. Rodger, M. J. Hannon, M. Coll, *Angew. Chem. Int. Ed.* **2006**, *45*, 1227–1231; c) B. Lippert, *Coord. Chem. Rev.* **2000**, *200*, 487–516.

[5] a) K. Aoki, in *Comprehensive Supramolecular Chemistry*, vol. 5 (Ed: J. M. Lehn), Pergamon Press, Oxford, **1995**, pp. 249–294; b) T. J. Kistenmacher, C. C. Chiang, P. Chalilpoyil, L. G. Marzilli, *J. Am. Chem. Soc.* **1979**, *10*, 1143–1148; c) J. Galy, A. Mosset, I. Grenthe, I. Puigdomenech, B. Sjöberg, F. Hultén, *J. Am. Chem. Soc.* **1987**, *109*, 380–386.

[6] a) B. Lippert, in *Nucleic – Acid Metal Ion Interaction*, (Ed: Nicholas V. Hud), The Royal Society of Chemistry, Cambridge, **2009**, pp. 39–74; b) D. Gupta, B. Lippert, *Dalton Trans.* **2009**, 4619–4634.

[7] a) B. Rosenberg, L. VanCamp, T. Krigas, *Nature* **1965**, *205*, 698–699; b) B. Rosenberg, L. VanCamp, J. E. Trosko, V. H. Mansour, *Nature* **1969**, *222*, 385–386.

[8] a) S. E. Sherman, D. Gibson, A. H. J. Wang, S. J. Lippard, *Science* **1985**, *230*, 412–417; b) S. E. Sherman, D. Gibson, A. H. J. Wang, S. J. Lippard, *J. Am. Chem. Soc.* **1988**, *110*, 7368–7381.

[9] a) M. Takahara, C. Rosenzweig, C. A. Frederick, S. J. Lippard, *Nature* **1995**, *377*, 649–652; b) P. M. Takahara, C. A. Frederick, S. J. Lippard, *J. Am. Chem. Soc.* **1996**, *118*, 12309–12321; c) V. Brabeck, in *Platinum-Based Drugs in Cancer Therapy*, (Ed: L. R. Kelland and N. P. Farrell), Humana Press Inc., New Jersey, **2000**, pp. 37–62.

[10] a) E. R. Jamieson, S. J. Lippard, *Chem. Rev.* **1999**, *99*, 2467–2498; b) J. Reedijk, *Chem. Rev.* **1999**, *99*, 2499–2510; c) E. Wong, C. M. Giandomenico, *Chem. Rev.* **1999**, *99*, 2451–2466; d) W. I. Sundquist, S. J. Lippard, *Coord. Chem. Rev.* **1990**, *100*, 293–322; e) D. Wang, S. J. Lippard, *Nat. Rev. Drug. Disc.* **2005**, *4*, 307–320; f) T. W. Hambley, *Coord. Chem. Rev.* **1997**, *166*, 181–223.

[11] M. J. Clarke, F. Zhu, D. R. Frasca, *Chem. Rev.* **1999**, *99*, 2511–2533; b) S. Ray, R. Mohan, J. K. Singh, M. K. Samantary, M. M. Shaikh, D. Panda, P. Ghosh, *J. Am. Chem. Soc.* **2007**, *129*, 15042–15053; c) L. Ronconi, P. J. Sadler, *Coord. Chem. Rev.* **2007**, *251*, 1633–1648; d) A. M. Pizarro, P. J. Sadler, in *Nucleic – Acid Metal Ion Interaction*, (Ed: Nicholas V. Hud), The Royal Society of Chemistry, Cambridge, **2009**, pp. 350–416; e) S. H. Van Ritz, P. J. Sadler, *Drug Discov. Today* **2009**, *14*, 1089–1097.

[12] J. P. Davidson, P. J. Faber, R. G. Fischer, Jr., S. Mansy, H. J. Peresie, B. Rosenberg, L. VanCamp, *Cancer Chemother. Rep. Part 1* 1975, 59, 287–300.

[13] a) B. Lippert, in *Cisplatin – Chemistry and Biochemistry of Leading Anticancer Drug*, (Ed: B. Lippert), VHCA Zürich and Willey-VCH, Weinhein, 1999, PP. 379–403; b) B. Lippert, *Coord. Chem. Rev.* **1999**, *182*, 263–295.

[14] A. P. Ginsberg, T. V. O'Halloran, P. E. Fanwick, L. S. Hollis, S. J. Lippard, *J. Am. Chem. Soc.* **1984**, *106*, 5430–5439.

[15] S. K. Aggarwal, R. W. Wagnertt, P. K. McAllister, B. Rosenberg, *Proc. Natl. Acad. Sci. U.S.A.* **1975**, *79*, 928–932.

[16] a) W. Bauer, S. L. Gonias, S. K. Kam, K. C. Wu, S. J. Lippard, *Biochemistry* **1978**, *17*, 1060–1068; b) M. S. Herrmann, A. D. Cardin, W. D. Behnke, J. R. Durig, *Biochemical Pharmacology* **1978**, *27*, 1571–1576.

[17] J. K. Barton, H. N. Rabinowitz, D. J. Szalda, S. J. Lippard, *J. Am. Chem. Soc.* **1977**, *99*, 2827–2829.

[18] a) J. K. Barton, S. A. Best, S. J. Lippard, R. A. Walton, *J. Am. Chem. Soc.* **1978**, *100*, 3785–3788; b) J. K. Barton, D. J. Szalda, H. N. Rabinowitz, J. V. Waszczak, S. J. Lippard, *J. Am. Chem. Soc.* **1979**, *101*, 1434–1441; c) J. K. Barton, C. Caravana, S. J. Lippard, *J. Am. Chem. Soc.* **1979**, *101*, 7269–7277; d) H. K. Mahtani, P. Stein, *J. Am. Chem. Soc.* **1989**, *111*, 1505–1506.

[19] P. K. Mascharak, I. D. Williams, S. J. Lippard, *J. Am. Chem. Soc.*, **1984**, *106*, 6428–6430.

[20] C. J. L. Lock, H. J. Peresie, B. Rosenberg, Graham Turnerla, *J. Am. Chem. Soc.* **1978**, *100*, 3371–3374.

[21] K. Sakai, K. Matsumoto, *J. Am. Chem. Soc.* **1989**, *111*, 3074–3075.

[22] a) T. V. O'Halloran, M. M. Roberts, S. J. Lippard, *J. Am. Chem. Soc.* **1984,** *106,* 6427–6428; b) T. V. O'Halloran, P. K. Mascharak, I. D. Williams, M. M. Roberts, S. J. Lippard, *Inorg. Chem.* **1987**, *26*, 1261–1270.

[23] B. Lippert, D. Neugebauer, *Inorg. Chem.* **1982**, *21*, 451–452; b) B. Lippert, H. Schöllhorn, U. Thewalt, *Inorg. Chem.* **1987**, *26*, 1736–1741.

[24] a) W. Micklitz, G. Müller, J. Riede, B. Lippert, *J. Chem. Soc., Chem. Commun.* **1987**, 76–78; b) W. Micklitz, G. Müller, B. Huber, J. Riede, F. Rashwan, J. Heinze, B. Lippert, *J. Am. Chem. Soc.* **1988**, *110*, 7084–7092.

[25] a) H. Rauter, E. C. Hillgeris, B. Lippert, *J. Chem. Soc., Chem. Commun.* **1992**, 1385–1386; b) H. Rauter, E. C. Hillgeris, A. Erxleben, B. Lippert, *J. Am. Chem. Soc.* **1994**, *116*, 616–624.

[26] a) C. D. Gutsche, *Calixarenes*, The Royal Society of Chemistry, Cambridge, **1989**; b) C. D. Gutsche, *Calixarenes Revisited*, The Royal Society of Chemistry, Cambridge, **1998**.

[27] A. Ikeda, S. Shinkai, *Chem. Rev.* **1997**, *97*, 1713–1734; b) J. S. Kim, D. T. Quang, *Chem. Rev.* **2007**, *107*, 3780–3799; c) L. Baldani, A. Casnati, F. Sansone, R. Ungaro, *Chem. Soc. Rev.* **2007**, *36*, 254–266; d) R. Joseph, B. Ramanujam, A. Acharya, A. Khutia, C. P. Rao, *J. Org. Chem.* **2008**, *73*, 5745–5758; d) U. Scheerder, P. M. J. van Duynhoven, J. F. J. Engberser and D. N. Reinhoudt, *Angew. Chem. Int. Ed.* **1996**, *35*, 1090–1093.

[28] R. Lalor, H. Baillie-Johnson, C. Redshaw, S. E. Matthews, A. Mueller, *J. Am. Chem. Soc.* **2008**, *1130*, 2892–2893; b) S. Blanchard, L Le Clainche, M. -N. Rager, B. Chansou, J. -P. Tuchagues, A. F. Duprat, Y. Le Mest, O. Reinaud, *Angew Chem. Int. Ed.* **1998**, *37*, 2732–2735; c) A. Visňjevac, J. Gout, N. Ingert, O. Bistri, O. Reinaud, *Org. Lett.* **2010**, *12*, 2044–2047.

[29] a) M. -X. Wang, *Chem. Commun.* **2008**, 4541–4551; b) W. Maes, W. Dehaen, *Chem. Soc. Rev.* **2008**, *37*, 2393–2402; c) B. König, M. H. Fonseca, *Eur. J. Inorg. Chem.* **2000**, 2303–2310.

[30] B. Botta, M. Cassani, I. D'Acquarica, D. Subissati, G. Zappia, D. Delle Monache, *Curr. Org. Chem.* **2005**, *9*, 1167–1202.

[31] a) P. A. Gale, J. L. Sessler, V. Král, *Chem. Commun.* **1998**, 1–8; b) P. A. Gale, P. Anzenbacher, J. L. Sessler, *Coord. Chem. Rev.* **2001**, *222*, 57–102.

[32] B. König, M. H. Fonseca, *Eur. J. Inorg. Chem.* **2000**, 2303–2310.

[33] a) J. A. R. Navarro, B. Lippert, *Coord. Chem. Rev.* **2001**, *222*, 219–250; b) J. A. R. Navarro, E. Barea, M. A. Galindo, J. M. Salas, M. A. Romero, M. Quirós, N. Masciocchi, S. Galli, A. Sironi, B. Lippert, *J. Solid State Chem.* **2005**, *178*, 2436–2451.

[34] a) H. Rauter, I. Mutikainen, M. Blomberg, C. J. L. Lock, P. Amo-Ochoa, E. Freisinger, L. Randaccio, E. Zangrando, E. Chiarparin, B. Lippert, *Angew. Chem. Int. Ed.* **1997**, *36*, 1296–1301; b) J. A. R. Navarro, E. Freisinger, B. Lippert, *Eur. J. Inorg. Chem.* **2000**, 147–151.

[35] J. A. R. Navarro, M. B. L. Janik, E. Freisinger, B. Lippert, *Inorg. Chem.* **1999**, *38*, 426–432.

[36] J. A. R. Navarro, E. Freisinger, B. Lippert, *Inorg. Chem.* **2000**, *38*, 2301–2305.

[37] M. A. Galindo, D. Olea, M. A. Romero, J. Gómez, P. del Castillo, M. J. Hannon, A. Rodger, F. Zamora, J. A. R. Navarro, *Chem. Eur. J.* **2007**, *13*, 5075–5081.

[38] a) Z. Qin, M. C. Jennings, R. J. Puddephatt, *Inorg. Chem.* **2002**, *41*, 3967–3974; b) N. Masciocchi, G. A. Ardizzoia, G. LaMonica, A. Maspero, A. Sironi, *Angew. Chem. Int. Ed.* **1998**, *37*, 3366–3369; c) M. J. Rauterkus, B. Krebs, *Angew. Chem. Int. Ed.* **2004**, *43*, 1300–1303; d) O. Sengupta, R. Chakrabarty, P. S. Mukherjee, *Dalton Trans.* **2007**, 4514–4516.

[39] E. Barea, J. A. R. Navarro, J. M. Salas, M. Quirós, M. Willermann, B. Lippert, *Chem. Eur. J.* **2003**, *9*, 4414–4421.

[40] E. Gil Bardají, E. Freisinger, B. Costisella, C. A. Schalley, W. Brüning, M. Sabat, B. Lippert, *Chem. Eur. J.* **2007**, *13*, 6019–6039.

[41] a) M. A. Galindo, A. Houlton, W. Clegg, R. W. Harrington, J. Dobado, F. Santoyo-Gonzalez, M. A. Romero, J. A. R. Navarro, *Chem. Commun*. **2008**, 3735–3737; b) M. A. Galindo, S. Galli, J. A. R. Navarro, M. A. Romero, *Dalton Trans.* **2004**, 2780–2785.

[42] J. -M. Lehn, *Supramolecular Chemistry-Concepts and Perspectives*, Wiley-VCH, Weinheim, **1995**.

[43] a) I. Haiduc, F. T. Edelmann, *Supramolecular Organometallic Chemistry*, Wiley-VCH, Weinheim, **1999**; b) P. D. Beer, P. A. Gale, D. K. Smith, *Supramolecular Chemistry*, Oxford University Press, **1999**.

[44] a) C. J. Pederson, *J. Am. Chem. Soc.* **1967**, *89*, 2495–2496; b) C. J. Pederson, *J. Am. Chem. Soc.* **1967**, *89*, 7017–7036.

[45] a) D. J. Cram, T. Kaneda, R. C. Helgeson, G. M. Lein, *J. Am. Chem. Soc.* **1979**, *101*, 6752–6754; b) D. J. Cram, T. Kaneda, R. C. Helgeson, S. B. Brown, C. B. Knobler, E. Maverick, K. N. Trueblood, *J. Am. Chem. Soc.* **1985**, *107*, 3645–3657; c) D. J. Cram, J. M. Cram, *Acc. Chem. Res.* **1978**, *11*, 8–14.

[46] a) J. -M. Lehn, *Struct. Bonding* **1973**, *16*, 1–69; b) J. -M. Lehn, *Acc. Chem. Res.* **1978**, *11*, 49–57.

[47] a) G. M. Whitesides, M. Boncheva, *Proc. Natl. Acad. Sci. USA* **2002**, *99*, 4769–4774; b) G. M. Whitesides, J. P. Mathias, C. T. Seto, *Science* **1991**, *254*, 1312–1319.

[48] F. Würthner, C. -C. You, C. R. Saha-Möller, *Chem. Soc. Rev.* **2004**, *33*, 133–146.

[49] a) M. Fujita, *Chem. Soc. Rev.* **1998**, *27*, 417–425; b) M. Fujita, M. Tominaga, A. Hori, B. Therrien, *Acc. Chem. Res.* **2005**, *38*, 369–378; c) J. K. Klosterman, Y. Yamuchi, M. Fujita, *Chem. Soc. Rev.* **2009**, *38*, 1714–1725.

[50] a) K. Severin, *Chem. Commun.* **2006**, 3859–3867; b) S. Leininger, B. Olenyuk, P. J. Stang, *Chem. Rev.* **2000**, *100*, 853–908; c) P. J.Stang, B. Olenyuk, *Acc. Chem. Res.* **1997**, *30*, 502–518; d) B. H. Northrop, Y. -R. Zheng, K. -W. Chi, P. J. Stang, *Acc. Chem. Res.* **2009**, *42*, 51554–1563; e) S. R. Seidel, P. J. Stang, *Acc. Chem. Res.* **2002**, *35*, 972–983.

[51] a) R. W. Saalfrank, H. Maid, A. Scheurer, *Angew. Chem. Int. Ed.* **2008**, *47*, 8794–8824; b) G. V. Oshovsky, D. N. Reinhoudt, W. Verboom, *Angew. Chem. Int. Ed.* **2007**, *46*, 2366–2393; c) G. F. Swiegers, T. J. Malefetse, *Chem. Rev.* **2000,** *100*, 3483–3537; d) A. W. Kleij, *Dalton Trans.* **2009**, 4635–4639.

[52] a) H. N. Miras, E. F. Wilsonw, L. Cronin, *Chem. Commun.* **2009**, 1297–1311; b) C. A. Schalley, A. Lützen, M. Albrecht, *Chem. Eur. J.* **2004**, *10*, 1072–1080; c) P. Thanasekarana, R. -T. Liaoa, Y. -H. Liua, T. Rajendrana, S. Rajagopalb, K. -L. Lua, *Coord. Chem. Rev.* **2005**, *249*, 1085–1110.

[53] a) C. H. M. Amijs, G. P. M. van Klink, G. van Koten, *Dalton Trans.* **2006**, 308–327; b) A. Kaiser, P. Bäuerle, *Top. Curr. Chem.* **2005**, *249*, 127–201.

[54] D. Fiedler, D. H. Leung, R. G. Bergman, K. N. Raymond, *Acc. Chem. Res.* **2005**, *38*, 349–358; b) F. A. Cotton, C. Lin, C. A. Murillo, *Acc. Chem. Res.* **2001**, *34*, 759–771.

[55] a) C. Janiak, *Dalton Trans.* **2003**, 2781–2804; b) M. J. Zaworotko, *Chem. Commun.* **2001**, 1–9; c) N. L. Rosi, J. Eckert, M. Eddaoudi, D. T. Vodak, J. Kim, M. O'Keeffe, O. M. Yaghi, *Science*, **2003**, *300*, 1127–1129; d) D. Britt, D. Tranchemontagne, O. M. Yaghi *Proc. Natl. Acad. Sci. USA* **2008**, *105*, 11623–11627; e) P. Horcajada, C. Serre, G. Maurin, N. A. Ramsahye, Fr. Balas, M. Vallet-Regí, M. Sebban, F. Taulelle, G. Férey, *J. Am. Chem. Soc.* **2008**, *130*, 6774–6780.

[56] a) S. L. James, *Chem. Soc. Rev.* **2003**, *32*, 276–288; b) S. Natarajan, P. Mahata, *Chem. Soc. Rev.* **2008**, *38*, 2304–2318; c) P. Horcajada, C. Serre, M. Vallet-Regi, M. Sebban, F. Taulelle, G. Ferey, *Angew. Chem. Int. Ed.* **2006**, *45*, 5974–5978; d) A. Corma, H. García, F. X. L. Xamena, *Chem. Rev.* **2010**, *110*, 4606–4605.

[57] M. Fujita, J. Yazaki, K. Ogura, *J. Am. Chem. Soc.* **1990**, *112*, 5645–5647.

[58] a) P. Mal, B. Breiner, K. Rissanen, J. R. Nitschke, *Science* **2009**, *324*, 1697–1699; b) S. Hiraoka, K. Harano, M. Shiro, M. Shionoya, *Angew. Chem. Int. Ed.* **2005**, *44*, 2727–2731; c) J. -P. Bourgeois, M. Fujita, M. Kawano, S. Sakamoto, K. Yamaguchi, *J. Am. Chem. Soc.* **2003**, *125*, 9260–9261; d) C. Sgarlata, J. S. Mugridge, M. D. Pluth, B. E. F. Tiedemann, V. Zito, G. Arena, K. N. Raymond, *J. Am. Chem. Soc.* **2010**, *132*, 1005–1009.

[59] a) T. Kawamichi, T. Haneda1, M. Kawano, M. Fujita, *Nature* **2009**, *461*, 633–635; b) T. Iwasawa, R. J. Hooley, J. Rebek Jr., *Science* **2007**, *317*, 493–496; c) R. Warmuth, *Angew. Chem. Int. Ed.* **1997**, *36*, 1347–1350; d) R. Warmuth, M. A. Marvel, *Angew. Chem. Int. Ed.* **2000**, *39*, 1117–1119..

[60] a) M. Yoshizawa, M. Tamura, M. Fujita, *Science* **2006**, *312*, 251–254; b) M. Yoshizawa, Y. Takeyama, T. Kusukawa, M. Fujita, *Angew. Chem. Int. Ed.* **2002**, *41*, 1347–1349; c) M. Yoshizawa, S. Miyagi, M. Kawano, K. Ishiguro, M. Fujita, *J. Am. Chem. Soc.* **2004**, *126*, 9172–9173; d) M. D. Pluth, R. G. Bergman, K. N. Raymond, *Science*, **2007**, *316*, 85–88.

2. Metallacalix[n]arenes of Varying Ring Size Derived from Non Symmetrical Pyrimidine Nucleobase Cytosine

2.1. Introduction

Cytosine is one of the main pyrimidine nucleobases present in nucleic acids. Neutral cytosine can theoretically exist in fourteen different forms if various tautomers and different rotamers, derived from different orientations of hydroxo–OH and imino–NH protons, are considered.[1] Out of 14 possible tautomers, only six are within 40 kJ mol^{-1} in the gas phase (Scheme 2.1). In the gas phase cytosine exists as a mixture of at least three main tautomers: the 2-oxo-4-amino form (II) and two 2-hydroxo-4-amino (I, III) forms, whose relative stabilities lie within 4 kJ mol^{-1} of each other.[2] The second 2-oxo-4-amino tautomer (VI) is about 7 kcal mol^{-1} less stable than I and III. Solvation has a dramatic influence on

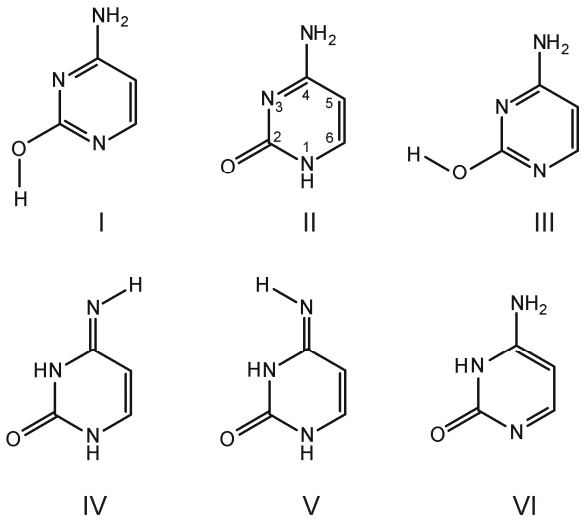

Scheme 2.1: Six predominant forms of cytosine in gas phase whose relative stabilities are within 40 kJ mol^{-1}.

the relative stabilities of different tautomers of neutral cytosine, however. All the tautomers are strongly destabilized with respect to the 1H-keto-amino (II) tautomer, which becomes dominant in solution. The 3H-keto-amino form (VI) is the second most stable one. However, it is about 24 kJ mol^{-1} less stable than the 1H-keto-amino tautomer.[2a,3] *Ab initio* calculations show that the solvent-induced destabilization of the 2-oxo-4-imino forms (IV & V) is smaller than for the 2-hydroxo-4-amino tautomers (I & III), which changes the relative population of these tautomers with respect to the situation in the gas phase.[2a] The most stable 2-oxo-4-imino form is preferred by about 4 kJ mol^{-1} over the most stable 2- hydroxo-4-amino form in aqueous solution. This finding agrees well with experimental evidence,

which precludes the existence of enol tautomers (I & III) in aqueous solution. X-ray crystal structure results indicate that unsubstituted cytosine (anhydrous and monohydrate) exists in 1H-keto-amino tautomeric form (II).[4,5] The Raman spectra of cytosine also show that the neutral cytosine has the 1H-keto-amino structure (II) in solution.[6] According to Raman spectroscopy, the removal of a proton from the free cytosine leads to an anion of type (VII), and N3 is the site of protonation (VIII) (Scheme 2.2).[6] The pK_a values of neutral cytosine are 4.58 (protonation at N3 site), 12.15 (deprotonation of N1-H)[7] and ca. 17 (deprotonation of the exocyclic amino group).[8]

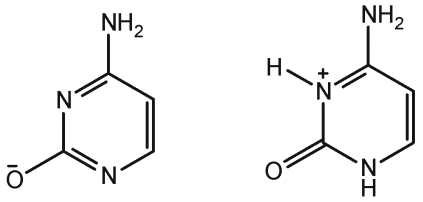

VII VIII

Scheme 2.2: View of preferred mono deprotonated (VII) and mono protonated (VIII) form of cytosine.

The primary metal binding site in neutral cytosine, which is present largely in 1H-keto-amino form (II) both in the solid state and in solution, is through the endocyclic N3 site.[9,10] However, metal ion coordination to the exocyclic O2 is also reported in a number of cases[11] and in few cases both N3 and O2 of cytosine simultaneously take part in metal binding either in a bridging fashion[12] or as a chelate.[13] The exocyclic N4 atom of cytosine does not take part in metal binding unless it is deprotonated.[14,15] Generation of organometallic compounds has also been observed with the model nucleobase 1-methylcytosine following metal coordination through its C5 position.[16] Possible metal binding patterns of cytosine are depicted in Scheme 2.3. A number of these patterns has been established crystallographically with the parent nucleobase cytosine.[17]

Metal ion coordination can be applied to stabilize rare nucleobase tautomers normally present in extremely low concentrations, and to crystallize them in their metal complexed forms in reasonable good yields. For example, metal complexation with the second most abundant 3H-keto-amino tautomer (VI) of cytosine is observed in a number of cases,[18,10b,10c] though 1H-keto-amino form (II) dominates the 3H-keto-amino tautomer (VI) by a factor of about 10^3 – 10^4 in aqueous solution. Similarly, metal coordination to the exocyclic amino group of 1-methylcytosine after initial deprotonation at this position and following reprotonation at N3, leads to a metalated form of the rare imino-oxo tautomer

(type IV or V).[14a,14c,19] The existence of a rare nucleobase tautomer may be responsible for base mispairing which, if undetected by repair enzymes, could lead to a point mutation.

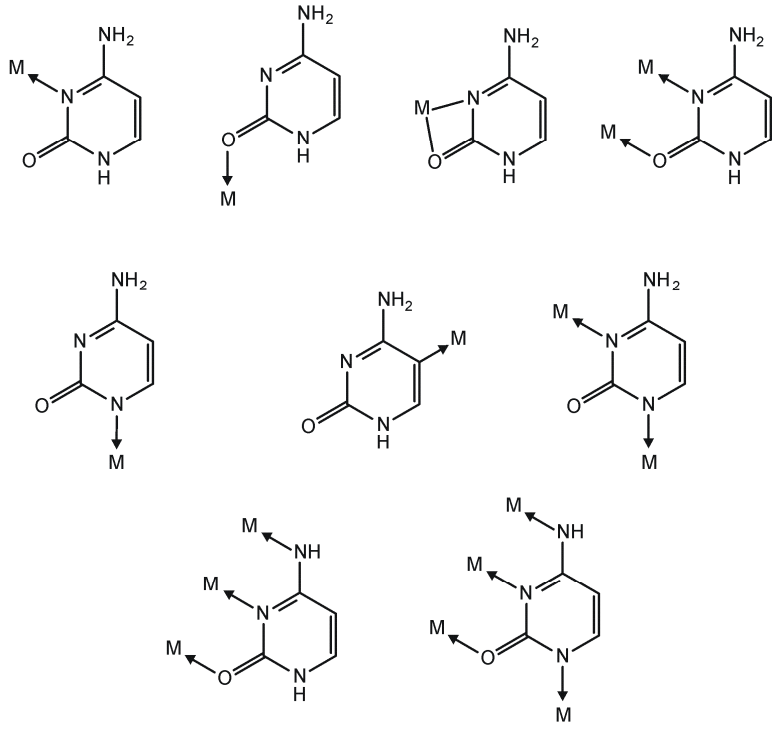

Scheme 2.3: Possible metal binding patterns of cytosine.

Metal migration and metal-mediated deamination has been the other phenomena found in metal-nucleobase complexes. Pt^{II} complexes of 1-methylcytosine can undergo metal migration from the kinetically preferred N3 site to the thermodynamically preferred N4 binding site in a process that can be facilitated either by redox chemistry[19a,20] or by pH.[21] It can also undergo metal-mediated deamination to a 1-methyluracil complex (Scheme 2.4).[21a,22]

Here, in the present work, Pt^{II} complexes of the parent (unsubstituted) nucleobase cytosine were studied to understand the effect of metal ions on acid-base equilibria of cytosine and also their ability to stabilize rare tautomeric forms of cytosine or of its monoanion. Cytosine can also form metallacycles of varying ring size via its endocyclic N1, N3 sites and these metallacycles have a strong propensity to accommodate additional metal entities at their exocyclic groups (N4, O2), resulting in the formation of multinuclear complexes. The complexity of so-called “platinum pyrimidine blues”,[23] a class of compounds once considered the second generation of Pt antitumor drugs after cisplatin,

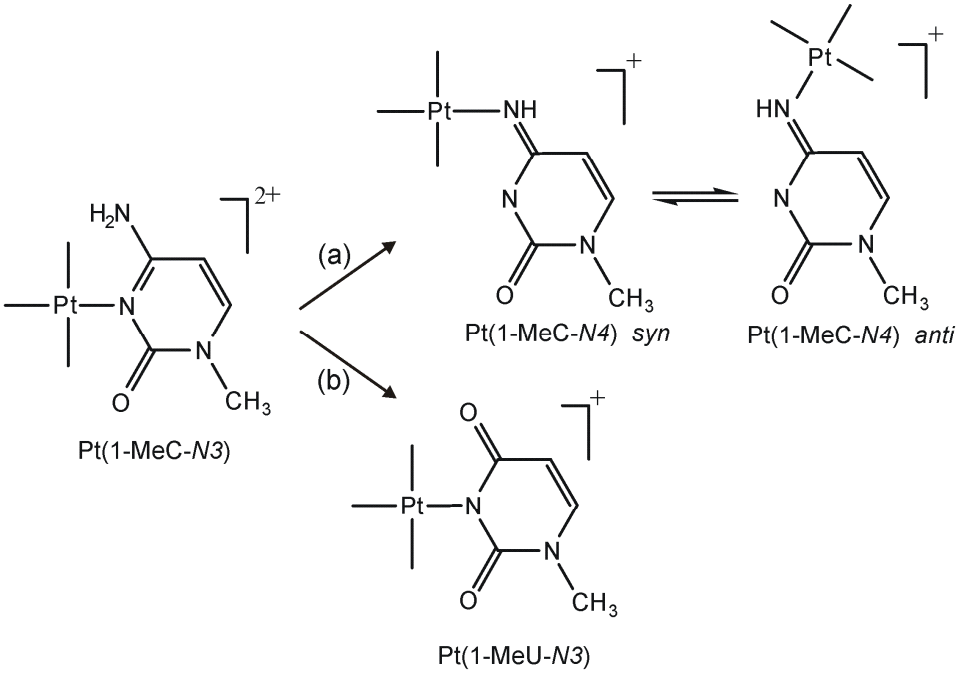

Scheme 2.4: Schematic diagram of (a) Pt^{II} migration from N3 to N4 site of 1-methylcytosine and (b) Pt^{II} mediated deamination of 1-methylcytosine.[22]

is possibly closely related to this propensity. Cytosine, being a low symmetrical ligand (C_s), can form random mixtures of isomers when combined with *cis*-a_2M^{II} entities (a_2 = amine or diamine, M = Pt, Pd). However, the number of possible isomers can be reduced to a single linkage isomer by applying preformed building blocks (see Section 2.12 for more details).

2.2. Observation of linkage isomers on the ^{1}H NMR scale

^{1}H NMR spectra of reaction mixtures of *cis*-$[Pt(NH_3)_2(D_2O)_2]^{2+}$ and cytosine (H_2C) at 40 ℃ in D_2O reveal the presence of multiple products, depending on pD and the ratio *r* between the reactants, especially within few hours after the start of reaction. However, with longer reaction time (66 h) and an excess of cytosine, the spectra become relatively simple (Figure 2.1). Under the conditions of the experiment, with Pt:H_2C = 1:4, formation of the N1 linkage isomer is hardly detectable (very weak doublets at δ = 7.80 ppm (H6) and 5.90 ppm (H5)). Resonances due to $Pt^{II}(H_2C\text{-}N1)_2$, $Pt^{II}(H_2C\text{-}N3)_2$, and free cytosine ($H_2C$) can be found in solution in a ratio 1:33:23. Most of the resonances are assigned from comparison with the spectra of isolated compounds and by their pD dependent ^{1}H NMR spectra. It is noteworthy to mention that the N1 linkage isomer $Pt^{II}(H_2C\text{-}N1)_2$ is formed even in acidic medium, where cytosine is partly protonated (pK_a of H_3C^+ is 4.58 ± 0.01[7]). There is no sign of formation of a *head-tail* dimer involving N3 and N4 coordination, hence

of $Pt_2^{II}(HC\text{-}N3,N4)_2$ (cytosine resonances to be expected upfield) or of the mixed linkage isomer $Pt^{II}(H_2C\text{-}N1)(H_2C\text{-}N3)$ under the condition of excess cytosine. When similar reactions are carried out between *cis*-$[Pt(NH_3)_2(D_2O)_2]^{2+}$ and cytosine in 1:1 ratio (pD = 2.9, 40 ℃, 1d), the spectrum becomes very complica ted and a number of new resonances appears in the low field section, three very intense ones and about five minor sets of cytosine-H6 resonances.

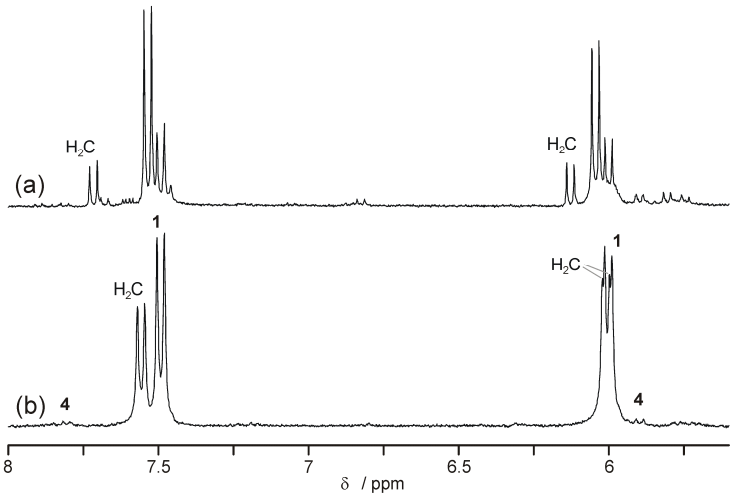

Figure 2.1: Low field section of ^{1}H NMR spectrum of a reaction mixture of *cis*-$[Pt(NH_3)_2(D_2O)_2]^{2+}$ and cytosine (a) r = 1:1, pD 2.9, 40 ℃, 24 h; (b) r = 1:4, pD 5 .8, 40 ℃, 66 h (See text for assignment of **1** and **4**).

The 1H-keto-amino tautomer II (Scheme 2.1) of cytosine is the preferred one in the gas phase and in aqueous medium, it exceeds the second most abundant one VI about 10^3 – 10^4 times. However, according to ^{1}H NMR spectra of a reaction mixture of *cis*-$(NH_3)_2Pt^{II}$ with cytosine, the distribution of different linkage isomers in D_2O at slightly acidic pD does not reflect this situation, and the N1 linkage isomer $Pt^{II}(H_2C\text{-}N1)_2$ is formed to an extent that greatly exceeds the natural abundance of tautomer VI. Earlier work on the *trans*-$(NH_3)_2Pt^{II}$ [10c] or $(dien)Pt^{II}$ [10b] systems also confirms this observation.

Similar reactions, carried out with $(en)Pd^{II}$ instead of *cis*-$(NH_3)_2Pt^{II}$, showed that the reaction mixture ($Pd:H_2C$ = 1:3) reaches equilibrium within 30 min of sample preparation at room temperature. Again, $Pd^{II}(H_2C\text{-}N3)_2$ is the dominant species in solution. This assignment is based on the pD dependence of the reaction mixture and also on the chemical shifts of the isolated compound. Interestingly, in case of Pd^{II} species, formation of the mixed linkage isomer $Pd^{II}(H_2C\text{-}N1)(H_2C\text{-}N3)$ can also be detected, albeit in very low percentage.

2.3. Synthesis and characterization of bis(nucleobase) complexes with cytosine-*N3* coordination

Three closely related complexes of composition *cis*-$[Pt(NH_3)_2(H_2C\text{-}N3)_2](NO_3)_2\cdot 2H_2O$ (**1**), $[Pt(en)(H_2C\text{-}N3)_2](NO_3)_2\cdot H_2O$ (**2**) and $[Pd(en)(H_2C\text{-}N3)_2](NO_3)_2\cdot 2H_2O$ (**3**) have been prepared by reacting the respective metal species *cis*-$[a_2M(H_2O)_2]^{2+}$ with 2 equivalents of cytosine in water at slightly acidic pH. *cis*-$[Pt(NH_3)_2(H_2C\text{-}N3)_2](NO_3)_2\cdot 2H_2O$ (**1**) has also been obtained from DMF by reacting *cis*-$[Pt(NH_3)_2(DMF)_2]^{2+}$ with 2 equivalents of cytosine. X-ray quality crystals were obtained in all three cases by slow evaporation of an aqueous solution of the respective compound and the structures were determined in all three cases.

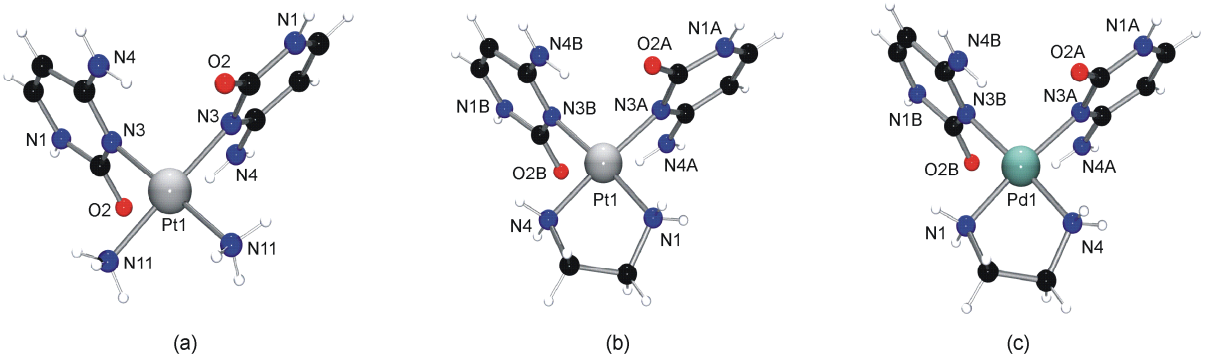

Figure 2.2: View of cations of (a) **1**, (b) **2** and (c) **3**. Counter anions (NO_3^-) and water are omitted for clarity

Compounds **1** and **3** crystallize in the centrosymmetric space group (C2/c), whereas compound **2** crystallizes in the triclinic space group (P-1). Views of the cations of compounds **1**, **2** and **3** are given Figure 2.2. Square-planar geometries of the metals are observed in all cases. Distances and angles between Pt and nucleobases are in the usual range. Selected bond distances and angles are listed in Table 2.1. Cytosine is coordinated to Pt through its N3 position. In all cases exocyclic O2 and N4 groups of two cytosine nucleobases are oriented in different directions of the Pt coordination plane; so the two nucleobases adopt a *head-tail* arrangement. The cations are consequently chiral and both enantiomers are present in the crystal. The *head-tail* arrangement of the nucleobases is stabilized by pairs of intramolecular hydrogen bonds between exocyclic O2 and $N4H_2$ groups. These H bond distances are 3.056(6) Å (in **1**), 2.955(4) and 3.042(5) Å (in **2**), as well as 3.041(4) and 3.000(4) Å (in **3**). The dihedral angles between MN_4 coordination planes and the cytosine nucleobases are 73.6° (in **1**), 80.9° and 81.4° (in **2**), as well as 82.7° and 84.8° (in **3**). The dihedral angles between cytosine planes are 82.5° (**1**), 72.0° (**2**), and 79.5° (**3**). There is a close similarity in the cation structures **1** – **3** with the corresponding 1-methylcytosine complex *cis*-$[Pt(NH_3)_2(1\text{-}MeC\text{-}N3)_2]^{2+}$ (1-MeC = 1-

methylcytosine).[24] The cations of **1** – **3** do not form hydrogen bonds involving simultaneously N1H and O2 sites of cytosines because donor/acceptor sites are blocked by nitrate counter anion (N1H) and ammine ligands of neighboring platinum entities (O2). However, these compounds display intermolecular hydrogen bonding between cytosines: N1H···O2 and $N4H_2$···O2, allowing the formation of monodimensional hydrogen bonded chains (Figure 2.3).

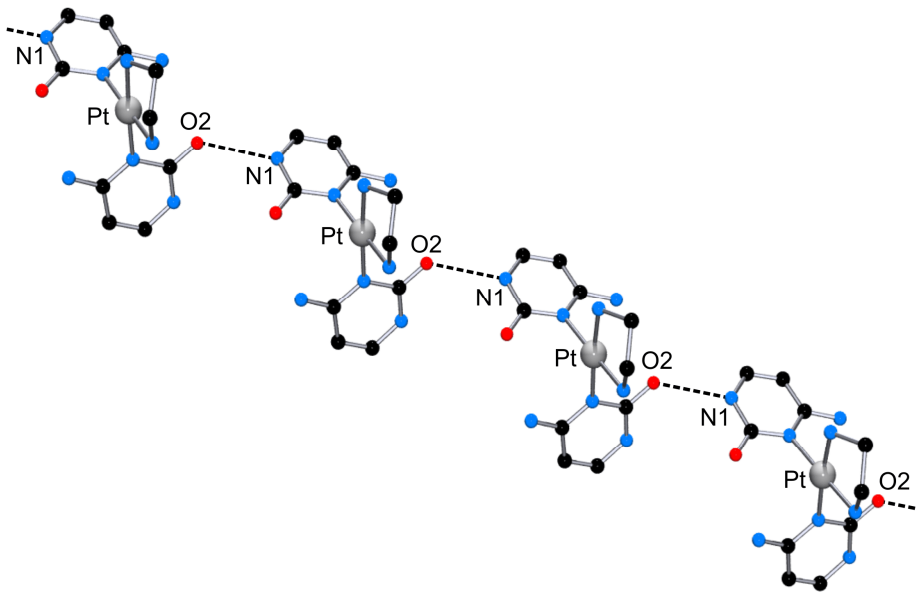

Figure 2.3: Monodimensional hydrogen bonded strand of cations of **2** involving N1(H) and O2 atoms.

Table 2.1a: Selected bond distances (Å) and angles (º) for compound **1**.

Pt1-N11, 2.039(4)	N11-Pt1-N11, 88.9(2)	N3-Pt1-N3, 90.7(2)
Pt1-N3, 2.042(4)	N11-Pt1-N3, 90.21(16)	N11-Pt1-N3, 178.92(18)

Table 2.1b: Selected bond distances (Å) and angles (º) for compound **2**.

Pt1-N1, 2.014(4)	N1-Pt1-N3A, 91.70(15)	N3A-Pt1-N4, 174.78(17)
Pt1-N4, 2.037(4)	N3B-Pt1-N4, 92.06(15)	N1-Pt1-N3B, 174.93(15)
Pt1-N3A, 2.034(4)	N3B-Pt1-N3A, 93.07(15)	Dihedral (PtN_4/H_2C), 80.9
Pt1-N3B, 2.027(4)	N1-Pt1-N4, 83.20(15)	Dihedral (PtN_4/H_2C), 81.4

Table 2.1c: Selected bond distances (Å) and angles (º) for compound **3**.

Pd1-N3A, 2.053(4)	N3B-Pd1-N3A, 92.98(13)	N1-Pd1-N3A, 174.76(15)
Pd1-N3B, 2.042(4)	N4-Pd1-N3A, 91.61(12)	N4-Pd1-N3B, 175.00(14)
Pd1-N1, 2.005(3)	N1-Pd1-N3B, 92.02(13)	Dihedral (PtN_4/H_2C), 82.7
Pd1-N4, 2.015(3)	N1-Pd1-N4, 83.44(13)	Dihedral (PtN_4/H_2C), 84.8

2.4. Synthesis of bis(nucleobase) complexes with cytosine-*N1* coordination

Cis-$Pt(NH_3)_2(HC\text{-}N1)_2 \cdot 3.25\ H_2O$ (**4**) was obtained in good yield from the reaction of *cis*-$[Pt(NH_3)_2(DMF)_2]^{2+}$ with 2 equivalents of sodium cytosinate (Na^+HC^-) in DMF. **4** crystallizes in the monoclinic space group C2/c. It has two crystallographically different molecules (Pt1, Pt2) in the unit cell. In both molecules, the two nucleobases adopt *head-tail* arrangements, as exocyclic O2 groups of two cytosine nucleobases are oriented in different directions of the PtN_4 coordination planes. Each complex is consequently chiral and occurs as pairs of enantiomers. A view of one of the two crystallographically independent molecules (Pt2) is provided in Figure 2.4. Monoanionic cytosine is coordinated to Pt through its N1 sites (Table 2.2). The dihedral angles between the PtN_4 coordination planes and the cytosine nucleobases are 57.7° (Pt1/A), 49.0° (Pt1/B), 44.1° (Pt2/C) and 67.3° (Pt2/D). The dihedral angles between cytosine planes are 71.1° (Pt1) and 74.2° (Pt2). The O2 sites of HC ligands are involved in intramolecular hydrogen bond formation with NH_3 ligands: N11···O2a, 3.000(6) Å, N12···O2b, 2.899(6) Å, N21···O2c, 2.853(7) Å, N22···O2d, 3.256(6) Å. A special feature of complex **4** is that the exocyclic O2 atom interacts with neighboring groups as expected for a sp^3 hybridized oxygen atom (Figure 2.5). This is reflected also in the slightly higher C-O2 bond length in **4** (C2a-O2a, 1.272(7) Å; C2b-O2b, 1.248(7) Å; C2c-O2c, 1.263(6); C2d-O2d, 1.259(7) Å) as compared to the free, anhydrous cytosine (1.241(3) Å). The Pt^{II} coordination to N1 site of deprotonated cytosine possibly causes a shift in hybridization of the exocyclic O2 towards sp^3 (Scheme 2.5). Unlike in its trans analogue,[10c] the Watson Crick type of base pairing involving O2, N3 and N4(H_2) site of cytosinate anion in **4** is not observed.

When **4** is compared with the corresponding N3 linkage isomers (**1** – **3**), a number of differences can be observed. In case of **4** the intramolecular H bonds between exocyclic O2 and $N4H_2$ groups seen with the N3 linkage isomer **1** – **3**, are missing. So the cation of

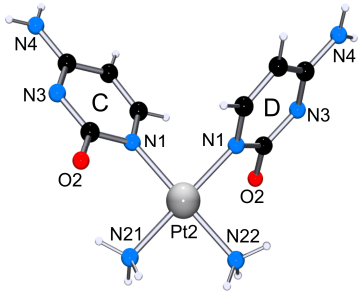

Figure 2.4: View of *cis*-[Pt(NH_3)$_2$(HC-*N1*)$_2$] (**4**)

Table 2.2: Selected bond distances (Å) and angles (º) for compound **4**.

Pt1-N1A, 2.017(4)	N1A-Pt1-N1B, 89.7(2)	N1B-Pt1-N12, 89.5(2)
Pt1-N1B, 2.031(5)	N12-Pt1-N11, 92.0(2)	N1A-Pt1-N12, 178.7(2)
Pt1-N12, 2.048(4)	N1A-Pt1-N11, 88.8(2)	N1B-Pt1-N11, 178.4(2)
Pt1-N11, 2.057(5)		
Pt2-N1C, 2.039(5)	N1D-Pt2-N1C, 87.36(18)	N1D-Pt2-N22, 91.58(18)
Pt2-N1D, 2.015(4)	N1C-Pt2-N21, 93.83(18)	N1D-Pt2-N21, 173.8(2)
Pt2-N21, 2.043(4)	N22-Pt2-N21, 87.69(18)	N22-Pt2-N1C, 175.5(2)
Pt2-N22, 2.038(5)		

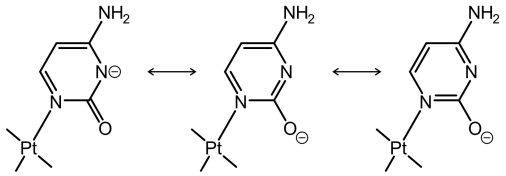

Scheme 2.5: Mesomeric forms of N1 bonded cytosinate ligand in **1**.

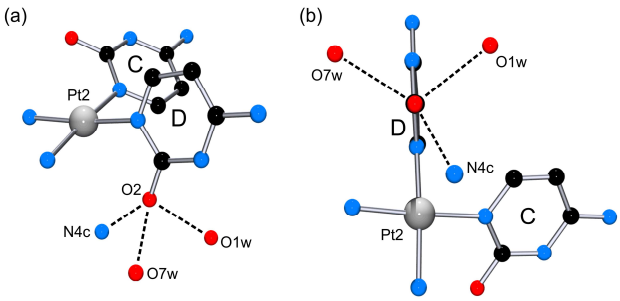

Figure 2.5: Side (a) and upper (b) views of the Pt2-molecule of **1**, showing the hydrogen bonding pattern for the atom O2 of cytosine ring D.

4 appears to be less rigid and more flexible. Also, **4** has a lower cytosine tilt angle as compared to the N3 linkage isomers **1** – **3** (ca. 74° – 84°). The internal bond angles of the cytosine in the N1 linkage isomer are significantly different from the corresponding N3 linkage isomers with the preferred 1H-keto-amino tautomer structures. A comparison of internal bond angles of cytosine in **1** and **4** is given in Table 2.3. For example, the C6–N1–C2, 122.5(5) bond angle in **1** is significantly higher than the corresponding bond angle in **4**. The corresponding *trans*-$(CH_3NH_2)_2Pt^{II}$ complex with cytosine also showed similar differences in bond angles.[10c]

Table 2.3: Comparison of internal bond angels (º) of cytosine ligand for compound **1** and **4**.

1	**4**	
C6-N1-C2, 122.5(5)	C6C-N1C-C2C, 116.1(5)	C6D-N1D-C2D, 118.6(5)
N1-C2-N3, 116.5(5)	N3C-C2C-N1C, 121.4(5)	N3D-C2D-N1D, 120.8(6)
C4-N3-C2, 121.0(4)	C4C-N3C-C2C, 120.8(5)	C4D-N3D-C2D, 118.8(5)
N4-C4-C5, 120.6(5) N3-C4-C5, 121.2(5)	N3C-C4C-C5C, 119.3(5)	N3D-C4D-C5D, 122.5(6)
C6-C5-C4, 117.8(5)	C6C-C5C-C4C, 117.8(6)	C6D-C5D-C4D, 115.8(6)
C5-C6-N1, 120.9(5)	C5C-C6C-N1C, 124.5(6)	N1D-C6D-C5D, 123.5(6)

2.5. ^{1}H NMR Spectra of 1, 2, 3, and 4

The ^{1}H NMR spectra of **1** – **4** in D_2O show discrete doublets due to cytosine H5 and H6 resonances. The chemical shifts of the aromatic protons with their coupling constants are

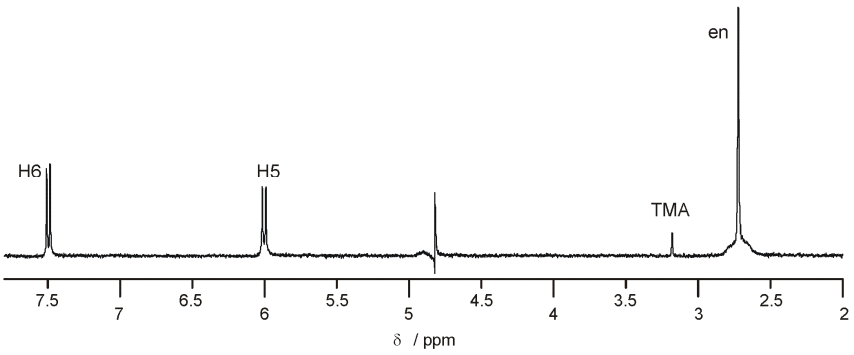

Figure 2.6: ^{1}H NMR spectrum of $[Pt(en)(H_2C\text{-}N3)_2](NO_3)_2 \cdot H_2O$ (**2**) in D_2O, pD 6.8 (TMA as internal reference, δ=3.18 ppm).

given in Table 2.4. A representative ^{1}H NMR spectrum of **2** is shown in Figure 2.6. In case of the corresponding trans complex with cytosine[10c] or 1-methylcytosine[25], both rotamers (*head-tail* and *head-head*) can be detected in solution, while this is not the case with cis isomers. Only single sets resonances are observed for each proton of cis isomers **1** – **4** in the ^{1}H NMR spectra, which probably suggests hindered rotation of individual bases due to steric congestion. The alternative, extremely fast rotation of the bases leading to averaged signals in the ^{1}H NMR, is less likely.

Table 2.4: The ^{1}H NMR chemical shifts of non-exchangeable protons for compounds **1** – **4** in D_2O. Coupling constants (^3J) are provided in brackets.

Compounds	pD	H6 ppm (^3J)	H5 ppm (^3J)
1	6.15	7.51 (7.3 Hz)	6.02 (7.3 Hz)
2	6.87	7.50 (7.3 Hz)	6.00 (7.3 Hz)
3	5.82	7.53 (7.2 Hz)	5.99 (7.2 Hz)
4	10.42	7.57 (6.8 Hz)	5.72 Hz (6.8 Hz)

2.6. Acid-base equilibria of 1, 2 and comparison with *N1* linkage isomer 4

pD-dependent ^{1}H NMR spectra for the *N3* linkage isomers *cis*-$[Pt(NH_3)_2(H_2C\text{-}N3)_2](NO_3)_2\cdot 2H_2O$ (**1**), $[Pt(en)(H_2C\text{-}N3)_2](NO_3)_2\cdot H_2O$ (**2**) and N1 linkage isomer *cis*-$Pt(NH_3)_2(HC\text{-}N1)_2\cdot 3.25H_2O$ (**4**) were recorded in order to determine their acid-base equilibria. With change in pD of the solution, the chemical shifts of non-exchangeable protons change as a consequence of protonation or deprotonation. Only a single pK_a value for the deprotonation of N1-H of both cytosines in **1** and **2** is deduced, but for its linkage isomer **4**, two pK_a values for deprotonation of N3 position can be calculated. While cytosine-H5 resonances in **1** and **2** are shifted upfield with increasing pD as a consequence of deprotonation, cytosine-H6 undergoes a downfield shift (Figure 2.7a). This situation is similar to that seen for *trans*-$[Pt(MeNH_2)_2(H_2C\text{-}N3)_2]^{2+}$ [10c] as well as $[Pt(NH_3)_3(H_2C\text{-}N3)]^+$.[10a] The p$K_a$ values for **1** derived for H6 and H5 are 9.95 ± 0.03 and 10.02 ± 0.03 in D_2O, corresponding to a value of ca. 9.40 ± 0.04 in H_2O. For $[Pt(en)(H_2C\text{-}N3)_2]^{2+}$ (**2**) a pK_a of 9.2 ± 0.04 (H_2O) was determined. Both values represent the mean of successive deprotonation steps of the two cytosine ligands, which are too close to be

resolved. Earlier work by Lippert and Sigel showed that the statistical expectation of ΔpK_a is 0.6 for two ligands behaving independently,[26] so individual pK_a values should then be $\geq$ 9.1 and $\leq$ 9.7 for **1** and ca. $\geq$ 8.9 and $\leq$ 9.5 for **2**. Thus, Pt^{II} coordination to the N3 position of cytosine shifts the pK_a value by ca. 2.8 – 3 log units from 12.15 in free cytosine to 9.4 in **1** and 9.2 in **2**.

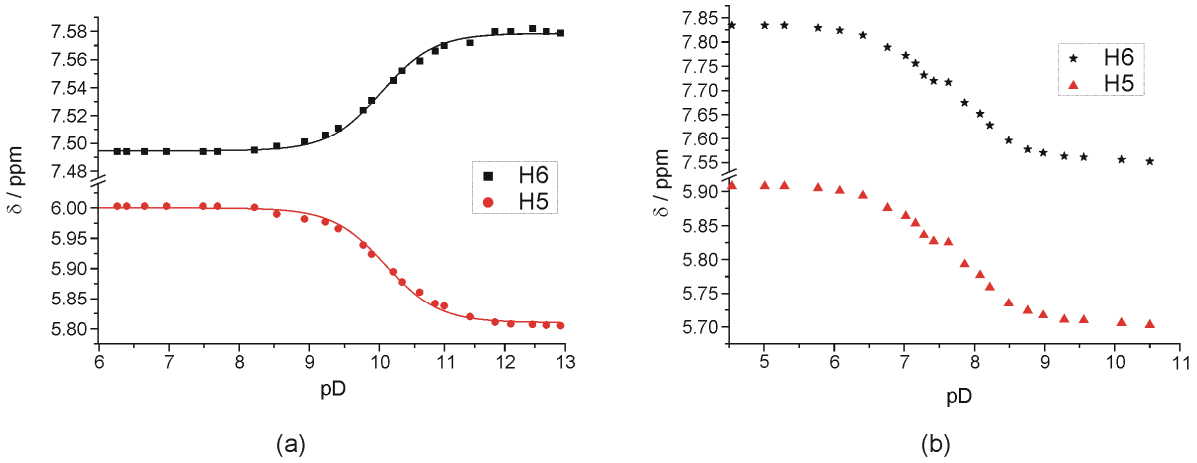

Figure 2.7: pD dependence of cytosine-H5 and -H6 resonances of (a) *cis*-$[Pt(NH_3)_2(H_2C\text{-}N3)_2](NO_3)_2$ (**1**) and (b) *cis*-$[Pt(NH_3)_2(HC\text{-}N1)_2]$ (**4**).

However, in case of *cis*-$Pt(NH_3)_2(HC\text{-}N1)_2 \cdot 3.25H_2O$ (**4**), both H5 and H6 resonances are downfield shifted upon protonation (Figure 2.7b). The pK_a values for *cis*-$[Pt(NH_3)_2(H_2C\text{-}N1)_2]^{2+}$ (**4b**) $\rightleftharpoons$ *cis*-$[Pt(NH_3)_2(H_2C\text{-}N1)(HC\text{-}N1)]^{+}$ (**4a**) and *cis*-$[Pt(NH_3)_2(H_2C\text{-}N1)(HC\text{-}N1)]^{+}$ (**4a**) $\rightleftharpoons$ *cis*-$[Pt(NH_3)_2(HC\text{-}N1)_2]$ (**4**) are 6.3 $\pm$ 0.2 and 7.5 $\pm$ 0.1 respectively (calculated for H_2O). Placing a Pt^{II} entity to the N1 site of cytosine in **4** acidifies strongly the N3H proton compared to free cytosine or N3 linkage isomers **1**, **2**. So the acidifying effect of Pt^{II} bonded to N1 affects markedly the N3H proton, while the acidifying effect of Pt^{II} bonded to N3 is less pronounced for N1H. The ΔpK_a (difference between two pK_a value) of 1.2 in **4,**

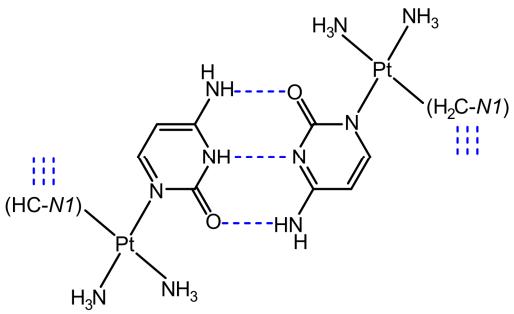

Scheme 2.6: Proposed homo base pairing between *cis*-$[Pt(NH_3)_2(H_2C\text{-}N1)(HC\text{-}N1)]^{+}$ (**4a**).

being higher than the statistically expected value of 0.6, clearly indicates that the two deprotonation sites are truly independent. This can be explained by the formation of homo cytosine base pairs **4a**, which are expected to lead to the formation of long chains and could have a stabilizing effect on the intermediate singly deprotonated form (Scheme 2.6).

2.7. Solution behavior of $[Pd(en)(H_2C\text{-}N3)_2](NO_3)_2\cdot 2H_2O$ (3)

The acid-base equilibrium for the Pd complex **3** can not be measured because a number of new resonances appear with change in pD of the solution. Unlike the Pt complexes, **3** is

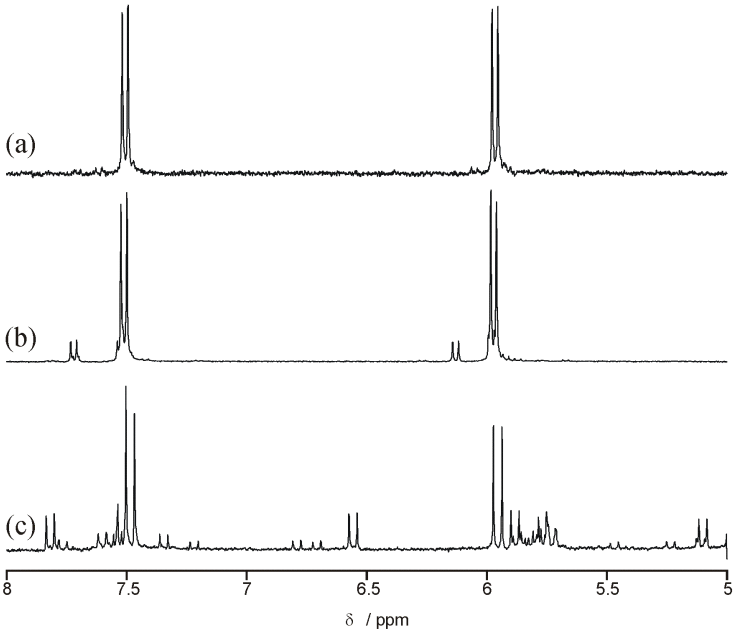

Figure 2.8: ^{1}H NMR spectra of (a) crystals of $[Pd(en)(H_2C\text{-}N3)_2](NO_3)_2\cdot 2H_2O$ (**3**) in D_2O, pD = 5.8; (b) **3** in D_2O kept at pD = 2.1 for 2d, RT; (c) **3** in D_2O kept at pD = 10.7 for 2d, RT.

unstable both at low pD as well as at high pD. The number of species formed in alkaline pD is comparatively higher. At low pD (pD 2.1, DNO_3), release of free cytosine (ca. 10%) is observed and formation of an additional minor product (< 3%) is indicated by the ^{1}H NMR spectrum (Figure 2.8). At alkaline pD (pD ≥ 9, NaOD), at least ten doublets for each H6 and H5 protons of cytosine are observed in the low field section of ^{1}H NMR spectra. No attempts have been made to assign all these resonances. Earlier work by Martin[27] showed that a multitude of products containing various *μ*-OH and *μ*-cytidinate species is formed in the Pd^{II}(en)/cytidine systems. However, in our case the use of cytosine may

even increase the number of feasible products because of the additional free N1 coordination site.

2.8. Hemideprotonated and fully deprotonated derivatives of 1

Two derivatives of **1**, namely *cis*-[Pt(NH_3)$_2$(H_2C-*N3*)(HC-*N3*)](NO_3)·H_2O (**5**) and *cis*-[Pt(NH_3)$_2$(HC-*N3*)$_2$]·4H_2O (**6**) were obtained from aqueous solution of **1** at different pH. As shown above, the pK_a value for deprotonation of N1H in **1** is ca. 9.4 (mean value for both cytosine ligands). Hemideprotonated complex **5** was obtained at pH 9.6, whereas the fully deprotonated **6** was obtained at pH 12.6. These values agree well with the observed pK_a values of **1**. Hemideprotonated **5** and fully deprotonated **6** crystallize in the tetragonal (I-42d) and the triclinic (P-1) space group, respectively. Views of the cation of **5** and of neutral **6** are provided in Figure 2.9. Selected structural features are given in Table 2.5. Like in **1**, the two nucleobases in **5** and **6** are arranged in *head-tail* orientation and are stabilized by intramolecular hydrogen bonding between exocyclic O2 and N4H_2 groups: 2.907(6) Å (for **5**); 2.916(8) and 3.123(8) Å (for **6**). The dihedral angles between cytosine planes are 84.9° (**5**) and 84.5° (**6**). The dihedral angles between PtN_4 coordination planes and cytosine are 84.4° (**5**), and 74.2° and 78.3° (**6**).

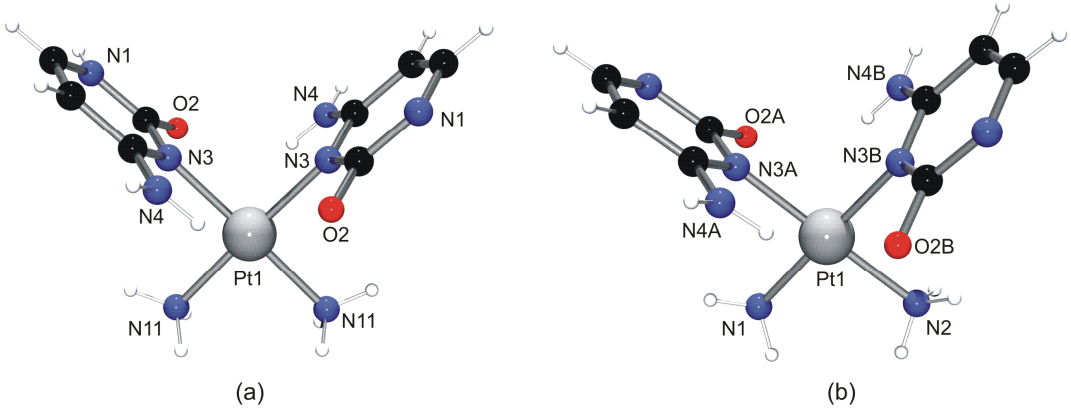

Figure 2.9: Views of (a) cation *cis*-[Pt(NH_3)$_2$(H_2C-*N3*)(HC-*N3*)]$^+$ of **5**, in which one of the cytosine bases is deprotonated at N1; and (b) the neutral species *cis*-[Pt(NH_3)$_2$(HC-*N3*)$_2$] (in **6**), which has both cytosine bases deprotonated at N1.

The effect of deprotonation of N1-H of cytosine bases is reflected in the internal bond angles of cytosines in **5** and **6**. For example, the internal bond angle C6–N1–C2 of 116.3(7)°, 117.3(7)° in fully deprotonated **6** is lower than the corresponding bond angle 120.2(5)° in hemideprotonated **5**. In the cation of **5**, short intermolecular hydrogen bonding

interactions of 2.732(9) Å between N1H and N1 sites gives rise to the formation of H-bonded polymeric chains (Figure 2.10).

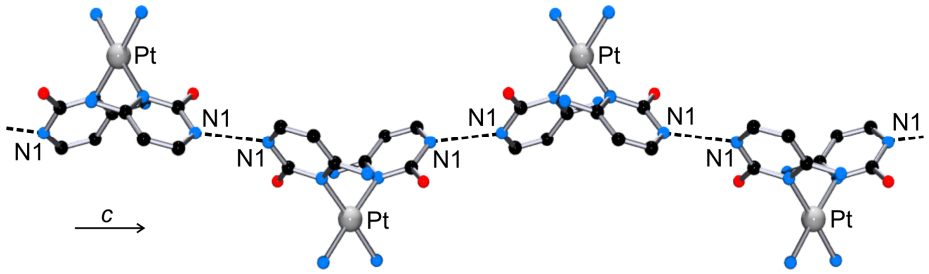

Figure 2.10: Monodimensional hydrogen bonded strand of **5** along the *c* axis.

Table 2.5a: Selected bond distances (Å) and angles (º) for compound **5**.

Pt1-N3, 2.034(5)	N3-Pt1-N11, 91.53(17)	N3-Pt1-N11, 177.8(2)
Pt1-N11, 2.035(5)	N3-Pt1-N11, 91.54(17)	C6-N1-C2, 120.2(5)
N3-Pt1-N3, 90.5(2)	N11-Pt1-N11, 86.4(3)	

Table 2.5b: Selected bond distances (Å) and angles (º) for compound **6**.

Pt1-N3A, 2.008(6)	N3A-Pt1-N3B, 91.6(2)	N2-Pt1-N3B, 88.1(2)
Pt1-N3B, 2.029(6)	N2-Pt1-N1, 90.8(3)	N3B-Pt1-N1, 179.0(3)
Pt1-N1, 2.060(6)	N3A-Pt1-N1, 89.4(3)	N3A-Pt1-N2, 179.7(3)
Pt1-N2, 2.022(6)	C6A-N1A-C2A, 116.3(7)	C6B-N1B-C2B, 117.3(7)

2.9. AgCl adducts of 4

AgCl adducts of **4** were obtained in low yield during the preparation of *cis*-$Pt(NH_3)_2$(HC-*N1*)$_2$·3.25 H_2O (**4**). Insufficient reaction time (10h in DMF, RT) causes incomplete precipitation of AgCl from the reaction mixture of *cis*-$[PtCl_2(NH_3)_2]$ with 2 equivalents of $AgNO_3$ and subsequent addition of sodium cytosinate to this reaction mixture leads to a mixture of **4** and its AgCl adducts **7**. Crystallization from water at room temperature produces two kinds of AgCl adducts, namely *cis*-$Pt(NH_3)_2$(HC-*N1*)$_2$·AgCl·xH_2O (**7a**) and *cis*-$[Pt(NH_3)_2$(HC-*N1*)$_2$Ag]Cl·3.5H_2O (**7b**), which were characterized by X-ray crystallography. A complete structural determination is not possible for **7a** due to the poor quality of the data set. In both **7a** and **7b**, Ag^+ is coordinated to the available N3 position of

the cytosinate ring, giving rise to the formation of a 1D polymeric structure. The only difference is that in **7a** the chloride anion and a water molecule are directly bonded to Ag^+ ion (Figure 2.11), unlike in **7b**. The apparent propensity of **4** to bind Ag^+ through its N3 sites was confirmed by the following experiment: **4** was added to a freshly prepared AgCl slurry (prepared from equivalent amounts of $AgNO_3$ and NaCl in water) and after 16h the remaining AgCl precipitate was filtered off, identified, and weighed. 45% of the original AgCl precipitate had dissolved.

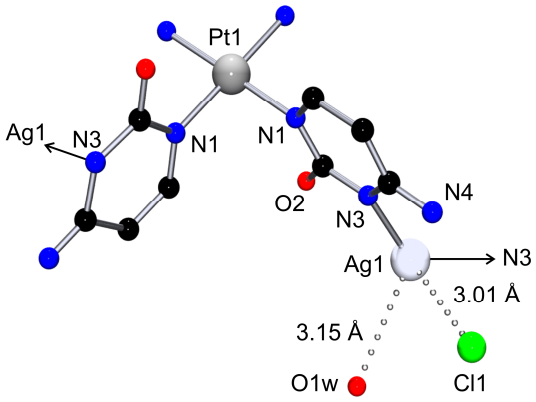

Figure 2.11: View of the monomer of *cis*-$Pt(NH_3)_2(CH\text{-}N1)_2 \cdot AgCl$ (**7a**).

Cis-$[Pt(NH_3)_2(HC\text{-}N1)_2Ag]Cl \cdot 3.5H_2O$ (**7b**) crystallizes in the triclinic space group (P-1). A view of the cation of **7b** is given in Figure 2.12. Cytosinate ligands are oriented in a *head-tail* arrangement, and intramolecular hydrogen bonding between exocyclic $N4H_2$ and O2 sites is absent. The dihedral angles between the PtN_4 coordination plane and the cytosinate ring are 79.4° (HC_A) and 81.1° (HC_B), far from the angles found in **4** (44.1° – 67.3°). The dihedral angle between cytosine bases is 81.5°. Ag-N3 bond distances are 2.154(14) Å (N3a) and 2.130(14) Å (N3b). The silver coordination angle of Ag1 (N3a-Ag1-N3b, 166.1(5)°) is in the range as reported in several examples of the cation $[Ag(NH_3)_2]^+$.[28] The coordination sphere of silver (Figure 2.13) is completed by a water molecule, intramolecular interactions with the O2 groups of the attached cytosine bases and N4 site of one cytosinate ring from a neighboring polymeric strand. Relevant distances are Ag1···O1w, 2.88(2) Å; Ag1···O2a, 3.009(13) Å; Ag1···O2b, 2.980(11) Å; Ag1···N4b, 3.003(16) Å.

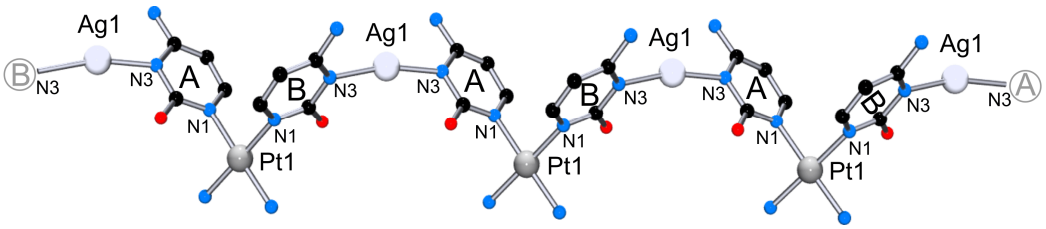

Figure 2.12: View of the coordination polymer *cis*-[Pt(NH$_3$)$_2$(HC-*N1*)$_2$Ag]Cl·3.5H$_2$O (**7b**).

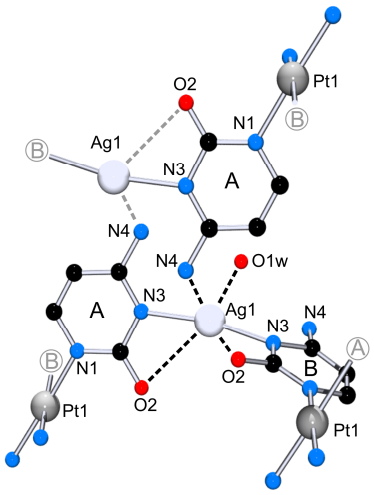

Figure 2.13: Detail of the coordination sphere of Ag1 in **7b**.

2.10. Unexpected side product: *head-tail* dimer with *N3,N4* bridging

During the course of preparation of *cis*-[Pt(NH$_3$)$_2$(H$_2$C-*N3*)$_2$]$^{2+}$ (**1**) from the reaction of *cis*-[Pt(NH$_3$)$_2$(H$_2$O)$_2$]$^{2+}$ with two equivalent of cytosine (H$_2$C) in water, the *head-tail* dimer *cis*-{[Pt(NH$_3$)$_2$(HC-*N3,N4*)]$_2$}(NO$_3$)$_2$ (**8**) was obtained in very small amount (5 – 6%) as a side product. The dimer **8** crystallizes in the monoclinic (C2/c) space group. Two *cis*-(NH$_3$)$_2$Pt^{II} entities coordinate to N3 and the mono deprotonated N4 site of cytosine in a *head-tail* arrangement (Figure 2.14). The cation is consequently chiral and both enantiomers are present in the crystal. Selected bond distances and bond angles are listed in Table 2.6. The dihedral angle between PtN$_4$ coordination planes is 30.8° and the dihedral angle between cytosine planes is 87.6°. The Pt-Pt separation of 2.9590(4) Å observed in **8** compares well with related diplatinum(II) compounds; e.g. 2.981(2) Å in *ht-cis*-[Pt(NH$_3$)$_2$(1MeC-*N3,N4*)$_2$]$_2^{2+}$,[29a] 2.981(3) Å in *ht*-[Pt(en)(1MeC-*N3,N4*)$_2$]$_2^{2+}$,[29b] and 2.974(1) Å in *ht-cis*-[Pt(NH$_3$)$_2$(1MeT-*N3,N4*)$_2$]$_2^{2+}$.[30] The Pt-Pt separation in diplatinum(III) complexes, e.g. 2.5982(4) Å in *ht*-[(SO$_4$)(en)Pt(1MeC-*N3,N4*)$_2$Pt(en)(SO$_4$)],[29b] is significantly shorter than in the diplatinum(II) complexes. There is a great similarity of the

cation of the dinuclear complex **8** with the analogous 1-methylcytosinato complex,[29,31] in which a CH_3 group substitutes for the proton at N1.

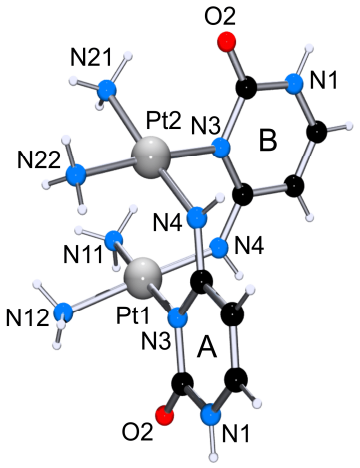

Figure 2.14: View of dinuclear cation *cis*-{[Pt$(NH_3)_2$(HC-*N3,N4*)]$_2$}$^{2+}$ (**8**), with both N1 sites protonated.

Table 2.6: Selected bond distances (Å) and angles (º) for compound **8**.

Pt1-N3A, 2.042(5)	N4B-Pt1-N3A, 89.7(2)	N11-Pt1-N12, 91.5(2)
Pt1-N4B, 1.991(5)	N4B-Pt1-N11, 88.39(19)	N3A-Pt1-N12, 90.3(2)
Pt1-N11, 2.034(5)	N11-Pt1-N3A, 178.1(2)	N4B-Pt1-N12, 177.8(2)
Pt1-N12, 2.056(5)	Pt1-Pt2, 2.9590(4)	
Pt2-N4A, 1.993(5)	N4A-Pt2-N3B, 89.8(2)	N4A-Pt2-N22, 88.4(2)
Pt2-N21, 2.049(4)	N22-Pt2-N21, 90.0(2)	N3B-Pt2-N21, 92.3(2)
Pt2-N22, 2.047(5)	N3B-Pt2-N22, 175.4(2)	N4A-Pt2-N21, 173.2(2)
Pt2-N3B, 2.021(5)		

An interesting feature in the crystal packing of **8** is that the ammine groups attached to the platinum atoms act as anion receptor, as reported previously with 1-methylcytosinato complexes.[31] Pairs of cations of **8** act as host and interact with two nitrate anion (Figure 2.15). One nitrate is hydrogen bonded to eight neighboring NH_3 groups and the distances are O21···N12, 3.111(8) Å, O21···N22, 3.446(8) Å, O22···N11, 3.334(7) Å, O22···N21, 2.945(6) Å. The second nitrate is locked via hydrogen bonding (O12···N11, 3.025(6) Å; O12···N21, 2.858(6) Å) and additional anion–π interactions. The distance of O11 to the centroid of cytosine-ring is 3.14 Å. Other sites of the cytosine bases

in **8** are involved in multiple hydrogen bonding with neighboring NH_3 groups and nitrate anions: O2a···H_3N11, 3.069 Å; N1bH···O11, 2.806 Å; O2b···N21, intramolecular H-bond of 2.988 Å; N4bH···O31, 2.996 Å. Moreover the cations of **8** display intermolecular hydrogen bonding interactions between cytosines (N1H···O2 (2.713 Å)), allowing the formation of monodimensional hydrogen bonded chains (Figure 2.16).

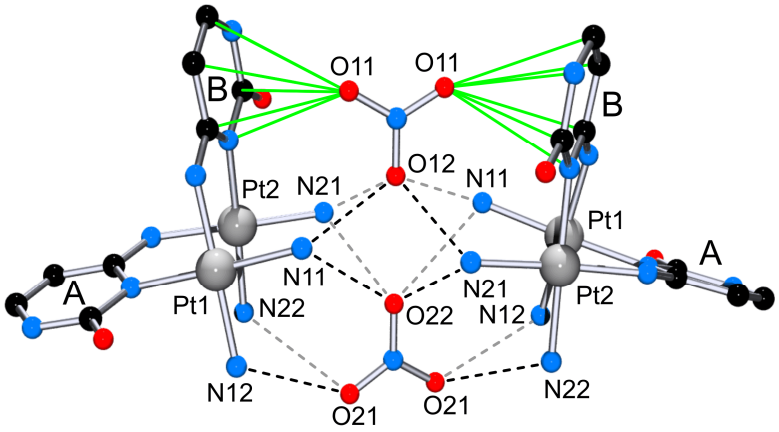

Figure 2.15: Pairs of cations of **8** act as effective anion receptors.

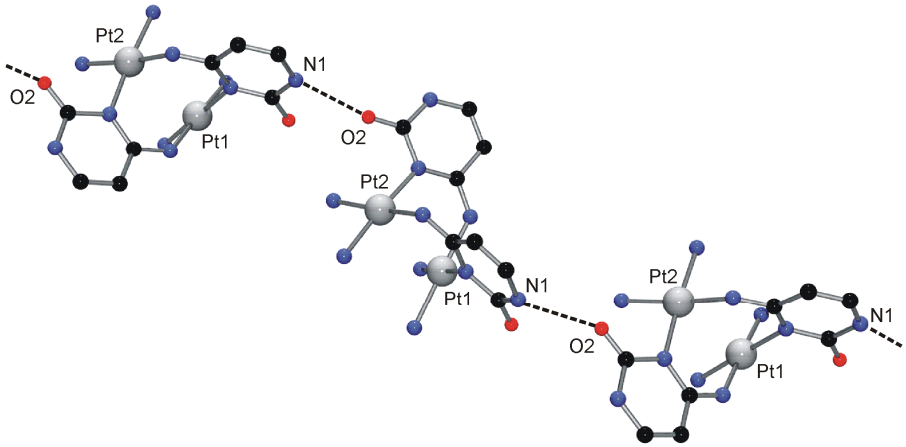

Figure 2.16: : Monodimensional hydrogen bonded strand of **8** involving N1(H) and O2 atoms

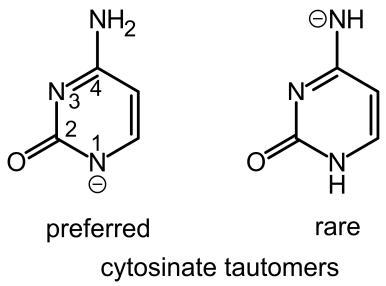

Scheme 2.7: Tautomeric forms for cytosinate. The preferred tautomer (left) is deprotonated at the N1 site. The rare tautomer is deprotonated at N4.

The cytosinate ligands seen in **8** represent rare tautomeric forms of the cytosine monoanion, which are stabilized by metal coordination through N3 and mono-deprotonated N4 (Scheme 2.7). Cytosine deprotonates at N1 position with a pK_a of 12.15 and the second deprotonation of exocyclic amino group occurs with a pK_a of ca. 17. So it is expected, that deprotonation of exocyclic amino group should not occur in aqueous medium. But the cytosinate monoanion present in **8** deprotonates at the N4 position, while carrying a proton at N1 position.

2.11. ^{1}H NMR spectrum and determination of pK_a value in 8

The ^{1}H NMR spectrum of **8** in D_2O (pD = 6.6) shows discrete doublets at 5.79 ppm and 6.82 ppm due to cytosine H5 and H6 resonances. The HC resonances of **8** are upfield shifted from those of **1**, differences being +0.26 ppm and +0.68 ppm. The dimer **8** is very stable in solution and there are no signs of complex decomposition within two days at room temperature in D_2O (pD = 2.1 with DCl). The pK_a value for deprotonation of N1-H in **8** was measured by pD dependent ^{1}H NMR spectroscopy. The cytosine-H5 is upfield shifted with increasing pD values, while cytosine-H6 undergoes a downfield shift (Figure 2.17). The pK_a values of **8** derived from H6 and H5 shifts, are 11.85 $\pm$ 0.02 and 11.99 $\pm$ 0.03 in D_2O, corresponding to a mean value of ca. 11.3 ± 0.09 in H_2O for deprotonation of the two cytosinate ligands in **8**.

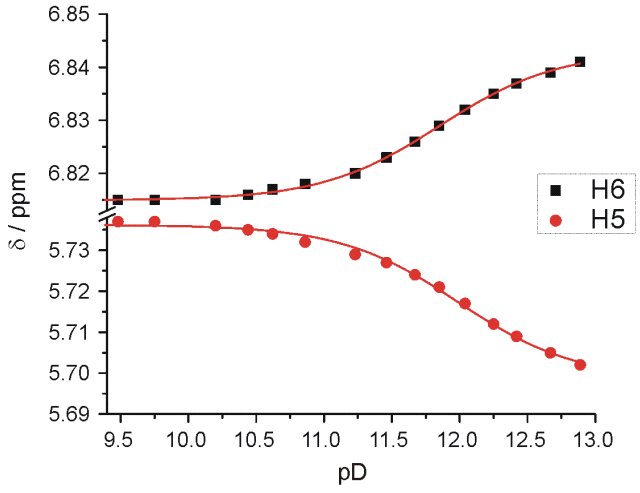

Figure 2.17: pD dependence of H6 and H5 protons in **8**.

2.12. "Directed" assembly of metallacalix[n]arenes with pyrimidine nucleobase ligands (cytosine) of low symmetry

In classical organic calix[n]arenes, methylene groups bridge *n* para-substituted phenols, yielding cyclic compounds.[32] Replacement of the CH_2 groups by numerous other groups or hetero atoms (e.g., O, NH, NR, S, etc) and of the phenols by other heterocyclic rings produces "heterocalix[n]aromatics".[33] Metallacalix[n]arenes are a class of discrete heterocalix[n]aromatics in which *n* heteroaromatic entities are bridged by *n* *cis*-square-planar metal units of type *cis*-a_2M^{II} (M = Pt or Pd; a = NH_3 or other monodentate ligand, a_2 = en, 2,2'-bpy) to produce cyclic structures.[34,35] Metallacalix[n]arenes can be obtained either in a spontaneous self-assembly process or in a stepwise fashion from preformed fragments. Depending on the symmetry of the bridging N-heterocyclic ligand, either *single species* or a *mixture of isomers* can be formed. Highly symmetrical (C_{2v}) heterocyclic ligands e.g. 2-aminopyrimidine, the deprotonated forms of 2-hydroxopyrimidine etc. (Scheme 2.8), in combination with square-planar metal entities *cis*-a_2M^{II}, can give rise to cyclic complex with a single connectivity pattern $[N,N\bullet]_n$. Depending on *n*, different conformers are possible. For example, for *n* = 4, the four conformations are cone, partial cone, 1,3-alternate, and 1,2-alternate (Scheme 2.9). However, low symmetrical pyrimidine ligands (C_s) are expected to produce a mixture of isomers as a result of random combinations of connectivities of the ditopic ligand, unless there is driving force such as specific molecular interactions (hydrogen bonding, steric repulsion etc.) which would lead to self-sorting. For each of these isomers, a large number of different conformers is possible. Recently Stang et al[36] and Schalley et al[37] discussed these possibilities with bidentate unsymmetrical bipyridine ligands where mixtures of isomers were formed. Similarly, with low-symmetrical pyrimidine ligands such as the mono or di- deprotonated

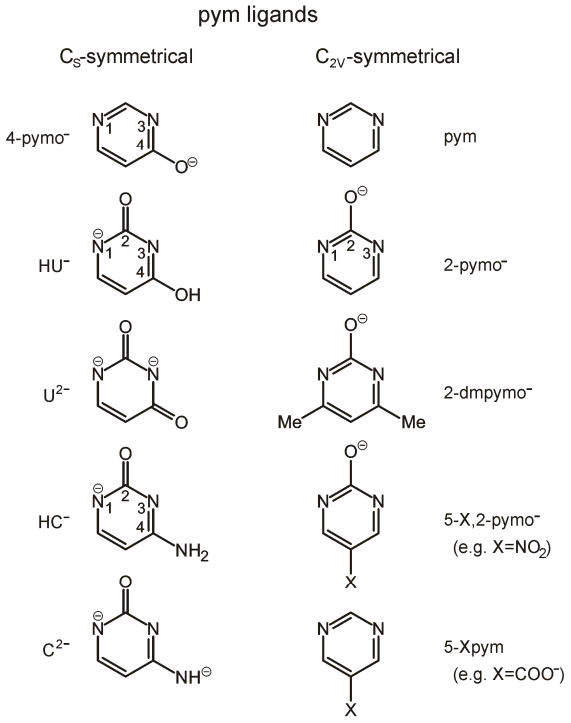

Scheme 2.8: C_s- and C_{2v}-symmetrical pyrimidine ligands.

forms of cytosine or uracil (point group C_s) and *cis*-a_2M^{II} forming cyclic tetramers, four types of cyclic isomers (I–IV) are feasible, which differ in the connectivities of N1 and N3 sites to the metal entities. For these four constitutional (linkage) isomers, numerous different conformational states are possible (Scheme 2.10). This situation becomes even more complicated, if different metals are employed simultaneously, e.g. Pt^{II} and Pd^{II}. It has, therefore, been a challenge to control the formation of a single, pure isomer of a self-assembled metallacycle that contains an unsymmetrical ligand as one of its building units. One feasible way towards this goal is to limit the number of reaction products by applying preassembled, kinetically inert corner fragments composed of metal and heterocyclic ligand. For example, the self-condensation of $[Pt(en)(HU\text{-}N1)(H_2O)]^+$ to the corresponding cyclic tetramer produces the isomer having exclusively the fully alternating N1,N3 • N1,N3 • N1,N3 • N1,N3 • connectivity (with • representing the metal entity).[34a,34b] Similarly, the bis(nucleobase) complex $[Pt(en)(HU\text{-}N1)(H_2C\text{-}N3)]^+$, upon reaction with (2,2'-bpy)Pd^{II} or (en)Pd^{II}, leads to the formation of a single linkage isomer.[35b] Here, in the current work, two types of kinetically inert preformed building blocks, namely *cis*-$[Pta_2(H_2C\text{-}N3)_2](NO_3)_2 \cdot xH_2O$ (a = NH_3, x = 2 (**1**); a_2 = en, x = 1 (**2**)) and *cis*-$Pt(NH_3)_2(HC\text{-}N1)_2 \cdot 3.25\ H_2O$ (**4**), have been applied and their reaction products with additional *cis*-a_2M^{II} entities will be discussed. As will be shown below, out of several possibilities, the favorable intramolecular hydrogen bonding and unfavorable steric interactions between exocyclic groups will lead to the formation of a single linkage isomer with a single conformational state.

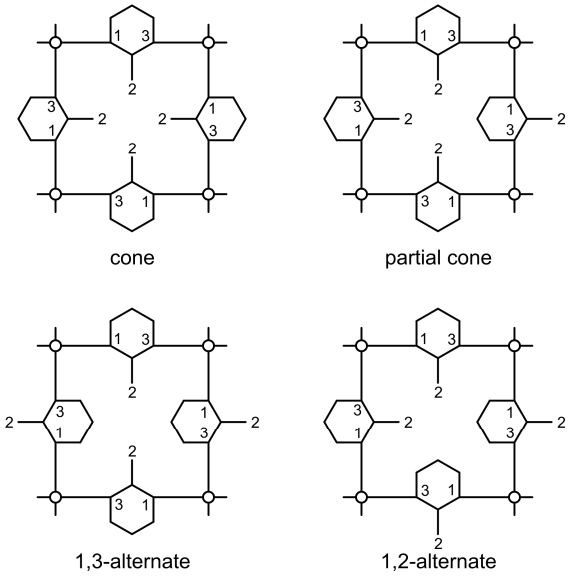

Scheme 2.9: Four possible rotamers of metallacalix[4]arene derived from highly symmetrical (C_{2v}) pym ligand.

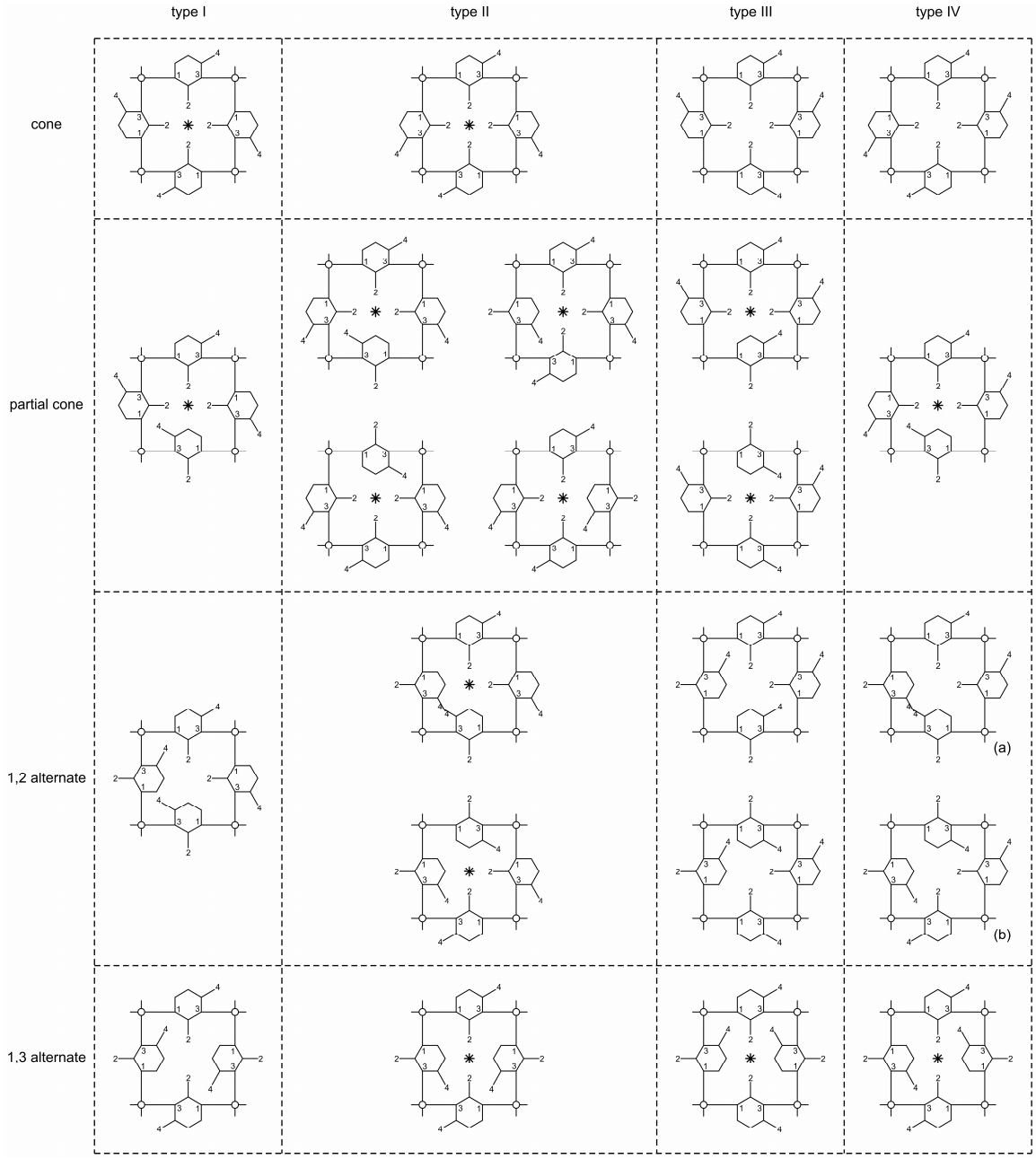

Scheme 2.10: Four different linkage isomers (types I - IV) of metallacalix[4]arenes containing C_s-symmetrical pym ligands with substituents at 2- and 4-positions (e.g. cytosine or uracil), and possible rotamer states of pym ligands. Stereoisomers with an asterisk are chiral.

2.13. Reaction of *cis*-$[Pt(NH_3)_2(HC\text{-}N1)_2]\cdot 3.25H_2O$ (4) with (2,2'-bpy)Pd^{II}

Reactions between **4** and $[Pd(2,2'\text{-bpy})(D_2O)_2]^{2+}$ were carried out in D_2O at different ratios (r = Pt:Pd) and the reactions were followed by ^1H NMR spectroscopy (Figure 2.18). There are some general points which should be noted: Some spectra display about four to five doublets for the H5 and H6 nucleobase resonances which clearly indicate the formation of multiple species during the course of reaction. When r is increased, e.g. to 3, the spectra become relatively simple and formation of one major species is observed.

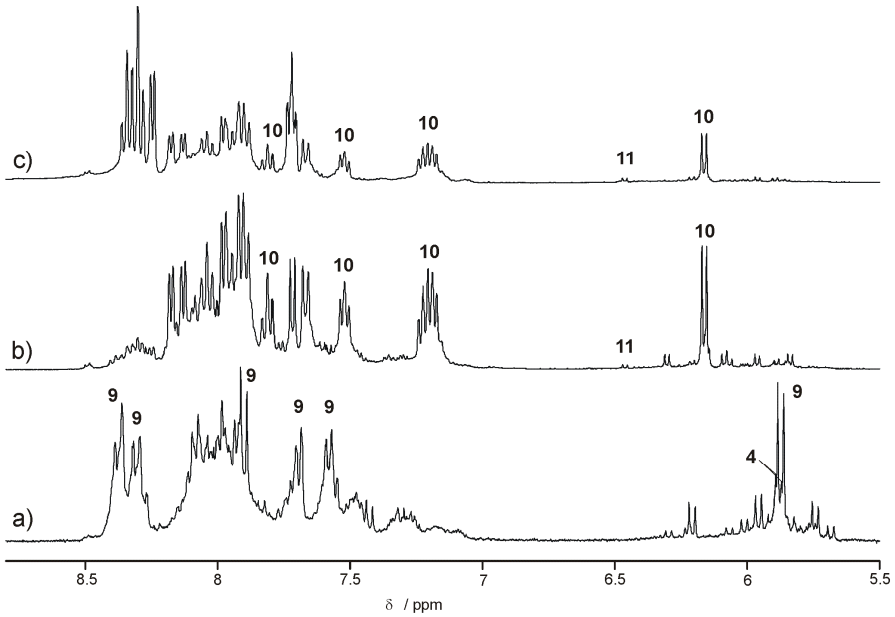

Figure 2.18: Low field sections of ^1H NMR spectra of a reaction mixtures of **4** with $[Pd(bpy)(D_2O)_2]^{2+}$ in D_2O (RT) at different ratios (r = Pt:Pd) after 24h: a) r = 1:1, pD 3.5; b) r = 1:2, pD 2.2; c) r = 1:3; pD 1.6.

2.14. Isolation of molecular box Pt_2Pd_2 (9)

Reaction of **4** with $[Pd(2,2'\text{-bpy})(H_2O)_2]^{2+}$ at 40 ℃ in water (r = 2:1 or r = 1:1) produces the cyclic tetranuclear complex *cis*-$[\{Pt(NH_3)_2(N1\text{-HC-}N3)_2Pd(2,2'\text{-bpy})\}_2](NO_3)_4\cdot 13H_2O$ (**9**). Slow evaporation of the reaction mixture (r = 2:1) at room temperature produces yellow crystals of **9**. Complex **9** crystallizes in the triclinic space group (P–1). The tetranuclear complex consists of four cytosinate ligands, two *cis*-$(NH_3)_2Pt^{II}$ entities and two (2,2'-bpy)Pd^{II} entities. A view of the tetranuclear complex is shown in Figure 2.19a. The cytosinate ligands (HC) are connected to Pt through their deprotonated N1 sites and Pd is bonded to N3 sites. The cytosinate ligands are oriented in *head-tail* arrangement. Ignoring the two different metal entities, the cyclic complex is of type IV (c.f. Scheme 2.10), hence

N1,N3•N3,N1•N1,N3•N3,N1• (with • representing the metal entity) and the four HC ligands in the complex adopt a 1,3-alternate conformation. The cation of **9** is chiral and both enantiomers are present in the crystals. Unlike in the starting complex **4**, intramolecular hydrogen bonding between exocyclic O2 and $N4H_2$ group of HC ligands at the two Pd centers in **9** is observed : N4bH···O2a, 2.883(11) Å; N4aH···O2b,2.993(11) Å; N4dH···O2c, 2.887(11) Å; N4cH···O2d, 2.858(11) Å. The four metal ions cross-linking N1

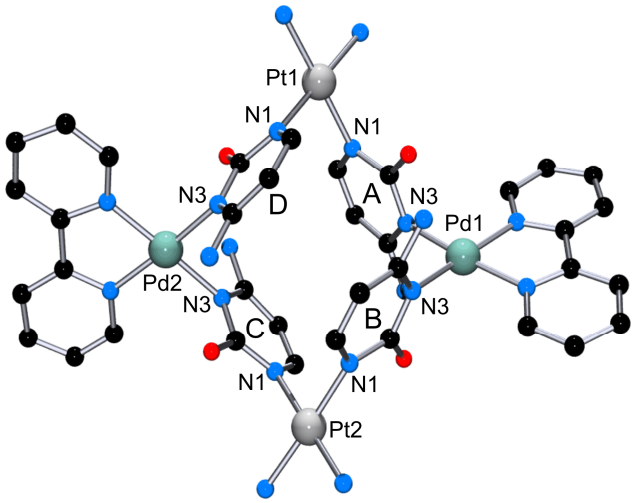

Figure 2.19a: Top view of cation of *cis*-[{Pt$(NH_3)_2$(*N1*-HC-*N3*)$_2$Pd(2,2'-bpy)}$_2$]$(NO_3)_4 \cdot 13H_2O$ (**9**). Nitrate anions and water molecules are removed for clarity.

and N3 sites of cytosinate ligands in complex **9** form a distorted square. The four metal ions are not coplanar and the distances from the best plane are 0.107 Å (average). Distances of metal ions at the sides of the square are Pt1-Pd1, 5.766 Å; Pd1-Pt2, 5.823 Å; Pt2-Pd2, 5.785 Å and Pd2-Pt1, 5.797 Å. The diagonal distances between Pt centers (Pt1-Pt2, 8.5708(7) Å) are longer than those involving Pd center (Pd1-Pd2, 7.7840(11) Å). The internal angle involving metal centers also deviate significantly from a perfect square: Pt1-Pd1-Pt2, 95.38°; Pd1-Pt2-Pd2, 84.22°; Pt2-Pd2-Pt1, 95.46° and Pd2-Pt1-Pd1, 84.62. The dihedral angles between the cytosine rings and the plane through Pt_2Pd_2 are 67.0° (HC_A), 66.4° (HC_B), 62.6° (HC_C) and 64.4° (HC_D). Dihedral angles between coordination planes of opposite metals are $Pt1N_4/Pt2N_4$, 87.1° and $Pd1N_4/Pd2N_4$, 88.4°, which shows that these planes are almost perpendicular to each other. Dihedral angles between square-planar coordination planes of the metals and the adjacent cytosine bases differ from ideal 90°, depending on the binding site ($Pt1N_4/HC_A$, 77.4°; $Pt1N_4/HC_D$, 74.6; $Pt2N_4/HC_B$, 74.6°; $Pt2N_4/HC_C$ 82.1°; $Pd1N_4/HC_A$, 83.2°; $Pd1N_4/HC_B$, 82.3; $Pd2N_4/HC_C$, 85.6°; $Pd2N_4/HC_D$ 88.0°). The opposite cytosine bases are inclined towards each other, which is reflected in their distances between different atoms of opposite pairs: C5A-C5C, 3.549 Å ; C2A-C2C,

5.785 Å; O2A-O2C, 7.035 Å and C5B-C5D, 3.555 Å; C2B-C2D, 5.849 Å; O2B-O2D, 6.937 Å. No π–π interactions between 2,2'-bpy ligands are present in the crystal packing.

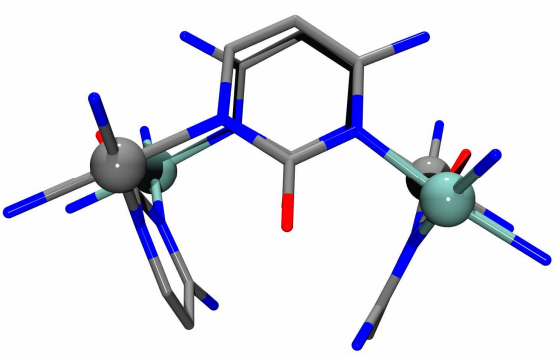

Figure 2.19b: Another view (side) of cation of **9**.

2.15. Isolation of Pt_2Pd_6 complex *cis*-[{$(NH_3)_2Pt$}$_2$(*N1*-C-*N3,O2,N4*)$_4${Pd(2,2'-bpy)}$_6$]$(NO_3)_8 \cdot 12H_2O$ (10)

Reaction of *cis*-$[Pt(NH_3)_2(HC\text{-}N1)_2]\cdot 3.25H_2O$ (**4**) with $[Pd(2,2'\text{-bpy})(H_2O)_2]^{2+}$ in r = 1:2 ratio in water produces the octanuclear complex **10**. Slow evaporation of an aqueous solution at room temperature yields crystals of reddish yellow color. Unfortunately, a complete structure determination was not possible because of poor quality crystal. A preliminary structure determination shows that it is an octanuclear complex (Figure 2.20) containing two *cis*-$(NH_3)_2Pt^{II}$, six (2,2'-bpy)Pd^{II} entities and 4 cytosinates (HC) . It can be considered as extended metallacalix[4]arene in which the exocyclic groups of connecting ligand are also utilized in metal coordination. The two *cis*-$(NH_3)Pt^{II}$ entities are connected to the deprotonated N1 sites of cytosine ligands and the two (2,2'-bpy)Pd^{II} are bonded to N3 positions to generate a Pt_2Pd_2 metallacalix[4]arene with $(N1,N3\bullet N3,N1\bullet)_2$ connectivity. The orientation of the cytosinate ligands is

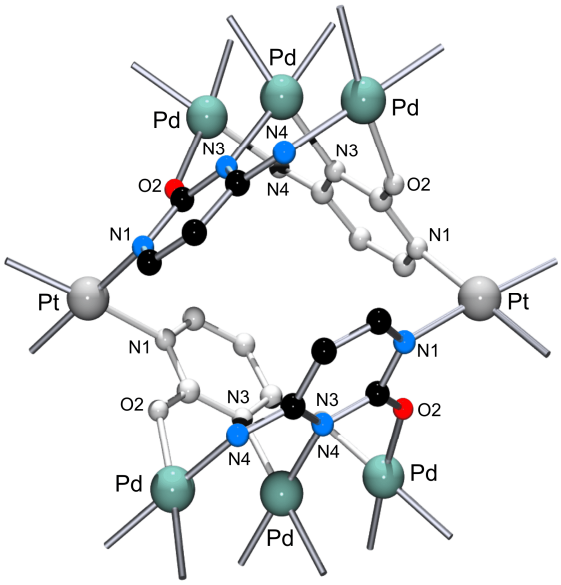

Figure 2.20: View of cation **10** (bpy attached to Pd atoms are omitted for clarity)

mutually *head-tail*. To this mixed metallacalix[4]arene scaffold, pairs of (2,2'-bpy)Pd^{II} units are added above and below the N3 bonded (2,2'-bpy)Pd^{II}, via deprotonated N4 positions and O2 sites of the cytosine bases. Consequently, the cytosine nucleobases in **10** are dianions (C^{2-}). The arrangement of stacks of three (2,2'-bpy)Pd^{II} units allows for extensive π–π stacking of the 2,2'-bpy rings, with Pd···Pd···Pd contacts of 2.796(3) – 2.815(3) Å between the three Pd ions.

2.16. ^{1}H NMR specrum of 10

The ^{1}H NMR spectrum of **10** in D_2O is shown in Figure 2.21. The integrated ratios of individual signals are consistent with the composition of **10**. The cytosine-H5 doublet is observed at 6.16 ppm (^3J = 7.03 Hz) and is well separated from all the other resonances. Three non-equivalent bpy–H5 doublets-of-doublets of equal intensities are expected,[38] which are indeed observed at 7.18, 7.22, and 7.55 ppm. The cytosine-H6 doublet can not be identified and is superimposed with other 2,2'-bpy resonances, which extend from 7.66 – 8.19 ppm. However, two well separated H6 doublets of 2,2'-bpy of equal intensities are observed at furthest low field at 8.13 and 8.17 ppm. The third one is buried under other 2,2'-bpy resonances.

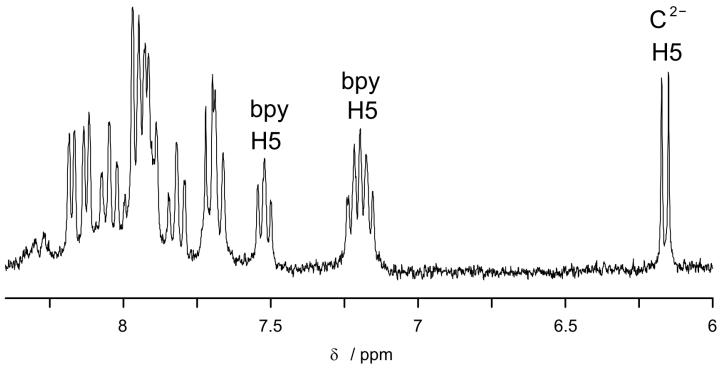

Figure 2.21: Low field section of ^{1}H NMR spectrum of **10** in D_2O (pD = 2.8).

When an excess NaCl is added to a solution of **10** in D_2O, formation of new sets of resonances due to an unknown species is observed. Rapid precipitation of yellow Pd(2,2'-bpy)Cl_2 is observed when the pD of a solution of **10** is lowered to 2.2 using DCl, and formation of **5** along with other unknown species is detected in the ^{1}H NMR spectra.

2.17. Displacement of N1 bonded *cis*-$(NH_3)_2Pt^{II}$ by (2,2'-bpy)Pd^{II}

When *cis*-$[Pt(NH_3)_2(HC\text{-}N1)_2]\cdot 3.25H_2O$ (**4**) is reacted with excess (3 or 4 equivalent) $[Pd(2,2'\text{-bpy})(H_2O)_2]^{2+}$ in water, a mixture of octanuclear metallacycles **10** and $[\{Pd(2,2'\text{-bpy})\}_8(C)_4](NO_3)_8\cdot 25H_2O$ (**11**) is obtained. Slow evaporation of an aqueous solution of reaction mixture produces red crystals of **11** along with a yellow precipitate **10**. The X-ray structural analysis shows that the complex **11** is octanuclear and contains eight (2,2'-bpy)Pd^{II} entities and four cytosine dianions (C^{2-}). Compound **11** was alternatively obtained in a self assembly reaction of (2,2'-bpy)Pd^{II} with cytosine (see Section 2.24 for details). It is surprising to see that the *cis*-$(NH_3)_2Pt^{II}$ entity has been completely replaced by (2,2'-bpy)Pd^{II} entities. In general, transmetallation reactions between Pd and Pt proceed in a way that the more labile Pd^{II} can be displaced by Pt^{II}. A possible reason of this unusual transmetallation reaction is that multifold binding of metal ions to the cytosine dianion – Pt at N1, Pd at N3, O2, N4 – weakens the individual coordination bonds sufficiently to permit metal substitution reactions, which under normal conditions would not take place. Hence, direct displacement of *cis*-$(NH_3)_2Pt^{II}$ in **4** by a (2,2'-bpy)Pd^{II} is unlikely to occur readily, but is apparently possible once several other sites in **4** are metalated as well. A view of cation of **11** is provided in Figure 2.22 (see Section 2.24 for details for structural details).

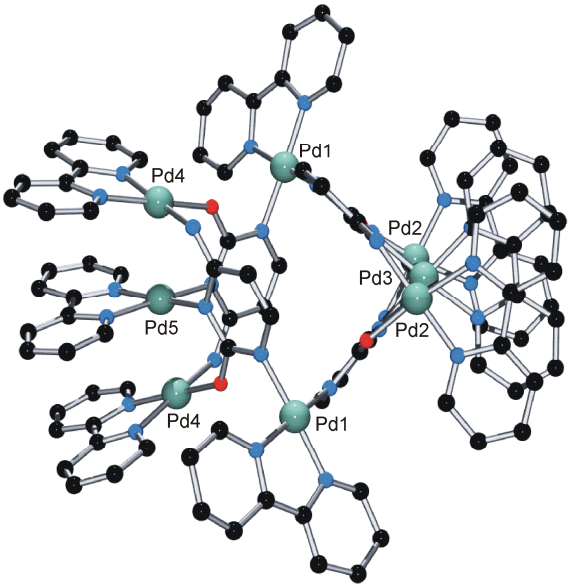

Figure 2.22: View of cation of octanuclear complex **11**.

2.18. Interchanging metals in metallacalix[4]arene

In addition to generating linkage isomers of the cytosine/cytosinate ligands, It is also possible to obtain metallacalix[4]arene with two different metal ions as the corner units and also with different am(m)ine ligands attached to the metal ions. Reaction of $[Pt(NH_3)_2(HC\text{-}N1)_2]$ (**4**) with (2,2'-bpy)Pd^{II} produces the cyclic tetramer **9** where *cis*-$(NH_3)_2Pt^{II}$ is coordinated to N1 sites of two cytosinates and (bpy)Pd^{II} bonded to two N3 sites. The isomer of **9**, with the two kinds of metal entities inverted (**12**) and an analogue of the latter (**13**) have been prepared and characterized (Scheme 2.11).

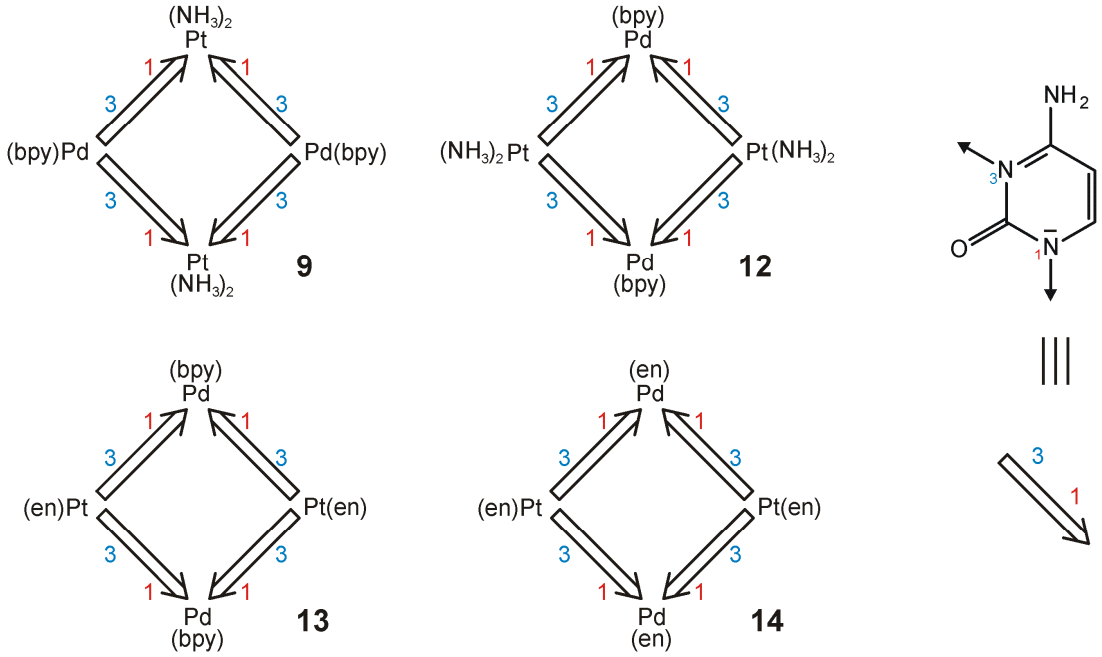

Scheme 2.11: Schematic views of cation **9**, **12**, **13** and **14**.

2.19. Crystal structures of 12 and 13

Reaction of *cis*-$[Pt(NH_3)_2(H_2C\text{-}N3)_2](NO_3)_2\cdot 2H_2O$ (**1**), $[Pt(en)(H_2C\text{-}N3)_2](NO_3)_2\cdot H_2O$ (**2**), respectively, with (2,2'-bpy)Pd^{II} in 1:1 ratio at high pH yields the molecular boxes *cis*-$[\{Pt(NH_3)_2(N3\text{-}HC\text{-}N1)_2Pd(2,2'\text{-}bpy)\}_2](NO_3)_4\cdot 9H_2O$ (**12**) and $[\{Pt(en)(N3\text{-}HC\text{-}N1)_2Pd(2,2'\text{-}bpy)\}_2](NO_3)_4\cdot 8.5H_2O$ (**13**). Views of cations of complexes **12** and **13** are shown in Figure 2.23. In both complexes, *cis*-$(NH_3)_2Pt^{II}$ entities are bonded to N3 sites while (2,2'-bpy)Pd^{II} are coordinated to deprotonated N1 sites of cytosinate ligands (HC). The ligands connectivity pattern in both complexes is of type IV in Scheme 2.10, viz. $(N1,N3\bullet N3,N1\bullet)_2$,

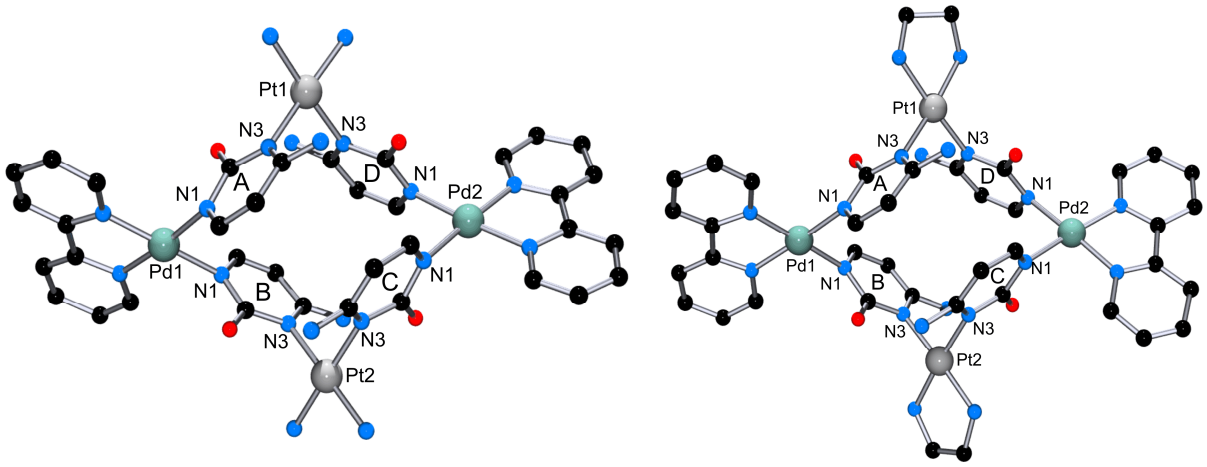

Figure 2.23: Top views of cations of **12** (left) and **13** (right).

(with • representing the metal entity). The cytosinate ligands adopt 1,3-alternate conformations in the solid state. Both cations are chiral and are present as a mixture of enantiomers. Like the starting compounds **1** and **2**, intermolecular hydrogen bonding between exocyclic O2 and N4H$_2$ groups at Pt centers are observed, namely: 3.213(9) Å, 2.852(8) Å, 3.033(9) Å, 2.922(9) Å in **12**, and 2.989(9) Å, 3.006(9) Å, 2.945(9) Å, 2.823(8) Å in **13**. The coordination planes of opposite metals are almost perpendicular to each other: 88.5° (**12**) and 87.1° (**13**) for Pt1N$_4$/Pt2N$_4$; and 80.1° (**12**) and 89.2° (**13**) for Pd1N$_4$/Pd2N$_4$. The four metal centers forming the Pt$_2$Pd$_2$ box are not in the same plane. Distances of the metal centers from the best plane are 0.133 – 0.136 Å in **12** and 0.060 – 0.062 Å in **13**. The metal-metal distances along the sides of the box range from 5.768 – 5.830 Å (**12**) and 5.758 – 5.854 Å (**13**). The diagonal distances across Pd (8.703 Å in **12**, 8.753 Å in **13**) are significantly longer than the distances across Pt centers (7.625 Å in **12**, 7.645 Å in **13**). Consequently the internal bond angle at the Pt center (97.88° and 96.96° in **12**; 98.34° and 97.07° in **13**) within the Pt$_2$Pd$_2$ box is larger than for the Pd center (82.15° and 75.32° in **12**; 81.91° and 82.58° in **13**). The nucleobases are inclined towards each other, with selected distances of C5a-C5c, 3.356 Å (**12**), 3.456 (**13**); O2a-O2c, 6.883 Å (**12**), 6.740 (**13**), and C5b-C5d, 3.632 Å (**12**), 3.864 Å (**13**); O2b-O2d, 7.268 Å (**12**), 6.989 Å (**13**). No π–π stacking interactions between 2,2'-bpy ligands are observed in the crystal packing.

2.20. Reaction of $[Pt(en)(H_2C\text{-}N3)_2](NO_3)_2\cdot H_2O$ (2) with $(en)Pd^{II}$

The ^1H NMR spectrum of a mixture of **2** and $[Pd(en)(D_2O)_2](NO_3)_2$ (r = 1:1) immediately after mixing at room temperature indicates the formation of two different species in solution, **14** and **15** (Figure 2.24). X-ray crystallography showed these two compounds to be cyclic ones. The resonances in ^1H spectrum are assigned from a comparison with the spectra of the isolated complexes (see below).

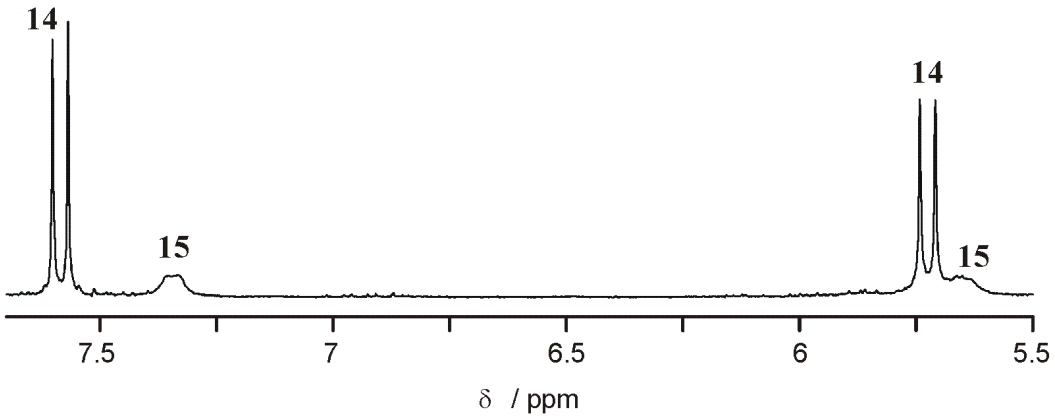

Figure 2.24: ^1H NMR spectrum of a mixture of $[Pt(en)(H_2C\text{-}N3)_2](NO_3)_2\cdot H_2O$ (**2**) and $[Pd(en)(D_2O)_2](NO_3)_2$ in D_2O, pD 7.5, RT.

2.21. Metallacalix[n]arenes with n = 4 and n = 6

Reaction of $[Pt(en)(H_2C\text{-}N3)_2](NO_3)_2\cdot H_2O$ (**2**) with $(en)Pd^{II}$ in 1:1 ratio at alkaline pH produces a mixture of a cyclic tetranuclear complex, $[\{Pt(en)(N3\text{-}HC\text{-}N1)_2Pd(en)\}_2](NO_3)_4\cdot 9.5H_2O$ (**14**), and of a cyclic hexanuclear complex, $[\{Pt(en)(N3\text{-}HC\text{-}N1)_2Pd(en)\}_3](NO_3)_6\cdot 18H_2O$ (**15**). X-ray quality crystals were obtained by slow evaporation of an aqueous solution of the reaction mixture at room temperature. The colorless, needle shaped crystals proved to be the metallacalix[4]arene **14**, whereas the colorless block-shaped crystals were found to be the metallacalix[6]arene **15**. Both compounds crystallize in the triclinic space group (P-1). In both compounds, Pt's remain bonded via N3 sites and Pd ions are connected to deprotonated N1 sites. The nucleobases are arranged in *head-tail* fashion with exocyclic O2 and $N4H_2$ sites of cytosinates at the two Pt centers pointing towards opposite directions. The four cytosinate ligands adopt 1,3-alternate conformations in both complexes. Consequently, the cations of **14** and **15** are chiral and both enantiomers are present in unit cells. The intramolecular hydrogen bonding between O2 and $N4H_2$ sites of cytosinate ligands bonded to Pt is maintained like in their parent

complex **2**. These distances are 3.031(9) Å, 2.942(8) Å, 2.892(8) Å and 2.909(8) Å in **14**; 2.87(2) Å, 3.10(3) Å, 3.06(3) Å, 3.06(2) Å, 2.99(2) Å, 2.89(2) Å in **15**.

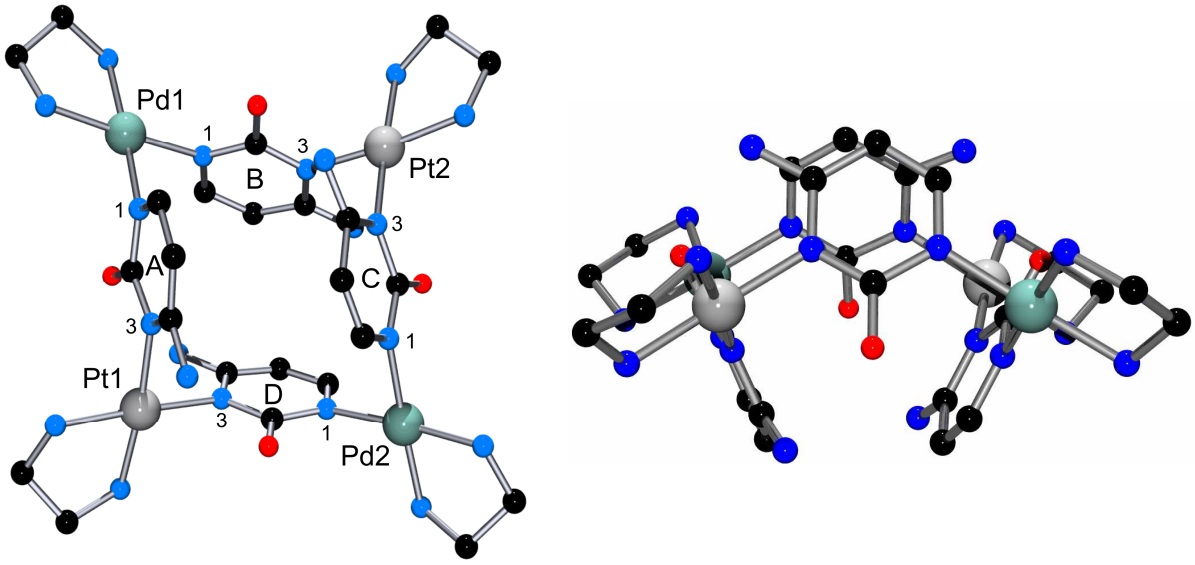

Figure 2.25: Top view (left) and side view (right) of cation of tetranuclear complex **14**.

Two different views of the tetranuclear cation **14** are shown in Figure 2.25. The ligand connectivity pattern in complex **14** is of type IV, viz. (N1,N3•N3,N1•)$_2$ (with • representing the metal entity) (see Scheme 2.10). The four metals forming the Pt_2Pd_2 core in cation **14** are found to lie roughly on the vertices of a diamond. The four metals are approximately in the same plane, with minor deviations of ca. 0.036 Å from the best plane. The distances (sides) between metal centers are Pt1-Pd1, 5.8017(7) Å, Pt1-Pd2, 5.7834(8) Å, Pt2-Pd1, 5.8014(8) Å, Pt2-Pd2, 5.7589(8) Å. The lengths of diagonal intermetallic distances are Pt1-Pt2, 8.6444(9) Å and Pd1-Pd2, 7.6928(5) Å. Angles within the Pt_2Pd_2 core deviate significantly from ideal right angles: Pd2-Pt1-Pd1, 96.519(11)°; Pt1-Pd1-Pt2, 83.058(10)°; Pd1-Pt2-Pd2, 96.794(11)°; Pt2-Pd2-Pt1, 83.593(10)°. Square-planar geometries around Pt and Pd are observed in all cases. Like in the tetranuclear complexes **9**, **12** and **13**, the opposite cytosine rings are inclined towards each other. The dihedral angles between cytosine rings and the planes through Pt_2Pd_2 are 65.2°(HC_A), 62.9°(HC_B), 62.7 (HC_C) and 67.0°(HC_D).

A view of the hexanuclear cation **15** is shown in Figure 2.26. All six cytosinate (HC) rings adopt 1,3-alternate conformations and, because of the resulting chirality, cations form a racemic mixture. The six metal ions (Pt1, Pt2, Pt3, Pd1, Pd2, Pd3) which form a hexagon within the metallacalix[6]arene **15**, are almost coplanar, with deviations of 0.07 –

0.34 Å from the best plane. Distances (side) between metal centers are: Pt1-Pd1, 5.8749(17) Å; Pd1-Pt2, 5.8543(18) Å; Pt2-Pd2, 5.7613(19) Å; Pd2-Pt3, 5.8602(18) Å; Pt3-Pd3, 5.8188(17) Å; Pd3-Pt1, 5.8257(17) Å. The distances between metal centers in the

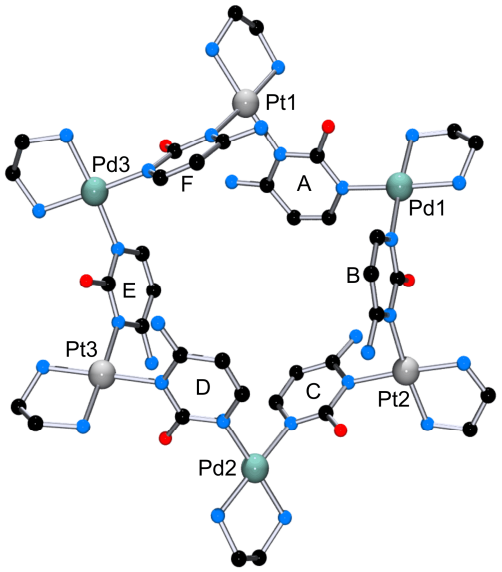

Figure 2.26: Top view of cation in hexanuclear complex **15**.

diagonals of the hexagon are: Pt1-Pd2, 11.7593(18) Å; Pt2-Pd3, 11.5389(17) Å; Pt3-Pd1, 11.6053(18) Å. The dihedral angles between cytosine rings and the plane through Pt_3Pd_3 are 53.5° (HC_A), 45.1° (HC_B), 54.0° (HC_C), 68.6° (HC_D), 48.7° (HC_E) and 63.7° (HC_F). All cytosine rings are significantly inclined towards the center of the hexagon defined by the metals. Opposite cytosine rings (A-D, B-E, C-F) are roughly parallel, with minor deviations (Figure 2.27). One nitrate anion is located in the cavity of the hexanuclear cation **15** (Figure 2.28), and it is almost perpendicular to the Pt_3Pd_3 plane (83.3°). This nitrate anion is sandwiched between cytosine rings B and E.

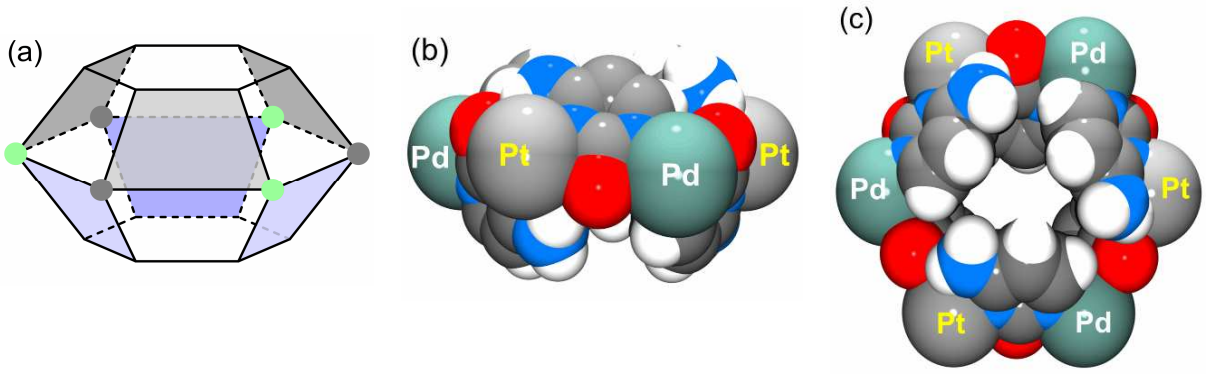

Figure 2.27: Schematic (a) and space filling (b, c) representations of cation **15**.

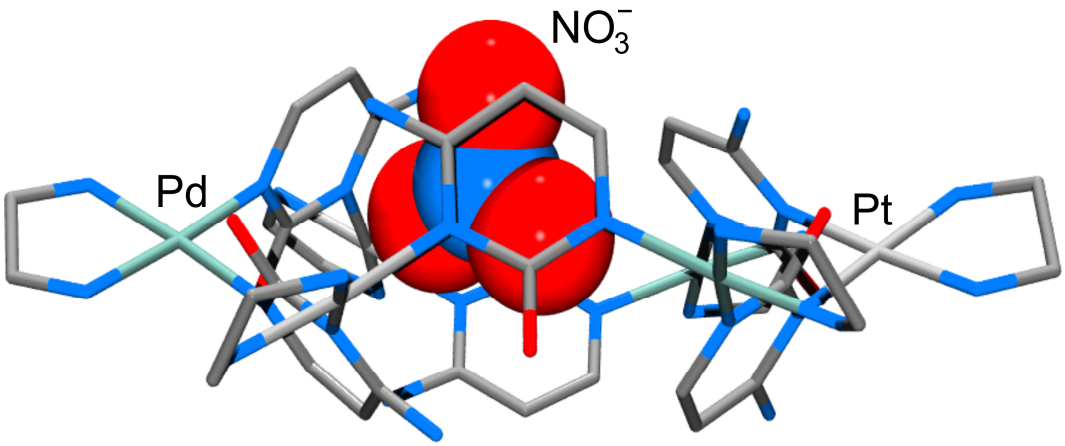

Figure 2.28: A view of cation of **15** with one of its counter anion NO_3^- trapped inside the cavity.

2.22. Homochiral self-sorting in tetranuclear and hexanuclear complex

The tetranuclear complexes **9**, **12**, **13** and **14** with their type IV connectivity pattern could exist in five different rotamer states (right column in Scheme 2.10). However, both the X-ray analysis of single crystals and the ^{1}H NMR spectra of the isolated complexes (see below) suggest the presence of a single rotamer (1,3-alternate) only in the solid state as well as in solution. This can possibly be explained by differential stabilities of individual rotamer species due to the presence of favorable hydrogen bonding and unfavorable steric repulsion between exocyclic groups of cytosinate ligands. The cone conformation and one of the two possible 1,2-alternate conformations (termed (a) in Scheme 2.10) do not have any possibility of intramolecular hydrogen bonding between exocyclic groups of the connecting ligands. The partial cone conformer can have two intramolecular hydrogen bonds. Finally, both the second 1,2-alternate rotamer (termed (b) in Scheme 2.10) and the 1,3-alternate rotamer allow formation of four intramolecular hydrogen bonds. This may suggest comparable stabilities of the two rotamers. However, a closer look reveals that in the 1,2-alternate rotamer (b), the cytosine-H6 protons of the *head-head* oriented Pd(HC-*N1*)$_2$ entities point toward each other, leading to repulsion (Scheme 2.12). Any attempt to relieve this repulsion by increasing the C6···C6 distance automatically increases the repulsion between the O2 groups. In contrast, the mutual *head-tail* arrangement of all four cytosine bases in the 1,3-alternate rotamer structure avoids this problem fully. It thus appears that the preferential formation of the 1,3-alternate structure is a consequence of both favorable hydrogen bonding formation (here: of four H bonds) and the absence of unfavorable interactions.

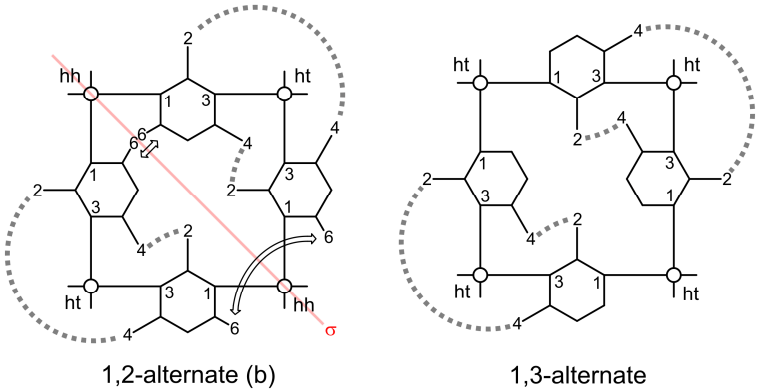

Scheme 2.12: Schematic views of two rotamers forming four intramolecular hydrogen bonds between exocyclic groups. (- - -) and ⇔ represent H-bonds and steric repulsions, respectively.

In the 1,3-alternate rotamer of the tetranuclear complex, the preformed building blocks *cis*-Pt(a)$_2$(HC-*N1*)$_2$ or *cis*-Pt(a)$_2$(HC-*N3*)$_2$ have identical chiralities, whereas in the 1,2-alternate rotamer (b) discussed here, these two units are of opposite chirality. Consequently, the 1,2-alternate rotamer (b) is to be considered a *meso* form. Exclusive formation of the 1,3-alternate rotamer implies that there is chiral self-sorting leading to the formation of the tetranuclear complex. The situation is similar with **15**: Out of the 10 possible rotamers of **15** with this connectivity pattern, only a single one crystallizes.

2.23. Comparison of ^{1}H NMR spectra of 9, 12, 13 and 14

The ^{1}H NMR spectra of complexes **9**, **12**, and **13** are given in Figure 2.29. ^{1}H NMR chemical shifts of all non exchangeable protons with coupling constant are provided in Table 2.7. The simplicity of the spectra suggests that in all cases a single rotamer exists in solution. The spectra of **12** and **13** are very similar, as the only difference is the replacement of two NH_3 ligands at each Pt (**12**) by an en ligand (**13**). The chemical shifts of cytosinate (HC) protons show a drastic change when (2,2'-bpy)Pd^{II} (in **12** and **13**) entities are replaced by (en)Pd^{II} entities (in **14**). The HC-H6 and HC-H5 resonances of **12** and **13** are downfield shifted (0.27 and 0.23 ppm, respectively), as compared to complex **14**. This appears to be a consequence of the acidifying and electron-withdrawing properties of the bpy ligand. The interchange of *cis*-(NH$_3$)$_2$Pt^{II} and (2,2'-bpy)Pd^{II} (compounds **9** and **12**) has a small effect on the HC resonances only (0.05 – 0.06 ppm). However, the H4 proton of 2,2'-bpy shows a major change in chemical shifts in **9** and **12**. The H4 doublet is observed at 7.70 ppm in **5**, yet at 8.10 ppm in **12**. The other bpy resonances are almost identical. As the H4 protons of the 2,2'-bpy ligand in both

compounds are pointing outside, hence are not affected by any intramolecular interactions with other ligands. These differences may be caused by differences in donor strengths (N3 of HC in **9**, N1 of HC in **12**) and/or differences in secondary interactions of Pd with the exocyclic groups (O2, $N4H_2$) of the HC ligands.

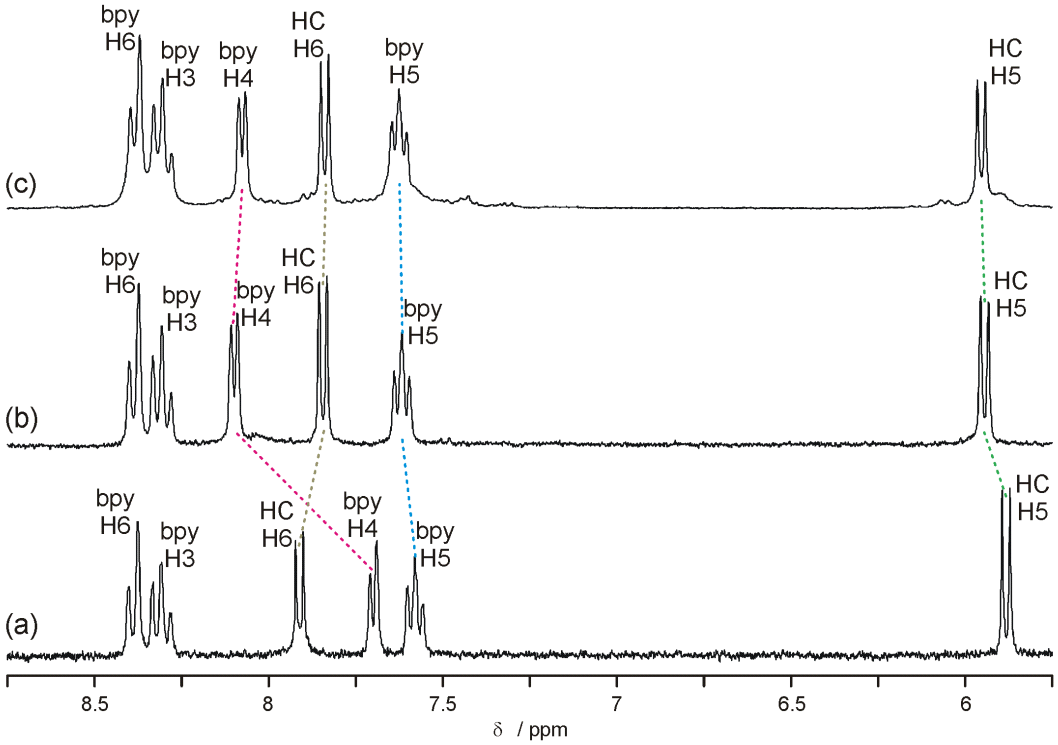

Figure 2.29: Low field section of ^{1}H NMR spectra of (a) *cis*-[{Pt(NH_3)$_2$(*N1*-HC-*N3*)$_2$Pd(2,2'-bpy)}$_2$](NO_3)$_4$·13H_2O (**9**); (b) *cis*-[{Pt(NH_3)$_2$(*N3*-CH-*N1*)$_2$Pd(2,2'-bpy)}$_2$](NO_3)$_4$·9H_2O (**12**) and (c) [{Pt(en)(*N3*-CH-*N1*)$_2$Pd(2,2'-bpy)}$_2$](NO_3)$_4$·8.5H_2O (**13**) in D_2O.

Table 2.7: ^{1}H NMR chemical shifts (δ ppm, D_2O) of different protons in cyclic compounds **9**, **12, 13** and **14**.

Compounds	pD	H6 / ppm (^3J)	H5 / ppm	Selected other resonances / ppm
9	7.1	7.91 (6.7 Hz)	5.89	7.58, 7.70, 8.31, 8.39 (bpy)
12	7.3	7.86 (6.7 Hz)	5.95	7.62, 8.10, 8.31, 8.39 (bpy)
13	7.8	7.86 (6.8 Hz)	5.96	7.63, 8.07, 8.31, 8.38 (bpy) 2.70 (en)
14	7.2	7.59 (6.6 Hz)	5.73	2.77 (en)

2.24. Decoration of exocyclic sites of metallacalix[4]arene with additional metal ions

Metal complexes of pyrimidine nucleobases have a strong propensity to coordinate additional transitional metal ions via their exocyclic groups (N4 and O2 in case of cytosine). For example, a series of multinuclear derivatives were prepared by utilizing exocyclic O2 and O4 sites of uracil anions in the cyclic tetranuclear complex [Pt(en)(HU-*N1*,*N3*)]$_4$(NO$_3$)$_4$.[16] However, reaction of cytosine (H$_2$C) with two equivalent [Pd(2,2'-bpy)(H$_2$O)$_2$]$^{2+}$ in water, in a self assembly process, produces a mixture of the octanuclear complex **11** and its isomeric complex **16**. The octanuclear complex [{Pd(2,2'-bpy)}$_8$(C)$_4$](NO$_3$)$_8$·25H$_2$O (**11**), which was also obtained in a transmetallation reaction from *cis*-[Pt(NH$_3$)$_2$(CH-*N1*)$_2$]·3.25H$_2$O (**4**), has been described above (see Section 2.17). Both isomeric complexes contain eight (bpy)Pd^{II} units and four dianionic cytosine ligands (C^{2-}). The octanuclear complex **16** cocrystallizes with half a molecule of Pd(2,2'-bpy)(NO$_3$)$_2$, hence as [{Pd(2,2'-bpy)}$_8$(C)$_4$]$_2$(NO$_3$)$_{16}$·Pd(2,2'-bpy)(NO$_3$)$_2$·60H$_2$O. These two isomeric

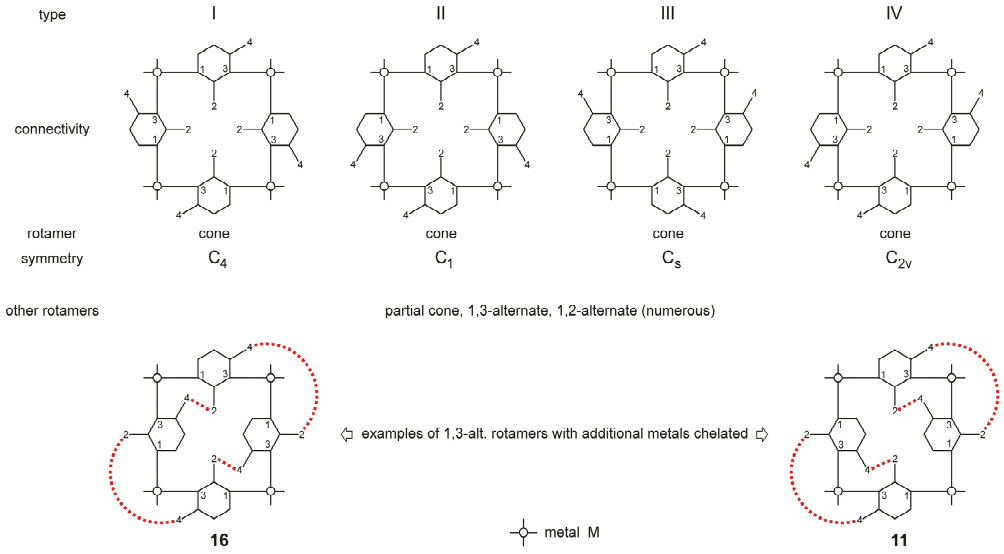

Scheme 2.13: Four principle linkage isomers of metallacalix[4]arenes I - IV derived from C$_s$-symmetrical pyrimidine ligands with cone forms (top) and two 1,3-alternate forms (of I and IV, bottom) show.

complexes can be considered as extended metallacalix[4]arenes in which exocyclic (N4 and O2) groups of cytosine ligand (C^{2-}) have been utilized for metal coordination. Four (2,2'-bpy)Pd^{II} entities coordinate to the endocyclic (N1, N3) sites of the cytosinate rings to give the basic metallacalix[4]arene structures with different connectivity patterns (type I in **16** and type IV in **11**; see Scheme 2.10 and Scheme 2.13). To this platform four additional (2,2'-bpy)Pd^{II} entities are added via the exocyclic groups of the cytosine ligands. The

difference in topology of the two cations is a result of the differences in mutual spatial dispositions of the exocyclic groups O2 and N4 of the cytosine rings, to which the four other (bpy)Pd^{II} entities are bonded (Scheme 2.13, lower part). In both complexes, cytosine rings are mutually *head-tail* and adopt the 1,3-alternate conformation.

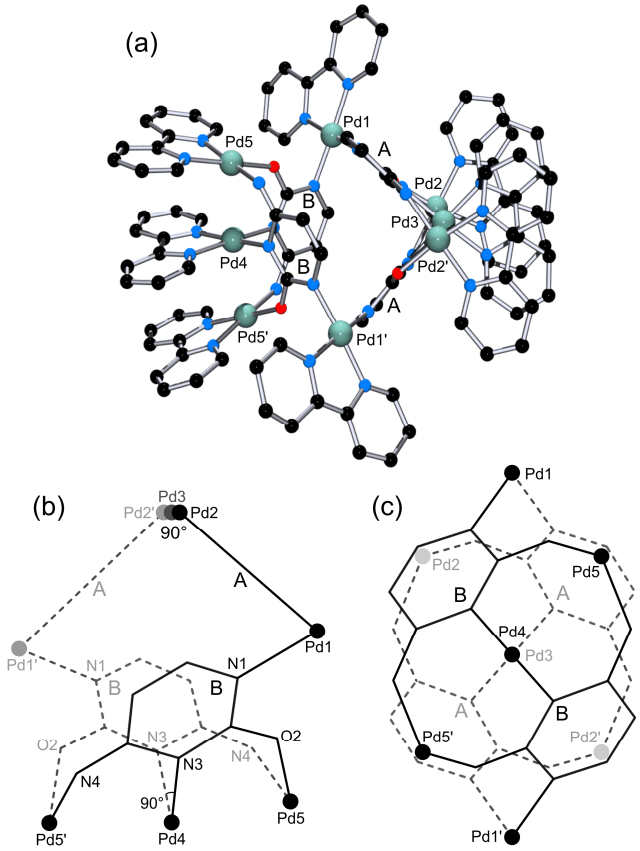

Figure 2.30: Full (a) and partial views (b, c) of cation **11**.

A view of cation **11** is shown in Figure 2.30. The basic metalla calix[4]arene in cation **11** has the (N1,N3•N3,N1•)$_2$ connectivity pattern (type IV) and the four exocyclic groups of two adjacent cytosine rings are in favorable orientations to bind *two* (bpy)Pd^{II} residues, thereby producing two stacks of Pd_3 units. The Pd···Pd distances of 2.8007(12) (Pd2···Pd3) and 2.8164(7) (Pd4···Pd5) Å in Pd_3 stacked entities are closely similar to those seen in a trinuclear PdPtPd compound with 1-methylcytosinato ligands.[39] Salient structural features of cation **11** are as follows: Pd1···Pd2, 4.8803(9) Å; Pd1···Pd5 4.7657(11) Å; Pd2-Pd3-Pd2, 170.08(4)°; Pd5-Pd4-Pd5, 171.15(4)°; Pd5-Pd1-Pd2, 124.57(2)°. The cation of **11** is chiral and both enantiomers are present in equal quantities. The coordination planes of opposite metals coordinated to endocyclic N1 and N3 sites of cytosine ring, are almost perpendicular to each other and the dihedral angles are 89.6° ($Pd1N_4$/$Pd1'N_4$) and 83.0° ($Pd3N_4$/$Pd4N_4$). Cytosine bases coordinated to Pd3 (A) and Pd4 (B) through N3 sites form almost perpendicular dihedral angles: 90.0° and 82.3°, respectively. Cytosine bases (A, B) bonded to Pd1 through N1 form an angle of 74.5°.

The octanuclear complex **16** crystallizes in the triclinic (P-1) space group. Figure 2.31 shows a view of cation **16**. The basic metallacalix[4]arene has a fully alternating (N1•N3)$_4$ connectivity (type I) pattern and exocyclic groups of C^{2-} ligands are oriented in such a way that only a single additional metal (bpy)Pd^{II} can be accommodated above or below the Pd atoms of the central metallacycle in a chelating fashion. The cation of **16** is analogous to

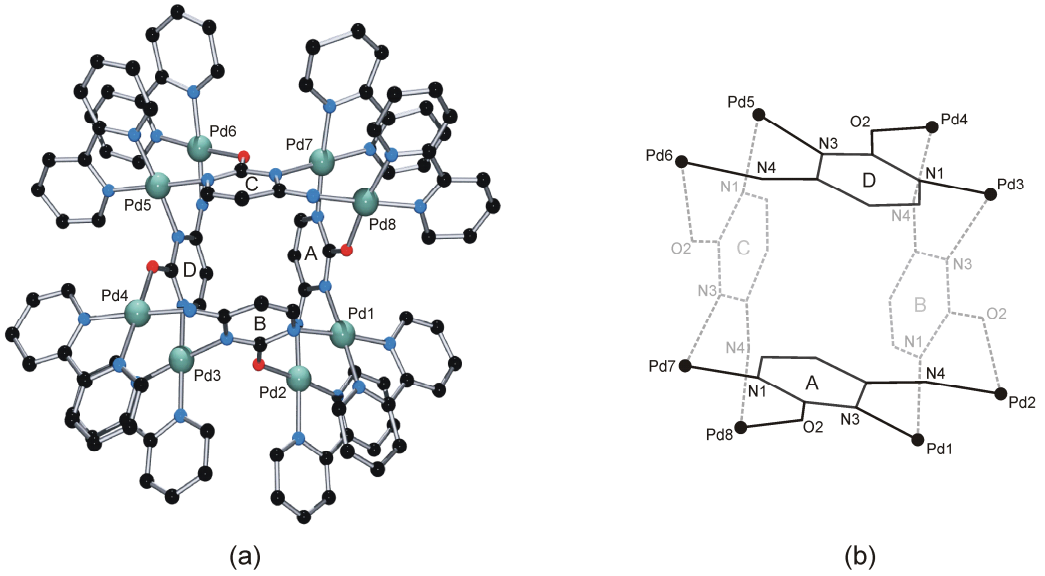

Figure 2.31: Top view (a) and schematic view (b) of cation **16**.

that seen in Pt_8 or mixed Pt_4M_4 complexes containing four uracil anions,[16] or in a mixed Pt_2Pd_6 cycle with alternating uracil and cytosine rings[35b] and a type I connectivity pattern. Unlike **11**, the cations of **16** are not chiral. Distances between pairs of Pd atoms are 2.8676(16) Å (Pd1···Pd2), 2.8329(15) Å (Pd3···Pd4),2.8346(17) Å (Pd5···Pd6), 2.8684(18) Å (Pd7···Pd8), 2.8361(15) Å (Pd9···Pd10), 2.8502(17) Å (Pd11···Pd12), 2.8514(16) Å (Pd13···Pd14), 2.8537(15) Å (Pd15···Pd16). The dihedral angles between planes of the cytosine ring are as follows: 79.0° (HC_A/HC_B), 76.0° (HC_B/HC_D), 79.1° (HC_D/HC_C) and 81.1° (HC_C/HC_A).

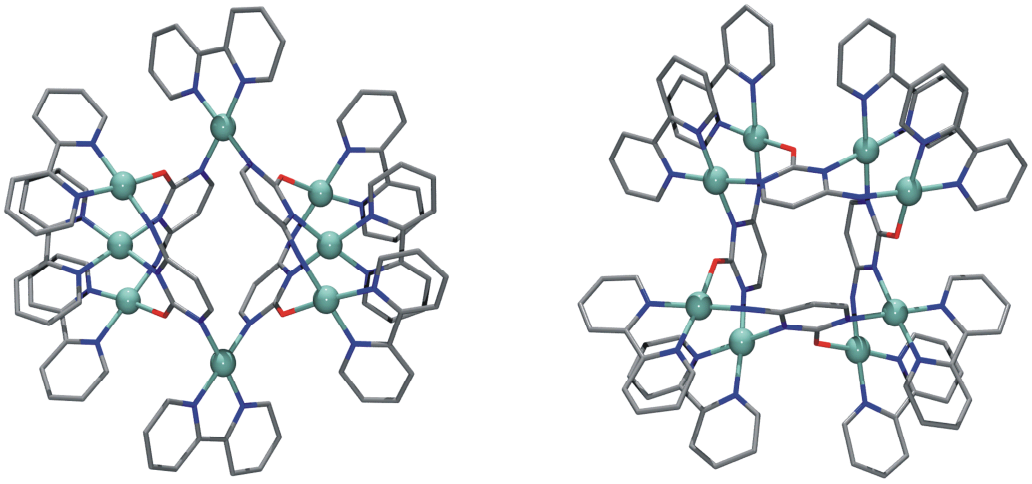

Figure 2.32: Comparison of cations **11** and **16**.

The cocrystallizing $Pd(bpy)(NO_3)_2$ connects two cations of **16** in a way as to produce an array of five Pd atoms (Figure 2.33). Distances between the central Pd (of $Pd(bpy)(NO_3)_2$) with the Pd atoms of the coordinated $(bpy)Pd^{II}$ units are longer (Pd4···Pd17, 3.409 Å; Pd16···Pd17, 4.669 Å) than between Pd atoms included in the cations of **16** (Pd3···Pd4, 2.8329(15) Å and Pd15···Pd16 2.8537(15) Å). In contrast to the difference between Pd-distances involving Pd17 (Δd = 1.26 Å), π–π stacking contacts between bpy rings are similar, however: Pd3-Pd4, 3.5 Å; Pd4-Pd17, 3.4 Å; Pd17-Pd16, 3.4 Å; Pd16-Pd17, 3.5 Å.

The four metal ions coordinated to the endocyclic N1, N3 sites of cytosine bases in **11** and **16**, which form the basic calix[4]arene moiety, lie perfectly in the same plane. The sides of the box range from 5.780 – 5.867 Å (**11**) and 5.754 – 5.875 Å (**16**). The diagonal distances are 8.441 Å (Pd1), 8.024 (Pd3-Pd4) Å in **11** and 8.198 Å (Pd1-Pd5), 8.242 Å (Pd3-Pd7) in **16**.

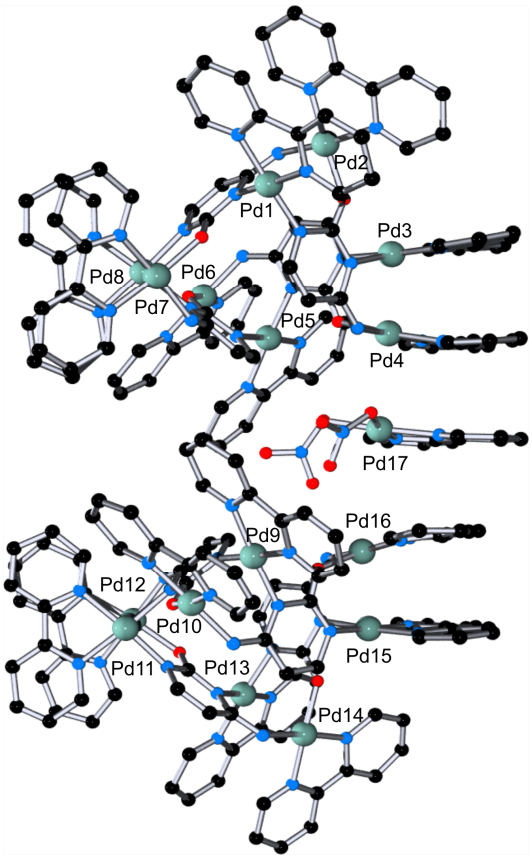

Figure 2.33: Section of crystal lattice of **16** with two octanuclear cations interacting with the extra $Pd(bpy)(NO_3)_2$.

2.25. ^{1}H NMR spectra of 11 and 16

The ^{1}H NMR spectra of **11** and **16** in D_2O are given in Figure 2.34. In both compounds, the cytosine–H5 doublets (**11**: 6.45 ppm; **16**: 6.46 ppm; ^3J = 7.02 Hz) occur furthest upfield and are well separated from all other resonances. The integrated intensities of all signals are consistent with the compostions of **11** and **16**. In the spectrum of **11** three doublets-of-doublets of equal intensities and the same intensity as cytosine-H5 are observed. The chemical shifts of these resonances (6.95, 7.18, 7.26 ppm) are characteristic of bpy-H5 signals of stacked (2,2'-bpy)Pd^{II} units.[38] They are assigned to the 12 bpy-H5 protons of the two Pd_3 stacks with three sets of non-equivalent bpy-H5 protons (of 2,2'-bpy rings with O2 and N4 donor sites of Pd, and bpy–H5 rings with two N3 donor sites of Pd). The doublet-of-doublet due to the four bpy-H5 resonances with Pd(C-*N1*)$_2$ coordination geometries is expected to be at lower field[38] and is superimposed with the other 2,2'-bpy resonances (as well as H6 of C^{2-}), which extend from 7.73 – 8.59 ppm. For **16** with its four Pd_2 stacks, likewise four bpy-H5 doublets-of-doublets are expected, two for each (2,2'-bpy)Pd^{II} entity. Three of these are observed (6.88, 7.27, 7.33 ppm) while the fourth one is buried under the other 2,2'-bpy resonances.

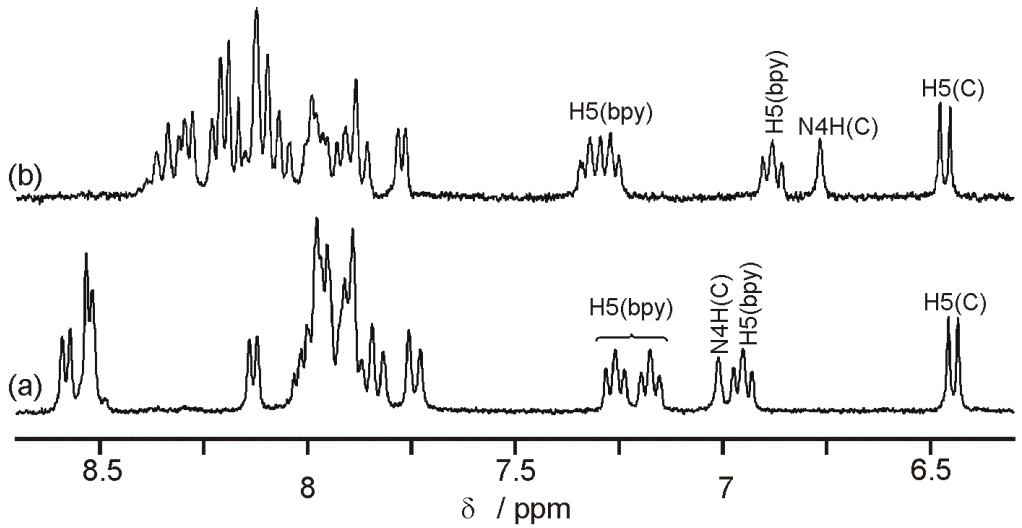

Figure 2.34: Low field section of ^{1}H NMR spectra of (a) **11** and (b) **16** in D_2O.

A noticeable detail of the spectra of **11** and **16** in D_2O is that in both cases the cytosine-N4H proton can be observed as a singlet at 7.01 and 6.77 ppm, respectively, in D_2O and that H→D exchange takes place only slowly. It most likely is a consequence of the reduced acidity of this proton following replacement of the other amino proton by Pd^{II}.

2.26. Conclusions

A series of metallacycles of different ring size, containing the parent pyrimidine nucleobase cytosine has been prepared in this work. Considering the formation of cyclic tetramers, low symmetrical ligands (C_s) could be expected to produce random mixtures of constitutional (linkage) isomers and rotamers. By utilizing a "directed" approach, hence by starting from preformed, kinetically inert corner units such as *cis*-$[Pt(a)_2(H_2C\text{-}N3)]^{2+}$ (**1**, **2**) or *cis*-$[Pt(a)_2(HC\text{-}N1)_2]$ (**4**) and by treating them with more labile $(en)Pd^{II}$ or $(2,2'\text{-bpy})Pd^{II}$ units, cyclic metallacalix[4]arenes (**9**, **12**, **13**, **14**) with a single connectivity pattern $(N1,N3\bullet N3,N1\bullet)_2$ and a single rotamer state (1,3-alternate) are obtained. A favorable head-tail arrangement in the starting compound and intramolecular hydrogen bonding between exocyclic site of cytosine rings either in the preformed corner units (in **12**, **13**, **14**) or during cyclization (in **9**) appears to be responsible for the formation of single rotamers. Inversion of *cis*-$(NH_3)_2Pt^{II}$ and $(bpy)Pd^{II}$ (compounds **9** and **12**) leads to differences in shape and dimensions of the constructs. Differences in electron distributions in the isomer **9** and **12** are reflected in their NMR spectra. The simultaneous formation of the cyclic tetramer **14** and the cyclic hexamer **16** also reflects the well-known phenomenon of supramolecular systems to find a balance between entropically and thermodynamically favorable conditions. Octanuclear metallacalix[4]arenes (**11** and **16**) have also been obtained in a self-assembly process from cytosine and the $(2,2'\text{-bpy})Pd^{II}$ entity. The difference in shape of **11** and **16** is due to the difference connectivity of the basic metallacalix[4]arene skeleton and the availability of exocyclic sites of cytosine for additional metal coordination.

2.27. References

[1] a) J. S. Kwiatkowski, B. Pullman, *Adv. Heterocycl. Chem.* **1975**, *18*, 199–335; b) J. Elguero, C. Marzin, A. R. Katritzky, P. Linda, *The Tautomerism of Heterocycles*, Academic Press, New York, **1976**, pp. 159.

[2] a) C. Colominas, F. J. Luque, M. Orozco, *J. Am. Chem. Soc.*, **1996**, *118*, 6811–6821; b) S. A. Trygubenko, T. V. Bogdan, M. Rueda, M. Orozco, F. J. Luque, J. Šponer, P. Slavíček, P. Hobza, *Phys. Chem. Chem. Phys.*, **2002**, *4*, 4192–4203.

[3] I. R. Gould, D. V. S. Green, P. Young, I. H. Hillier, *J. Org. Chem.* **1992**, *57*, 4434–4437.

[4] a) D. L. Barker, R. E. Marsh, *Acta Crystallogr.* **1964**, *17*, 1581–1587; b) R. J. McClure, B. M. Craven, *Acta Crystallogr., Sect. B* **1973**, *29*, 1234–1238.

[5] a) P. Munshi, T. N. G. Row, *Acta Crystallogr., Sect. B* **2006**, *62*, 612–626; b) M. Eisenstein, *Acta Crystallogr., Sect. B* **1988**, *44*, 412–426; c) S. Neidle, A. Achari, M. Rabinovitch, *Acta Crystallogr., Sect. B* **1976**, *32*, 2050–2053; d) G. A. Jeffrey, Y. Kinoshita, *Acta Crystallogr.* **1963**, *16*, 20–28.

[6] R. C. Lord, G. J. Thomas, Jr., *Spectrochim. Acta Part A: Molecular Spectroscopy* **1967**, *23*, 2551–2591.

[7] J.J. Christensen, J.H. Rytting, R.M. Izatt, *J. Phys. Chem.* **1967**, *71*, 2700–2705.

[8] R. Stewart, M.G. Harris, *Can. J. Chem.* **1977**, *55*, 3807–3811.

[9] See, e.g.: a) M. Palaniandavar, I. Somasundaram, M. Lakshminarayanan, H. Manohar, *J. Chem. Soc., Dalton Trans.* **1996**, 1333–1340; b) G. De Munno, S. Mauro, T. Pizzino, D. Viterbo, *J. Chem. Soc., Dalton Trans.* **1993**, 1113–1119; c) L. S. Hollis, A. R. Amundsen, E. W. Stern, *J. Med. Chem.* **1989**, *32*, 128–136.

[10] a) S. Jaworski, H. Schöllhorn, P. Eisenmann, U. Thewalt, B. Lippert, *Inorg. Chim. Acta* **1988**, *153*, 31–38; b) W. Brüning, I. Ascaso, E. Freisinger, M. Sabat, B. Lippert, *Inorg. Chim. Acta* **2002**, *339*, 400–410; c) W. Brüning, E. Freisinger, M. Sabat, R. K. O. Sigel, B. Lippert, *Chem. Eur. J.* **2002**, *8*, 4681–4692.

[11] a) G. Cervantes, J. J. Fiol, A. Terron, V. Moreno, J. R. Alabart, M. Aguilo, M. Gomez, X. Solans, *Inorg. Chem.* **1990**, *29*, 5168–5173; b) G. De Munno, M. Medaglia, D. Armentano, J. Anastassopoulou, T. Theophanides, *J. Chem. Soc., Dalton Trans.* **2000**, 1625–1629; c) M. A. Geday, G. De Munno, M. Medaglia, J. Anastassopoulou, T. Theophanides, *Angew. Chem. Int. Ed.* **1997**, *36*, 511–513; d) D. Armentano, G. De Munno, R. Rossi, *New. J. Chem.* **2006**, *30*, 13–17.

[12] K. Aoki, M. A. Salam, *Inorg. Chim. Acta*, **2001**, *316*, 50–58.

[13] M. Concepció Caplloncha, A. García-Rasoa, A. Terróna, M. Cristina Apellab, E. Espinosa, E. Molins, *J. Inorg. Biochem.* **2001**, *85*, 173–178.

[14] a) J. Müller, E. Zangrando, N. Pahlke, E. Freisinger, L. Randaccio, B. Lippert, *Chem. Eur. J.* **1998**, *4,* 397–405; b) L. Yin, P. J. Sanz Miguel, W. –Z. Shen, B. Lippert, *Chem. Eur. J.* **2009**, *15*, 10723–10726; c) H. Schöllhorn, R. Beyerle-Pfnür, U. Thewalt, B. Lippert, *J. Am. Chem. Soc.* **1986**, *108*, 3680–3688.

[15] A. Khutia, P. J. Sanz Miguel, B. Lippert, *Inorg. Chem.* **2010**, *49*, 7635–7637.

[16] H. Rauter, I. Mutikainen, M. Blomberg, C. J. L. Lock, P. Amo-Ochoa, E. Freisinger, L. Randaccio, E. Zangrando, E. Chiarparin, B. Lippert, *Angew. Chem. Int. Ed.* **1997**, *36*, 1296–1301.

[17] a) B. Lippert, *Coord. Chem. Rev.* **2000**, *200*, 487–516; b) B. Lippert, in *Nucleic – Acid Metal Ion Interaction*, (Ed: Nicholas V. Hud), The Royal Society of Chemistry, Cambridge, **2009**, pp. 39–74; c) D. Gupta, B. Lippert, *Dalton Trans.* **2009**, 4619–4634.

[18] A. L. Beauchamp, M. Simard, *Acta Crystallogr., Sect. A* **1984**, *40*, C67–C67.

[19] a) B. Lippert, H. Schöllhorn, U. Thewalt, *J. Am. Chem. Soc.* **1986**, *108*, 6616–6621; b) R. Beyerle-Pfnür, H. Schöllhorn, U. Thewalt, B. Lippert, *J. Chem. Soc. Chem. Commun.* **1985**, 1510–1511.

[20] a) F. Pichierri, D. Holthenrich, E. Zangrando, B. Lippert, L. Randaccio, *J. Biol. Inorg. Chem.* **1996**, *1*, 439–445; b) J. Müller, F. Glahé, E. Freisinger, B. Lippert, *Inorg. Chem.* **1999**, *38*, 3160–3166.

[21] a) J. E. Šponer, P. J. Sanz Miguel, L. Rodriguez-Santiago, A. Erxleben, M. Krumm, M. Sodupe, J. Šponer, B. Lippert, *Angew. Chem. Int. Ed.* **2004**, *43*, 5396–5399; b) P. J. Sanz Miguel, P. Lax, M. Willermann, B. Lippert, *Inorg. Chim. Acta* **2004**, *257*, 4552–4561.

[22] P. J. Sanz Miguel, P. Lax, B. Lippert, *J. Biol. Inorg. Chem.* **2006**, *100*, 980–991.

[23] J. P. Davidson, P. J. Farber, R. G. Fischer, jr.; S. Masy, H. J. Peresie, B. Rosenberg, L. VanCamp, *Cancer Chemother. Rep., Part I*, **1975**, *59*, 287–300.

[24] a) R. Faggiani, B. Lippert, C. J. L. Lock, *Inorg. Chem.* **1982**, *21*, 3210–3216; b) H. Schöllhorn, U. Thewalt, G. Raudaschl-Sieber, B. Lippert, *Inorg. Chim. Acta* **1986**, *124*, 207–211.

[25] D. Holthenrich, I. Sóvágó, G. Fusch, A. Erxleben, E. C. Fusch, I. Rombeck, B. Lippert, *Z. Naturforsch. B* **1995**, *50*, 1767–1775.

[26] a) B. Song, G. Feldmann, M. Bastian, B. Lippert, H. Sigel, *Inorg. Chim. Acta* **1995**, *235*, 99–109; b) G. Schröder, B. Lippert, M. Sabat, C. J. L. Lock, R. Faggiani, B. Song, H. Sigel, *J. Chem. Soc. Dalton Trans.* **1995**, 3767–3775.

[27] U. K. Häring, R. B. Martin, *Inorg. Chim. Acta.* **1983**, *78*, 259–267.

[28] Z. -L. You, H. -L. Zhu, W. -S. Liu, *Acta Cryst. E.* **2004**, *60*, m1903–m1905.

[29] a) R. Faggiani, B. Lippert, C. J. L. Lock, R. A. Speranzini, *J. Am. Chem. Soc.* **1981**, *103*, 1111–1120; b) V. M. Djinovic, M. Galanski, V. B. Arion, B. K. Keppler, *Dalton Trans.* **2010**, *39*, 3633–3643.

[30] C. J. L. Lock, H. J. Peresie, B. Rosenberg, Graham Turnerla, *J. Am. Chem. Soc.* **1978**, *100*, 3371–3374.

[31] P. J. Sanz Miguel, M. Roitzsch, L. Yin, P. M. Lax, L. Holland, O. Krizanovic, M. Lutterbeck, M. Schürmann, E. C. Fusch, B. Lippert, *Dalton Trans.* **2009**, 10774–10786.

[32] a) C. D. Gutsche, *Calixarenes*, The Royal Society of Chemistry, Cambridge, 1989; b) C. D. Gutsche, *Calixarenes Revisited*, The Royal Society of Chemistry, Cambridge, **1998**; c) J. S. Kim, D. T. Quang, *Chem. Rev.* **2007**, *107*, 3780–3799.

[33] a) M. -X. Wang, *Chem. Commun.* **2008**, 4541–4551; b) W. Maes, W. Dehaen, *Chem. Soc. Rev.* **2008**, *37*, 2393–2402; c) B. König, M. H. Fonseca, *Eur. J. Inorg. Chem.* **2000**, 2303–2310; c) P. A. Gale, P. Anzenbacher, J. L. Sessler, *Coord. Chem. Rev.* **2001**, *222*, 57–102.

[34] a) H. Rauter, E. C. Hillgeris, B. Lippert, *J. Chem. Soc., Chem. Commun.* **1992**, 1385–1386; b) H. Rauter, E. C. Hillgeris, A. Erxleben, B. Lippert, *J. Am. Chem. Soc.* **1994**, *116*, 616–624; c) J. A. R. Navarro, E. Freisinger, B. Lippert, *Inorg. Chem.* **2000**, *38*, 2301–2305.

[35] a) E. Barea, J. A. R. Navarro, J. M. Salas, M. Quirós, M. Willermann, B. Lippert, *Chem. Eur. J.* **2003**, *9*, 4414 –4421; b) E. Gil Bardají, E. Freisinger, B. Costisella, C. A. Schalley, W. Brüning, M. Sabat, B. Lippert, *Chem. Eur. J.* **2007**, *13*, 6019 – 6039.

[36] L. Zhao, B. H. Northrop, Y. -R. Zheng, H. -B. Yang, H. J. Lee, Y. M. Lee, J. Y. Park, K. -W. Chi, P. J. Stang, *J. Org. Chem.* **2008**, *73*, 6580–6586.

[37] A. Rang, M. Engeser, N. M. Maier, M. Nieger, W. Lindner, C. A. Schalley, *Chem. Eur. J.* **2008**, *14*, 3855–3859.

[38] W. -Z. Shen, G. Trötscher-Kaus, B. Lippert, *Dalton Trans.* **2010**, 8203–8214.

[39] D. Holthenrich, E. Zangrando, E. Chiarparin, B. Lippert, L. Randaccio, *J. Chem. Soc., Dalton. Trans.* **1997**, 4407–4410.

3. Complexes of *cis*-$(NH_3)_2Pt^{II}$ with Parent (Unsubstituted) Uracil

3.1. Introduction

Uracil is a naturally occurring pyrimidine derivative and one of the major nucleobases found in RNAs. Uracil can exist in six tautomeric forms I – VI (Scheme 3.1). However, if different orientations of hydroxyl (–OH) protons are considered, then the total

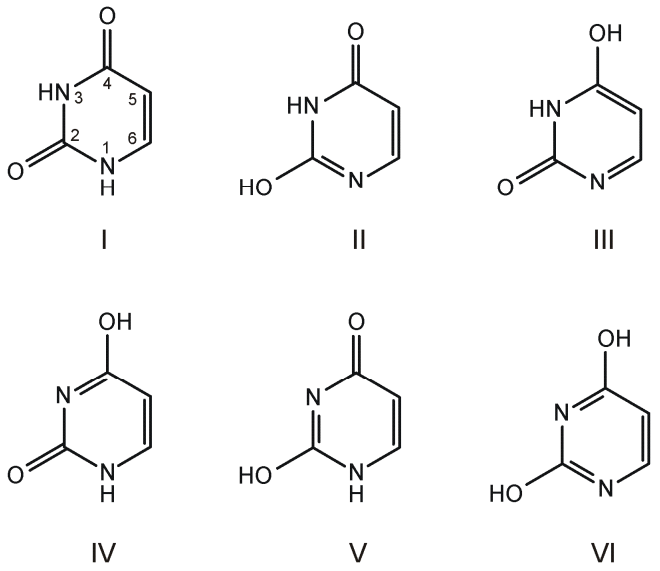

Scheme 3.1: Six tautomeric forms of unsubstituted neutral uracil

number of isomers will be thirteen.[1] The 1H,3H-diketo tautomer (I) is most stable both in gas phase as well as in solution.[2] The enol or dienol tautomeric forms of uracil are higher in energy than the diketo form I. The relative stabilities of the enol or dienol forms of uracil "still remains unclear".[2] The 2H,4H-dienol form VIa is the only minor tautomer of uracil which is present in aqueous medium beside the preferred tautomer I, but it is about 40 kJ mol^{-1} less stable than I. X-ray crystallography showed that uracil exists in the 1H,3H-diketo tautomer form (I) in solid state as well.[3]

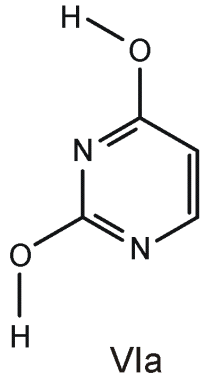

VIa

Uracil has two deprotonation steps because of the presence of two different acidic protons at N1 and N3. The macroscopic pK_a value for deprotonation of uracil leading to the formation of uracil monoanion is 9.33 ± 0.05[4] and the second deprotonation of uracil occurs with a pK_a of

14.20.[5] The proton at the N3 site of uracil is somewhat more acidic than the proton at N1 site, leading to the microscopic pK_a values of 9.43 ± 0.05 for N(3)H and 10.02 ± 0.31 for N(1)H.[4] Mono deprotonation of uracil can lead to the formation of two tautomers of uracil monoanions, either N3 deprotonated uracil or N1 deprotonated uracil (Scheme 3.2). The N1 deprotonated form of uracil is less polar than the N3 deprotonated uracil because of greater delocalization of its negative charge. Consequently the former tautomer is favored in solvents of low dielectric constant, e.g. dimethylformamide ($\varepsilon_{25\,℃}$ = 36.7).[6] However, in water ($\varepsilon_{25\,℃}$ ≈ 78) at alkaline pH, the two tautomers co-exist in comparable amounts.

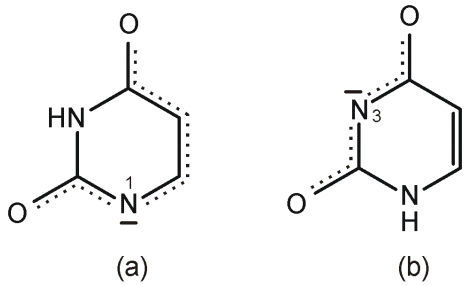

(a) (b)

Scheme 3.2: Structure of (a) N1 deprotonated uracil and (b) N3 deprotonated uracil

Metal coordination to the *neutral* uracil has been reported for several transition metal ions,[7] but X-ray structure analyses are scarce. The thermodynamic stability of these complexes is generally low. Coordination of the O4 site of unsubstituted uracil with $HgCl_2$ has been established by X-ray crystallography.[8] Metal complexes with uracil *monoanion* have been reported and characterized crystallographically. Zn complexes coordinated to different ring N sites (N1 and N3) of uracil have been described.[9] A recently reported example showed that coordination of Zn with N1 and N3 tautomers of uracil can occur simultaneously within the same complex.[10] Pt^{II} coordination complexes with the deprotonated N1 site of uracil have generally been prepared in the less polar solvent DMF.[11] Coordination of Pt^{II} to the deprotonated N3 site of the unsubstituted uracil is somewhat difficult to obtain. So far only a single X-ray crystal structure, *cis*-[$Pt(NH_3)_2$(HU-*N3*)Cl], has been reported.[12] Interestingly it was prepared at acidic pH = 4-5, under which condition uracil is present in its neutral form. Concerning its formation, it has been suggested that initial binding of Pt^{II} to a carbonyl oxygen atom takes place, followed by base deprotonation and metal migration to the N3 site.[13] A cyclic tetramer complex, $[\{Pt(en)(UH\text{-}N1,N3)\}_4]^{4+}$, has been prepared through self-assembly of the mononuclear N1 platinated uracil complex $[Pt(en)(HU\text{-}N3)(H_2O)]^+$.[12,14] This complex represents a minor tautomer of the uracil monoanion which has a movable proton between its exocyclic O2

and O4 groups. A series of multinuclear derivatives has been prepared from this tetranuclear complex utilizing the exocyclic oxygen atoms of uracil.[15] As has been discussed in detail in the previous chapter (Section 2.12), for low symmetrical ligands (C_s), a series of linkage isomers and numerous rotamers can be obtained when considering formation of metallacycle with square planar *cis*-a_2M^{II} entities (a = amine, a_2 = diamine; M = Pt, Pd). On the other hand, the number of possible isomers can be reduced to a single one by applying preformed building block. The tetranuclear complex $[\{Pt(en)(UH\text{-}N1,N3)\}_4]^{4+}$ has strictly alternating $(N1,N3\bullet)_4$ connectivities (• represents the metal entity) and is stabilized in a 1,3-alternate conformation through hydrogen bonding between exocyclic O2 and O4(H) sites of *head-tail* oriented uracil moieties. In principle the same connectivity patterns of uracil can be obtained during the reaction of the preformed corner stone *cis*-$[Pta_2(HU\text{-}N1)(HU\text{-}N3)]$ with additional *cis*-a_2M^{II} entities (a = NH_3, a_2 = en, 2,2'-bpy; M = Pt, Pd) (see below). The aim of this chapter is to describe the preparation of kinetically inert uracil building blocks such as the N3 linkage isomer *cis*-$[Pta_2(HU\text{-}N3)_2]$, or the mixed N1,N3 linkage isomer *cis*-$[Pta_2(HU\text{-}N1)(HU\text{-}N3)]$ and to characterize the species formed when reacted with additional metal entities.

3.2. Solution behavior of *cis*-$[Pt(NH_3)_2(HU\text{-}N3)Cl]$ (17)

Complex 1**7** has previously been prepared through the reaction of *cis*-$PtCl_2(NH_3)_2$ with uracil in 1:1 ratio at low pH 4-5 in very low yield (8%).[12] In the current work, several variations in reaction conditions (changes in pH, temperature) have been made to improve the yield of this reaction, yet these attempts were not successful. A mixture of components was formed during this reaction which required separation by sephadex G-10 chromatography. Attempts to prepare the bis(uracil) complex *cis*-$[Pt(NH_3)_2(HU\text{-}N3)_2]$ from the reaction of *cis*-$[Pt(NH_3)_2Cl_2]$ with excess uracil (2-4 equivalent, pD 4-5 with 1M NaOH, 5d at 40 ℃ or 60 ℃) in water proved likewise unsu ccessful.

pD dependant ^{1}H NMR spectra of *cis*-$[Pt(NH_3)_2(HU\text{-}N3)Cl]$ (**17**) were recorded in order to evaluate its acid-base equilibria. The chemical shifts of uracil-H6 and uracil-H5 in **17** change with pD of the solution (Figure 3.1). At alkaline pD, uracil-H5 is upfield shifted, whereas uracil-H6 undergoes a downfield shift. The pK_a values determined for the deprotonation of exocyclic N1-H are 12.03 ± 0.03 (H6) and 12.32 ± 0.05 (H5) in D_2O, corresponding to a value of 11.55 ± 0.14 in H_2O (mean value). So Pt^{II} coordination to the

N3 site of uracil acidifies the N1H by ca. 2.6 log units (pK_{a2} of uracil is 14.20[5]). Protonation of the exocyclic O2, O4 sites in **17** occurs at low pH (pK_a = 0.02 in H_2O).

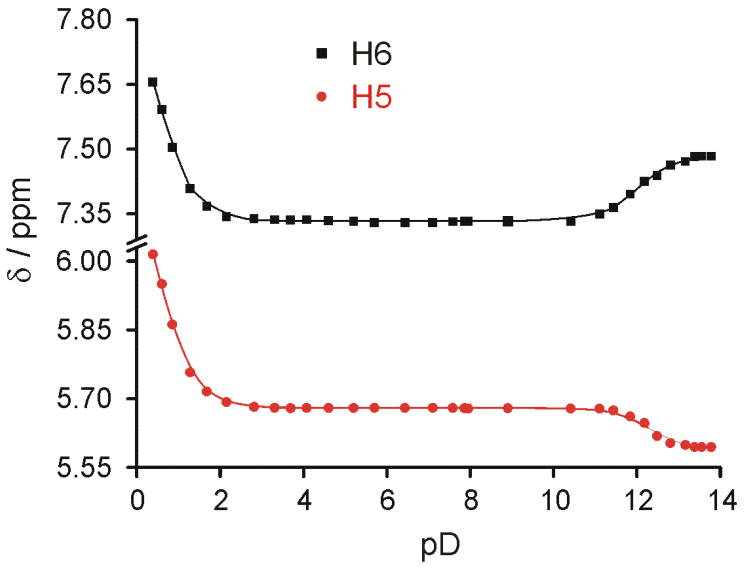

Figure 3.1: pD dependence of uracil-H6 and -H5 resonances in **17**.

3.3. Synthesis of mixed linkage isomer with N1,N3 coordination

The mixed linkage isomer *cis*-[$Pt(NH_3)_2$(HU-*N1*)(HU-*N3*)]·H_2O (**18**) was prepared by reacting the N1 linkage isomer *cis*-[$Pt(NH_3)_2$(HU-*N1*)Cl] with uracil (H_2U) at 40 ℃ (pH = 4-5) in water. Mixtures of species are formed during the course of this reaction, as indicated by ^{1}H NMR spectroscopy. Methanol was eventually used to remove unreacted uracil from the solid and repeated recrystallization of the mixture from water produced finally pure complex **18**. The yield of the reaction was only 12% and all attempts to improve the yield of this reaction remained unsuccessful. Surprisingly, starting with [Pt(en)(HU-*N1*)Cl] and reacting it with free uracil, did not produce the desired product; rather it lead to the formation of [Pt(en)(HU-*N1*)$_2$]. The identity of [Pt(en)(HU-*N1*)$_2$] was confirmed by elemental analysis and comparison of its ^{1}H NMR spectrum with that of an authentic sample.[11]

3.4. ^{1}H NMR spectrum and acid-base equilibria of *cis*-[Pt$(NH_3)_2$(HU-*N1*)(HU-*N3*)]·H_2O (18)

The ^{1}H NMR spectrum of complex **18** in D_2O is shown in Figure 3.2. The spectrum displays discrete doublets for H5 and H6 protons of the two differently bonded uracil rings (A and B). The chemical shifts (δ, ppm; D_2O, pD 7.2) of these protons are 5.51, 7.58 (ring A) and 5.66, 7.33 (ring B). This assignment of protons of rings A and B is based on a comparison of its pD dependence and also on a comparison with the chemical shifts of the mono(uracil) complex of *cis*-$(NH_3)_2Pt^{II}$ namely, *cis*-[Pt$(NH_3)_2$(HU-*N1*)Cl] and *cis*-[Pt$(NH_3)_2$(HU-*N3*)Cl]. The H5 and H6 protons of ring A appear furthest upfield and furthest downfield, respectively, compared to the corresponding protons in ring B (Figure 3.2).

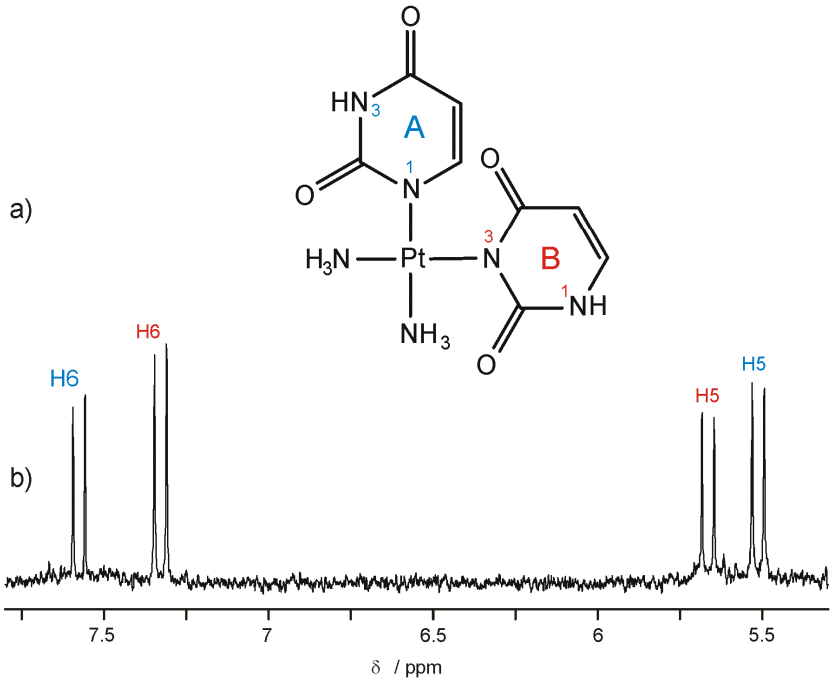

Figure 3.2: a) Structure of *cis*-[Pt$(NH_3)_2$(HU-*N1*)(HU-*N3*)] (**18**); b) ^{1}H NMR spectrum of **18** in D_2O, pD = 7.2.

^{1}H NMR spectra of complex **18** were recorded in D_2O at different pD values in order to evaluate the pK_a value for deprotonation of the acidic protons. Both H5 and H6 in the N1 platinated uracil (ring A) are shifted upfield with increasing pD values. However, H6 of the N3 platinated uracil (ring B) shows a downfield shift and H5 undergoes an upfield shift with increasing pD (Figure 3.3). The behavior of uracil-H6 and uracil-H5 in ring B towards changes in pD values of solution, is thus similar to that seen for the N3 coordinated mono(uracil) complex of Pt^{II}, *cis*-[Pt$(NH_3)_2$(HU-*N3*)Cl] (**17**). The pK_a values derived for deprotonation of acidic protons in **18** are 12.13 ± 0.01 (ring A) and 11.99 ± 0.02 (ring B) in

H_2O. Within the error limits, the acidity of N1-H (ring B) and N3-H (ring A) in complex **18** are practically identical.

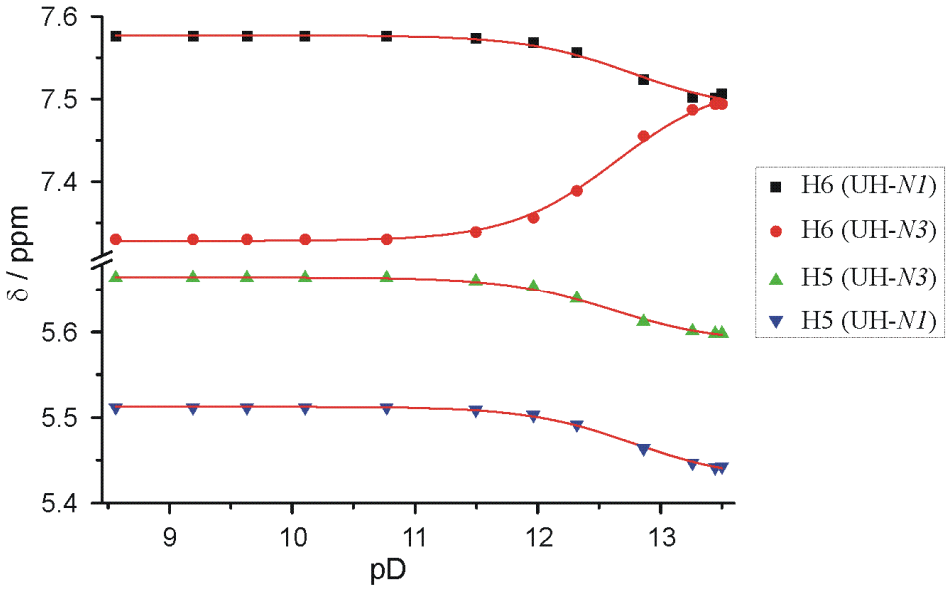

Figure 3.3: pD dependence of uracil-H6 and uracil-H5 resonances in complex **18**.

3.5. Reaction of *cis*-[Pt$(NH_3)_2$(HU-*N1*)(HU-*N3*)] (18) with *cis*-$(NH_3)_2Pt^{II}$

Reaction of the mixed linkage isomer **18** with an additional *cis*-a_2M^{II} entity can lead to the formation of cyclic metallacalix[4]arenes with two different connectivity patterns, either (A) with a fully alternating $(N1,N3\bullet)_4$ sequence similar to that seen in the cation of [Pt(en)(UH-*N1*,*N3*)$_4$]$(NO_3)_4$[12] or (B) with a (N1,N3•N1,N3•N3,N1•N3,N1•) sequence (• representing metal entities) (Scheme 3.3).

Reaction of the mixed linkage isomer **18** with *cis*-$[Pt(NH_3)_2(D_2O)]^{2+}$ (*r* =1:1) in D_2O was followed by ^{1}H NMR spectroscopy (Figure 3.4). Mixtures of species formed within hours after the start of the reaction and numerous resonances (>8) for uracil-H6 can be observed. Resonances due to starting complex **18** can not be identified even in the ^{1}H NMR spectrum recorded within 2h after start of the reaction (spectrum (a) in Figure 3.4). This clearly indicates that complex **18** reacts rapidly with *cis*-$[Pt(NH_3)_2(D_2O)]^{2+}$. Some of the H6 resonances appear as pseudo triplets due to partial isotopic exchange at the uracil-H5 site. For a cyclic tetranuclear species, one could expect to observe a single set of uracil resonance for (A) and two sets of uracil resonances with equal intensities for (B). The

cyclic tetramer (A) (M = *cis*-$(NH_3)_2Pt^{II}$ in this case) should have very similar chemical shifts as $[\{Pt(en)(UH\text{-}N1,N3)\}_4]^{4+}$, since the only difference is the replacement of en by the NH_3

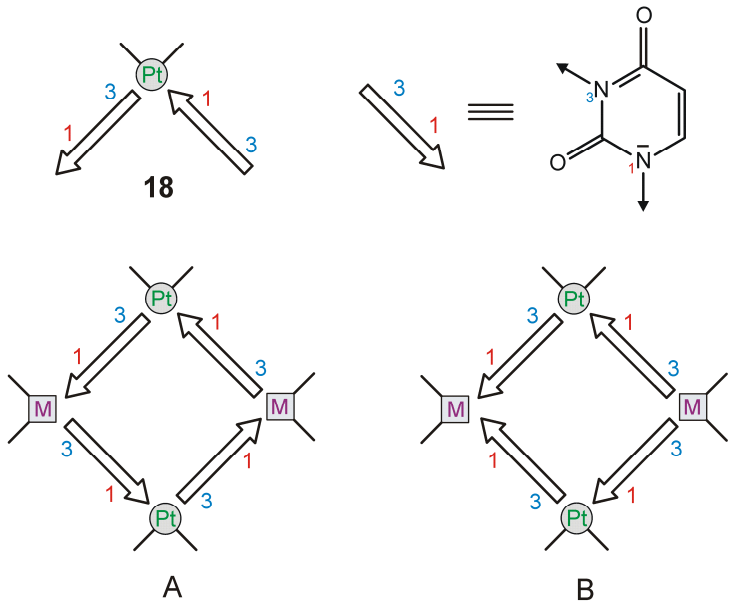

Scheme 3.3: Schematic representation of two feasible metallacalix[4]arenes A and B formed by the reaction of **18** with a *cis*-a_2M^{II} entity.

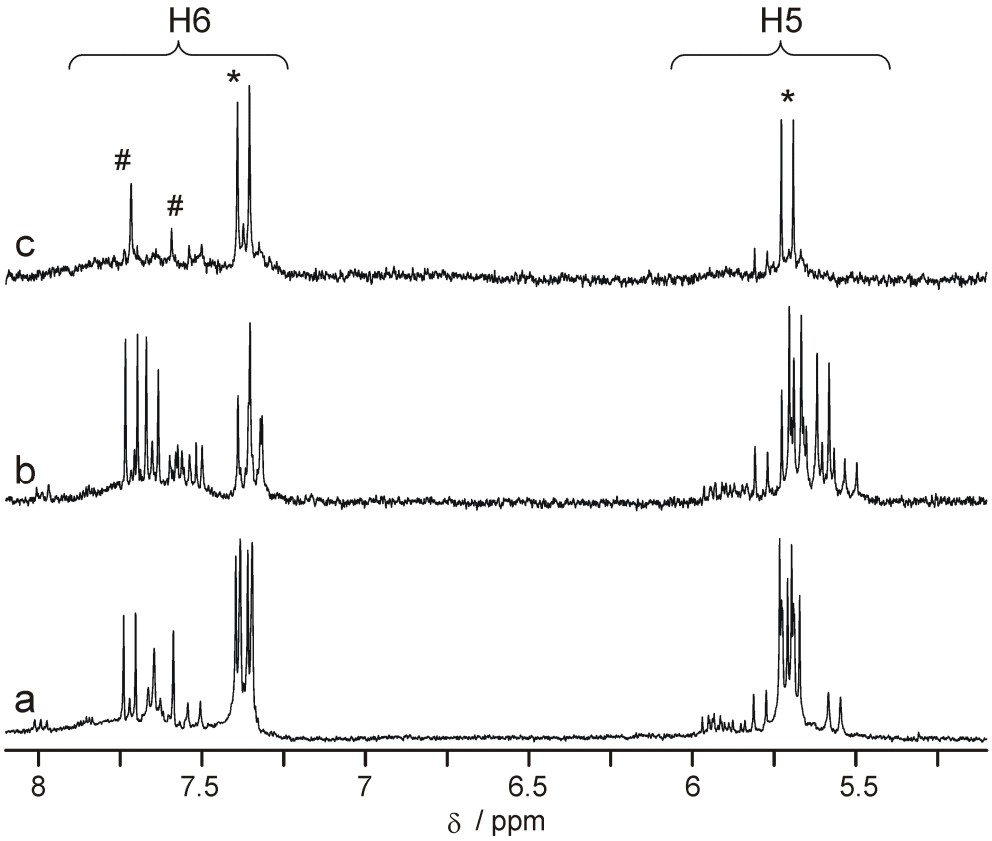

Figure 3.4: ^1H NMR spectra of a reaction mixture of **18** with *cis*-$[Pt(NH_3)_2(D_2O)_2]^{2+}$ in D_2O, pD 4.7, at different time intervals: (a) t = 2h, (b) t = 12h and (c) t = 24 h.

groups. However, comparison of chemical shifts of $[\{Pt(en)(UH\text{-}N1,N3)\}_4]^{4+}$ (with spectra (a-c) in Figure 3.4) does not give any indication of formation of the cyclic tetramer (A). Likewise, the spectra are inconsistent with formation of (B). After 1 day, formation of an unknown major species is observed in solution (marked with * in Figure 3.4) along with several minor species. Some of these minor species (#) appear as singlets due to complete isotopic exchange of H5. Attempts to isolate this major species remained unsuccessful.

3.6. Reaction of *cis*-$[Pt(NH_3)_2(HU\text{-}N1)_2]$ (19) with *cis*-$(NH_3)_2Pt^{II}$

Earlier work on *cis*-$[Pt(NH_3)_2(HU\text{-}N1)_2]$ (**19**) has shown that cyclic complexes of varying size can be prepared when **19** is reacted with kinetically labile *cis*-a_2Pd^{II} (a_2 = en, 2,2'-bpy) metal entities.[16] Here, reactions of **19** with additional *cis*-$(NH_3)_2Pt^{II}$ entity have been carried out in order to prepare metallacalix[4]arene composed exclusively of Pt^{II} entities. Reactions between these two species (*r* = 1:1) have been followed by ^1H NMR spectroscopy in D_2O (Figure 3.5). The pD value of the solution decreases rapidly within

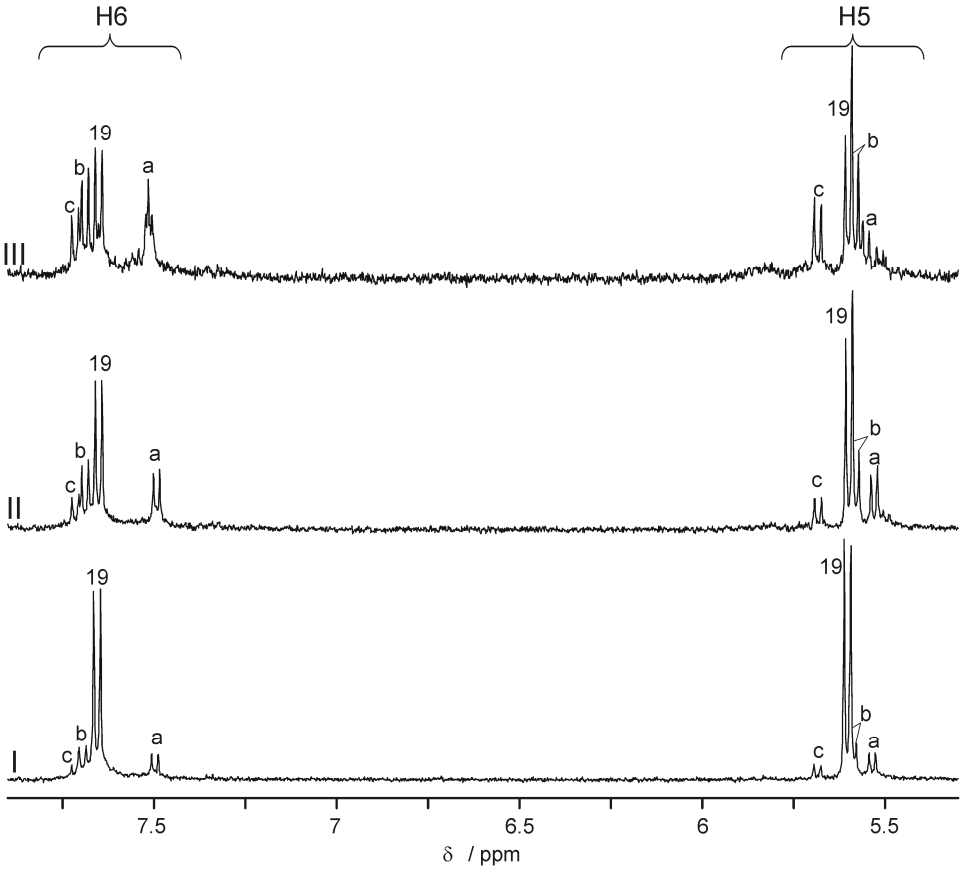

Figure 3.5: ^1H NMR spectra of a reaction mixture of **19** with *cis*-$[Pt(NH_3)_2(D_2O)_2]^{2+}$ (*r* = 1:1) in D_2O after (I) 2h, pD 4.1, (II) 12h, pD 3.8, (III) 24h, pD 3.6.

few hours after the start of the reaction. This clearly indicates that metal coordination takes place at the N3 sites of the uracilate anions in **19**, following deprotonation. Besides the starting complex *cis*-[$Pt(NH_3)_2$(HU-*N1*)$_2$] (**19**), three new uracil resonances (a, b and c) can be detected at an early stage of the reaction in the ^{1}H NMR spectra. Resonances (a) and (b) have equal intensity, clearly visible in the spectra (I) and (II) in Figure 3.5. So it suggests the formation of a complex in which the coordination environments of two uracil rings are different. This complex is tentatively assigned to *cis*-[(HU-*N1*)$Pt(NH_3)_2$(*N1*-U-*N3*)$Pt(NH_3)_2(H_2O)]^+$ (X). The resonances due to N1,N3 bridged uracilate dianion in (X) are

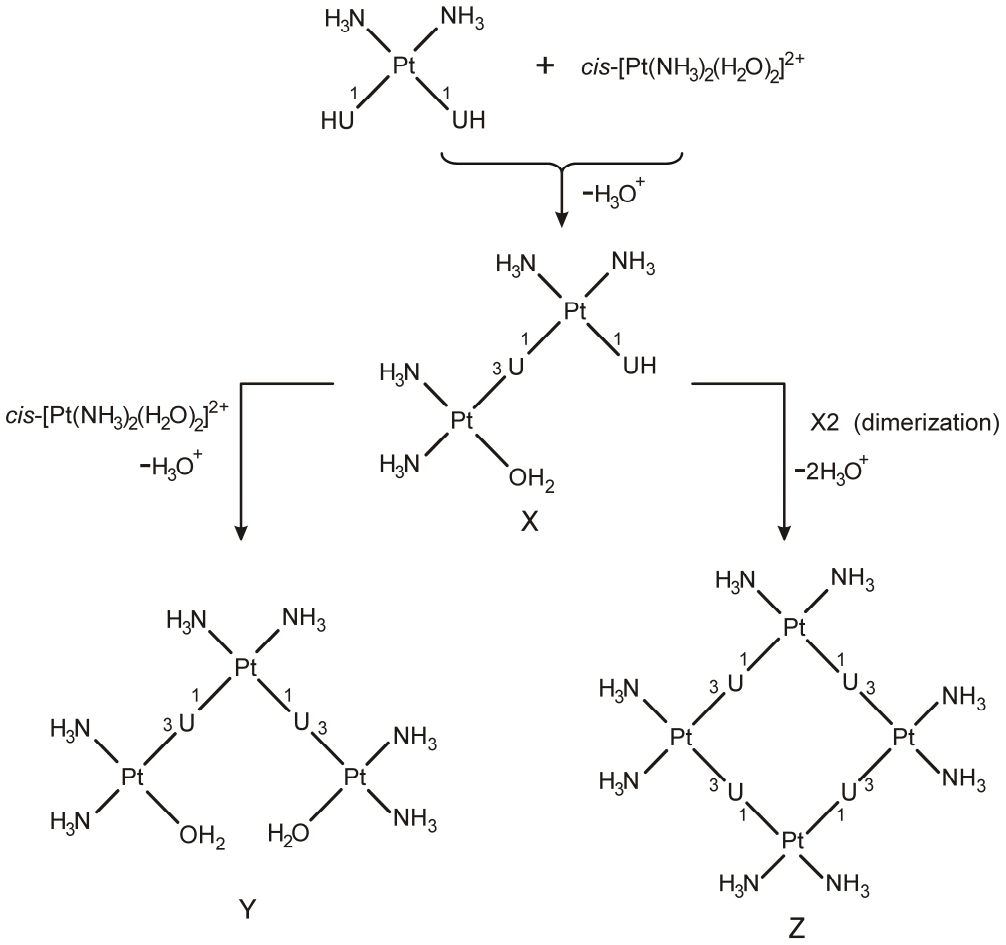

Scheme 3.4: Schematic diagram of formation of X, Y and Z.

expected to appear in the downfield region, hence at 5.59 and 7.69 ppm (resonances of (b)). The N1 coordinated uracilate monoanion in (X) would then be at 5.34 and 7.50 ppm (resonances (a)), and uracil-H6 of this uracil ligand undergoes slow isotopic exchange after longer reaction times. Concerning the nature of the other uracil species with resonances (c) at 5.68 and 7.71 ppm, we can see that it does not undergo any isotopic exchange even after longer reaction time. These resonances should be due to a species

which is highly symmetrical. We can therefore assign this species to either the open structure *cis*-$[(H_2O)Pt(NH_3)_2(N3\text{-HU-}N1)Pt(NH_3)_2(N1\text{-HU-}N3)Pt(NH_3)_2(H_2O)]^{2+}$ (Y) or the cyclic tetramer *cis*-$[\{(NH_3)_2Pt(N3\text{-U-}N1)_2Pt(NH_3)_2\}_2]$ (Z) (Scheme 3.4). The species Y could give rise to the formation of various rotamers and is also expected to be very reactive due to the presence of two free coordination sites. But the resonances of (c) do not disappear with time, so we can simply rule out the open structure (Y). Therefore it is proposed that the resonances (c) may correspond to the symmetrical tetranuclear species Z.

Reactions carried out between **19** and an excess of *cis*-$[Pt(NH_3)_2(D_2O)_2]^{2+}$ also do not give much additional information. Attempts to crystallize any of these new species formed in this reaction were not successful.

3.7. Conclusion

Reactions of unsubstituted bis(uracil) complexes of *cis*-$(NH_3)_2Pt^{II}$, namely of *cis*-$[Pt(NH_3)_2(HU\text{-}N1)(HU\text{-}N3)]$ (**18**) and *cis*-$[Pt(NH_3)_2(HU\text{-}N1)_2]$ (**19**) with *cis*-$[(NH_3)_2Pt(H_2O)_2]^{2+}$ have been carried in an attempt to obtain metallacalix[4]arene. Reactions followed by ^1H NMR spectra showed the formation of several new species in solution. However, despite several attempts, the new species formed could not be isolated.

3.8. References

[1] J. S. Kwiatkowski, B. Pullman, *Adv. Heterocycl. Chem.* **1975**, *18*, 199–335.

[2] J. Rejnek, M. Hanus, M. Kabeláč, F. Ryjáček, P. Hobza, *Phys. Chem. Chem. Phys.* **2005**, *7*, 2006–2017.

[3] a) G. S. Parry, *Acta Crystallogr.* **1954**, *7*, 313–320; b) R. Gerdil, *Acta Crystallogr.* **1961**, *14*, 333–344; c) K. Ozeki, N. Sakabe, J. Tanaka, *Acta Crystallogr. Sect. B* **1969**, *25*, 1038–1045.

[4] C. F. Moreno-Luque, E. Freisinger, B. Costisella, R. Griesser, J. Ochocki, B. Lippert, H. Sigel, *J. Chem. Soc., Perkin Trans. 2*, **2001**, 5005–5011.

[5] J. R. DeMember, F. A. Wallace, *J. Am. Chem. Soc.* **1975**, *97*, 6240–6245.

[6] B. Lippert, *J. Raman Spectrosc.* **1979**, *8*, 274–278.

[7] M. Goodgame, D. A. Jakubovic, *Coord. Chem. Rev.*, **1987**, *79*, 97–134.

[8] J. A. Carrabine, M. Sundaralingam, *Biochemistry*, 1**971**, *10*, 292–299.

[9] a) M. Ruf, K. Weis, H. Vahrenkamp, *Inorg. Chem.* **1997**, *36*, 2130–2137; b) C. Bazzicalupi, A. Bencini, E. Berni, A. Bianchi, S. Ciattini, C. Giorgi, P. Paoletti, B. Valtancoli, *Eur. J. Inorg. Chem.* **2001**, 629–632.

[10] I. Escorihuela, L. R. Falvello, M. Tomás, E. P. Urriolabeitia, *Cryst. Growth Des.* **2004**, *4*, 655–657.

[11] B. Lippert, *Inorg. Chem.* **1981**, *20*, 4326–4343.

[12] H. Rauter, E. C. Hillgeris, A. Erxleben, B. Lippert, *J. Am. Chem. Soc.* **1994**, *116*, 616–624

[13] D. Gupta, B. Lippert, *Dalton Trans.* **2009**, 4619–4634.

[14] H. Rauter, E. C. Hillgeris, B. Lippert, *J. Chem. Soc., Chem. Commun.* **1992**, 1385–1386.

[15] H. Rauter, I. Mutikainen, M. Blomberg, C. J. L. Lock, P. Amo-Ochoa, E. Freisinger, L. Randaccio, E. Zangrando, E. Chiarparin, B. Lippert, *Angew. Chem. Int. Ed.* **1997**, *36*, 1296–1301.

[16] E. Gil Bardají, *Ph.D. Dissertation*, Technische Universität Dortmund, **2007**.

4. Hybrids between classical calix[4]arene and metallacalix[4]arene derived from uracil based ligands

4.1. Introduction

In classical calix[n]arenes, methylene groups bridge n para-substituted phenols, yielding cyclic compounds.[1] Interest in calixarenes primarily results from their ability to function as hosts for small molecules or ions as well as their metal binding properties, either in the cavity or at the periphery.[2] In metallacalix[n]arene, the ditopic N,N'-heterocyclic ligands replace the original phenol entities and cis blocked square planar *cis*-a_2M^{II} [a = NH_3, a_2 = en, 2,2'-bpy; M = Pt, Pd) substitute the methylene bridges[3] (Scheme 4.1). A number of cyclic metallacalix[n]arene complexes with different ring sizes (n = 3,[4] 4,[3,5] 6,[6] 8[7]) have been prepared and characterized with the heterocyclic pyrimidine ligands, including the parent pyrimidine nucleobases such as uracil and cytosine. These metallacalix[n]arene

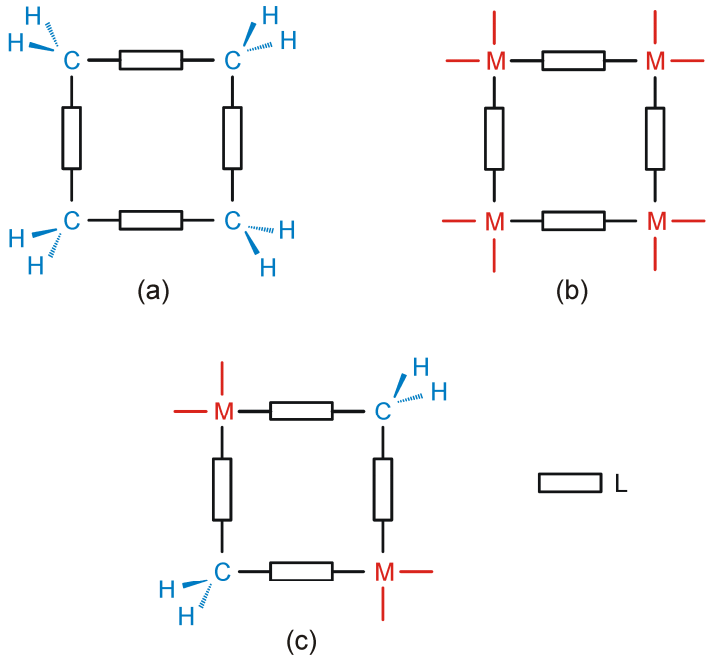

Scheme 4.1: Schematic views of (a) classical calix[4]arene, (b) metallacalix[4]arene, L = uracil anion and square-planar M units (M = Pt^{II}, Pd^{II}) and (c) hybrid based on L = bis(1-methyluracil-5-yl)methane and square-planar M units (M = Pt^{II}, Pd^{II}).

complexes have the propensity to coordinate additional metal entities through the exocyclic sites of pyrimidine ligands (O2, O4 in uracil; O2, N4 in cytosine), resulting in the formation of multinuclear complexes with short intermetallic distances.[8] These macrocyclic compounds have the ability to act as host for anions[9] as well as cations.[10]

Some of these compounds display surprising effects on the structure of double-stranded DNA.[11]

In this chapter, two ditopic ligands based on the pyrimidine nucleobase 1-methyluracil, bis(1-methyluracil-5-yl)methane (L1) and its phenyl derivative L2 (Scheme 4.2) are presented and their reaction products with *cis*-a_2M^{II} units will be discussed. Ligands L1 and L2 have potential metal coordination sites and can coordinate to metal ions through their endocyclic N3 sites and/or exocyclic O2, O4 sites. Reactions of these ligands with *cis*-a_2M^{II} entities are expected to produce cyclic species, hence hybrids between classical calix[n]arene and metallacalix[n]arenes. These hybrids represent a new distinct class of finite supramolecular architectures. The term “hybrid” has been coined since these metallacycles, based on uracil moieties, contain both methylene groups and square-planar *cis*-a_2Pt^{II} units (Scheme 4.1).

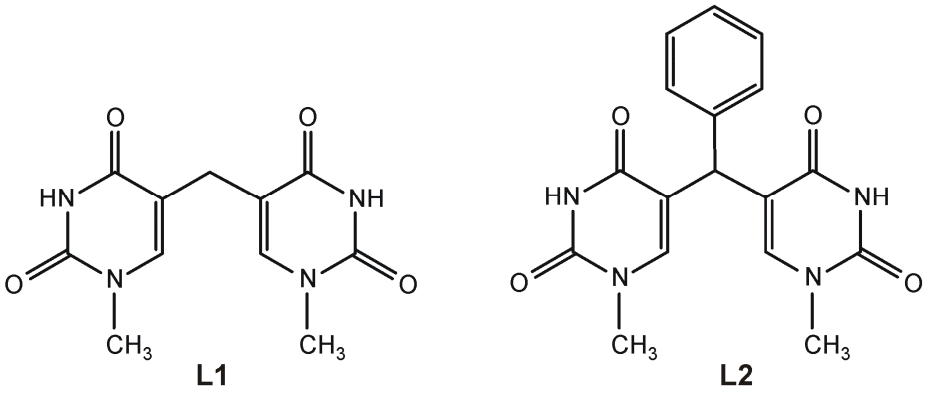

Scheme 4.2: Views of ligand L1 and L2.

4.2. Synthesis of bis(1-methyluracil-5-yl)methane (L1) and its phenyl derivative (L2)

The acid catalyzed condensation of 1-methyluracil (1-MeUH) with paraformaldehyde or benzaldehyde produces L1 and L2, respectively, in high yield (Scheme 4.3).[12] The ligands were obtained as pure white solids. The ^{1}H NMR spectra of L1 and L2, recorded in Me_2SO-d_6 are consistent with their compositions. The spectra of the free ligands have their ^{1}H NMR resonances (δ, ppm; Me_2SO-d_6) at N1(H), 11.27 s, C(6)H, 7.43 s, N(1)CH_3, 3.20 s, CH_2, 3.06 s in L1 and N1(H), 11.32 s, C(6)H, 7.03 s, CH(-Ph), 5.09 s, N(1)CH_3, 3.19 s, Ph, 7.32–7.18, m in L2.

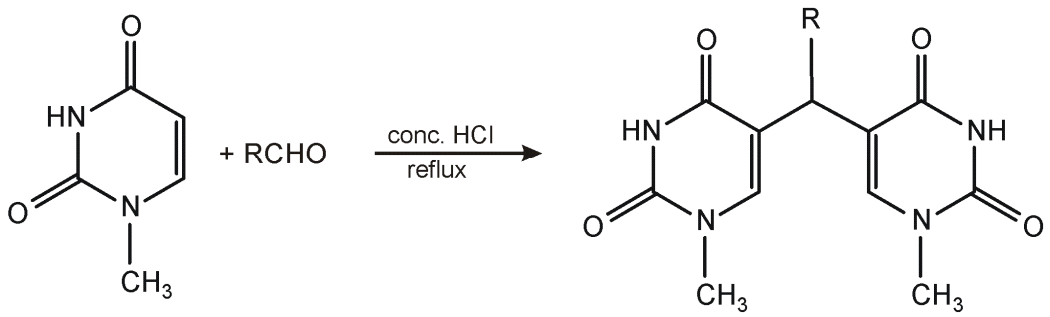

Scheme 4.3: Synthesis of ligands L1 (R = H) and L2 (R = Ph) from 1-methyluracil.

4.3. Determination of pK_a value of L1 and L2

The ^{1}H NMR spectra of L1 and L2 in D_2O were recorded at different pD values to determine their acid-base equilibria. These ligands are extremely insoluble in D_2O at neutral pD, but they dissolve in alkaline media after removal of the N3-H protons. The H6 and $-CH_3$ protons of 1-methyluracil in L1 and L2 are shifted downfield with increasing

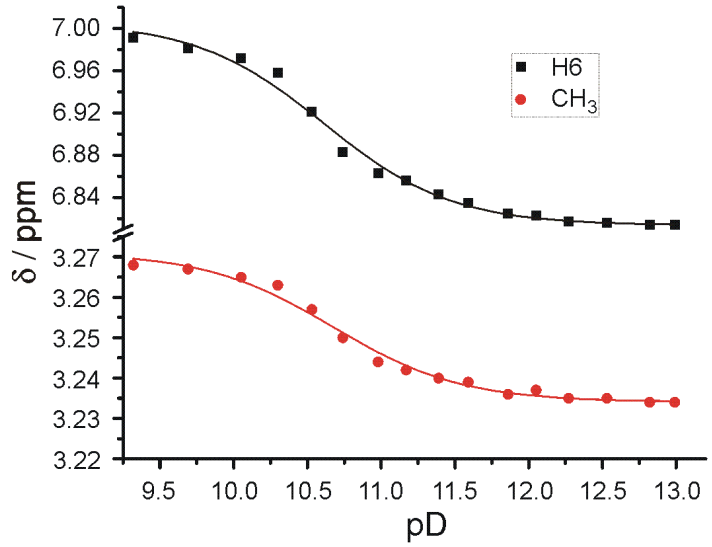

Figure 4.1: pD dependence of uracil-H6 and $-CH_3$ resonances in L2.

pD value of the solution. The pK_a value derived for L1 and L2 are 10.02 ± 0.02 and 10.05 ± 0.04 respectively (calculated for H_2O). These values represent a mean value for successive deprotonation steps of the two uracil ligands. Individual pK_a values should then be ca. ≥ 9.72 and ≤ 10.32 for L1 and ca. $\underline{\geq}$ 9.75 and $\underline{\leq}$ 10.35 for L2. A representative graph of the ^{1}H NMR chemical shifts (δ, ppm) versus pD of the solution for ligand L2 is provided

in Figure 4.1. As compared to 1-methyluracil (pK_a = 9.63 ± 0.05[13]), the ligands L1 and L2 are thus somewhat less acidic.

4.4. Reaction of *cis*-$(Ph_3P)_2Pt^{II}$ with L1: synthesis of hybrid

Reaction of $PtCl_2$(COD) with an excess of L1 (3 equiv) in the presence of PPh_3 (2 equiv) and excess of Ag_2O in refluxing CH_2Cl_2 for 24 h yielded the metallacycle *cis*-[$Pt(PPh_3)_2$(L1'-*N3*)]$_2$·4H_2O (**20**) (with L1' = dianion of bis(1-methyluracil-5-yl)methane (L1)). Single crystals were obtained upon slow evaporation of a $CHCl_3$/MeOH solution. The ^{1}H as well as $^{31}P\{^1H\}$ NMR spectra of **20** in $CDCl_3$ are fully consistent with the presence of a single, highly symmetrical species in solution. Chemical shifts (δ, ppm) are as follows: N(1)CH_3, 2.77 s, C(6)H, 6.93 s, CH_2, 3.13 s, Ph, 7.0–7.25, 7.60 m. [This reaction was originally carried out by a former post doctoral student Dr. Neeladri Das in our group. After his leaving, I repeated this reaction to calculate its yield and also to get elemental analysis data.] The neutral molecule **20** consists of two *cis*-$Pt^{II}(PPh_3)_2$ moieties and two dianions of L1. Two different views of **20** are provided in Figure 4.2. The two *cis*-$Pt(PPh_3)_2$ entities are connected to the deprotonated N3 sites of two L1 ligands, leading to the formation of an "open molecular box". The four uracil rings adopt a 1,3-alternate conformation. The two Pt atoms and the two C atoms of the methylene bridges are co-planar. The four uracil rings are almost perpendicular to this plane (79.3(2)° and 78.9(2)°). Within each diuracilate entity the methyl groups adopt a transoid orientation. The distance between the two Pt atoms is 9.0264(7) Å, that between the two CH_2 groups 6.508(17) Å.

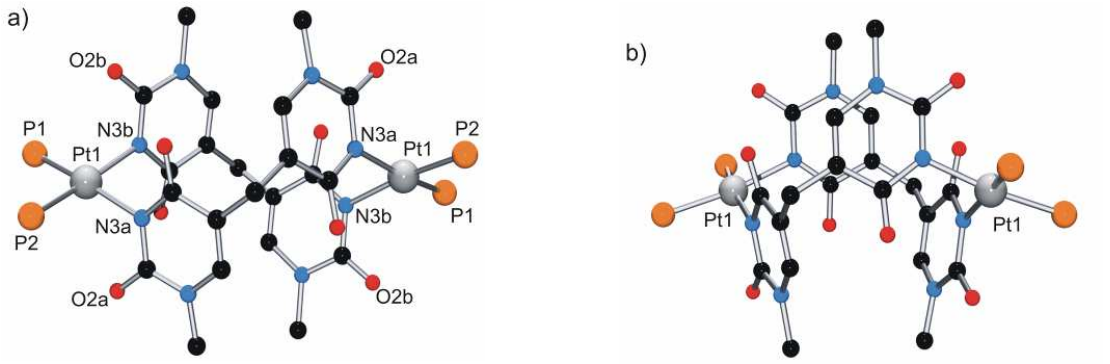

Figure 4.2: Views of the molecular structure of **20**. Ph_3 groups attached to P have been omitted for clarity.

4.5. Reaction of (2,2'-bpy)Pt^{II} with L1 and L2

Reaction of [Pt(2,2'-bpy)$(H_2O)_2$]$(NO_3)_2$ with L1 in water (1:1 ratio) yielded a Pt_4 "open molecular box" {[Pt(2,2'-bpy)]$_2$(L1'-*N3*,*O4*)}$_2(NO_3)_4 \cdot 8H_2O$ (**21**) (with L1' = dianion of L1). In contrast to L1, ligand L2 does not produce a cyclic complex when reacted with [Pt(2,2'-bpy)$(H_2O)_2$]$(NO_3)_2$. Rather it leads to the formation of an acyclic complex {[(2,2'-bpy)Pt]$_2$(L2'-*N3*,*O4*)$_2$}$(NO_3)_2 \cdot 41H_2O$ (**22**) (with L2' = monoanion of L2). X-ray quality red colored crystals of **21** and **22** were obtained upon slow evaporation of an aqueous solution at room temperature. A second derivative of complex **21** with different cell constant was obtained when the same reaction was carried out in different metal to ligand (2:1) ratio.

The tetranuclear complex **21** crystallizes in the orthorhombic (Fddd) space group. Figure 4.3 gives a view of the cation of **21** and selected structural features are listed in Table 4.1. The cation of **21** consists of four (2,2'-bpy)Pt^{II} entities and two L1' ligands. Each Pt is simultaneously bonded to a deprotonated N3 position of L1 ligand and to an O4 site in a *head-tail* fashion. The complex **21** can be considered as extended calix[4]arene in which exocyclic O4 sites of uracil rings also take part in metal coordination. As in complex **20**, the uracil moieties retain the transoid orientation of the N(1)CH_3 groups and the overall 1,3-alternate conformation of the uracil rings. The distance between N-methyl groups is ca. 9.5 Å and that between methylene groups is ca. 6.5 Å. Distances between platinum centers across the calix core are 7.8466(14) and 7.5200(14) Å.

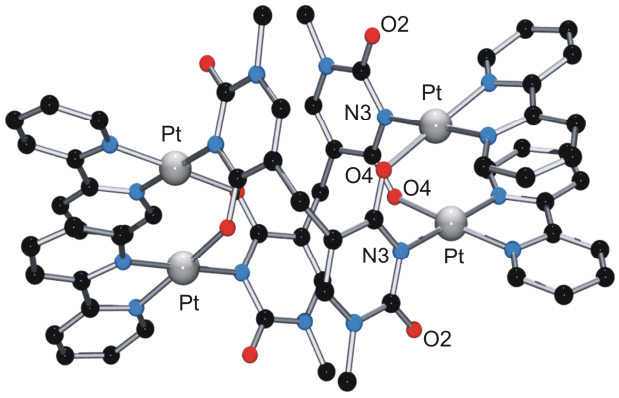

Figure 4.3: View of the molecular cation **21**. Counter anions and water molecules are omitted for clarity.

Table 4.1: Selected bond distances (Å) and angles (º) for compound **21**.

Pt1-N11, 1.989(14)	N11-Pt1-N21, 80.7(6)	N11-Pt1-N3, 99.1(6)
Pt1-N21, 2.010(13)	N21-Pt1-O4, 94.2(5)	O4-Pt1-N3, 86.1(5)

Pt1-O4, 2.023(11)	N21-Pt1-N3, 178.7(5)	N11-Pt1-O4, 174.2(5)
Pt1-N3, 2.062(13)	Pt-Pt, 2.8583(12) Å	

The 2,2'-bpy entities in complex **21** are stacked and the Pt atoms within the stacked Pt(2,2'-bpy) entities are rather close for a diplatinum(II) complex, namely 2.8583(12) Å. In the crystal packing, several cations of complex **21** are stacked on top of each other, leading to the formation of one dimensional array of 2,2'-bpy units (Figure 4.4). The intra planar spacing between these 2,2'-bpy planes is 3.75 Å, while the inter planar spacing between these 2,2'-bpy planes is 3.51 Å.

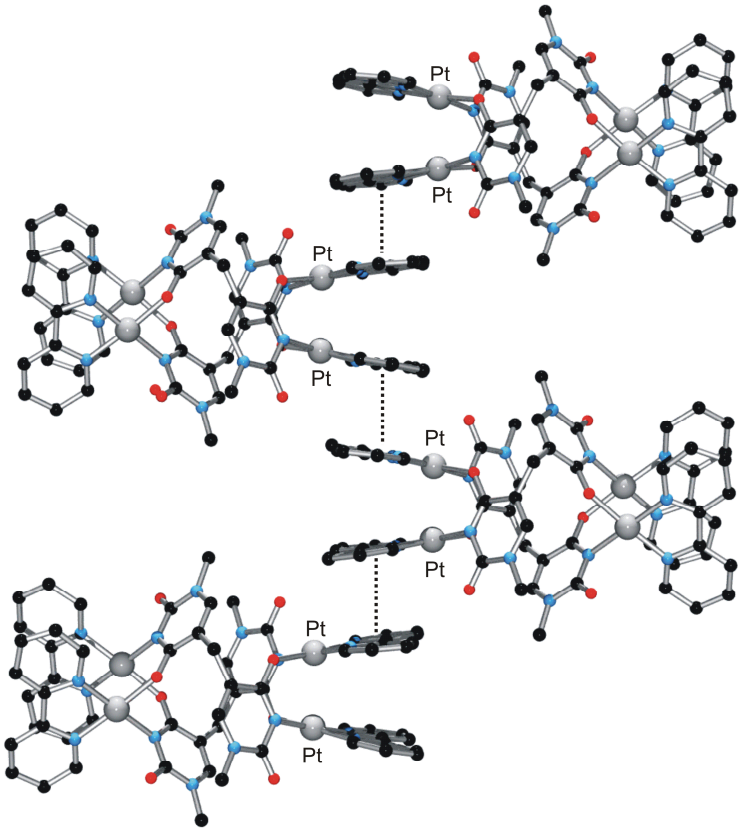

Figure 4.4: A view showing the stacking of 2,2'-bpy entities in the cations of **21**.

The dinuclear complex **22** crystallizes in the monoclinic (C2/c) space group. A view of the cation of **22** is shown in Figure 4.5. Selected structural parameters are enlisted in Table 4.2. The cation of **22** consists of two stacked (2,2'-bpy)Pt^{II} entities and two mono deprotonated L2 ligands. Only one uracil ring in L2 ligand is coordinated to Pt where as other uracil ring remains uncoordinated. Each Pt is coordinated to N3 and O4 sites in a *head-tail* arrangement. The C5 position of ligand L2' attached to the phenyl ring is chiral,

and both diastereomers, (R,R) and (S, S) are present in the crystals in 1:1 ratio. Unlike ligand L1, ligand L2 does not yield a cyclic complex with (2,2'-bpy)Pt^{II}. The steric bulk of the phenyl groups in L2 probably inhibit the formation of the metallacycle in this case. The distance between two Pt centers within the stacked Pt^{II}(2,2'-bpy) entities is 2.8588(6) Å.

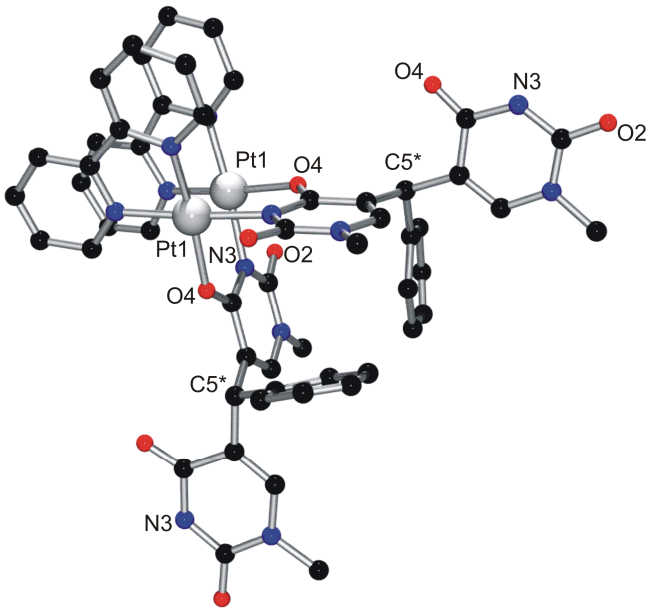

Figure 4.5: View of the molecular cation of **22**. Counter anions and water molecules are removed for clarity.

Table 4.1: Selected bond distances (Å) and angles (º) for compound **22**.

Pt1-N3A, 2.028(6)	N21-Pt1-N3A, 96.9(3)	N11-Pt1-O4A, 95.8(2)
Pt1-O4A, 2.029(5)	N21-Pt1-N11, 80.8(3)	N3A-Pt1-O4A, 86.8(2)
Pt1-N11, 2.005(6)	N11-Pt1-N3A, 176.0(3)	N21-Pt1-O4A, 173.7(2)
Pt1-N21, 1.974(6)	Pt1-Pt1, 2.8588(6)	

4.6. ^{1}H NMR spectra of compounds 21 and 22

The ^{1}H NMR spectra of complex **21** and **22** in D_2O are shown in Figure 4.6 and Figure 4.7 respectively. The integrated intensities of individual signals are consistent with the respective composition of **21** and **22**. In complex **21**, uracil-H6, N1-CH_3 and methylene protons are observed at 7.93, 3.67 and 3.69 ppm respectively. Two non-equivalent bpy–H5 doublets-of-doublets of equal intensities are observed at 7.28 and 7.62 ppm. One bpy-

H6 resonances is observed at 8.35 ppm, while the other bpy-H6 is buried under other 2,2'-bpy resonances which extend from 8.02 – 8.21 ppm.

The two uracil rings in ligand L2' of complex **22** are non equivalent, which is reflected in the ^{1}H NMR spectrum of complex **22** in D_2O. Two different resonances of equal intensities for each H(6) and N1-CH_3 groups are observed. They are appear at 7.45, 6.81 ppm (H6) and 3.41, 3.26 ppm (N1-CH_3). The benzyl proton is observed at 5.38 ppm. The resonances of 2,2'-bpy and phenyl protons are superimposed on each other and have not been identified individually.

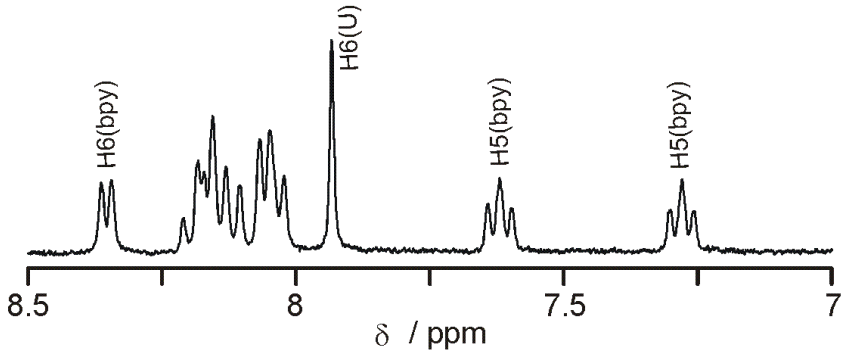

Figure 4.6: Low field ^{1}H NMR spectrum of complex **21** in D_2O.

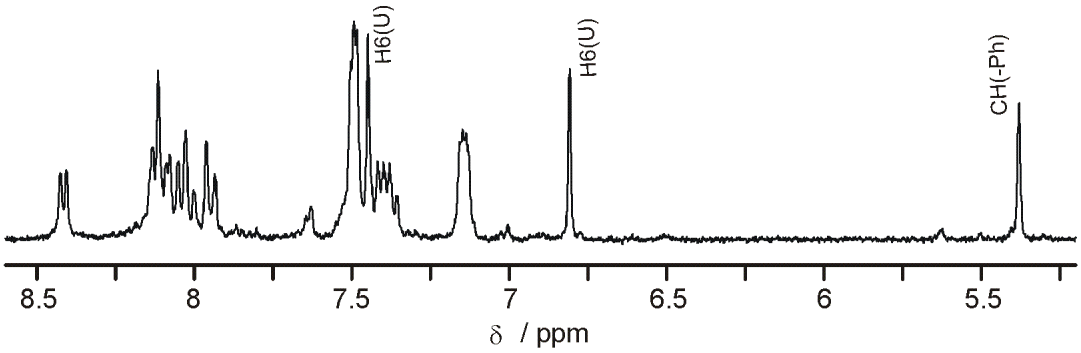

Figure 4.7: Low field ^{1}H NMR spectrum of complex **22** in D_2O.

4.7. Reaction of *cis*-$(NH_3)_2Pt^{II}$ with L1

Reaction of *cis*-$(NH_3)_2Pt^{II}$ entity with ligand L1 is very interesting because its reaction is highly dependent on reaction conditions such as concentration of reactants or pH of the solution. Three multinuclear complexes of different compositions were isolated from the reaction of *cis*-$[Pt(NH_3)_2(H_2O)_2]^{2+}$ with ligand L1 (*r* = 2:1), depending on reaction

conditions. Preliminary structural analyses showed that they have the following composition: {[*cis*-$(NH_3)_2Pt]_4$(L1'-*N3*,*O4*)$_2$}$(NO_3)_4$ (**23**), {[*cis*-$(NH_3)_2Pt]_4$(L1'-*N3*,*O4*)(L1'-*N3*,*O4,O2*)}$(NO_3)_4$ (**24**), and {[*cis*-$(NH_3)_2Pt]_4$(L1'-*N3*,*O4*)$_2$} {[*cis*-$(NH_3)_2Pt]_4$(L1'-*N3*,*O4*)(L1'-*N3*,*O4,O2*)}$(NO_3)_8$ (**25**). A typical ^{1}H NMR spectrum of a reaction mixture of *cis*-$[Pt(NH_3)_2(D_2O)_2]^{2+}$ and L1 in D_2O isn shown in Figure 4.8. The complexity of the spectrum suggests that mixtures of species were formed during this reaction. Some of the

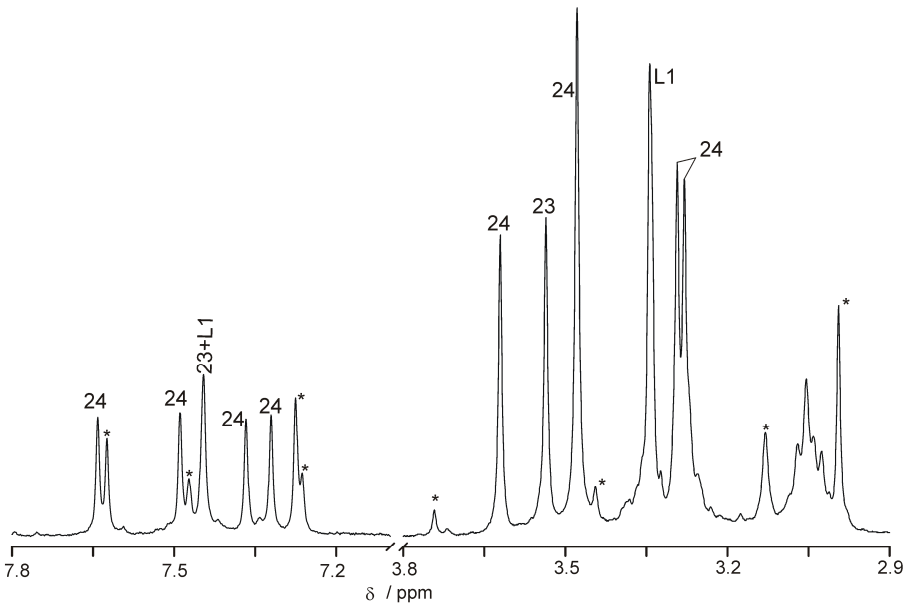

Figure 4.8: Section of ^{1}H NMR spectrum of a mixture of *cis*-$[Pt(NH_3)_2(D_2O)_2]^{2+}$ and L1 in D_2O (pD 4.8, 2d, 40 ℃).

resonances are assigned to free ligand (L1) as well as complex **23** and **24** based on the chemical shifts of isolated complexes. The species marked with (*) can not be identified at this moment. These resonances could be due to some intermediate species (either open or cyclic structures).

4.7.1. Crystal structure and ^{1}H NMR spectrum of 23

The complex {[*cis*-$(NH_3)_2Pt]_4$(L1'-*N3*,*O4*)$_2$}$(NO_3)_4$ (**23**) was prepared in water at 40 ℃ in the reaction of *cis*-$[Pt(NH_3)_2(H_2O)_2]^{2+}$ with ligand L1 (*r* = 2:1), with the *pH of the solution repeatedly adjusted to 5* by means of a 1M NaOH solution during the course of reaction. The cation of complex **23** consists of four *cis*-$(NH_3)Pt^{II}$ entities and two di-deprotonated L1' ligands. The *head-tail* arranged Pt^{II} entities are coordinated to O4 and deprotonated N3 sites of L1' ligands. A view of complex **23** is shown in Figure 4.9. The uracil rings in complex **23** adopt a 1,3-alternate conformation. The ligand L1' retains its transoid

orientation. The two uracil rings in L1' are almost perpendicular to each other: 87.4° and 88.2°. The Pt-Pt distances within each *head-tail* arranged *cis*-$(NH_3)_2Pt^{II}$ entities are 2.965 Å. The calixarene core in complex **23** is more extended as compared to complex **20** or complex **22**. The distances between N-methyl groups are ca. 10.28 Å and 10.35 Å, and that between methylene groups is ca. 6.73 Å. Distances between the platinum centers across the calix core are ca. 7.32 and 7.24 Å. Several hydrogen bonding interactions among NH_3 groups, non coordinated exocyclic oxygens, water of crystallization and nitrate anions are observed in the crystal packing.

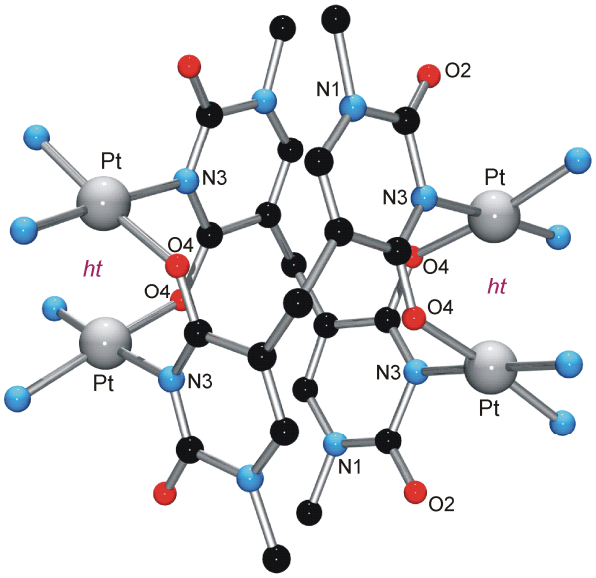

Figure 4.9: View of cation of **23**.

The ^{1}H NMR spectrum of the tetranuclear complex {[*cis*-$(NH_3)_2Pt]_4$(L1'-*N3*,*O4*)$_2$}$(NO_3)_4$ (**23**) in D_2O is shown in Figure 4.10. **23** displays its ^{1}H NMR resonances (δ, ppm, D_2O) at 7.45, 3.54 and 3.08 ppm. Because of the symmetrical coordination mode of both uracil rings in the L1' ligands, one set of resonances is observed in the ^{1}H NMR spectrum.

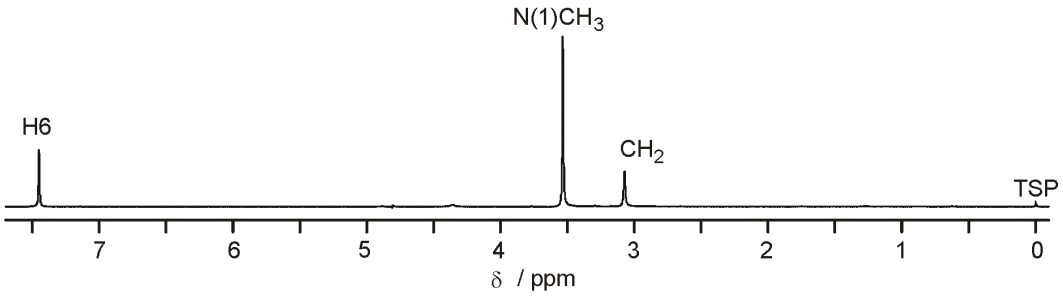

Figure 4.10: ^{1}H NMR spectrum of complex **23** in D_2O (TSP as internal reference).

4.7.2. Synthesis and characterization of 24 and 25

Reaction of *cis*-$[Pt(NH_3)_2(H_2O)_2](NO_3)_2$ entities with ligand L1 at 2:1 ratio in water yielded the tetranuclear complex {[*cis*-$(NH_3)_2Pt]_4$(L1'-*N3*,*O4*)(L1'-*N3*,*O4,O2*)}$(NO_3)_4$ (**24**). Because of the presence of four non-equivalent uracil rings in complex **24** (unsymmetrical coordination modes of ligand L1') (see Figure 4.12 for its crystal structure), four uracil-H6 singlets of equal intensities are expected to be observed in its ^{1}H NMR spectrum. However, the ^{1}H NMR spectrum of isolated solids in D_2O (Figure 4.11) shows the presence of five uracil-H6 resonances, one of which (7.45 ppm) can be identified as complex **23**. So the other four resonances at 7.65, 7.50, 7.37 and 7.32 ppm are assigned to four different uracil-H6 protons in complex **24**. This clearly suggests that both **23** and **24** are formed simultaneously in this reaction, and depending on the reaction conditions either **23** or **24** can be isolated, and occasionally even **25**. The cation of **25** contains simultaneously cations of tetranuclear **23** *and* **24** (see below). The appearance of five uracil-H6 singlets (in Figure 4.11) in almost 1:1:1:1:1 ratio tentatively suggests that complex **24** is formed in great excess compared to complex **23**.

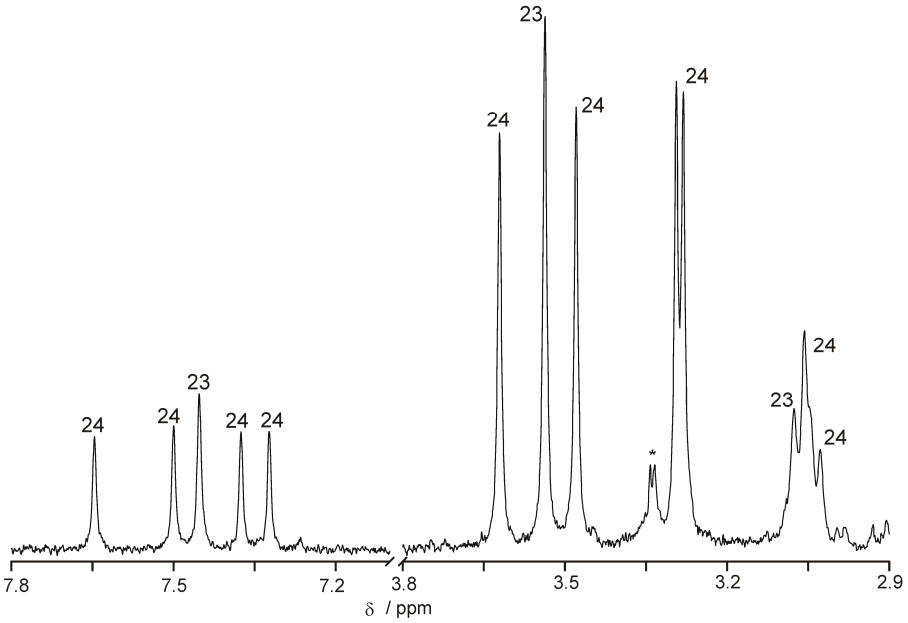

Figure 4.11: Section of ^{1}H NMR spectrum of isolated solid from the reaction of *cis*-$[Pt(NH_3)_2(H_2O)_2](NO_3)_2$ and L1 (*r* = 2:1) in water (pH adjusted to 5 at start of reaction), 40 ℃. (* unknown impurity)

A view of the tetranuclear cation **24** is shown in Figure 4.12. The cation consists of four *cis*-$(NH_3)Pt^{II}$ entities and two di-deprotonated L1' ligands. The two *cis*-$(NH_3)Pt^{II}$ entities (Pt1, Pt2) are coordinated to N3 and O4 sites of uracil in L1' ligands in *head-tail* orientations. The two other *cis*-$(NH_3)Pt^{II}$ units (Pt3, Pt4) are coordinated to the uracil rings

in *head-head* arrangement. The ligand retains its transoid orientation and the uracil rings are arranged in 1,3-alternate conformation. The Pt-Pt separations (Pt1-Pt2, 2.911 Å; Pt3-Pt4, 2.925 Å) are shorter as compared to complex **23**. The distances between N-methyl groups are ca. 9.221 Å, 9.170 Å and between methylene groups are ca. 6.883 Å apart. Distances between platinum centers across the calix core ca. 7.95 and 7.74 Å. Perfect square-planar coordination geometries are observed around Pt1 and Pt2, whereas Pt3 and Pt4 deviate from the ideal situation: O4-Pt1-N3, 90.05°; O4-Pt2-N3, 90.10; N3-Pt3-N3, 85.86° and O4-Pt4-O2, 93.62°.

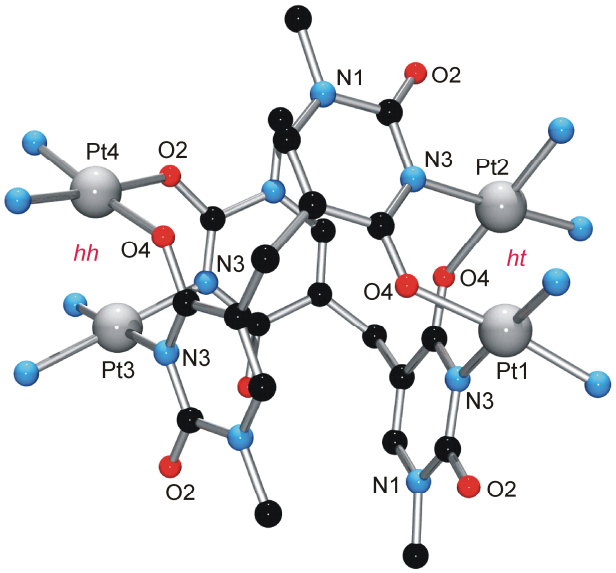

Figure 4.12: View of cation **24**.

The cation of complex **25** is composed of two different tetranuclear units, namely the cation of **24**, $\{[cis\text{-}(NH_3)_2Pt]_4(L1'\text{-}N3,O4)(L1'\text{-}N3,O4,O2)\}^{4+}$ and the cation of **23**, $\{[cis\text{-}(NH_3)_2Pt]_4(L1'\text{-}N3,O4)_2\}^{4+}$. The structural features of these two tetranuclear units in complex **25** are similar to the individual cations **24** and **23**. The uracil rings adopt 1,3-alternate conformations and the ligand L1' retains its transoid orientation. In the crystal packing of complex **25**, one of the eight nitrate anions is perfectly stacked between two uracil rings (A and B), showing a typical anion-π interaction.[14] A view of cation **25** with a nitrate anion stacked between two different tetranuclear units, is shown in Figure 4.13. The distances from the centroid of uracil ring A and ring B to the plane of the NO_3^- anion are 3.037 Å and 3.258 Å.

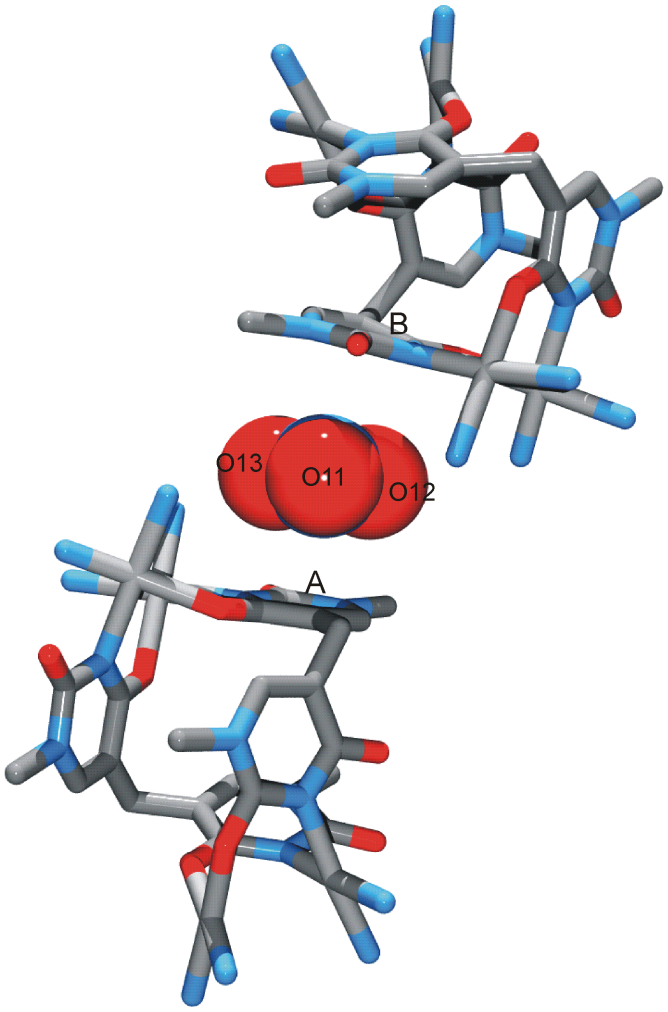

Figure 4.13: View of cation **25** with one of its nitrate anions stacked between two uracil rings from two different tetranuclear units.

4.8. Conclusion

Reaction of uracil based ditopic ligand L1 with different *cis*-a_2Pt^{II} entities produces a series of multinuclear complexes. These metallacycles are termed hybrids between classical calix[4]arenes and metallacalix[4]arenes because they contain both bridging methylene groups and *cis*-a_2Pt^{II} entities. Depending on the steric requirements of the co-ligands at the metal center (*cis*-a_2M^{II}, M = Pt), two (**20**) or four (**21**, **23**, **24**) metal entities can be accommodated, leading to neutral (**20**) or cationic (**21**, **23**, **24**) complexes. Moreover the steric bulk of the ligand L (L1 vs L2) dictates the final shape of the metal complex – tetranuclear metallacycle (**21**) in case of ligand L1 and dimeric, yet acyclic metal complex (**22**) in case of ligand L2 using the same metal corner unit Pt^{II}(2,2'-bpy). This has been

attributed to steric congestion caused by the phenyl ring. Reaction of *cis*-$(NH_3)_2Pt^{II}$ entity with L1 produces cyclic complexes (**23**, **24**, **25**) of different composition depending on concentration and pH of the solution.

4.9. References

[1] a) C. D. Gutsche, *Calixarenes*, The Royal Society of Chemistry, Cambridge, **1989**; b) C. D. Gutsche, *Calixarenes Revisited*, The Royal Society of Chemistry, Cambridge, **1998**.

[2] a) A. Ikeda, S. Shinkai, *Chem. Rev.* **1997**, *97*, 1713–1734; b) J. S. Kim, D. T. Quang, *Chem. Rev.* **2007**, *107*, 3780–3799; c) L. Baldani, A. Casnati, F. Sansone, R. Ungaro, *Chem. Soc. Rev.* **2007**, *36*, 254–266; d) R. Joseph, B. Ramanujam, A. Acharya, A. Khutia, C. P. Rao, *J. Org. Chem.* **2008**, *73*, 5745–5758.

[3] a) H. Rauter, E. C. Hillgeris, B. Lippert, *J. Chem. Soc., Chem. Commun.* **1992**, 1385–1386; b) H. Rauter, E. C. Hillgeris, A. Erxleben, B. Lippert, *J. Am. Chem. Soc.* **1994**, *116*, 616–624.

[4] a) Z. Qin, M. C. Jennings, R. J. Puddephatt, *Inorg. Chem.* **2002**, *41*, 3967–3974; b) M. J. Rauterkus, B. Krebs, *Angew. Chem. Int. Ed.* **2004**, *43*, 1300–1303.

[5] A. R. Navarro, E. Freisinger, B. Lippert, *Inorg. Chem.* **2000**, *38*, 2301–2305.

[6] E. Barea, J. A. R. Navarro, J. M. Salas, M. Quirós, M. Willermann, B. Lippert, *Chem. Eur. J.* **2003**, *9*, 4414–4421.

[7] E. Gil Bardají, E. Freisinger, B. Costisella, C. A. Schalley, W. Brüning, M. Sabat, B. Lippert, *Chem. Eur. J.* **2007**, *13*, 6019–6039.

[8] a) H. Rauter, I. Mutikainen, M. Blomberg, C. J. L. Lock, P. Amo-Ochoa, E. Freisinger, L. Randaccio, E. Zangrando, E. Chiarparin, B. Lippert, *Angew. Chem. Int. Ed.* **1997**, *36*, 1296–1301; b) J. A. R. Navarro, E. Freisinger, B. Lippert, *Eur. J. Inorg. Chem.* **2000**, 147–151.

[9] J. A. R. Navarro, M. B. L. Janik, E. Freisinger, B. Lippert, *Inorg. Chem.* **1999**, *38*, 426–432.

[10] J. A. R. Navarro, E. Freisinger, B. Lippert, *Inorg. Chem.* **2000**, *38*, 2301–2305.

[11] M. A. Galindo, D. Olea, M. A. Romero, J. Gómez, P. del Castillo, M. J. Hannon, A. Rodger, F. Zamora, J. A. R. Navarro, *Chem. Eur. J.* **2007**, *13*, 5075–5081.

[12] S. Kumar, V. Malik, N. Kaur, K. Kaur, *Tetrahedron Lett.* **2006**, *47*, 8483–8487.

[13] C. F. Moreno-Luque, E. Freisinger, B. Costisella, R. Griesser, J. Ochocki, B. Lippert, H. Sigel, *J. Chem. Soc., Perkin Trans. 2*, **2001**, 5005–5011.

[14] P. Gamez, T. J. Mooibroek, S. J. Teat, J. Reedijk*, Acc. Chem. Res.* **2007**, *40*, 435–444.

5. Influence of Metal (Pt^{II}, Pd^{II}) Coordination on the Equilibrium of 2,2'-Dipyridylketone (dpk) with its Hydrated *gem*-Diol Form (dpk·H_2O)

5.1. Introduction

Di-2-pyridyl ketone (dpk), a widely used ligand in metal coordination chemistry,[1,2] can act as monodentate, chelating or bridging ligand, depending on the metal ions and the nature of anions (Scheme 5.1). It can also undergo nucleophilic addition of solvent during reaction

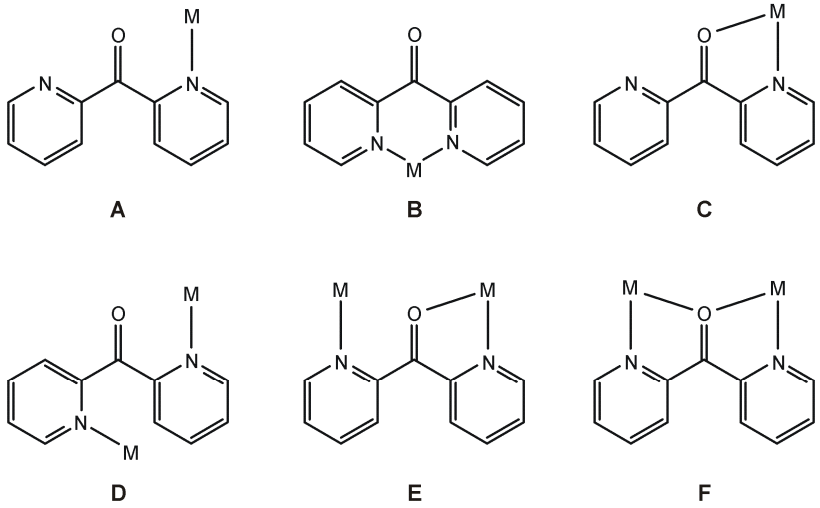

Scheme 5.1: Different coordination modes of 2,2'-dipyridylketone (dpk)

on its carbonyl group, leading to the formation of solvated forms of 2,2'-dipyridyl ketone.[3] When reaction is carried out in water, the hydrated form, known as the geminal diol form is generated (Scheme 5.2). A geminal diol is any organic compound, having two hydroxyl groups (-OH) at the same carbon atom. There is always an equilibrium between ketone and its hydrated form in aqueous solution. The equilibrium constant for the conversion of formaldehyde to methanediol is 10^3 while that of hexafluoroacetone to its hydrated form is 10^6. The strongly electron withdrawing nature of the CF_3 group increases the electrophilic nature of the carbonyl group and thus shifts the equilibrium in favor of its hydrated form. Some organic compounds such as decahydroxycyclopentane and dodecahydroxycyclohexane are stable only in their geminal diol form. The electrophilic nature of carbonyl groups can also be increased by metal coordination to the carbonyl oxygen (direct polarization) or by metal coordination to another site (induced polarization).[1a] In case of di-4-pyridyl ketone, the hydration at the carbonyl carbon atom

occurs to remove the ring strain after metal coordination.[4] However, it is not surprising to find both di-2-pyridyl ketone (dpk) and its hydrated form (dpk·H_2O) within the same multinuclear complexes.[5]

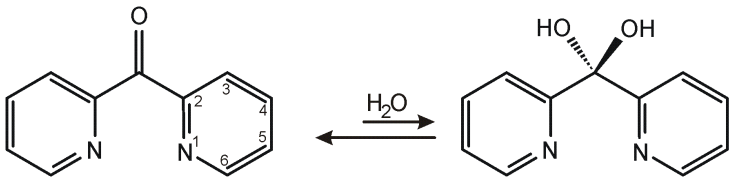

Scheme 5.2: Conversion of dpk into dpk·H_2O in presence of H_2O.

The aim of this chapter is to understand the solution behavior of the free ligand di-2-pyridylketone and its diaqua complexes $[M(dpk)(H_2O)_2]^{2+}$ (M = Pt^{II} and Pd^{II}), and in particular to rationalize their ^{1}H NMR spectra. As will be shown below, the formation of the *gem*-diol form is rapid in the case M = Pd^{II} because of its fast kinetics. In contrast, with M = Pt^{II} the conversion from dpk to its *gem*-diol form is slow, allowing the separation of μ-OH bridged trinuclear hydrolysis product containing two dpk·H_2O ligands and a dpk ligand simultaneously.

5.2. ^{1}H NMR spectra of free ligand

The ^{1}H NMR spectrum of the free ligand dpk in DMSO-d_6 displays the characteristic signal patterns of pyridyl rings substituted at the 2-position[6] (Figure 5.1). The chemical shifts (δ)

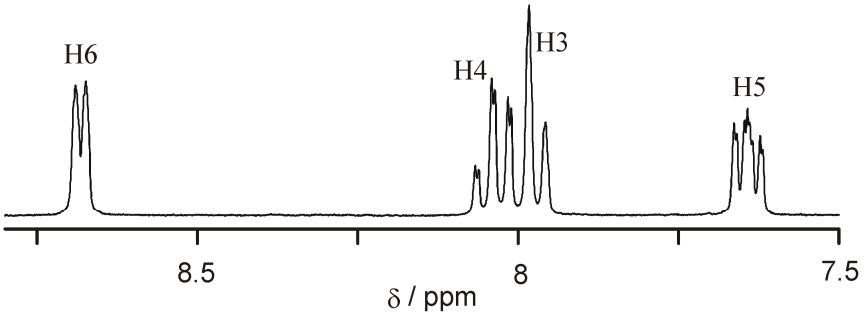

Figure 5.1: ^{1}H NMR spectrum of di-2-pyridylketone in DMSO-d_6.

with coupling constant for different protons are: H6 at lowest field (8.66 ppm, d, ^3J = 4.8 Hz), H4 (8.03 ppm, dd, ^3J = 7.5 Hz; ^4J = 1.2 Hz), H3 (7.97 ppm, d, ^3J = 7.5 Hz) and H5 (7.64 ppm, ddd, ^3J = 7.2 Hz; ^3J = 4.8 Hz; ^4J = 1.2 Hz). The H4 and H3 resonances are in part superimposed.

The ^{1}H NMR spectrum of dpk recorded in D_2O is very similar that of DMSO spectrum with little differences in chemical shifts values (H6, 8.65 ppm; H5, 7.73 ppm; H4, 8.10 ppm; H3, 8.06 ppm). However, in contrast to the DMSO spectrum, a number (at least six) of minor resonances (d, ddd) are observed. Intensities of these minor resonances are *ca.* 3 – 5% of those of the main resonances (Figure 5.2). This observation clearly suggests that addition of H_2O to the carbonyl group of dpk occurs even in the absence of a metal. So the equilibrium constant for the conversion of dpk to dpk·H_2O is *ca.* 0.04 (dpk + H_2O $\rightleftharpoons$ dpk·H_2O). The appearance of more than four minor peaks in the ^{1}H NMR spectrum is due to the fact that the free dpk·H_2O ligand exists in more than one conformation, which do not interconvert quickly on the NMR time scale.

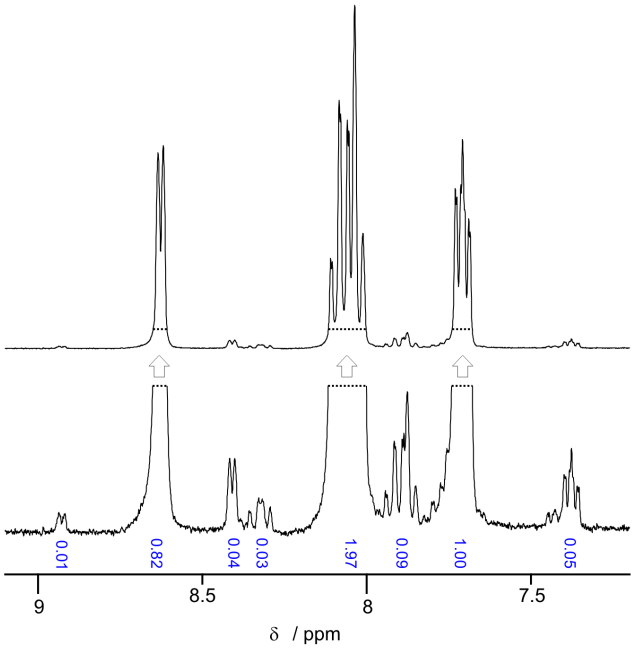

Figure 5.2: Low field section of the ^{1}H NMR spectrum of dpk in D_2O. Resonances of the minor species are assigned to dpk·D_2O.

5.3. Synthesis and crystal structure of $[Pd(dpk·H_2O)_2](NO_3)_2·2H_2O$ (26)

The reaction of $[PdCl_2(dpk·H_2O)]$ (**27**, see below) with 2 equivalents $AgNO_3$ in water produces $[Pd(dpk·H_2O)_2](NO_3)_2·2H_2O$ (**26**) in good yield. The fact that we have obtained the 1:2 complex **26** from a 1:1 starting compound (**27**) is a clear indication that a symmetrization reaction of the type $[Pd(dpk·H_2O)(H_2O)_2]^{2+}$ $\rightleftharpoons$ $0.5[Pd(dpk·H_2O)_2]^{2+}$ + $0.5[Pd(H_2O)_4]^{2+}$ takes place. Slow evaporation of an aqueous solution of **26** at room temperature produces colorless crystals. The complex **26** crystallizes in the monoclinic

($P2_1/c$) space group. Two different views of cation **26** are shown in Figure 5.3. Selected structural features are listed in Table 5.1. The cation of **26** is closely similar to that of the reported Cl^- [7] and ClO_4^- salts.[8] Pd-N distances are (2.018(2) and 2.034(2) Å) in the usual range. Pd has also two weak contacts with the O1 atoms of the hydroxyl groups (2.826(2) Å) and consequently Pd has a (4+2) coordination geometry. The two pyridine rings of dpk·H_2O are at an angle of 64° and the C12-C4-C22 angle is with 109.0(2)° close to the ideal tetrahedral angle. The pairs of pyridine rings in **26** are partially intramolecularly stacked, and the H6 atoms of the pyridine rings fall within the π-electron systems of adjacent pyridine rings. The perpendicular lines from H6 to the pyridine planes, with which the H6 protons stack, are 2.57 (H26 to ring 1) and 2.56 Å (H16 to ring 2).

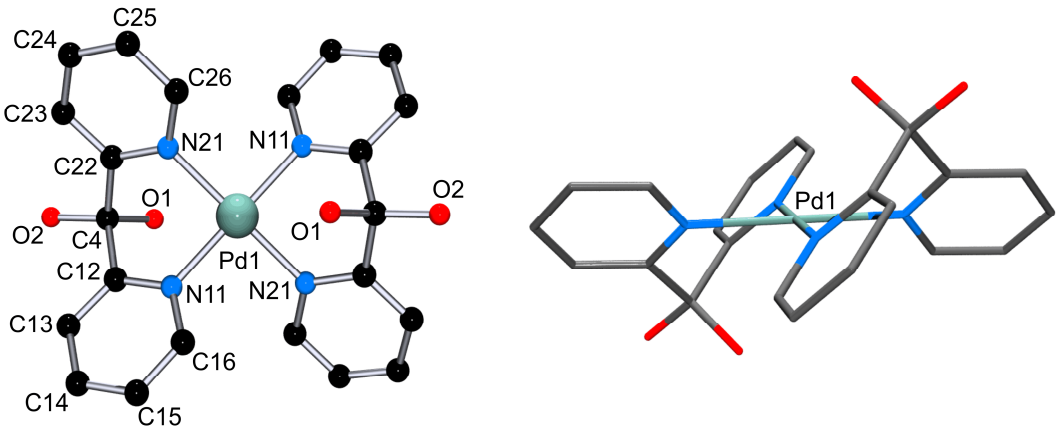

Figure 5.3: Top and side views of the cation of compound **26** with atom numbering scheme.

Table 5.1: Selected bond distances (Å) and angles (º) for compound **26**.

Pd1-N11, 2.018(2)	N11-Pd1-N21, 92.77(8)	N11-Pd1-N11, 180.00(11)
Pd1-N21, 2.034(2)	N11-Pd1-N21, 87.23(8)	N21-Pd1-N21, 180
Pd1-O1, 2.826(2)	-	C12-C4-C22, 109.0(2)

5.4. ^{1}H NMR spectrum of [Pd(dpk·H_2O)$_2$](NO$_3$)$_2$·2H_2O (26)

The ^{1}H NMR spectrum of **26** in D_2O consists of two sets of resonances: Intense ones (**I**), which are attributed to complex **26**, and very minor ones (**II**), which have relative intensities of *ca.* 2% of the intense ones. The H5 signal of **26** (**I**) is observed at 7.51 ppm (ddd, ^3J = 7.6 Hz; ^3J = 5.5 Hz; ^4J = 1.8 Hz). The signals of the three other protons overlap strongly and occur between 8.23 – 8.28 ppm. The H6 resonance of **26** is shifted upfield

relative to that of free dpk. The observed upfield shift of H6 is a consequence of partial intramolecular stacking between pyridyl entities, which affects H6 most. The ^{1}H NMR spectrum of **26** in DMSO-d_6 is provided in Figure 5.4. It also shows the existence of two species **I** and **II** in this solvent. The relative intensities of the minor component **II** amount to

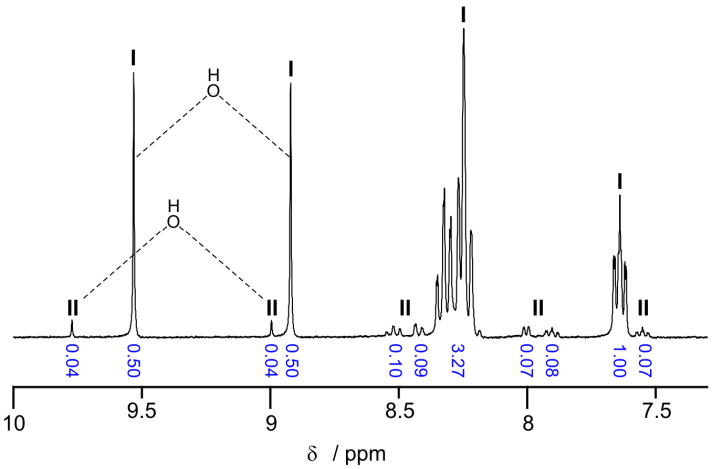

Figure 5.4: Low field section of ^{1}H NMR spectrum of **26** in DMSO-d_6 and integrals of individual resonances.

ca. 7 – 8%. The H5 resonance of **I** appears at 7.64 ppm, whereas H6, H4 and H3 overlap between 8.18 – 8.35 ppm. The two singlets at 8.92 and 9.53 ppm are attributed to the OH protons of the dpk·H_2O ligand. The OH groups pointing towards the Pd appear further downfield (9.53 ppm). The minor species **II** is assigned to a mixed ligand complex, $[Pd(dpk{\cdot}H_2O)(dpk)]^{2+}$. This assignment is based on the following arguments: First, two OH resonances of 1:1 intensity occurs at 8.99 and 9.77 ppm. Second, for the two non-equivalent ligands, eight sets of pyridyl resonances are to be expected. At least six sets of pyridyl resonances of the proper relative intensities can be differentiated. Third, there is no pyridine resonance in the range > 8.5 ppm as typically seen for 1:1 complexes with either dpk or dpk·H_2O ligands, thus strongly implying structures in which the H6 resonances are exposed to the π-systems of the pyridyl rings. This observation suggests that complex **26** exists in solution in equilibrium with a small amount of the mixed-ligand species, hence $[Pd(dpk{\cdot}H_2O)_2]^{2+} \rightleftharpoons [Pd(dpk{\cdot}H_2O)(dpk)]^{2+} + H_2O$. In DMSO-$d_6$ the amount of the mixed ligand species **II** is higher than in D_2O. A possible reason of this finding is that the hygroscopic nature of DMSO shifts the equilibrium to the right.

5.5. Synthesis of [$PdCl_2$(dpk·H_2O)] (27)

[$PdCl_2$(dpk·H_2O)] (**27**) was prepared via three different routes: (a) By reaction of K_2PdCl_4 with 1 equiv of dpk, (b) by reaction of [Pd(dpk·$H_2O)_2$]($NO_3)_2$ (**26**) with 1 equiv of K_2PdCl_4, and (c) by reaction of $PdCl_2$ with dpk, as reported in the literature.[3] Single crystals were obtained from an aqueous solution (prepared according to (b)), and proved to be **27** by X-ray analysis and comparison with the reported X-ray structure in the literature.[3] The IR spectra of products obtained through routes (a) and (b) were completely identical, with the most intense absorptions at 3353 and 3259 cm^{-1} (*v* OH). The product obtained according to procedure (c) displayed major differences in its IR spectrum (3000 – 3500 cm^{-1} range) *e.g.*, its most intense *v* OH modes were at 3353, 3253 and 3175 cm^{-1}. This suggests that route (c) produced a mixture of compounds and not exclusively **27** (see also ^{1}H NMR spectra). As will be shown below, in moist DMSO an equilibrium of species exists containing both the dpk and the dpk·H_2O ligands. This feature does not seem to explain the differences in IR spectra. Specifically, only a single IR band of moderate intensity is observed at 1605 – 1608 cm^{-1} in the Pd complexes, whereas the *v* C=O in dpk occurs at 1682 cm^{-1} and represents the most intense of all IR bands. So procedure (c) gave a mixture of [$PdCl_2$(dpk·H_2O)] (**27**) and [Pd(dpk·$H_2O)_2$][$PdCl_4$]. IR spectra of both compounds are expected to be rather similar.

5.6. ^{1}H NMR spectrum of [$PdCl_2$(dpk·H_2O)] (27)

^{1}H NMR spectra of **27** prepared via the three different routes, with DMSO-d_6 as solvent, are provided in Figure 5.5. The ^{1}H NMR spectrum of **27,** prepared according to procedure (c) and recorded immediately after dissolving the solid, unambiguously reveals the presence of [Pd(dpk·$H_2O)_2$]$^{2+}$ (I), in addition to resonances due to [$PdCl_2$(dpk·H_2O)] (III) and [$PdCl_2$(dpk)] (IV). The species I, III, and IV are present in different relative amounts in all cases. Species I has its highly characteristic OH resonances at 9.56 and 8.91 ppm, which largely disappear within 20 h. This suggests that **27**, prepared according to the literature method, contained a fraction of [Pd(dpk·$H_2O)_2$][$PdCl_4$], which symmetrizes according to [Pd(dpk·$H_2O)_2$][$PdCl_4$] $\rightleftharpoons$ 2[$PdCl_2$(dpk·$H_2O)_2$]. Both III and IV have their H6 doublets at low field (8.92 and 9.08 ppm, respectively), thereby proving the absence of π-stacking of H6. III has its other resonances at 7.54 ppm (H5), 7.96 ppm (H3), 8.10 ppm (H4), as well as 8.39 and 8.83 (OH protons). Relative signal intensities are fully consistent with this interpretation. For species IV (H5, 7.91 ppm; H3, 8.17 ppm; H4, 8.36 ppm; H6,

9.08 ppm) no resonances due to OH protons are detected and consequently the compound is assigned to a mono(chelate) complex containing the dpk ligand, hence [$PdCl_2$(dpk)]. The spectrum of IV is quantitatively very similar to that of the Pt analogue **28**.

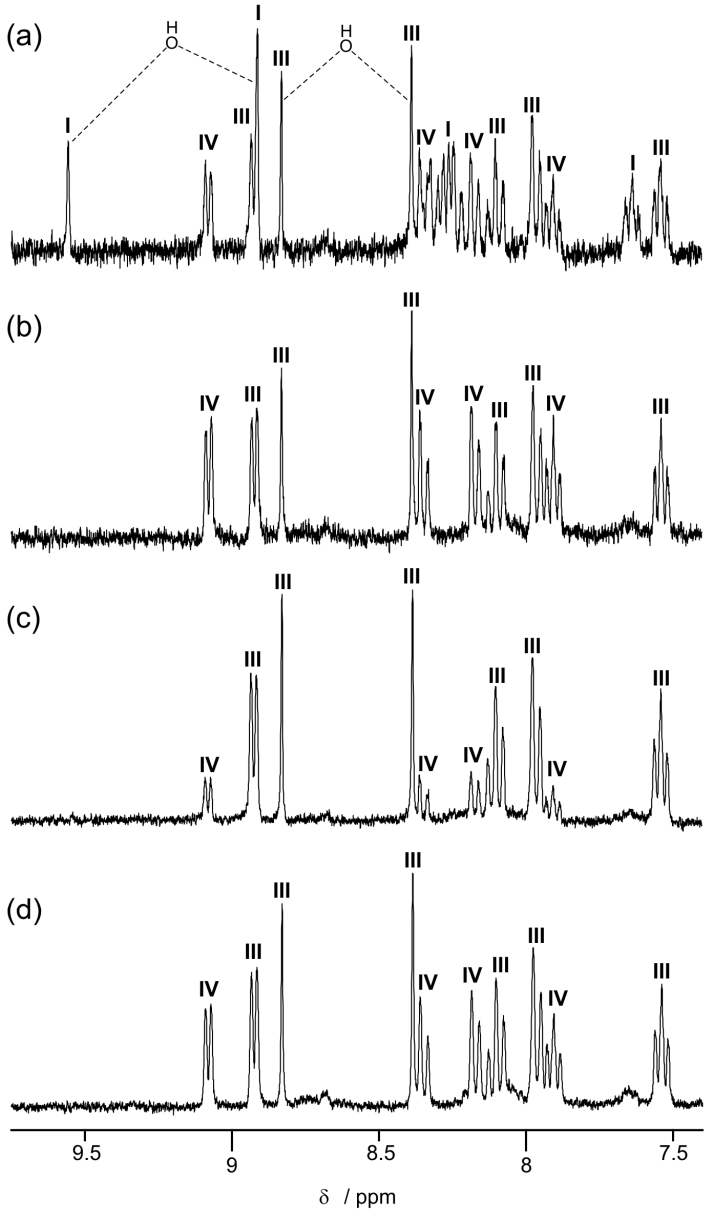

Figure 5.5: Low field sections of ^{1}H NMR spectra of (a) **27** (prepared according to procedure (c)) immediately after dissolving and (b) after 16 h, (c) **27** (prepared according to procedure (a)) after 1 h and (d) **27** (prepared from [$Pd(dpk·H_2O)_2$]$(NO_3)_2$ (**26**) and K_2PdCl_4, procedure (b)) immediately after dissolving in DMSO-d_6.

5.7. Synthesis and ^{1}H NMR spectrum of [$PtCl_2$(dpk)] (28)

[$PtCl_2$(dpk)] (**28**) was prepared from K_2PtCl_4 and dpk in water as described in the literature.[5] **28** displays in its ^{1}H NMR spectrum (DMSO-d_6) a more pronounced separation

of the individual pyridyl resonances than in the free ligand. The H6 doublet occurs at 9.12 ppm, the ddd of H4 is centered at 8.38 ppm, the H3 doublets is at 8.16 ppm, and the ddd of H5 is highest upfield at 7.88 ppm. There are several sets of minor pyridyl resonances (few %), one of which can be identified as that of free dpk. Platinum complexes having Pt-Cl bonds have a tendency to undergo solvolysis when kept in coordinating solvent like DMSO. However, treatment of **28** with $AgNO_3$ (2 equiv or 4 equiv) in DMSO-d_6 gives a complicated ^{1}H NMR spectrum (Figure 5.6) which does not contain any of the resonances seen for [$PtCl_2$(dpk)] in this solvent. This observation suggests that solvolysis of Cl^- ligand is not dominant, unless Cl^- is precipitated by Ag^+. Spectra of samples of **28**, when treated with 2 or 4 equiv of $AgNO_3$ look virtually identical. Two sets of signals (V, VI) can be differentiated and are due to two species having non-equivalent pyridyl entities. The presence of two singlets at 8.70 and 9.15 ppm suggests that signals of V correspond to a dpk·H_2O ligand.

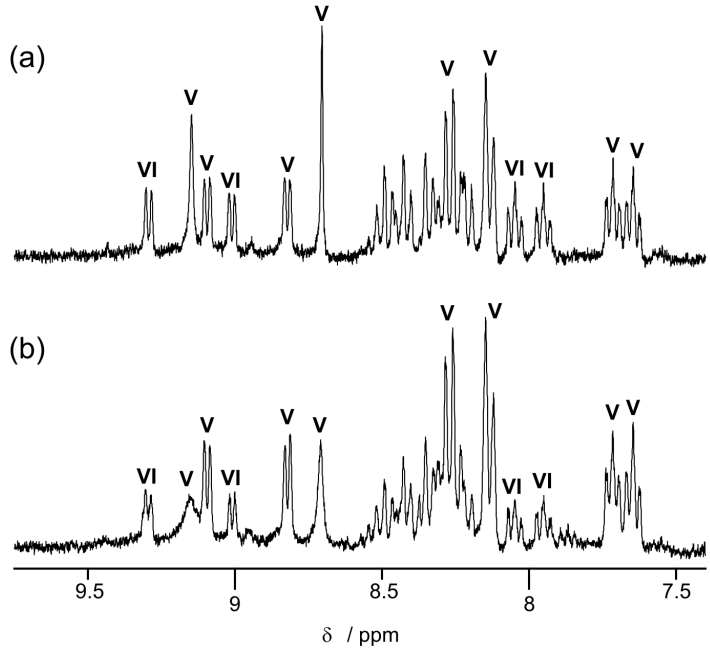

Figure 5.6: Low field sections of ^{1}H NMR spectra of a solution after treating [$PtCl_2$(dpk)] (**28**) with 2 equivalents of $AgNO_3$ (a) after 16 h (b) after 2 d in DMSO-d_6.

Treatment of [$PtCl_2$(dpk)] (**28**) with 2 equiv. $AgNO_3$ in water for 2d at room temperature (pD 2.05) gives a ^{1}H NMR spectrum which indicates the presence of two species, a major one (H5 at 7.58 ppm, ddd, 1H; *ca.* 8.20 ppm, superposition of H3 and H4, 2H; H6 at 8.66 ppm, d, 1H) and a minor one (7.87 ppm, ddd, 1H; 8.30 ppm, d, 1H, 8.38 ppm, ddd, 1H; 8.78 ppm, d, 1H). The ratio between major (VII) and minor species (VIII) amounts to *ca.* 3:1 (Figure 5.7).

The major component VII is assigned to $[Pt(D_2O)_2(dpk·H_2O)]^{2+}$ and the minor one (VIII) to $[Pt(D_2O)_2(dpk)]^{2+}$, based on the findings with $[PdCl_2(dpk·H_2O)]$ (III) and $[PdCl_2(dpk)]$ (IV) (see above), which likewise display characteristic differences in chemical shifts of the pyridyl protons in chelated dpk·H_2O and dpk.

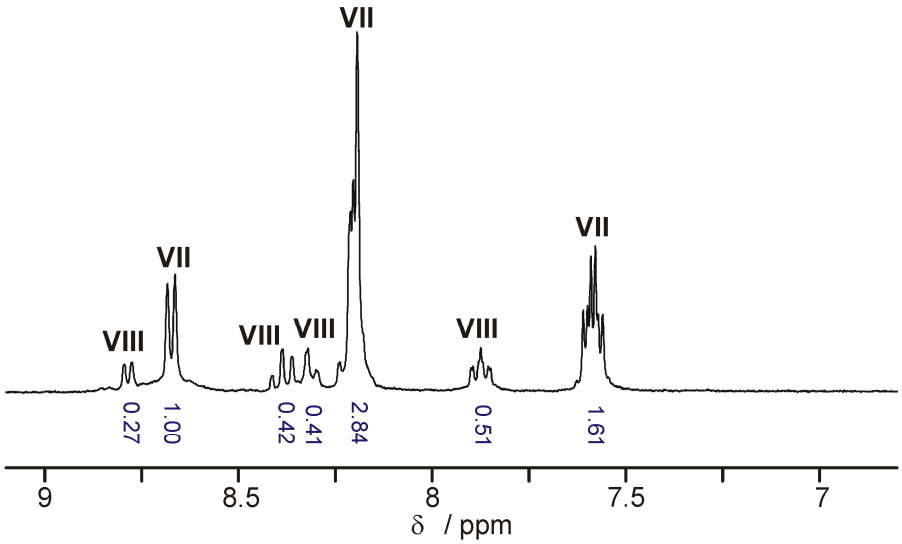

Figure 5.7: Low field section of ^{1}H NMR spectrum of a mixture obtained from $[PtCl_2(dpk)]$ (**28**) with 2 equiv. $AgNO_3$ (pD = 2.2; 40 ℃, 2 d) in D_2O.

5.8. Synthesis and crystal structure of $[Pt_3(\mu\text{-}OH)_3(dpk·H_2O)_2(dpk)](NO_3)_3·4.5H_2O$ (29)

Reaction of $[PtCl_2(dpk)]$ (**28**) with 2 equivalents of $AgNO_3$ at 60 – 70 ℃ for three days yielded the trinuclear complex $[Pt_3(\mu\text{-}OH)_3(dpk·H_2O)_2(dpk)](NO_3)_3·4.5H_2O$ (**29**). Cyclo-tri-μ-OH species derived from the antitumor agent *cis*-$[PtCl_2(NH_3)_2]$ have been known in the literature.[9,10] Slow evaporation of an aqueous solution of **29** at room temperature produces the yellow crystals. The trinuclear complex **29** crystallizes in the monoclinic (C2/c) space group. Two different views of cation **29** are shown in the Figure 5.8 and selected structural parameters are listed in Table 5.2. The X-ray crystal structure of **29** reveals that two of the three chelating ligands of the cation have undergone addition of water to give the di-2-pyridylmethanediol (*gem*-diol). The three μ-OH ligands are located on the same side of the Pt_3 plane, hence the three chelate rings adopt a cone conformation (Figure 5.8). Pt-N (1.981(7) 2.027(8) Å) and Pt-O (2.005(6) – 2.050(6) Å) distances[9,10] are normal, as are Pt···Pt distances (Pt1···Pt2, 35614(6) Å; Pt2···Pt3, 3.1738(6) Å and Pt3···Pt1, 3.2834(6) Å). The three hydroxo ligands form an almost

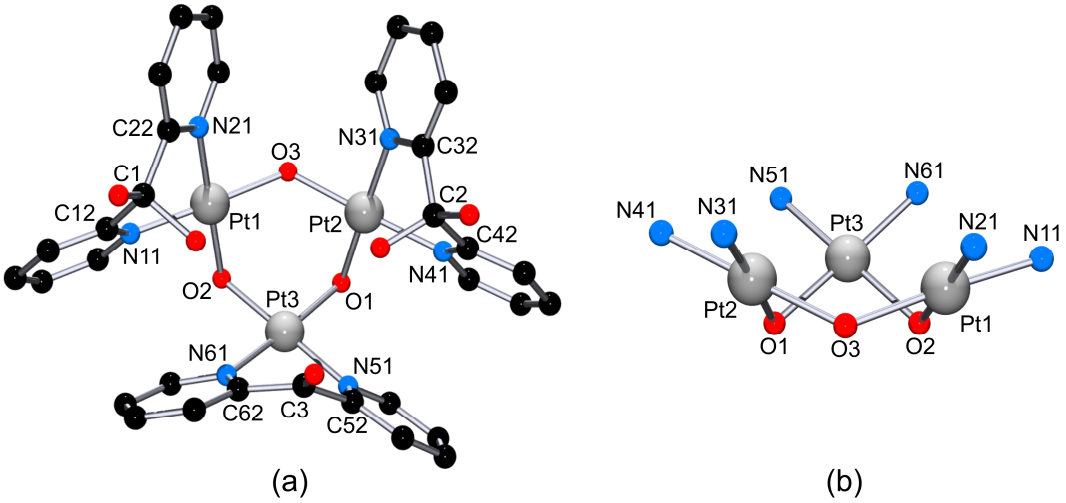

Figure 5.8: (a) View of cation **29** with atom numbering scheme. (b) View from the vector Pt3-midpoint (Pt2-Pt1). The dpk and dpk·H_2O ligands are omitted for clarity.

Table 5.2: Selected bond distances (Å) and angles (º) for compound **29**.

Pt1-N11, 1.981(7)	N11-Pt1-N21, 89.9(3)	O2-Pt3-O1, 89.5(2)
Pt1-N21, 2.006(8)	N11-Pt1-O2, 90.0(3)	N51-Pt3-Pt2, 92.0(2)
Pt1-O2, 2.031(6)	N21-Pt1-O3, 90.3(3)	O2-Pt3-Pt2, 89.01(18)
Pt1-O3, 2.031(6)	O2-Pt1-O3, 89.8(3)	N21-Pt1-O2, 178.7(3)
Pt2-N31, 2.012(9)	O3-Pt2-N31, 89.9(3)	N11-Pt1-O3, 176.8(3)
Pt2-N41, 2.027(8)	N31-Pt2-N41, 88.0(3)	O3-Pt2-N41, 177.9(3)
Pt2-O1, 2.050(6)	O3-Pt2-O1, 90.8(3)	N31-Pt2-O1, 177.8(3)
Pt2-O3, 2.005(6)	N41-Pt2-O1, 91.3(3)	N51-Pt3-O2, 178.9(3)
Pt3-N51, 1.989(8)	O3-Pt2-Pt3, 81.4(2)	N61-Pt3-O1, 174.8(3)
Pt3-N61, 1.990(8)	N51-Pt3-N61, 89.9(3)	C62-C3-C52, 119.5(8)
Pt3-O1, 2.016(6)	N61-Pt3-O2, 89.8(3)	C42-C2-C32, 108.8(9)
Pt3-O2, 2.010(6)	N51-Pt3-O1, 90.9(3)	C22-C1-C12, 115.2(9)
Pt1-Pt2, 3.5614(6)	Pt2-Pt3, 3.1738(6)	Pt3-Pt1, 3.2834(6)
O1-O2, 2.835(8)	O2-O3, 2.868(9)	O3-O1, 2.887(9)

equilateral triangle (O1···O2, 2.835(8) Å; O2···O3, 2.868(9) Å and O3···O1, 2.887(9) Å), whereas the triangle formed by the C4 positions of dpk and dpk·H_2O ligands is more irregular (4.51 – 6.36 Å). The oxygen atoms of the dpk ligand and of the closest OH

groups of the dpk·H_2O ligands form likewise an irregular triangle with distances between 3.139(9) Å and 4.027(11) Å. A comparison of the 6-ring chelates formed by the dpk and dpk·H_2O reveals the following differences: the two pyridine rings of dpk are at an angle of 42°, and the C62-C3-C52 angle is with 119.5(8)° clo se to the ideal sp^2 angle. In contrast, the two pyridine rings of the two dpk·H_2O ligands are at angles of 60° and 53°, respectively. Only the C42-C2-C32 angle (108.8(9)°) approaches the ideal sp^3 angle, whereas the corresponding angle at the other dpk·H_2O ligand (C22-C1-C12) is larger than expected (115.2(9)°).

The cation of **29** binds, at its upper periphery, one of the three nitrate anions (Figure 5.9) in the following way: One of the nitrate oxygen atoms (O11) forms hydrogen bonding contacts with hydroxo groups of the dpk·H_2O ligands (2.604(11), 2.620(12) Å), while a second nitrate oxygen (O13) is sandwiched between two pyridyl rings (distances to centroids of pyridyl rings are 3.00 and 3.16 Å), suggesting a typical anion-π interaction.[11]

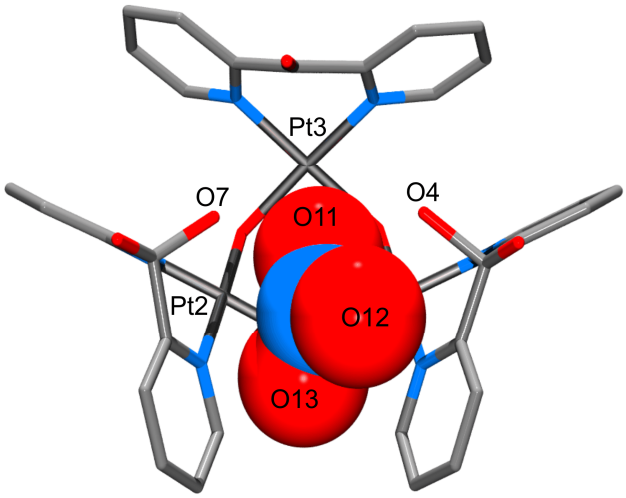

Figure 5.9: View of cation **29** with one of the three NO_3^- anions bonded at its periphery.

5.9. ^{1}H NMR spectrum of complex 29

The ^{1}H NMR spectrum of **29** displays multiple sharp resonances (d, ddd) scattered over the shift range 7.1 – 8.8 ppm (Figure 5.10). Based on relative intensities, the resonances can be separated into three sections (8.55 – 8.80 ppm: 1H; 7.72 – 8.24 ppm: 2H; 7.12 – 7.60 ppm: 1H), but a more detailed assignment is not possible. Assuming a static structure of cation **29**, three sets of pyridyl resonances could have been expected. However, a

change in dpk·H_2O $\rightleftharpoons$ dpk + H_2O equilibria or/and a partial interconversion of the $Pt_3(OH)_3$ framework could be expected to lead to a considerably larger number of resonances.

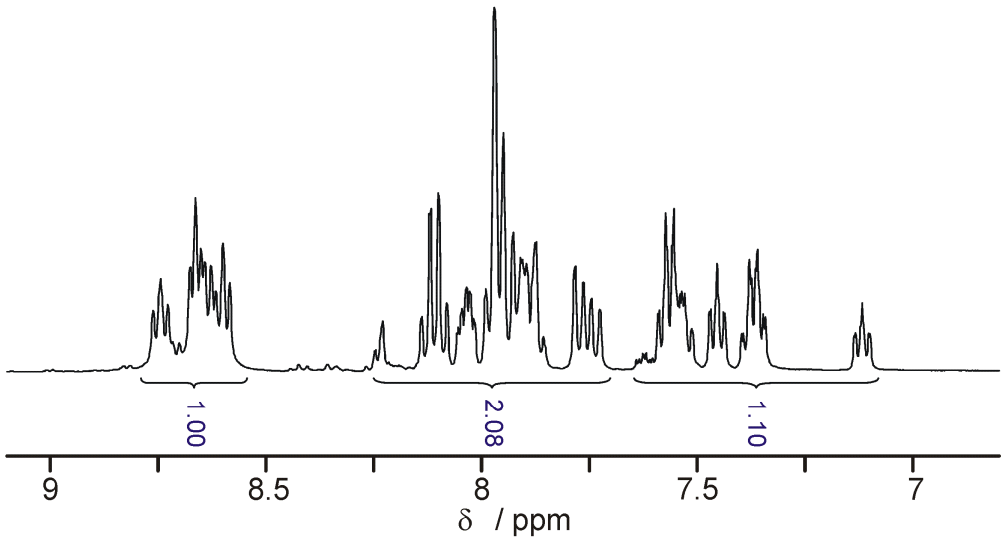

Figure 5.10: Low field section of ^{1}H NMR spectrum of crystalline **29** in D_2O with relative intensities of group of resonances given.

5.10. Conclusion

The well known equilibrium between ketones and their *gem*-diol forms has been studied for di-2-pyridylketone. The equilibrium constant, K = dpk·H_2O/dpk in D_2O has been estimated by ^{1}H NMR spectroscopy to be around 4×10^{-2}. When complexed to *cis*-$[Pt(D_2O)_2]^{2+}$, the *gem*-diol ligand dpk·H_2O becomes strongly favored and K = dpk·H_2O/dpk increases to *ca.* 3. A trinuclear Pt^{II} complex (**29**) has been isolated which contain both (dpk·H_2O) and dpk ligands. With Pd^{II} the situation is similar, hence dpk, when chelating Pd^{II}, is largely converted into dpk·H_2O in the presence of water (neat water or water content of DMSO). The crystal structure of Pd^{II} with dpk·H_2O ligands (compound **26**) seemingly suggests that there is a complete conversion to dpk·H_2O. However, this is not the case and in fact the reverse reaction Pd(dpk·H_2O) → Pd(dpk) + H_2O is likewise possible. There is an additional complication with Pd^{II} in that there are symmetrization reactions of type $[PdL_2][PdCl_4] \rightleftharpoons 2\ PdLCl_2$ (L = dpk or dpk·H_2O), which occur readily.

5.11. References

[1] a) G. S. Papaefstathiou, S. P. Perlepes, *Comm. Inorg. Chem.* **2002**, *23*, 249–274; b) T. C. Stamatatos, C. G. Efthymiou, C. C. Stoumpos, S. P. Perlepes, *Eur. J. Inorg. Chem.* **2009**, 3361–3391; c) S. Sarkar, B. Sarkar, N. Chanda, S. Kar, S. M. Mobin, J. Fiedler, W. Kaim, G. K. Lahiri, *Inorg. Chem.* **2005**, *44*, 6092–6099.

[2] J. C. Knight, A. J. Amoroso, P. G. Edwards, R. Prabaharan, N. Singh, *Dalton. Trans.* **2010**, *39*, 8925–8936.

[3] G. Annibale, L. Canovese, L. Cattalini, G. Natile, M. Biagini-Cingi, A. -M. Manotti-Lanfredi, A. Tiripicchio, *J. Chem. Soc., Dalton Trans.* **1981**, 2280–2287.

[4] M. Fujita, M. Aoyagi, K. Ogura, *Inorg. Chim. Acta* **1996**, *246*, 53–57.

[5] M. J. Rauterkus, B. Krebs, *Angew. Chem. Int. Ed.* **2004**, *43*, 1300–1303.

[6] W.-Z. Shen, G. Trötscher-Kaus, B. Lippert, *Dalton Trans.* **2009**, 8203–8214.

[7] S. O. Sommerer, A. J. Jircitano, B. L. Westcott, K. A. Abboud, J. A. Krause Bauer, *Acta Crystallogr., Sect. C* **1997**, *53*, 707–710.

[8] Y. -M. Li, X. -W. Zhao, J. -L. Zhang, *Acta Crystallogr., Sect. E* **2007**, *63*, m2585–m2585.

[9] R. Faggiani, B. Lippert, C. J. L. Lock, B. Rosenberg, *Inorg. Chem.* **1977**, *16*, 1192–1196.

[10] R. Faggiani, B. Lippert, C. J. L. Lock, B. Rosenberg, *Inorg. Chem.* **1978**, *17*, 1941–1945.

[11] P. Gamez, T. J. Mooibroek, S. J. Teat, J. Reedijk*, Acc. Chem. Res.* **2007**, *40*, 435–444.

6. Molecular Architectures Derived from Metal Ions and the Flexible 3,3'-Bipyridine Ligand. Unexpected Dimer with Hg(II)

6.1. Introduction

3,3'-Bipyridine (3,3'-bpy) is a versatile ligand widely used in coordination chemistry. Because of the resulting flexibility from rotation about the C(3)-C(3') single bond, it can give rise to *cis*- and *trans*- conformers (Scheme 6.1). There are several reports in the

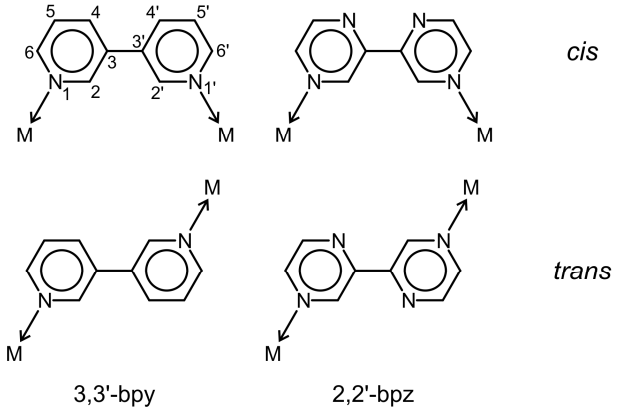

Scheme 6.1: *cis* and *trans* orientation of pyridine and pyrazine rings in 3,3'-bpy and 2,2'-bpz.

literature on polymeric structures containing *cis*-[1] and in particular *trans*-arranged 3,3'-bpy ligands,[2] yet none with a discrete molecular metallacycle. 4,7-phenanthroline ligands which can be considered rigid analogous of 3,3'-bpy, yields triangular metallacycles when reacted with *cis*-a_2M^{II} units (a_2 = diamine; M = Pd or Pt).[3] So in principle, it is also possible to synthesize discrete metallacycle utilizing flexible 3,3'-bpy as the connecting ligand. Feasible discrete cyclic and polymeric metal complexes derived from 3,3'-bpy are shown in Scheme 6.2. A series of cyclic metal complexes of various size has been reported with the structurally related 2,2'-bpz (2,2'-bipyrazine) ligand.[4]

Here in this chapter, the heterocyclic 3,3'-bpy ligand is reacted with different transition metal ions and metal entities, namely Ag(I), Hg(II), enPd(II), *cis*-$(NH_3)_2$Pt(II) as well as *trans*-a_2Pt(II) (a = NH_3), in an attempt to produce discrete cyclic complexes.

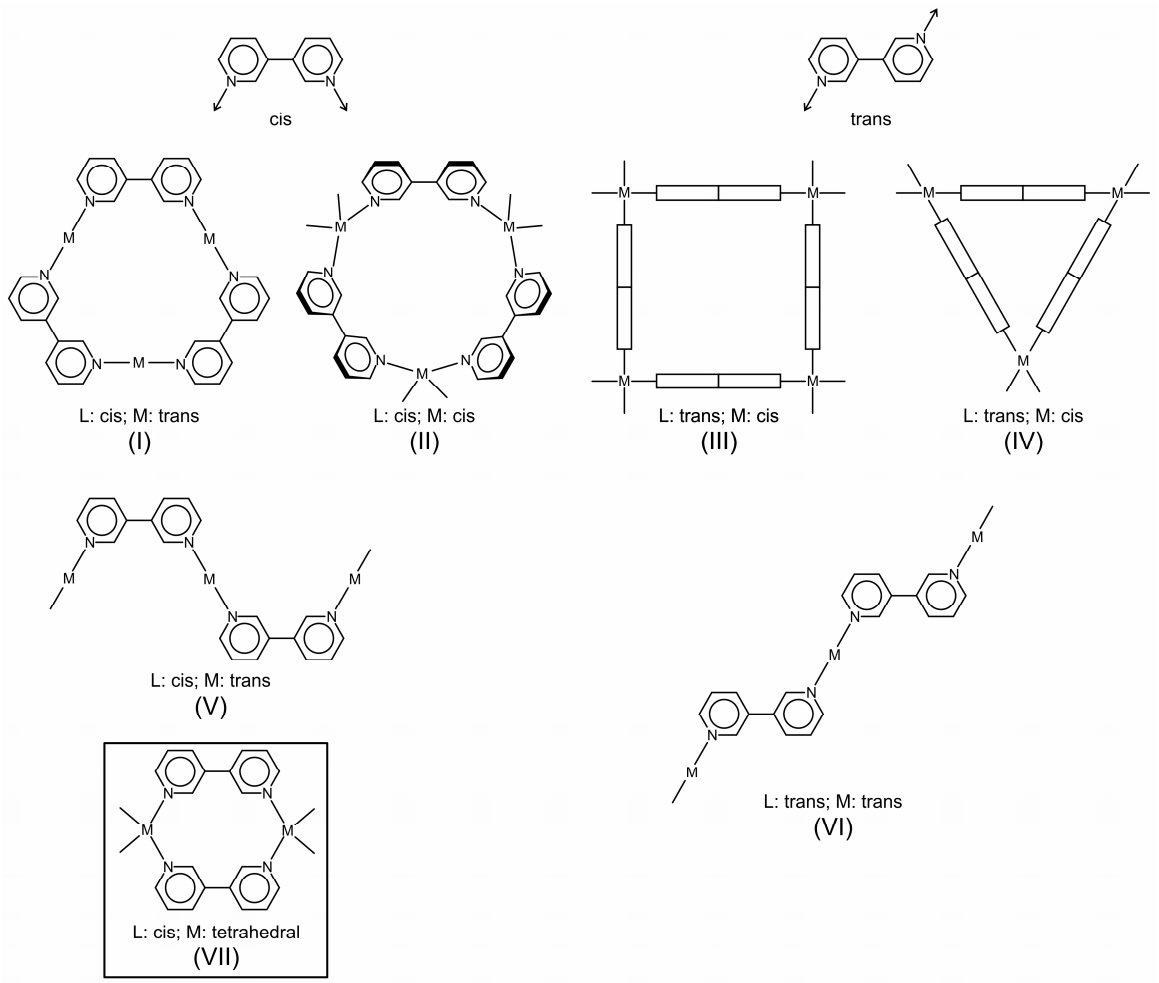

Scheme 6.2: Feasible discrete (I – IV) and polymeric (V, VI) structures of 3,3'-bpy metal complexes. Shown is also the novel discrete dinuclear complex (VII) reported here.

6.2. ^{1}H NMR spectra of 3,3'-Bipyridine

3,3'-Bipyridine was prepared by Ni(0) catalyzed homocoupling reaction of reaction of 3-bromopyridine.[5] The ^{1}H NMR spectrum of the free 3,3'-bpy ligand in D_2O (pD 6.8) is given in Figure 6.1a. It shows the resonances (D_2O, δ, ppm) at 8.77 (H2), 8.55 H(4), 8.11 H(6) and 7.56 H(5). All resonances show splitting due to long-range coupling. For example, the H2 signal is split into a doublet due to coupling with H4 (1.5 Hz) and additionally displays coupling with H5 (0.7 Hz). ^{1}H NMR spectra of 3,3'-bpy were recorded at different pD of the solution in order to determine its pK_a value. Upon protonation, all resonances are downfield shifted, with H6 affected most (Figure 6.1b). pK_a values for $[3,3'\text{-bpyH}]^+$ and $[3,3'\text{-bpyH}_2]^{2+}$, as determined by pD dependent ^{1}H NMR spectroscopy, are 4.58 ± 0.1 and 2.71 ± 0.1 (values converted to H_2O), respectively. These values compare with 4.3 and *ca.*

0.3 for 2,2'-bpy, and 0.45 and –1.35 for 2,2'-bpz, and reflect the higher basicity of 3,3'-bpy as compared to two other ligands.

^{1}H NMR resonances of 3,3'-bpy in D_2O display a moderate sensitivity on concentration, which is consistent with intermolecular stacking. For example, when going from 0.0125 M to 0.125 M, upfield shifts are 0.06 ppm (H2), 0.03 ppm (H4), 0.05 ppm (H6), and 0.04 ppm (H5).

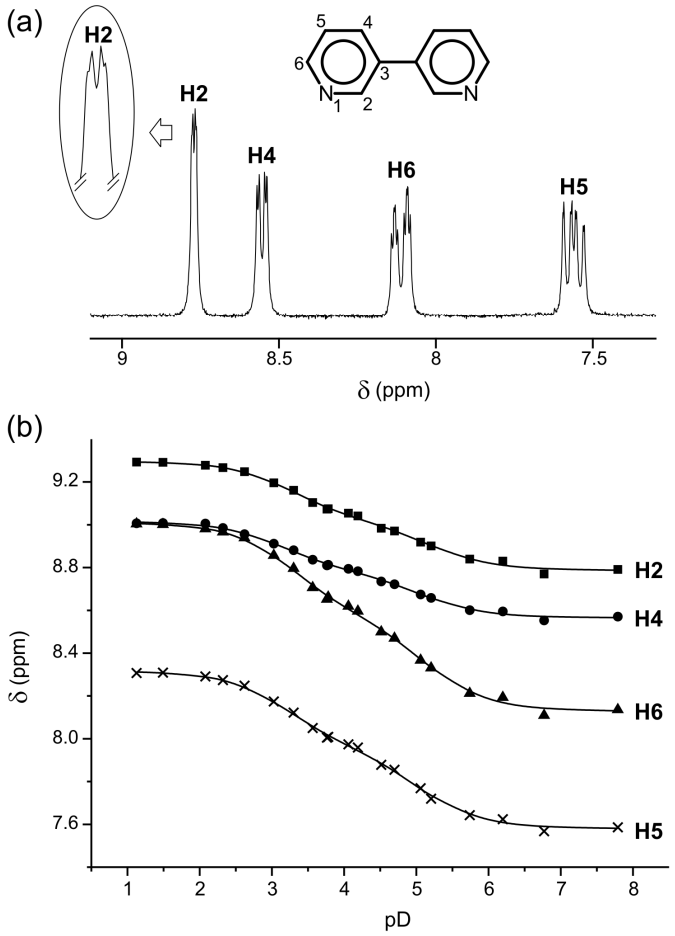

Figure 6.1: (a) Low field section of ^{1}H NMR spectrum of 3,3'-bpy (D_2O, pD = 6.8), focusing on splitting of the H2 resonances. (b) pD dependence of H2, H4, H6 and H8 resonances of free 3,3'-bipyridine.

6.3. Ag^+ and Hg^{2+} coordination

Addition of Ag^+ ions to an aqueous solution of 3,3'-bpy in D_2O expectedly does not reveal resonances due to individual species, but rather gives only averaged signals of the free ligand and the various Ag complexes as a consequence of fast exchange. A similar

situation applies to mixtures of 3,3'-bpy and Hg(II) acetate. The spectrum of the dinuclear Hg(II) complex **31** (see below) has its ^{1}H resonances (δ, ppm; D_2O, pD 5.2) at 8.97, 8.73, 8.44 and 7.88 as well as 2.02 (acetate). No coupling of any of the 3,3'-bpy resonances with the ^{199}Hg isotope is observed, as in a previously reported case.[6]

6.3.1. Synthesis and crystal structure of {[Ag(3,3'-bpy)](ClO$_4$)·H$_2$O}$_n$ (30)

The polymeric complex {[Ag(3,3'-bpy)](ClO$_4$)·H$_2$O}$_n$ (**30**) was prepared by the reaction of free ligand 3,3'-bpy and AgClO$_4$ in water. **30** crystallizes in the monoclinic ($P2_1/c$) space group. Views of complex **30** are shown in Figure 6.2 and selected structural parameters are listed in Table 6.1. The 3,3'-bpy ligands adopt *trans*-conformations with a twist angle of 27.9(1)° between pyridine halves. The dihedral angle between two pyridyl rings coordinated to Ag1 is 7.2(1)°. The silver atom (Ag1) shows a distorted octahedral coordination sphere (Figure 6.2a), with two 3,3'-bpy ligands at the apical positions (Ag1-N1, 2.181(3) Å; Ag1-N11, 2.189(3) Å). The equatorial coordination is completed by a water molecule (Ag1-O1w, 2.722(3) Å), two perchlorate counter anions (Ag1-O13, 2.773(4) Å; Ag1-O13', 2.861(4) Å) and an argentophilic interaction[7] with a neighbor silver atom (Ag···Ag, 3.3751(8) Å). The crystal packing is based on π–π stacking and argentophilic interactions between polymer strands.

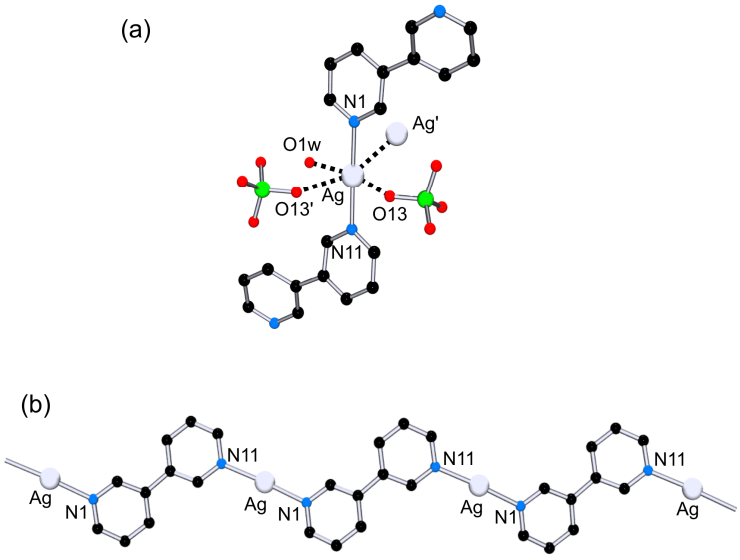

Figure 6.2: (a) Detail of the coordination sphere of the silver atom in **30**. (b) Polymeric motif between Ag1 and 3,3'-bpy bridging ligands in **30**.

An upper view of the *ac* plane evidences the presence of voids in the structure (Figure 6.3a), which consist of two sets of hydrogen bond-based perchlorate-water

polymers. These polymers are built by connecting water molecules of crystallization and perchlorate anions. Each O1w forms two hydrogen bonds with two perchlorate anions: ···O14-Cl1-O12···(H1w)O1w(H2w)···O14-Cl1-O12··· (Figure 6.3b). Distances involving O1w are: O1w···O12, 2.969(5) Å; O1w···O14, 2.886(5) Å;O12···O1w···O14, 119.5(2)°.

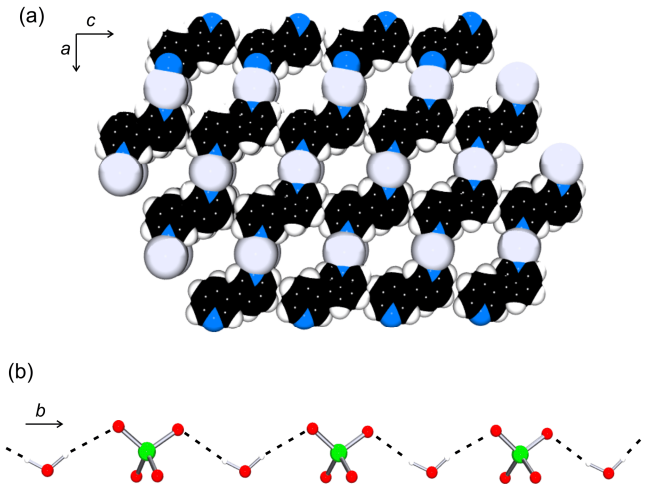

Figure 6.3: (a) Section of the packing pattern in **30** (excluding H_2O and ClO_4^-), including voids along the *b* direction. (b) Water-perchlorate hydrogen bonded polymer inserted along the packing tunnels of **30**.

Table 6.1: Selected bond distances (Å) and angles (º) for compound **30**.

Ag1-N1, 2.181(3)	N1-Ag1-N11, 174.37(13)	N11-Ag1-Ag1', 76.06(9)
Ag1-N11, 2.189(3)	O13-Ag1-Ag1, 157.52(8)	N11-Ag1-O13, 87.31(11)
Ag1-Ag1, 3.3751(8)	O1w-Ag1-O13, 168.17(10)	N11-Ag1-O13', 92.86(11)
Ag1-O1w, 2.722(3)	N1-Ag1-Ag1', 108.03(9)	N11-Ag1 O1W 95.33(11)
Ag1-O13, 2.773(4)	N1-Ag1-O13, 84.58(11)	Ag1'-Ag1-O1w, 78.60(7)
Ag1-O13', 2.861(4)	N1-Ag1-O13', 87.48(11)	O1w-Ag1-O13, 83.13(10)
Bpy-rings, 27.86(7)	N1-Ag1-O1w, 89.35(11)	O13-Ag1-O13', 85.22(10)
py-Ag-py', 7.19(10)		O13-Ag1-Ag1', 113.22(7)

6.3.2. Synthesis and crystal structure of $[Hg(3,3'\text{-bpy})(CH_3COO)_2]_2 \cdot 3H_2O$ (31)

Reaction of 3,3'-bpy with $Hg(CH_3COO)_2$ in water yielded the dinuclear complex $[Hg(3,3'\text{-bpy})(CH_3COO)_2]_2 \cdot 3H_2O$ (**31**). The colorless crystals were obtained by slow evaporation of

an aqueous solution at room temperature. **31** crystallizes in the triclinic (P-1) space group. Figure 6.4 gives a view of complex **31** and selected structural parameters are listed in Table 6.2. The 3,3'- bpy ligands adopt a *cis*-conformation of the two pyridyl rings, with a twist angle of 30.4(2)°, and act as bridges between two mercury centers. The coordination geometry of each Hg ion is distorted tetrahedral, enclosing two 3,3'-bpy entities and two chelating/semi-chelating acetates. Hg-N (Hg1-N1a, 2.274(3) Å; Hg1-N1b, 2.263(3) Å) and Hg-O distances (Hg1-O11, 2.490(3) Å; Hg1-O12, 2.392(3) Å; Hg1-O21, 2.286(3) Å; Hg1-O22, 2.762(3) Å) are in the normal range. Both 3,3'- bpy ligands and their bonded mercury atoms are almost coplanar with a tendency towards a boat conformation (distance from Hg1 to the plane defined by N1a,N1b,N1a',N1b' is 0.58 Å). Both acetate ligands form a dihedral angle of 79.23(16)° with each other. The ligand containing O11,O12 is roughly coplanar with the pyridyl rings (7.27(27)°, 23.28(23)°), whereas the other acetate ligand (with O21,O22) is roughly perpendicular (78.33(15), 72.81(14)°). Multiple hydrogen bonding is observed in the crystal packing. Besides hydrogen bonding, the crystal packing includes π–π- and anion–π-interactions. N1a-pyridyl rings are pairwise π–π stacked (3.5 Å), and both rings are involved in an additional anion–π-interaction with O11 (O11···centroid, 3.47 Å).

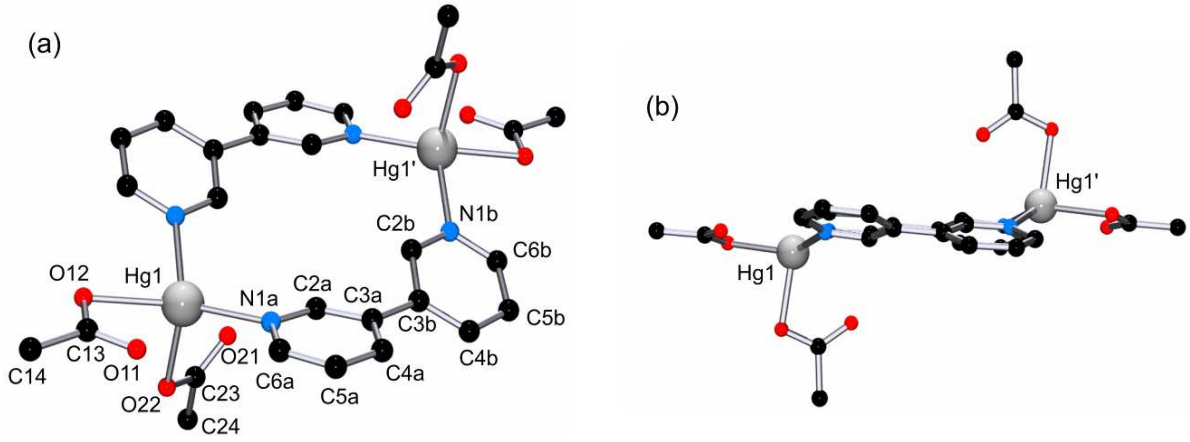

Figure 6.4: (a) View of **31** with atom numbering scheme. (b) Side view of **31**, evidencing a boat conformation of the mercury atoms with respect to the 3,3'-bpy ligands.

Table 6.2: Selected bond distances (Å) and angles (º) for compound **31**.

Hg1-N1a, 2.274(3)	N1a-Hg1-N1b, 114.74(11)	N1b-Hg1-O21, 115.85(11)
Hg1-N1b, 2.263(3)	N1a-Hg1-O11, 88.58(11)	O11-Hg1-O12, 53.82(11)
Hg1-O11, 2.490(3)	N1a-Hg1-O12, 140.71(12)	O11-Hg1-O21, 93.87(10)

Hg1-O12, 2.392(3)	N1a-Hg1-O21, 103.25(12)	O12-Hg1-O21, 91.53(11)
Hg1-O21, 2.286(3)	N1b-Hg1-O11, 134.38(12)	Bpy-rings, 30.43(16)
Hg1-O22, 2.762(3)	N1b-Hg1-O12 89.72(12)	py-Hg-py', 30.43(16)

6.4. Reaction of 3,3'-bipyridine with enPd^{II} and *cis*-(NH$_3$)$_2$Pt^{II}

Reactions of 3,3'-bpy with [Pd(en)(H$_2$O)$_2$](NO$_3$)$_2$ and *cis*-[Pt(NH$_3$)$_2$(H$_2$O)$_2$](NO$_3$)$_2$ (1:1 ratio) give products of 1:1 stoichiometry [{Pd(en)(3,3'-bpy)}(NO$_3$)$_2$]$_n$ (**32**) and *cis*-[{Pt(NH$_3$)$_2$(3,3'-bpy)}(PF$_6$)$_2$]$_n$ (**33**). Despite several attempts, crystals suitable for X-ray crystallography can not be obtained. However, the appearance of single sets of 3,3'-bpy resonances in the ^{1}H NMR spectra of **32** and **33** indicates the formation of cyclic compounds. Chemical shifts (δ, ppm; D$_2$O, TMA as internal reference) are as follows: **32**, 9.15, 8.84, 8.27, 7.69 ppm (3,3'-bpy) and 2.98 (en); **33**, 8.99, 8.95, 8.23, 7.67 (3,3'-bpy). When TSP was used as a reference, shifts differed by 0.1 ppm (**32**) and 0.09 ppm (**33**), suggesting that the TSP anion interacts with the cations of **32** and **33**.[8] The high resolution MS of a sample of **33**

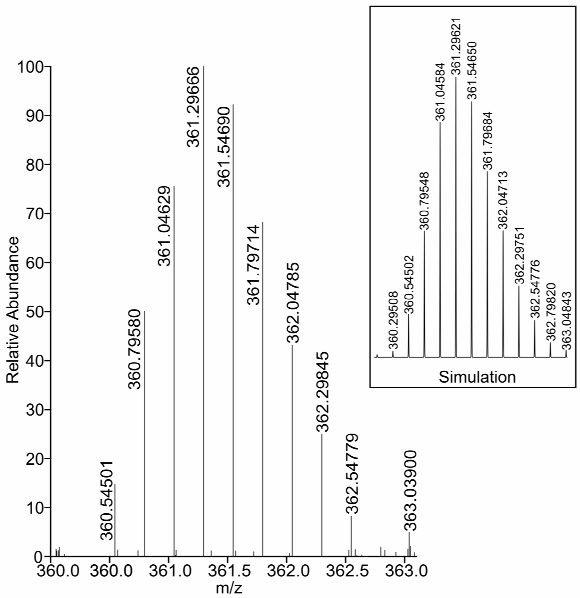

Figure 6.5: HRMS spectrum of complex **33**: Observed and calculated pattern for [M–(PF$_6$)$_4$]$^{4+}$.

was carried out and confirmed a triangular structure (see (II) or (IV) in Scheme 6.2). The mass spectrum displayed peaks due to [M–(PF$_6$)]$^+$: 1880.08114 (calcd. 1880.07904), (M–(PF$_6$)$_2$]$^{2+}$: 867.55844 (calcd. 867.55828) and [M–(PF$_6$)$_4$]$^{4+}$: 361.29666 (calcd. 361.29621).

The HRMS spectrum of $[M–(PF_6)_4]^{4+}$ is given in Figure 6.5 and compared with the simulated spectrum.

6.5. Reaction with *trans*-$[Pt(NH_3)_2(H_2O)_2]^{2+}$

Reactions of 3,3'-bpy with *trans*-$[Pt(NH_3)_2(D_2O)_2](NO_3)_2$ were carried out with different ratios between 3,3'-bpy and the Pt^{II} species (10:1, 2:1, 1:1, 1:10) on the ^1H NMR scale in D_2O. The spectra change with time, but within 2–3 d at 50 ℃, constant spectra are obtained. In the case of a large excess of ligand over Pt (10:1), the spectrum reveals the presence of a major species attributed to *trans*-$[Pt(NH_3)_2(3,3'\text{-bpy})_2]^{2+}$ and excess 3,3'-bpy (Figure 6.6). The two sets of pyridine resonances of the coordinated 3,3'-bpy ligands of the 1:2 complex are assigned on the basis of their relative intensities. The H2 and H4 resonances of the free ligand are very much broadened, and those of H2, H4, and H6 are upfield shifted by *ca.* 0.2, 0.08, and 0.14 ppm, respectively. The broadness of H2 and H4 resonances may be due to the presence of different rotamers of the 1:2-Pt complex. Reaction carried out on a preparative scale did not yield pure products. So the self-assembly process of *trans*-$(NH_3)_2Pt^{II}$ and 3,3'-bpy does not lead to a preferred single product, unlike in the case of $enPd^{II}$ and *cis*-$(NH_3)_2Pt^{II}$.

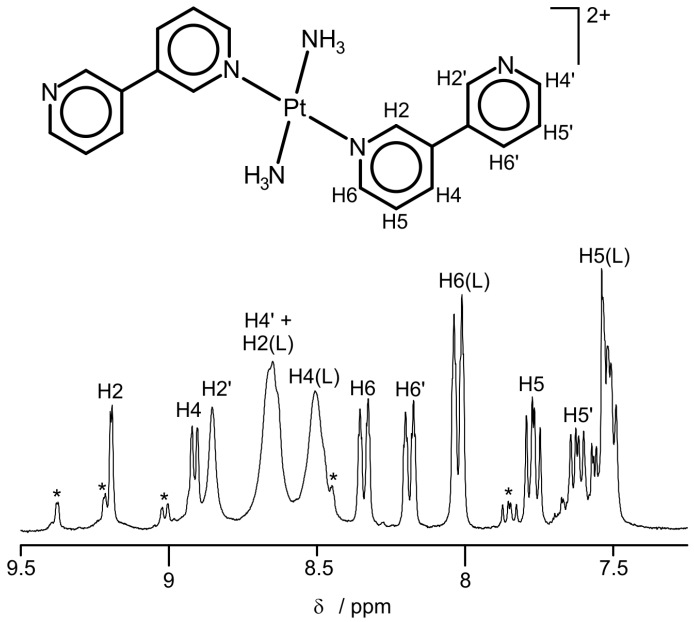

Figure 6.6: ^1H NMR spectrum of mixture of *trans*-$[Pt(NH_3)_2(D_2O)_2]^{2+}$ and 3,3'-bpy (L) in ratio 1:10 after 2 d, 50℃, D_2O, pD = 6.65. Main resonances are assigned to the 1:2 complex and free ligand; minor resonances (*) are not assigned.

6.6. Conclusion

The flexible ditopic ligand 3,3'-bipyridine forms with $Hg(CH_3COO)_2$ and *cis*-$[Pt(NH_3)_2(H_2O)_2](PF_6)_2$ discrete di- and trinuclear cycles **31** and **33**, respectively. The solid state structure of the Hg(II) complex **31** is unique in that it represents the smallest possible entity of any cyclic complex. In contrast, **33** is a cyclic trinuclear compound, proved by HRMS spectrometry. On the NMR time scale, **31** is kinetically labile in aqueous solution, but **33** is inert. The 3,3'-bpy ligand also forms a 1-D polymeric complex **30** with $AgNO_3$.

6.7. References

[1] R. L. LaDuca, M. P. Desciak, R. S. Rarig, Jr., J. A. Zubieta, *Z. Anorg. Allg. Chem.* **2006**, *632*, 449–453.

[2] R. S. Rarig, Jr., R. Lam, P. Y. Zavalij, J. K. Ngala, R. L. LaDuca, Jr., J. E. Greedan, J. Zubieta, *Inorg. Chem.* **2002**, *41*, 2124–2133.

[3] a) M. A. Galindo, J. A. R. Navarro, M. A. Romero, M. Quiros, *Dalton Trans*. **2004**, 1563-1566; b) S. –Y. Yu, H. Huang, H. -B. Liu, Z. -N. Chen, R. Zhang, M. Fujita, *Angew. Chem. Int. Ed.* **2003**, *42*, 686–690.

[4] a) J. A. R. Navarro, B. Lippert, *Coord. Chem. Rev.* **2001**, *222*, 219–250.

[5] M. Tiecco, L. Testaferri, M. Tingoli, D. Chianelli, M. Montanucci, *Synthesis* **1984**, 736–738.

[6] M. Krumm, E. Zangrando, L. Randaccio, S. Menzer, A. Danzmann, D. Holthenrich, B. Lippert, *Inorg. Chem.* ***1993***, *32*, 2183–2189.

[7] See, e.g.: a) G. Meyer, M. Sehabi, I. Pantenburg, in *Design and Construction of Coordination Polymers* (Eds. M. C. Hong, L. Chen), J. Wiley & Sons, Hoboken, USA, **2009**, pp. 1–23; b) A. J. Blake, N. R. Champness, P. Hubberstey, W. -S. Li, M. A. Withersby, M. Schröder, *Coord. Chem. Rev.* **1999**, *183*, 117–138.

[8] J. A. R. Navarro, M. B. L. Janik, E. Freisinger, B. Lippert, *Inorg. Chem.* **1999**, *38*, 426–432.

7. Discrete as well polymeric metal complexes of 1,4,5,8-tetra-azaphenanthrene (TAP) ligand and its derivative

7.1. Introduction

1,4,5,8-tetra-azaphenanthrene (TAP) is a versatile ligand in metal coordination chemistry. While it acts as a chelating ligand in most cases,[1] monodentate as well as distinct bridging modes are also possible.[2] Different binding modes of this ligand are depicted in Scheme 7.1. It can be considered as rigid analogue of 2,2'-bipyrazine (2,2'-bpz), in which the two pyrazine rings are fixed in *cis* orientation. With 2,2'-bpz, a number of discrete molecular entities have been characterized, which include a flat triangular structure, 3D triangular entities of different shapes (prism, vase), as well as a tetranuclear open box.[3] In all these cases the N4/N4' positions are involved in metal coordination, occasionally complemented by addition of metal chelation via N1/N1', and influenced by counter anions.

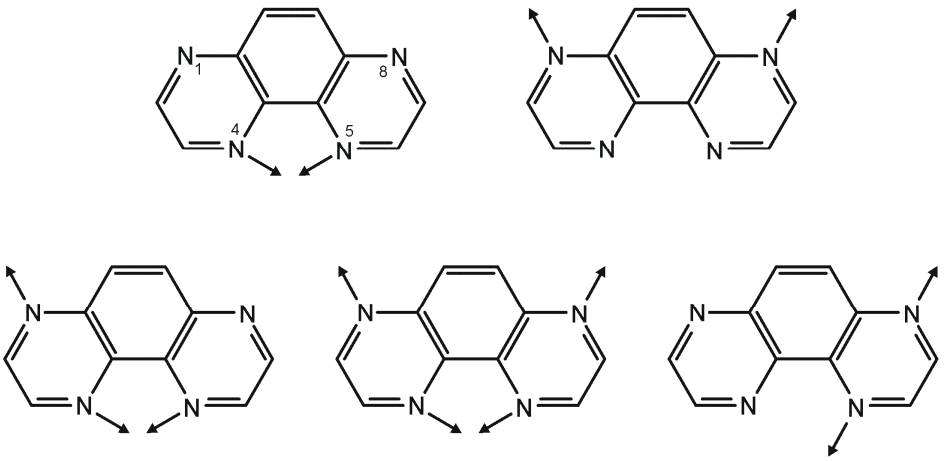

Scheme 7.1: Schematic diagram of different coordination modes of 1,4,5,8-tetra-azaphenanthrene ligand (L3).

Here in this chapter, two heterocyclic N-based ligands, 1,4,5,8-tetra-azaphenanthrene (L3) and its derivative (L4) (Scheme 7.2) have been prepared according to the published literature procedure,[4] and their reaction products with different transition metal ions and metal entities such as *cis*-a_2M^{II} (a = am(m)ine, a_2 = diamine; M = Pt, Pd), Ag^+, Hg^{2+}, Zn^{2+} will be discussed. As will be shown below, a series of metal complexes has been synthesized and characterized by X-ray crystallography. The ligands L3 and L4 coordinate to the metal ions either in a chelating or both as a chelating and monodentate fashion, depending on the metal ions or metal entities.

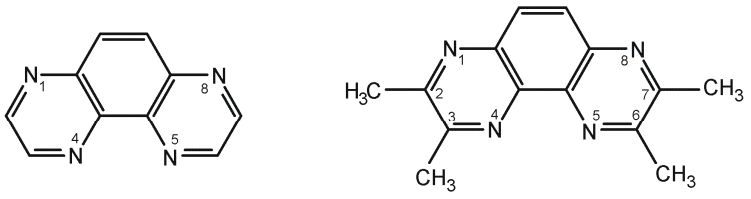

Scheme 7.2 Structures of 1,4,5,8-tetra-azaphenanthrene (L3) and 2,3,6,7-tetramethyl 1,4,5,8-tetra-azaphenanthrene(L4)

7.2. Synthesis of ligand L3 and L4

The ligands L3 and L4 were synthesized in high yield starting from 4-nitro-*o*-phenylenediamine in a step-wise manner (Scheme 7.3).[4] Ligand L4 is poorly soluble in water. The ^{1}H NMR spectra of L3 and L4, recorded in D_2O and $CDCl_3$, are consistent with their compositions. The ^{1}H spectrum of L3 in D_2O is shown in Figure 7.1. The chemical shifts in D_2O (pD = 7.5) are 8.93, 8.92, 7.83 ppm for L3 and 7.83, 2.79, 2.73 ppm for L4. In $CDCl_3$, the ligands have their resonances (δ, ppm) at 9.16 (d, ^3J = 2.0 Hz), 9.10 (d), 8.35 (s) in L3 and 8.13 (s), 2.90 (s), 2.80 (s) in L4.

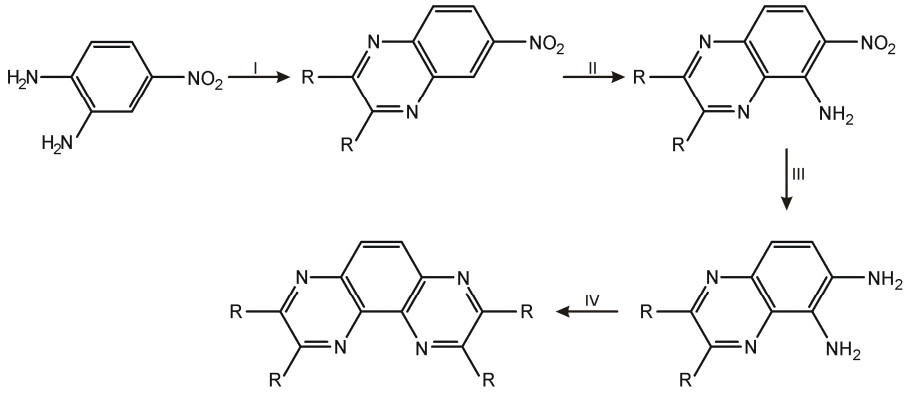

Scheme 7.3: Synthesis of ligands L3 (R = H) and L4 (R = CH_3); Reagents: (I) RCO-COR in EtOH, (II) NH_2OH/KOH in EtOH, (III) N_2H_4/10% Pd-C, (IV) RCO-RCO in EtOH.[4a]

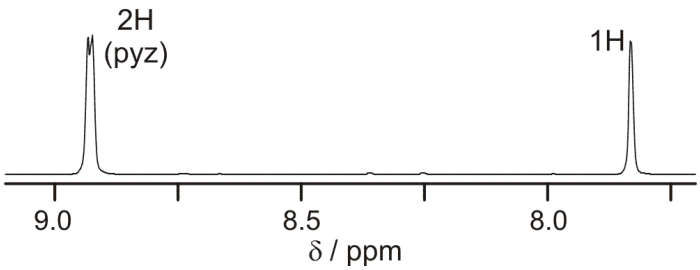

Figure 7.1: Low field section of ^{1}H NMR spectrum of L3 in D_2O.

Single crystals of L4·2H_2O were obtained by slow evaporation of an aqueous methanolic (1:1) solution at room temperature. It crystallizes in orthorhombic (Pca2(1)) space group. A view of L4·2H_2O is shown in Figure 7.2. The bond distances and angles are in the normal range. The two water molecules of crystallization make hydrogen bonds with two nitrogen atoms of pyrazine rings in L4, resulting in the formation of linear 1-D polymeric hydrogen bonded chain (Figure 7.3). The hydrogen bond distances are, for example, N11-O2w, 2.92 Å; N24-O1w, 3.00 Å; O1w-O2w, 2.76, 2.77 Å. The heterocyclic L4 ligands are stacked on each other with a ring centroid to plane separation of 3.37 Å,

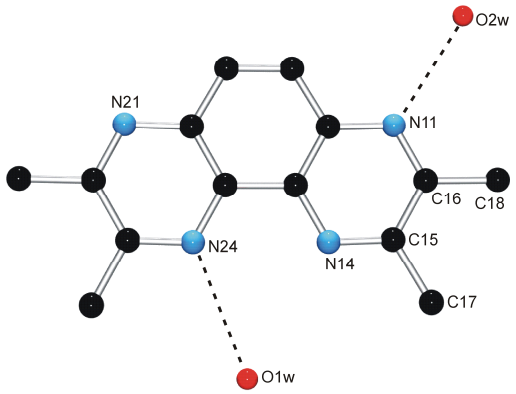

Figure 7.2: Molecular structure of L4·2H_2O.

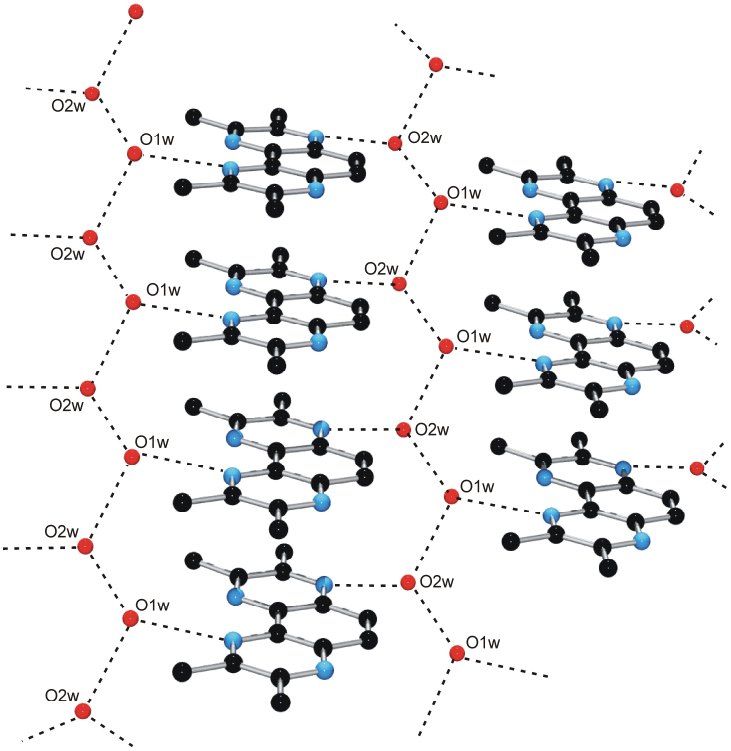

Figure 7.3: View of hydrogen bonded polymeric network in L4·2H_2O.

representing significant π–π interactions. This value, observed in case of L4 ligand, is similar to that seen in L3 (3.34 Å)[2] and 2,2'-bpz ligands (3.36 Å).[2]

7.3. Reaction of L3 with *cis*-a_2Pt^{II} (a = NH_3, en)

Reactions between *cis*-$[Pt(NH_3)_2(D_2O)_2](NO_3)_2$ and L3 at different ratios (*r* = 1:1, 2:1) were followed by ^{1}H NMR spectroscopy in D_2O. The spectra change with time, but within 3-4 days constant spectra are obtained. The resonances due to free ligand L3 can no longer be found. When *r* = 1:1, signals of one major species are observed, along with resonances due to two or three minor species. The major species has chemical shifts at 10.27, 9.65 (d, pyz); 8.97 (s) ppm. With excess of Pt^{II} species (2 equiv.), also formation of one major species is observed at 10.20 (s); 9.84, 9.43 (d, pyz) ppm in the ^{1}H NMR spectra (Figure

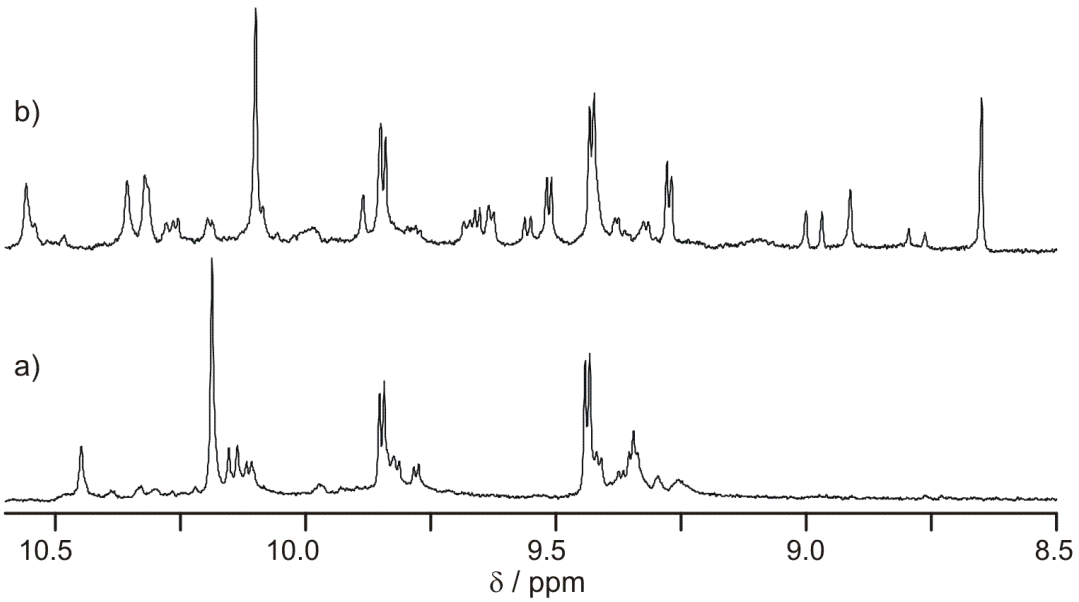

Figure 7.4: Low field sections of ^{1}H NMR spectra of a reaction mixtures of (a) *cis*-$[Pt(NH_3)_2(D_2O)_2](NO_3)_2$ and L3 (*r* = 2:1) at 40 ℃; (b) $[Pt(en)(D_2O)_2](NO_3)_2$ and L3 (*r* = 2:1) at 40 ℃ after 2 days.

7.4a). The resonances of aromatic protons are downfield shifted by +0.91, +0.51 and +2.37 ppm from those of free ligand. Similarly, the reaction between $[Pt(en)(D_2O)_2](NO_3)_2$ and L3 produces mixtures of species as observed in ^{1}H NMR spectra (Figure 7.4b). Reactions carried out in preparative scale also did not produce pure compounds.

7.4. Reactions of L3 and L4 with (en)Pd^{II}

The reactions of L3 and L4, respectively, with $[Pd(en)(H_2O)_2](NO_3)_2$ in water yielded the monochelate complexes $[Pd(en)(L3)](NO_3)_2 \cdot H_2O$ (**34a**) and $[Pd(en)(L4)](NO_3)_2 \cdot 1.5H_2O$ (**35**). $[Pd(en)(L3)](ClO_4)_2 \cdot 2H_2O$ (**34b**) was also isolated as its perchlorate salt. Single crystals were obtained during the slow evaporation of aqueous solution of **34a**, **34b**, and **35** at room temperature. **34a** crystallizes in monoclinic ($P2_1/c$) space group and **35** crystallizes in the triclinic (P-1) space group. Views of cations **34a** and **35** are shown in Figure 7.5. Selected bond distances and angles are listed in Table 7.1. In both compounds, ligands (L3 and L4) are coordinated to Pd^{II} in a chelating fashion. Pd-N

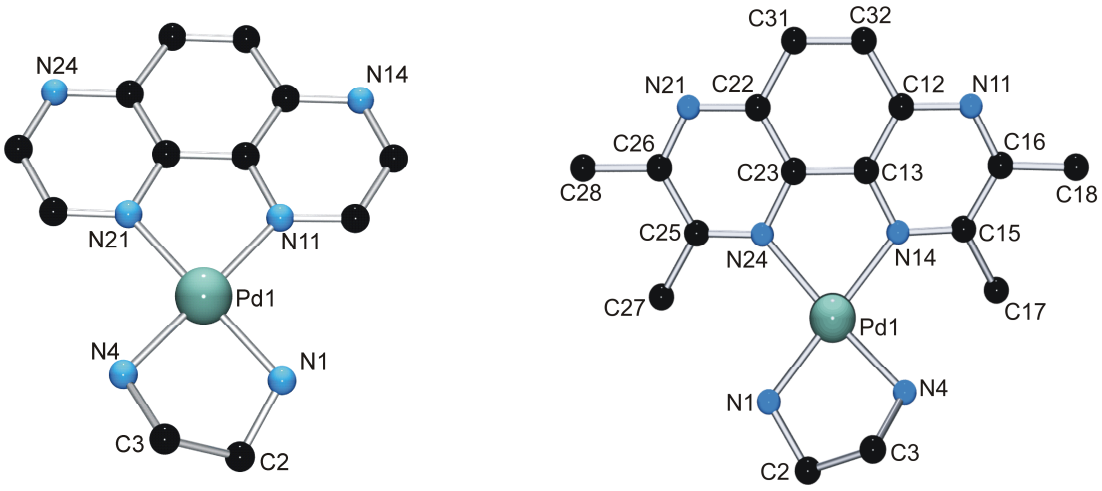

Figure 7.5: Views of cations **34a** (left) and **35** (right).

distances are in the normal range and in both complexes, the bond angles around Pd slightly deviate from the ideal square planar geometry (see Table 7.1). In complex **34a**, Pd lies roughly in the same plane as the aromatic L3 ligand. But the ethylenediamine attached to the Pd shows the expected pucker, and the distances of C2 and C3 from the plane of ligand L3 are +0.45 and -0.36 Å, respectively. However, in case of complex **35**, the situation is completely different. Both ethylenediamine as well as Pd do not lie in the plane of the aromatic L4 ligand, possible due to steric effect exerted by the attached methyl groups. The distances of different atoms of (en)Pd^{II} entitiy from the plane of L4 ligand are Pd1 0.64 Å; N1, 1.48 Å; N4, 1.52 Å; C2, 2.14 Å; and C3, 2.68 Å. In both complexes, several hydrogen bonding interactions are observed, which involve NH_2 groups of the en ligand, nitrate anions and water of crystallization. They represent the main motif in the crystal packing.

The aromatic L4 ligands in complex **35** are stacked on each other (Figure 7.6) and the distances from centroid of one ring to planes of adjacent L4 ligands are 3.28 and 3.26 Å.

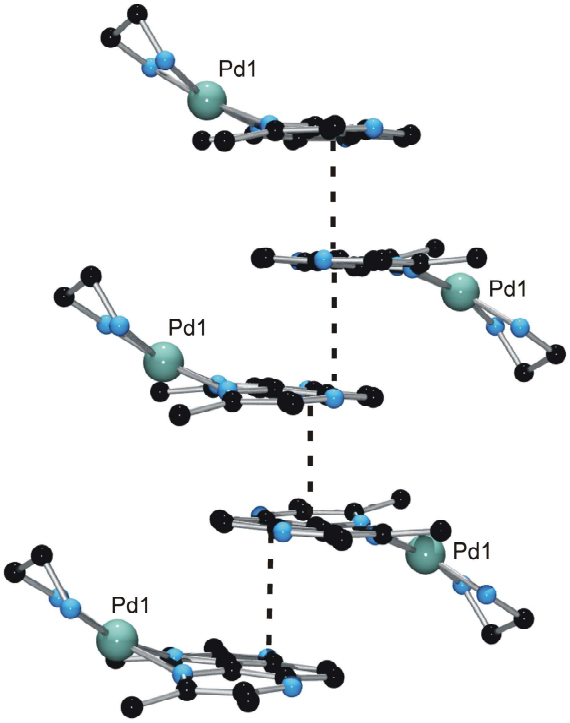

Figure 7.6: View of stacked L4 ligands in cations of **35**.

Table 7.1a: Selected bond distances (Å) and angles (º) for compound **34a**.

Pd1-N1, 2.022(2)	N11-Pd1-N1, 96.96(10)	N11 Pd1-N4, 177.48(9)
Pd1-N4, 2.018(2)	N4-Pd1-N1, 83.69(10)	N1-Pd1-N21, 176.96(9)
Pd1-N11, 2.016(2)	N4-Pd1-N21, 97.47(10)	N11-Pd1-N21, 82.01(10)
Pd1-N21, 2.047(2)		

Table 7.1b: Selected bond distances (Å) and angles (º) for compound **35**.

Pd1-N1, 2.032(3)	N4-Pd1-N1, 81.89(14)	N4-Pd1-N24, 168.37(14)
Pd1-N4, 2.027(3)	N4-Pd1-N14, 96.03(14)	N1-Pd1-N14, 172.61(14)
Pd1-N14, 2.060(3)	N14-Pd1-N24, 81.02(12)	N1-Pd1-N24, 99.60(13)
Pd1-N24, 2.088(3)		

The ^{1}H NMR spectrum of **34a**, recorded in D_2O (pD 6.9), displays its resonances at 9.49 (d, ^3J = 2.7 Hz), 8.93 (d), 8.63(s) (for L3) as well as 3.09 (s, en) ppm (Figure 7.7). Similarly, complex **35** shows its ^{1}H NMR resonances (D_2O, pD 7.1) at 8.33 (s), 2.91 (s), 2.90 (s) (for L4) and 2.84 ppm (en).

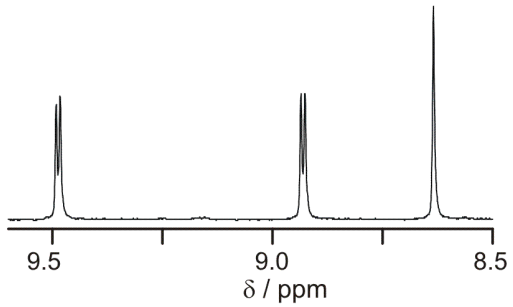

Figure 7.7: Low field section of ^{1}H NMR spectrum of **34a** in D_2O.

7.5. Reaction of 34a with additional metal entities or metal ions

Complex $[Pd(en)(L3)](NO_3)_2 \cdot H_2O$ (**34a**) has two non-coordinated nitrogen atoms, available for additional metal ion binding and these can be used to generate high-nuclearity derivatives. Depending on the metal ions used, it can either lead to the formation of discrete metallacycles or polymeric species (Scheme 7.4).

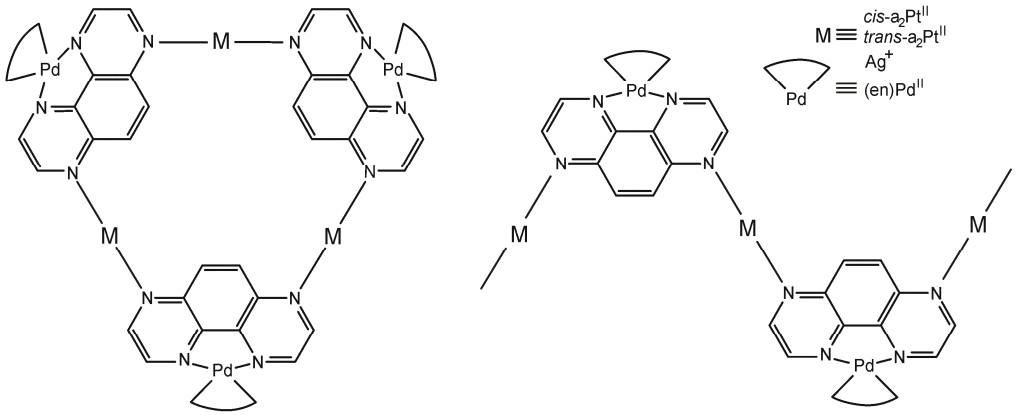

Scheme 7.4: Schematic views of feasible discrete triangular metallacycle (left) and polymeric species (right), which can be obtained in the reaction of **34a** with different metal entities.

Reactions between **34a** and different metal entities or metal ions, such as *cis*-a_2M^{II} (a = NH_3, en; M = Pt, Pd) and Ag^+ ion have been carried out with the aim to obtain discrete metallacycles. Reactions followed by ^{1}H NMR spectroscopy showed that there is, rather

unexpectedly, no reaction between $[Pd(en)(H_2O)_2]^{2+}$ and **34a** even after 7d at 40 ℃. In its ^1H NMR spectrum two separate resonances due to ethylenediamine (en) are observed (3.09 ppm for en in **34a** and 2.64 ppm for free $[Pd(en)(D_2O)_2]^{2+}$) which is a clear indication that $(en)Pd^{II}$ in complex **34a** is neither exchanging rapidly with free $[Pd(en)(D_2O)_2]^{2+}$ nor that it is bonded to the available N atoms.

However, *cis*-$[Pt(NH_3)_2(H_2O)_2](NO_3)_2$ and *trans*-$[Pta_2(H_2O)_2](NO_3)_2$ (a = NH_3, CH_3NH_2) react moderately with complex **34a** in D_2O. Typical ^1H NMR spectra, recorded after 3 days at 40 ℃, are shown in Figure 7.8. The spectra do n ot change with time afterwards. Along

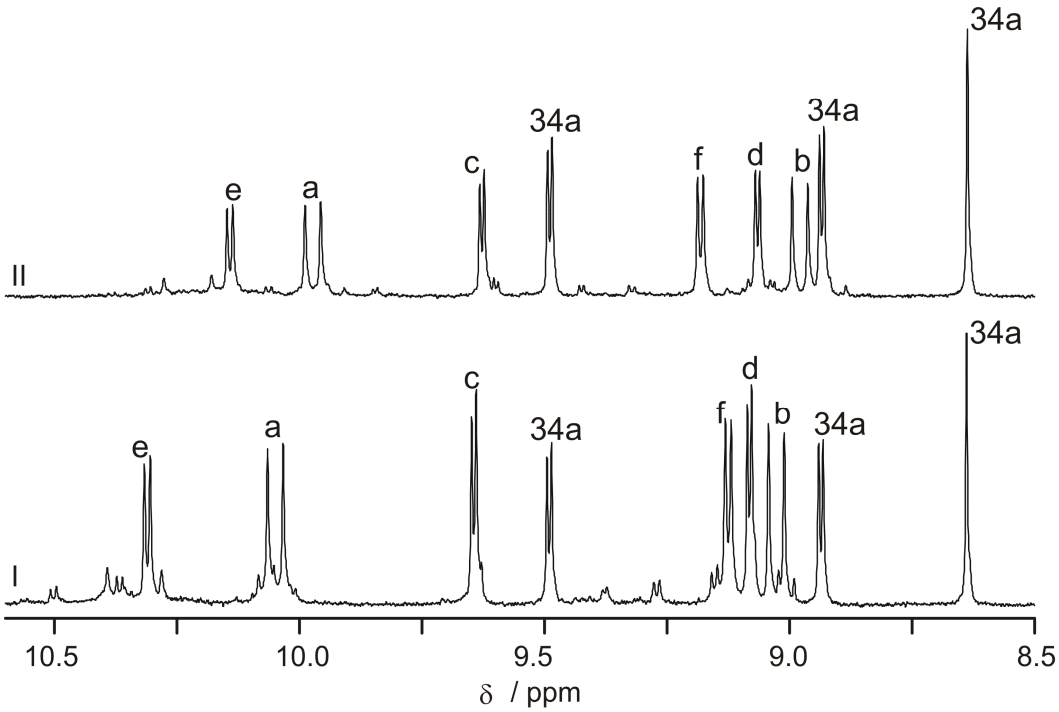

Figure 7.8: Low field section of ^1H NMR spectra of reaction mixtures of (I) **34a** and *trans*-$[Pt(CH_3NH_2)_2(H_2O)_2](NO_3)_2$; (II) **34a** and *cis*-$[Pt(NH_3)_2(H_2O)_2](NO_3)_2$ in D_2O.

with resonances due to complex **34a**, six additional major peaks (a – f) are observed at 10.14, 9.97, 9.63, 9.18, 9.07, 9.02 ppm (in case of reaction between *cis*-$(NH_3)_2Pt^{II}$ and **34a**) and 10.31, 10.05, 9.64, 9.13, 9.08, 9.03 ppm (for *trans*-$(CH_3NH_2)_2Pt^{II}$ and **34a**). These new peaks have equal intensities in the spectra recorded after 12 h, 1 day and 3 days from the start of the reaction. This suggests that these new resonances belong to the same species. Moreover, all of these new peaks appear as doublets. This is only possible when the coordination of the L3 ligand in complex **34a** to a metal ion takes place in a non-symmetrical ways (only one out of two available nitrogen atoms coordinate to the metal

ion), which makes the two pyrazine rings as well as the bridging protons (e & f in Scheme 7.5) non-equivalent. A comparison of integral ratios of aromatic L3 ligand with the *trans*-$(CH_3NH_2)_2Pt^{II}$ entity suggests the formation of a 1:1 (Pd:Pt) complex (Scheme 7.5, (I)). The six new doublets can be grouped in three pairs displaying identical ^3J coupling constants of 9.6 Hz, 3.5 Hz, and 2.7 Hz. The assignment used in Figure 7.8 (for comparison see Scheme 7.5) is a tentative one. While for protons (c) and (d) the low value of 2.7 Hz is logical (2.7 Hz in **34a**), the two other sets ((a) and (b), 9.6 Hz; (e) and (f), 3.5 Hz) might be interchanged. The assignment followed here is corroborated by comparison with a trinuclear complex of 4,7-phenanthroline and $(en)Pt^{II}$, in which the protons adjacent to the Pt coordination site display a ^3J coupling constant of 8.5 Hz.[5] However, as the electronic status of a pyridine ligand (in 4,7-phen) is different from that in a pyrazine ring (**34a**), this uncertainty persists.

The ^{1}H NMR spectra of reaction mixtures, carried out with excess Pt^{II} (2 equiv.), do not show any improvement concerning relative intensities of individual resonances. Resonances of the starting complex **34a** are still present in significant amounts. Reactions were also carried out on a preparative scale; however, it was not possible to obtain pure products from these reactions.

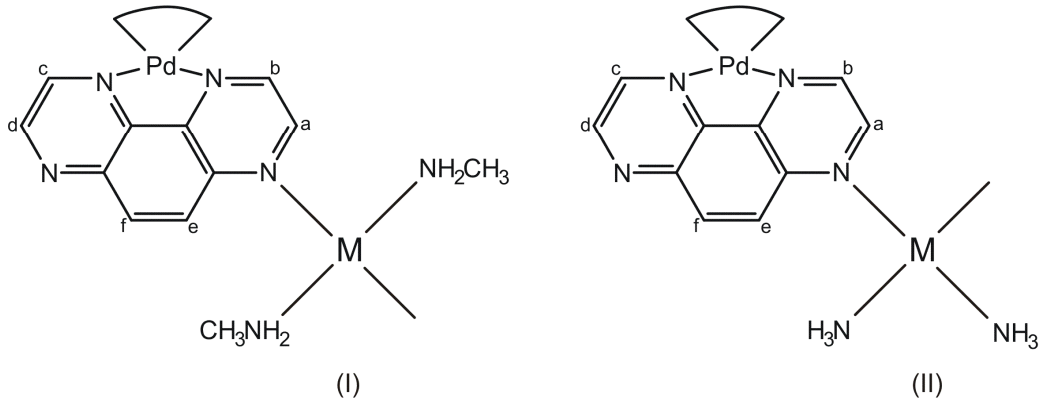

Scheme 7.5: proposed 1.1 (Pd:Pt) complex from the reaction of $[Pd(en)(L3)](NO_3)_2{\cdot}H_2O$ (**34a**) with (I) *trans*-$[Pt(CH_3NH_2)_2(H_2O)_2](NO_3)_2$; (II) *cis*-$[Pt(NH_3)_2(H_2O)_2](NO_3)_2$. Structure (II) is not verified (even though likely to be true).

The reaction between **34a** and $AgNO_3$ was also carried out in water to obtain either discrete or polymeric species of the types shown in Scheme 7.4. However, much to our surprise, a metal complex was isolated, which by X-ray crystal structure determination, showed that it is a polymeric complex $\{[Ag(L3)]_2Ag(NO_3)_3{\cdot}3H_2O\}_n$ (**36**), containing Ag^I ions only. Thus, $(en)Pd^{II}$ was completely replaced by Ag^I ions in this transmetallation reaction.

Slow evaporation of reaction mixtures at 4 ℃ yield ed single crystals of **36**. Complex **36** crystallizes in the monoclinic (C2/c) space goup. A view of **36** is given in Figure 7.9 and selected structural parameters are listed in Table 7.2. There are two types of silver ions (Ag1, Ag2) in the complex **36**. Ag1 coordinates to the chelating N (N11, N21) sites of the L3 ligand and also to the N14 site of a second L3 ligand, which gives rise to a coordination polymer strand. Two of these polymer strands run in antiparallel direction, and they are connected by a second silver ion (Ag2). The coordination sphere of Ag2 is distorted tetrahedral, and consists of two N atoms (N24, N24) of L3 ligands from two neighbouring polymer strands as well as two oxygen atoms of the two coordinated nitrate anions. Ag-N and Ag-O bond distances are in the normal range (Table 7.2). The two L3 ligands, which are bonded to Ag1 or Ag2 make a dihedral angle of 45.6°.

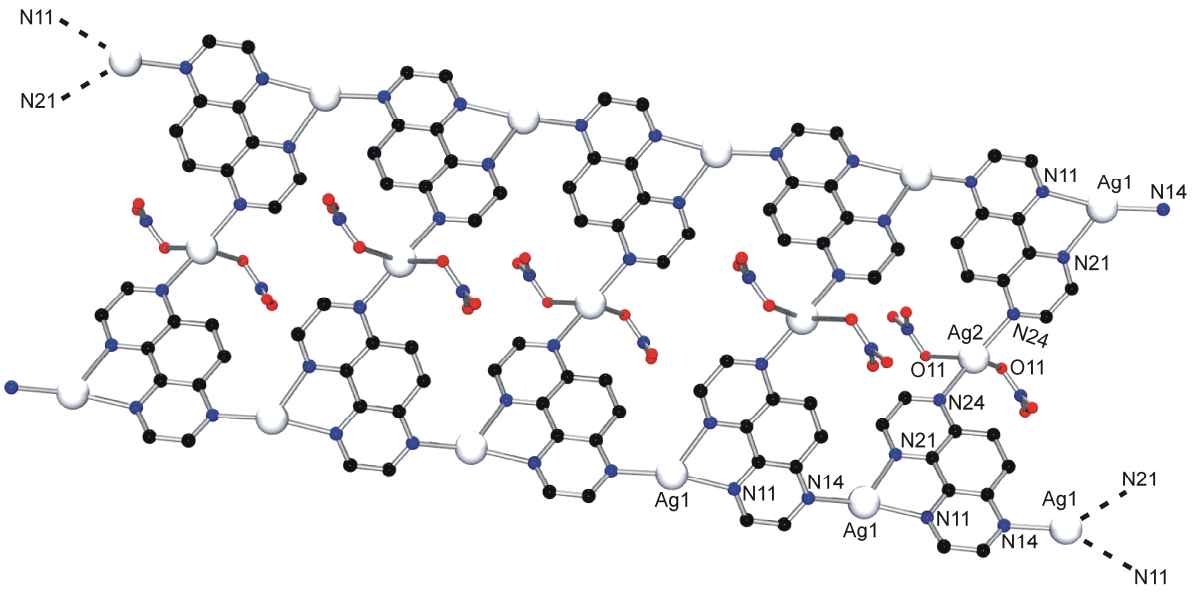

Figure 7.9: Section of polymeric structure of $\{[Ag(L3)]_2Ag(NO_3)_3 \cdot 3H_2O\}_n$ (**36**).

Table 7.2: Selected bond distances (Å) and angles (º) for compound **36**.

Ag1-N11, 2.356(6)	N11-Ag1-N21, 71.0(2)	N24-Ag2-O11, 85.4(2)
Ag1-N14, 2.233(6)	N14-Ag1-N11, 155.7(2)	O11-Ag2-O11, 70.0(3)
Ag1-N21, 2.379(6)	N14-Ag1-N21, 125.1(2)	N24-Ag2-N24, 149.9(3)
Ag2-N24, 2.218(6)	Ag2-O11, 2.564(6)	N24-Ag2-O11, 120.4(2)

7.6. Crystal structure of [Pd(L3)($CH_3COO)_2$] (37)

Reaction of L3 with $Pd(OAc)_2$ in dichloromethane yielded single crystals of [Pd(L3)($CH_3COO)_2$] (**37**). The complex **37** crystallizes in the monoclinic ($P2_1/c$) space group. A view of the neutral molecule **37** is shown in Figure 7.10. Selected structural features are listed in Table 7.3. The ligand L3 coordinates to $Pd(OAc)_2$ in a chelating

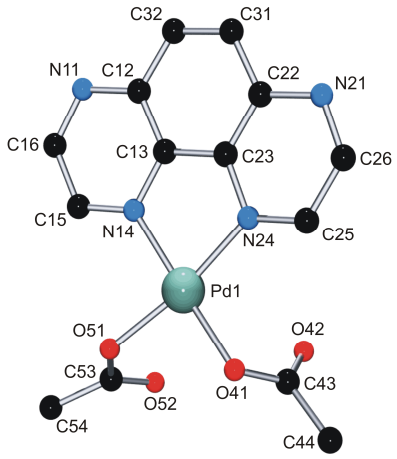

Figure 7.10: Molecular structure of neutral [Pd(L3)($CH_3COO)_2$] (**37**).

fashion. Pd-N (2.020(2), 2.026(2) Å) and Pd-O (2.0197(19), 2.0035(18) Å) bond distances are in the normal range. The bond angles around Pd deviate slightly from the ideal square-planar geometry. The acetates in complex **37** behave as monodentate ligands; only one of the two oxygen atoms is coordinated to Pd. The two acetate ligands make a dihedral angle of 76.7° and 65.2° with the $Pd1N_2O_2$ coordination plane. The dihedral angle between the two acetate ligands is 78.9°. Significant anion-π interaction is observed in the crystal packing. The distance of O41 or O51 to centroid of the adjacent pyrazine rings is 2.99 Å.

Table 7.3: Selected bond distances (Å) and angles (º) for compound **37**.

Pd1-N14, 2.020(2)	O51-Pd1-O41, 91.95(8)	O41-Pd1-N14, 174.65(8)
Pd1-N24, 2.026(2)	N14-Pd1-N24, 82.16(9)	O51-Pd1-N24, 170.49(8)
Pd1-O41, 2.0197(19)	O41-Pd1-N24, 95.20(9)	
Pd1-O51, 2.0035(18)	O51-Pd1-N14, 90.19(8)	

7.7. Crystal structure of polymeric $[Hg(L3)(CH_3COO)_2]_n$ (38)

Reaction of L3 with $Hg(OAc)_2$ in water yielded the polymeric complex $[Hg(L3)(CH_3COO)_2]_n$ (**38**). Single crystals of **38** were obtained by slow evaporation of an aqueous solution at room temperature. The complex crystallizes in the triclinic (P-1) space group. A view of the monomer unit of polymeric complex **38** is shown in Figure 7.11 and selected structural parameters are listed in Table 7.4. Hg-N distances (2.375(5), 2.493(5) Å) are in the normal range, as seen in various complexes of Hg(II).[5] Hg-O bond distances show considerable variations (Hg1-O1 and Hg1-O3 are markedly longer than Hg1-O2 and Hg1-O4), suggesting a semi-chelation of the acetate ligands. The bond angles about Hg(II) are highly irregular, and they are between 69.07(18)° and 158.71(13)°. The dihedral angle

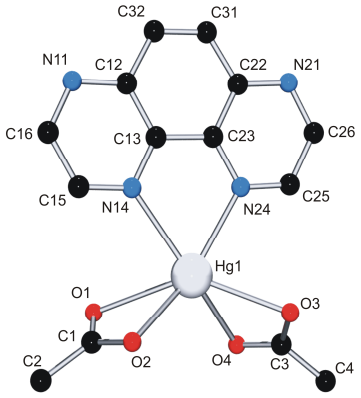

Figure 7.11: Structure of mononuclear unit of $[Hg(L3)(CH_3COO)_2]_n$ (**38**).

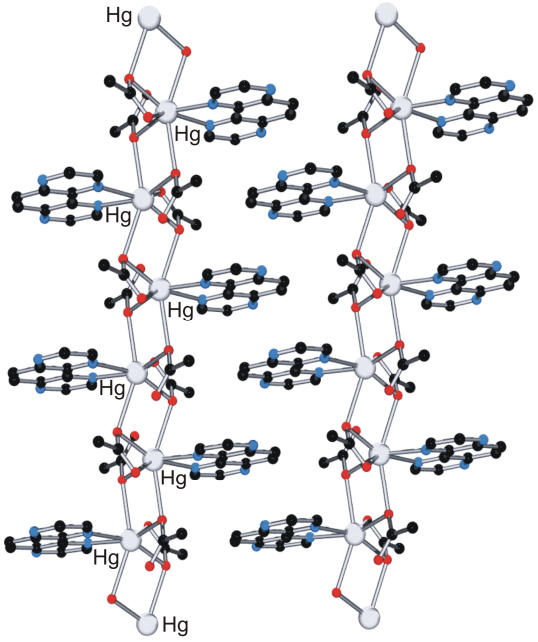

Figure 7.12: Structure of polymeric $[Hg(L3)(CH_3COO)_2]_n$ (**38**).

between two acetate ligands is 80.8°. The dihedral angles between L3 ligand and the two acetates are 66.3° and 66.9°. The coordination sphere of Hg(II) consists of two chelating N atoms from ligand L3 and four oxygens from two chelating acetate ligands. The Hg(II) has also two weak contacts with two oxygen atoms (O2, O4) from two neighbouring actetate ligands, which produces a one-dimensional polymeric strand of complex **38** (Figure 7.12). These Hg-O distances (2.68, 2.70 Å) are significantly longer than those to the (semi-) chelating acetates, yet they are well below the sum of the van der Waals radii of Hg (1.73 Å[6]) and O (1.4 Å), thereby qualifying them as bonds. Thus, the coordination number of Hg(II) in complex **38** is 8, or possibly better 4+2+2. Complex **38** shows its resonances (δ, ppm, D_2O) at 9.56, 9.21, 8.62 and 2.05 in the ^1H NMR spectrum.

Table 7.4: Selected bond distances (Å) and angles (º) for compound **38**.

Hg1-N14, 2.375(5)	O4-Hg1-O2, 95.56(14)	O4-Hg1-N14, 156.22(15)
Hg1-N24, 2.493(5)	O4-Hg1-N24, 93.31(16)	N14-Hg1-O2, 106.54(16)
Hg1-O1, 2.540(4)	N14-Hg1-N24, 69.07(18)	O2-Hg1-N24, 158.71(13)
Hg1-O2, 2.378(4)	N14-Hg1-O1, 79.47(16)	N24-Hg1-O1, 140.67(16)
Hg1-O3, 2.734(3)	O2-Hg1-O1, 52.97(12)	O4-Hg1-O1, 108.26(14)
Hg1-O4, 2.263(4)		

7.8. Crystal Structure of $[Ag(CF_3COO)(L3)_2]$ (39)

$[Ag(CF_3COO)(L3)_2]$ (**39**) was obtained from the reaction of L3 with $Ag(CF_3COO)$ in $CHCl_3$. $[Ag(CF_3COO)(L3)_2]$ (**39**) crystallizes in the monoclinic (C2/c) space group. A view of **39** is shown in Figure 7.13 and selected structural parameters are listed in Table 7.5. The coordination sphere of Ag consists of two L3 ligands and one CF_3COO^- ligand. Both the trifluoro acetate and L3 ligands coordinate to Ag^I in chelating fashions. Ag-N bond distances (2.413(2), 2.448(2) Å) are significantly shorter that Ag-O (2.613 Å) distances. The two L3 ligands form a dihedral angle of 75.8°. The dihedral angle between CF_3COO^- and L3 ligands is 54.35°. Strong anion-π interaction is observed in the crystal packing of complex **39**. The fluorine atoms of the CF_3COO^- ligand interact with the π cloud of adjacent pyrazine rings of the L3 ligands. The distance from F atoms to the centroid of the pyrazine ring is 2.68 Å.

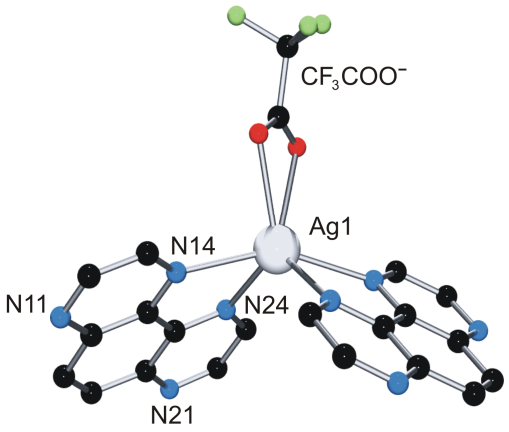

Figure 7.13: Structure of $[Ag(CF_3COO)(L3)_2]$ (**39**)

Table 7.5: Selected bond distances (Å) and angles (º) for compound **39**.

Ag1-N14, 2.413(2)	N14-Ag1-N24, 69.09(8)	N14-Ag1-N24, 96.67(8)
Ag1-N24, 2.448(2)	N14-Ag1-N24, 69.10(8)	N14-Ag1-N14, 119.81(11)
	N14-Ag1-N24, 96.67(8)	N24-Ag1-N24, 152.22(11)

7.9. Structure of polymeric $\{[Ag_4(L3)_2(SO_4)_2]\cdot H_2O\}_n$ (40)

Reaction of L3 with Ag_2SO_4 in water yielded the polymeric complex $\{[Ag_4(L3)_2(SO_4)_2]\cdot H_2O\}_n$ (**40**). Single crystals were obtained by the slow evaporation of an aqueous solution of reaction mixture at room temperature. A preliminary structural analysis confirms that it is a polymeric complex (Figure 7.14). The sulphate anions are also involved in silver coordination.[8] Three out of four nitrogen atoms in L3 coordinate to the

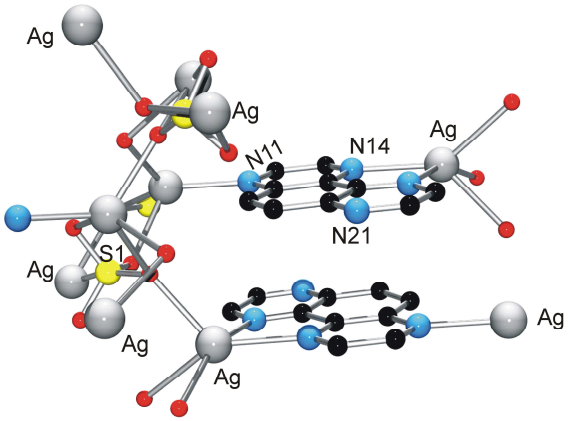

Figure 7.14: Section of polymeric complex **40**.

Ag^{+} ion. Ag-O distances are significantly longer than the Ag-N bonds. The coordination sphere of Ag^{I} is distorted trigonal-bipyramidal. In the polymeric network of complex **40** the adjacent aromatic L3 ligands are stacked on each other and the distance from the centroid of one ring to the plane of adjacent L3 ligand is 3.26 Å.

7.10. Structure of polymeric $\{[Ag_2(L4)_2(H_2O)_2](ClO_4)_2{\cdot}H_2O\}_n$ (41)

$\{[Ag_2(L4)_2(H_2O)_2](ClO_4)_2{\cdot}H_2O\}_n$ (**41**) was prepared from the reaction of L4 with $AgClO_4$ in $CHCl_3$. The polymeric complex **41** crystallizes in the monoclinic ($P2_1/c$) space group. A view of **41** is shown in Figure 7.15 and selected structural parameters are listed in Table 7.6. Complex **41** has two different Ag^{I} (Ag1, Ag2) units. The coordination environment

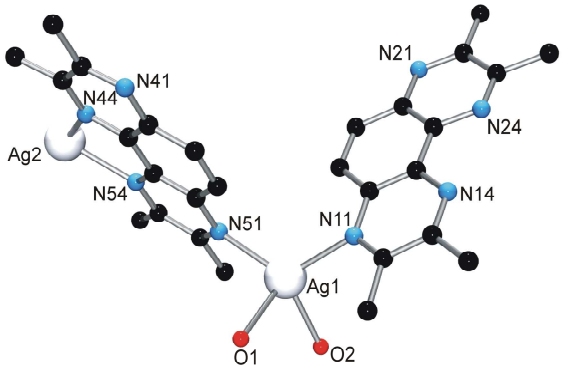

Figure 7.15: Monomeric unit of $\{[Ag_2(L4)_2(H_2O)_2](ClO_4)_2{\cdot}H_2O\}_n$ (**41**)

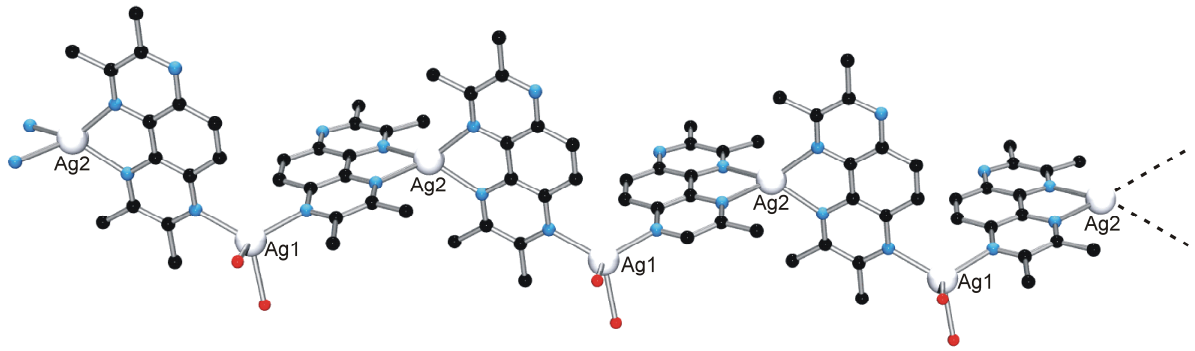

Figure 7.16: Structure of polymeric complex **41**.

around both Ag metal ions is distorted tetrahedral. The two L4 ligands coordinate with Ag2 in a chelating fashion to give $Ag2(L4)_2$ units and these units are connected by metal (Ag1) coordination through its available N11 and N51 coordination sites, leading to the formation

of a one-dimensional polymer. The coordination sphere of Ag1 consists of two nitogen atoms from two adjacent L4 ligands (Ag1-N11, 2.293(3); Ag1-N51, 2.299(2) Å) and two water molecules (Ag1-O1, 2.400(2); Ag1-O2, 2.395(2) Å). The N11-Ag1-N51 bond angle is 119.04(8)°. The two adjacent L4 ligands, which are coordinated to either Ag1 or Ag2, are almost perpendicular to each other (84.2°). The water molecules coordinated to Ag1 are involved in multiple hydrogen bonding interactions with ClO_4^- anions, water of crystallization and non-coordinated N sites (N41, N21) of L4 ligands.

Table 7.6: Selected bond distances (Å) and angles (º) for compound **41**.

Ag1-N11, 2.293(3)	O2 Ag1 O1 85.03(8)	N44 Ag2 N54 73.90(9)
Ag1-N51, 2.299(2)	N11 Ag1 O2 98.62(8)	N24 Ag2 N14 74.40(9)
Ag1-O2, 2.395(2)	N11-Ag1-N51, 119.04(8)	N54 Ag2 N14 121.23(8)
Ag1-O1, 2.400(2)	N51 Ag1 O1 104.37(8)	N24 Ag2 N54 127.39(9)
Ag2-N24, 2.265(2)	N51 Ag1 O2 117.24(8)	N44 Ag2 N14 133.82(9)
Ag2-N44, 2.268(2)	N11 Ag1 O1 127.59(9)	N24 Ag2 N44 134.49(8)
Ag2-N54, 2.309(3)	Ag2 N14 2.322(3)	

7.11. Crystal structure of $[Ag_3(NO_3)_2(L4)_4][Ag(L4)_2](NO_3)_2\cdot 8H_2O$ (42)

Reaction of L4 with $AgNO_3$ yielded complex $[Ag_3(NO_3)_2(L4)_4][Ag(L4)_2](NO_3)_2\cdot 8H_2O$ (**42**). Complex **42** crystallizes in the monoclinic (C2/c) space group. A view of **42** is shown in Figure 7.11. Selected bond distances and angles are listed in Table 7.7. **42** consists of two independent units: $[Ag(L4)_2]$ and $[Ag_3(NO_3)_2(L4)_4]$. In $[Ag(L4)_2]$, both L4 ligands coordinate to Ag through their chelating nitrogen atoms. But in $[Ag_3(NO_3)_2(L4)_4]$ two terminal L4 ligands act as chelate, while the other two L4 ligands coordinate to Ag both as chelate and monodentate fashion. The coordination environment of all four Ag^I ion is distorted tetrahedral. The L4 ligands in $[Ag(L4)_2]$ make a dihedral angle of 58.5°. In $[Ag_3(NO_3)_2(L4)_4]$ unit, the dihedral angle between two adjacent L4 ligands is 58.8° at Ag3 and 59.3° at Ag2 or Ag2'. There are weak π-π stacking interactions between these two independent units in crystal packing and the distances being 3.29 – 3.36 Å. The nitrate anions which are coordinated to Ag2 or Ag2' ion displays significant anion- π interaction in the crystal lattice.

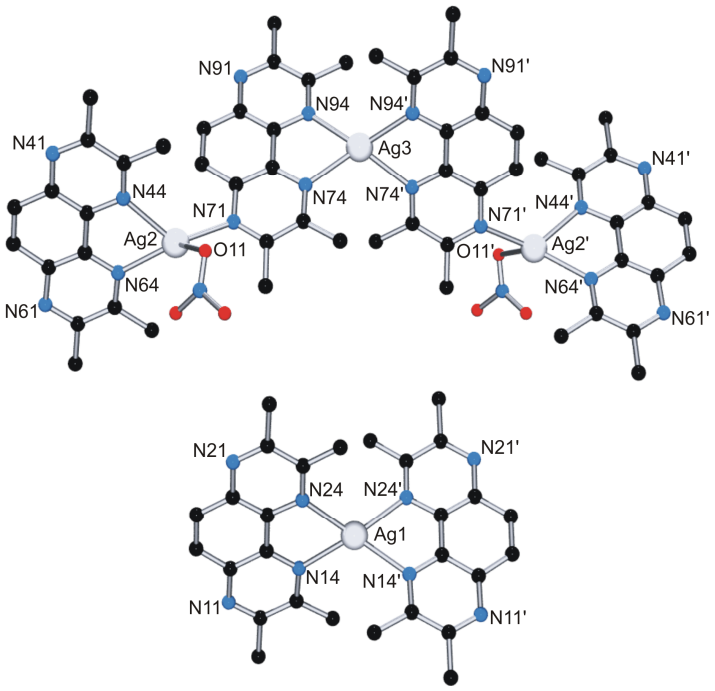

Figure 7.17: View of the two cations of $[Ag_3(NO_3)_2(L4)_4][Ag(L4)_2](NO_3)_2{\cdot}8H_2O$ (**42**).

Table 7.7: Selected bond distances (Å) and angles (º) for compound **42**.

Ag1-N24, 2.318(6)	N24-Ag1-N24, 116.7(3)	N71-Ag2-N64, 141.4(2)
Ag1-N24, 2.318(6)	N24-Ag1-N14, 73.4(2)	N71-Ag2-N44, 126.0(2)
Ag1-N14, 2.350(6)	N24-Ag1-N14, 73.4(2)	N64-Ag2-N44, 73.4(2)
Ag1-N14, 2.350(6)	N24-Ag1-N14, 144.0(2)	N74-Ag3-N74, 113.4(3)
Ag2-O11, 2.468(11)	N14-Ag1-N14, 120.2(3)	N94-Ag3-N74, 74.1(2)
Ag2-N44, 2.382(6)	N24-Ag1-N14, 144.0(2)	N94-Ag3-N74, 143.1(2)
Ag2-N64, 2.300(6)	N64-Ag2-O11, 125.9(3)	N94-Ag3-N74, 143.1(2)
Ag2-N71, 2.242(6)	N44-Ag2-O11, 93.8(3)	N94-Ag3-N74, 74.1(2)
Ag3-N74, 2.327(6)	N71-Ag2-O11, 88.8(3)	N94-Ag3-N94, 122.8(3)
Ag3-N74, 2.327(6)	Ag3-N94, 2.287(6)	Ag3-N94, 2.287(6)

7.12. Reactions of L3 and L4 with Zn^{2+}

The reaction of L3 with $Zn(NO_3)_2$ yielded crystals of $[Zn(L3)_2(NO_3)_2]$ (**43**). It crystallizes in monoclinic (C2/c) space group. A view of **43** is shown in Figure 7.18 and selected structural parameters are listed in Table 7.8. Complex **43** consists of two L3 ligands and

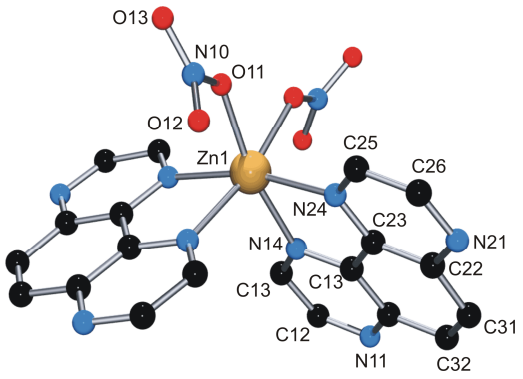

Figure 7.18: Structure of $[Zn(L3)_2(NO_3)_2]$ (**43**).

two coordinated nitrate (NO_3^-) anions. The coordination sphere of Zn in complex **43** is distorted octahedral. Zn-N and Zn-O distances are in the normal range. The L3 ligands coordinate to Zn^{2+} through their chelating nitrogen atoms.

Table 7.8: Selected bond distances (Å) and angles (º) for compound **43**.

Zn1-O11, 2.0861(16)	O11-Zn1-O11, 77.01(9)	O11-Zn1-N14, 94.24(7)
Zn1-N14, 2.1573(18)	N14-Zn1-N24, 77.36(7)	N14-Zn1-N14, 95.24(10)
Zn1-N24, 2.1675(18)	N14-Zn1-N24, 92.93(7)	N24-Zn1-N24, 165.70(10)
Zn1-N24, 2.1674(18)	O11-Zn1-N24, 94.93(7)	O11-Zn1-N14, 168.82(7)
	O11-Zn1-N24, 96.25(7)	

Complex $[Zn(L4)_2(H_2O)][Zn(L4)(H_2O)_3](ClO_4)_4{\cdot}5H_2O$ (**44**) was obtained from the reaction of L4 with $Zn(ClO_4)_2$. Complex **44** crystallizes in the triclinic (P-1) space group. Figure 7.19 gives a view of complex **44** and selected structural parameters are listed in

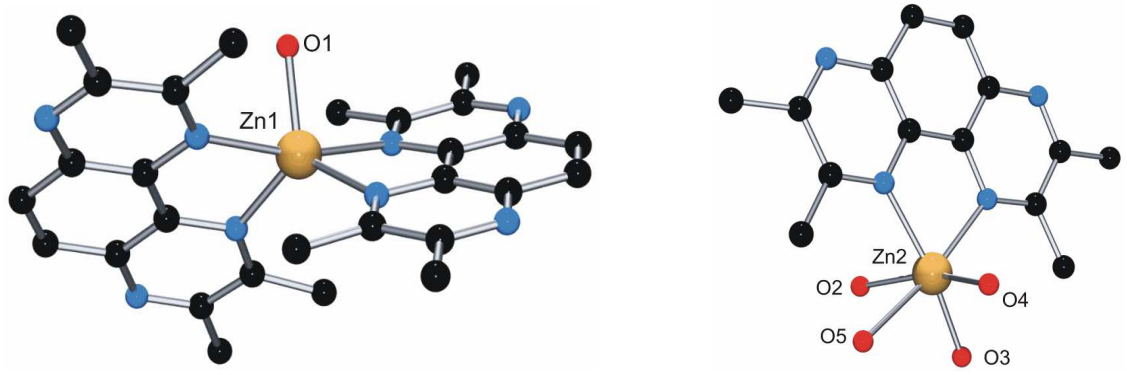

Figure 7.19: View of cations of $[Zn(L4)_2(H_2O)][Zn(L4)(H_2O)_3](ClO_4)_4{\cdot}5H_2O$ (**44**).

Table 7.9. Complex **44** contains two independent units: $[Zn(L4)_2(H_2O)]^{2+}$ and $[Zn(L4)(H_2O)_3]^{2+}$. In both units L4 ligands coordinate to Zn^{2+} as chelates. In the first unit $[Zn(L4)_2(H_2O)]^{2+}$, the coordination environment of Zn^{2+} is distorted trigonal bipyrimidal, and in second unit the environment of Zn^{2+} is distorted octahedral. Water molecules of crystallization and perchlorate (ClO_4^-) anions are involved in multiple hydrogen bonding.

Table 7.8: Selected bond distances (Å) and angles (º) for compound **44**.

Zn1-O1, 1.995(5)	N54-Zn1-N44, 80.20(18)	O1-Zn1-N24 116.50(19)
Zn1-N54, 2.092(4)	O1-Zn1-N44, 82.65(18)	N24-Zn1-N44 104.77(17)
Zn1-N24, 2.098(4)	N24-Zn1-N14, 80.40(17)	N14-Zn1-N44 165.3(2)
Zn1-N14, 2.165(4)	O1-Zn1-N14, 82.76(19)	O1-Zn1-N54 122.69(18)
Zn1-N44, 2.177(5)	N54-Zn1-N24, 120.70(18)	N54-Zn1-N14 109.31(18)
Zn2-O2, 1.995(5)	O4-Zn2-N74, 94.8(3)	O2-Zn2-N84, 84.3(2)
Zn2-O3, 2.031(5)	O2-Zn2-O5, 74.6(4)	O4-Zn2-O2, 157.0(3)
Zn2-N74, 2.187(7)	O3-Zn2-O5, 86.6(3)	O3-Zn2-N84, 169.0(2)
Zn2-N84, 2.195(7)	N84-Zn2-O5, 90.8(3)	O3-Zn2-N74, 104.6(3)
Zn2-O5, 2.338(10)	N74-Zn2-N84, 78.4(2)	O2-Zn2-N74, 107.9(2)
O2-Zn2-O3, 84.7(2)	O4-Zn2-O3, 93.1(2)	N74-Zn2-O5, 168.5(3)
O4-Zn2-N84, 97.1(2)	O4-Zn2-O5, 82.5(4)	O4-Zn2-O2, 157.0(3)

7.13. Conclusion

Two tetradentate ligands, L3 and L4, were reacted with various metal ions and metal entities. A series of discrete as well as polymeric complexes were isolated and characterized by single crystal X-ray crystallography. The isolated complexes can be divided into three classes, based on their modes: class A, B, C (Scheme 7.5). In the majority of complexes, coordination to metal ions is as chelate. The following complexes fall into class A in which L3 or L4 acts as chelating ligand only: $[Pd(en)(L3)](NO_3)_2{\cdot}H_2O$ (**34a**), $[Pd(en)(L3)](ClO_4)_2{\cdot}2H_2O$ (**34b**), $[Pd(en)(L4)](NO_3)_2{\cdot}1.5H_2O$ (**35**), $[Pd(L3)(CH_3COO)_2]$ (**37**), $[Hg(L3)(CH_3COO)_2]_n$ (**38**), $[Ag(CF_3COO)(L3)_2]$ (**39**), $[Zn(L3)_2(NO_3)_2]$ (**43**), $[Zn(L4)_2(H_2O)][Zn(L4)(H_2O)_3](ClO_4)_4{\cdot}5H_2O$ (**44**). In two compounds, $\{[Ag_4(L3)_2(SO_4)_2]{\cdot}H_2O\}_n$ (**40**) and $\{[Ag_2(L4)_2(H_2O)_2](ClO_4)_2{\cdot}H_2O\}_n$ (**41**), three nitrogen atoms

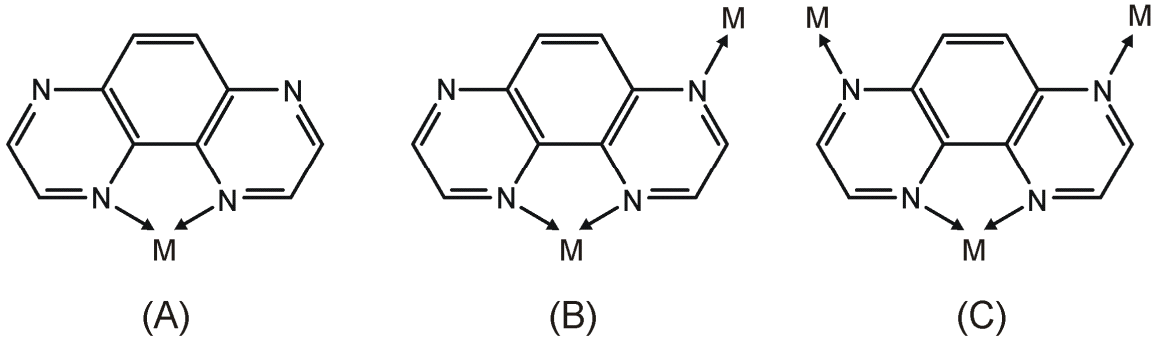

Scheme 7.5

out of four take part in metal coordination (Class B). Only in one case, namely in complex $\{Ag(L3)]_2Ag(NO_3)_3{\cdot}3H_2O\}_n$ (**36**), all four nitrogen atoms are coordinated to the metal ions. Complex $[Ag(L4)_2][Ag_3(L4)_4](NO_3)_4$ (**42**) contains two independent units, which shows both class A as well as class B type metal coordination. Unfortunately, no example of a discrete metallacycle could be verified.

7.14. References

[1] a) A. Kirsch-De Mesmaeker, L. Jacquet, J. Nasielski, *Inorg. Chem.* **1988**, *27*, 4451–4458; b) L. Jacquet, J. M. Kelly, A. Kirsch-De Mesmaeker, *J. Chem. Soc., Chem. Commun.* **1995**, 913–914; c) J. A. Real, M. Carmen Munoz, E. Andres, T. Granier, B. Gallois, *Inorg. Chem.* **1994**, *33*, 3587–3594; d) D. M. D'Alessandro, M. S. Davies, F. R. Keene, *Inorg. Chem.* **2006**, *45*, 1656–1666

[2] A. J. Blake, N. R. Champness, P. A. Cooke, J. E. B. Nicolson, C. Wilson, *J. Chem. Soc.*, *Dalton Trans*. **2000**, 3811–3819.

[3] a) J. A. R. Navarro, B. Lippert, *Coord. Chem. Rev.* **2001**, *222*, 219–250; b) R. -D. Schnebeck, L. Randaccio, E. Zangrando, B. Lippert, *Angew. Chem. Int. Ed.* **1998**, *37*, 119–121; c) R. -D. Schnebeck, E. Freisinger, B. Lippert, *Angew. Chem. Int. Ed.* **1999**, *38*, 168–171; d) R. -D. Schnebeck, E. Freisinger, B. Lippert, *Chem. Commun.* **1999**, 675–676; e) R. -D. Schnebeck, E. Freisinger, F. Glah, B. Lippert, *J. Am. Chem. Soc.* **2000**, *122*, 1381–1390.

[4] R. Nasielski-Hinkens, M. Benedek-Vamos, *J. Chem. Soc. Parkin Trans. 1* **1975**, 1229–1229; b) R. Nasielski-Hinkens, J. Kotel, T. Lecloux, J. Nasielski, *Synth. Commun.* **1989**, *19*, 511–514.

[5] S. -Y. Yu, H. Huang, H. -B. Liu, Z. -N. Chen, R. Zhang, M. Fujita, *Angew. Chem. Int. Ed.* **2003**, *42*, 686–690.

[6] F. Zamora, M. Sabat, B. Lippert, *Inorg. Chim. Acta.* **1998**, *167*, 87–91.

[7] A. J. Canty, G. B. Decon, *Inorg. Chim. Acta.* **1980**, *45*, L225–L227.

[8] K. V. Domasevitch, I. A. Gural'skiy, P. V. Solntsev, E. B. Rusanovb, A. N. Chernegab, *Acta Cryst. C63*, **2007**, m259–m263.

Summary

English Version

The synthesis of discrete as well as polymeric metal complexes has received great attention in recent years because of their wide potential applications in chemistry. In chapter 1, various complexes of Pt^{II} and Pd^{II} with the unsubstituted pyrimidine nucleobase cytosine are discussed, including their characterization by X-ray crystallography. pD dependant ^1H NMR spectra in D_2O were also recorded to determine relevant pK_a values. The *head-tail* dimer *cis*-{[Pt$(NH_3)_2$(HC-*N3,N4*)]$_2$}$(NO_3)_2$ (**8**) contains a truly rare tautomer form (Figure S1) of the cytosine monoanion, stabilized by twofold metal coordination through N3 and N4. While cytosine deprotonates at N1 with a pK_a ~ 12.15, the cytosine anion present in **8** has lost a proton from the exocyclic amino group, while still maintaining the proton at N1. The cations of complex **8** behave as anion receptors via directional hydrogen bonding of their attached NH_3 ligands. Also, the synthesis of multinuclear metal complexes of various ring sizes with the parent (unsubstituted) pyrimidine nucleobase

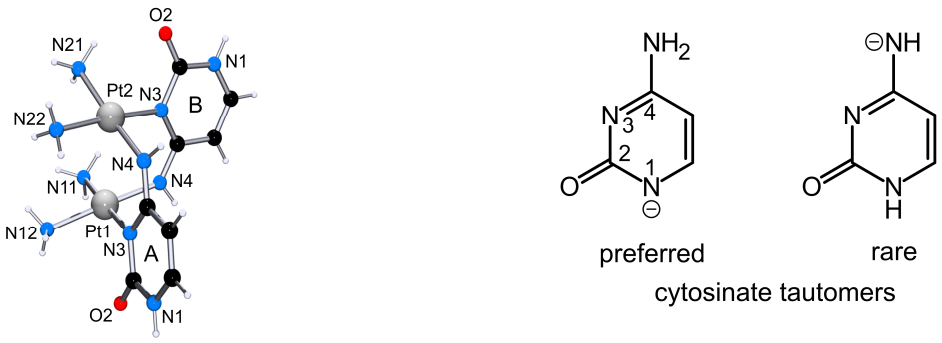

Figure S1: Structure of cation **8** (left) and tautomeric forms for cytosinate monoanion (right).

cytosine is discussed in chapter 1. These cyclic metal complexes are termed metallacalix[n]arenes because of their structural similarity with classic calix[n]arenes. Cytosine, being a low symmetrical ligand (C_s), can give rise rise to the formation of random mixtures of cyclic isomers and numerous rotamers when combined with *cis*-a_2M^{II} (a = am(m)ine, a_2 = diamine; M = Pt, Pd) entites. However, when a directed approach is followed, hence kinetically inert preformed building blocks such as *cis*-[Pta_2(H_2C-*N3*)$_2$]$^{2+}$ (a = NH_3, **1**; a_2 = en, **2**) and *cis*-[Pta_2(HC-*N1*)$_2$] (a = NH_3; **4**) are applied, single linkage isomers can be obtained upon addition of kinetically labile metal entities such as *cis*-a_2Pd^{II} (a_2 = en; 2,2'-bpy). The intramolecular hydrogen bonding between exocyclic O2 and

$N(4)H_2$ groups of cytosines lock these molecules in 1,3-alternate conformations. For example, reaction of *cis*-$[Pt(NH_3)_2(HC\text{-}N1)_2]$ (**4**) with $[Pd(2,2'\text{-bpy})(H_2O)_2](NO_3)_2$ yielded the cyclic tetramer *cis*-$[\{Pt(NH_3)_2(N1\text{-}HC\text{-}N3)_2Pd(2,2'\text{-bpy})\}_2](NO_3)_4 \cdot 13H_2O$ (**9**) (Figure S2), where *cis*-$(NH_3)_2Pt^{II}$ is coordinated to N1 sites of two cytosinates and $(bpy)Pd^{II}$ bonded to two N3 sites. Complex **9** has a N1,N3•N3,N1•N1,N3•N3,N1• (with • representing

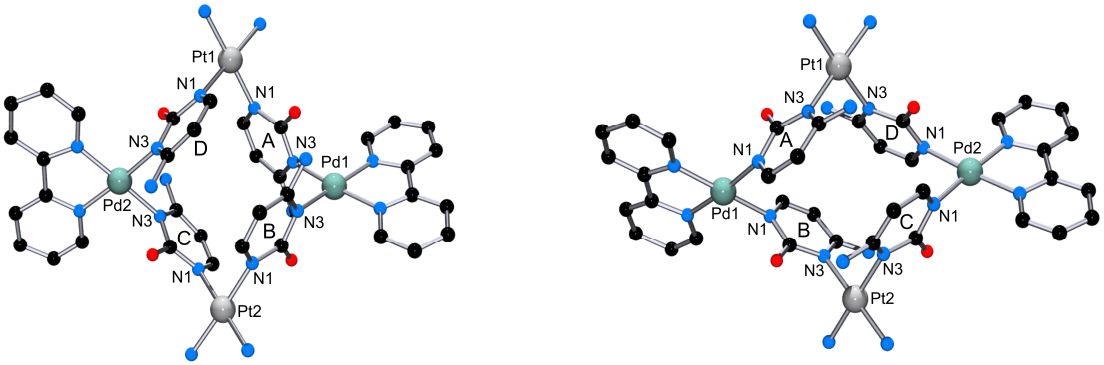

Figure S2: Structure of cation **9** (left) and **12** (right).

the metal entity) connectivity pattern and a 1,3-alternate conformation. It is also possible to obtain metallacalix[4]arenes with two different metal ions as the corner units and also with different am(m)ine ligands attached to the metal ions. The isomer of **9**, with the two kinds of metal entities inverted, *cis*-$[\{Pt(NH_3)_2(N3\text{-}HC\text{-}N1)_2Pd(2,2'\text{-bpy})\}_2](NO_3)_4 \cdot 9H_2O$ (**12**) (Figure S2) and an analogue of the latter, $[\{Pt(en)(N3\text{-}HC\text{-}N1)_2Pd(2,2'\text{-bpy})\}_2](NO_3)_4 \cdot 8.5H_2O$ (**13**), have likewise been prepared and characterized. Inversion of *cis*-$(NH_3)_2Pt^{II}$ and $(bpy)Pd^{II}$ (compounds **9** and **12**) leads to differences in shape and dimensions of the constructs. Differences in electron distributions in the isomers **9** and **12** are also reflected in their ^1H NMR spectra. Reaction of $[Pt(en)(H_2C\text{-}N3)_2]^{2+}$ (**2**) with

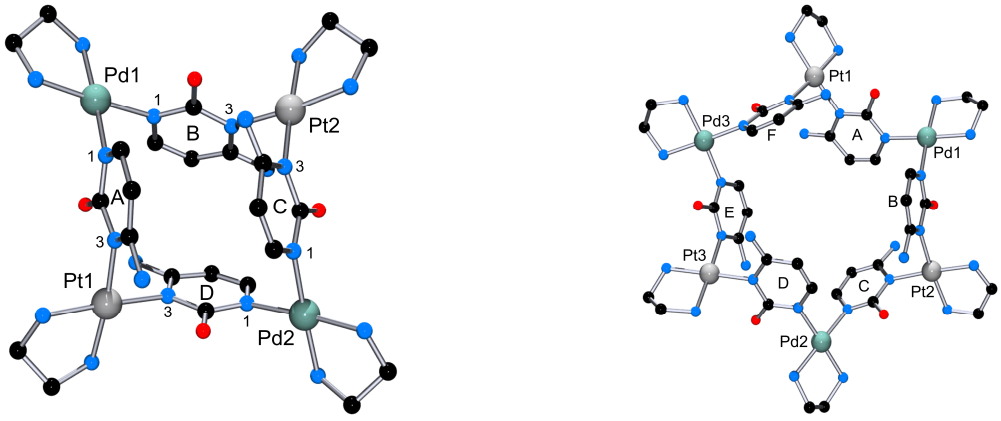

Figure S3: Structure of cations of tetramer **14** (left) and hexamer **15** (right).

$[Pd(en)(H_2O)_2](NO_3)_2$ produced a mixture containing both a cyclic tetramer $[\{Pt(en)(N3\text{-}HC\text{-}N1)_2Pd(en)\}_2](NO_3)_4\cdot 9.5H_2O$ (**14**) and a cyclic hexamer $[\{Pt(en)(N3\text{-}HC\text{-}N1)_2Pd(en)\}_3](NO_3)_6\cdot 18H_2O$ (**15**) (Figure S3). Simultaneous formation of cycles of different ring size (**14**, **15**) reflects the well-known phenomenon of supramolecular systems to find a balance between entropically and thermodynamically favorable conditions. The exocyclic O2 and $N(4)H_2$ groups of such complexes can be used for further metal coordination to generate octanuclear derivatives with short metal-metal distances. Two octanuclear complexes, **11** and **16** (Figure S4), have been prepared, starting from $[Pd(2,2'\text{-bpy})(H_2O)_2](NO_3)_2$ and cytosine. The differences in topology of the two cations is a result of the differences in mutual spatial dispositions of the exocyclic groups O2 and N4 of the cytosine rings, to which the four other $(bpy)Pd^{II}$ entities are bonded.

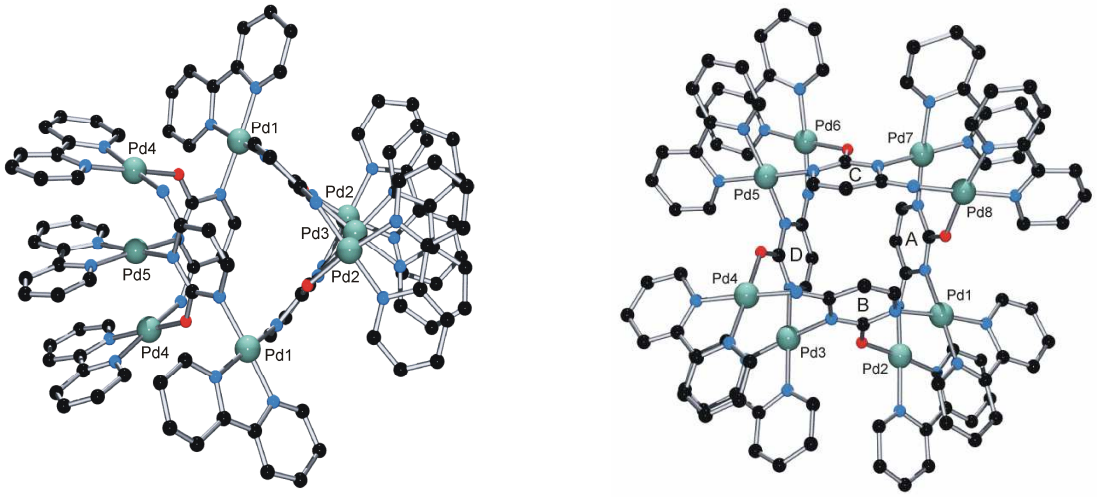

Figure S4: Structure of cations **11** (left) and **16** (right).

In chapter 2, attempts to synthesize metallacalix[n]arenes containing the unsubstituted nucleobase uracil are described. Particularly *cis*-$[Pt(NH_3)_2(HU\text{-}N1)(HU\text{-}N3)]$ (**18**) and *cis*-$[Pt(NH_3)_2(HU\text{-}N1)_2]$ (**19**) have been reacted with the *cis*-$(NH_3)_2Pt^{II}$ entity. Though the reactions carried out on the ^1H NMR scale showed formation of various new species, attempts to isolate any of these species were unsuccessful. The nature of "platinum pyrimidine blues" derived from unsubstituted pyrimidine bases such as uracil, cytosine is not fully understood because of their very complex behavior. However, the results of this thesis (chapters 1 and 2) provide a deeper understanding of this class of "blues".

In chapter 3, a series of multinuclear complexes is described, which were prepared through reactions of 1-methyluracil (1-MeUH) based ligands (L1 and L2) with *cis*-a_2M^{II}

entities. This class of metallacycles can be considered hybrids between classical calix[4]arenes and metallacalix[4]arenes because of the presence of both methylene as well as *cis*-a_2M^{II} entities as bridging units (Figure S5). The exocyclic O2 and O4 sites of uracil can also be used to generate high nuclearity derivatives. Reaction of L1 with *cis*-$[Pt(NH_3)_2(H_2O)_2](NO_3)_2$ is very interesting because, depending on reaction conditions (concentration, pH of the solution), cyclic metallacycles of different composition have been obtained.

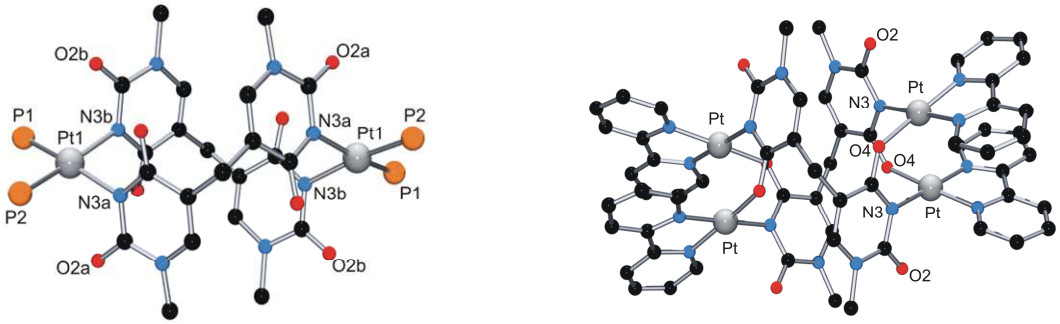

Figure S5: Structures of neutral *cis*-$[Pt(PPh_3)_2(L1'\text{-}N3)]_2 \cdot 4H_2O$ (**20**) (left) and cation of $\{[Pt(2,2'\text{-bpy})]_2(L1'\text{-}N3,O4)\}_2(NO_3)_4 \cdot 8H_2O$ (**21**) (right).

In chapter 4, the well know equilibrium between ketone and geminal diol form has been studied for di-2-pyridyl ketone (dpk) (Scheme S1) and its metal complexes (Pt^{II}, Pd^{II}) by ^{1}H NMR spectroscopy in D_2O and DMSO-d_6. For the free ligand, the equilibrium constant between the ketone (dpk) and the *gem*-diol (dpk·H_2O) forms is 0.04. In presence of kinetically labile Pd^{II}, the *gem*-diol form is highly favored and in fact the reverse reaction Pd(dpk·H_2O) → Pd(dpk) + H_2O is likewise realized. With Pt^{II}, because of its slower kinetics, it is possible to obtain a trinuclear complex $[Pt_3(\mu\text{-}OH)_3(dpk\cdot H_2O)_2(dpk)](NO_3)_3 \cdot 4.5H_2O$ (**29**) which contains both dpk as well as dpk·H_2O ligands.

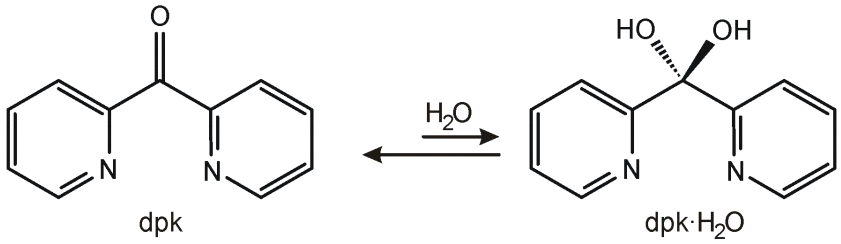

Scheme S1: Conversion of dpk to dpk·H_2O.

In chapters 5 and 6, heterocyclic nitrogen based ligands (3,3'-bpy, 1,4,5,8-tetra-azaphenanthrene) have been prepared and their reaction products with transition metal ions and metal entities are reported. Reaction of 3,3'-bpy with $Hg(OAc)_2$ yielded the dinuclear complex $[Hg(3,3'\text{-bpy})(CH_3COO)_2]_2 \cdot 3H_2O$ (**31**) (Figure S6) which represents the smallest possible entity of any cyclic complex. With tetra-azaphenanthrene based ligands (L3, L4), the synthesis of various polymeric metal complexes is described, with a number of compounds characterized by X-ray crystallography. An unusual transmetallation reaction is observed in the reaction of $[Pd(en)(L3)](NO_3)_2 \cdot H_2O$ (**34a**) with $AgNO_3$, resulting in the formation of the polymeric complex $\{[Ag(L3)]_2Ag(NO_3)_3 \cdot 3H_2O\}_n$ (**36**).

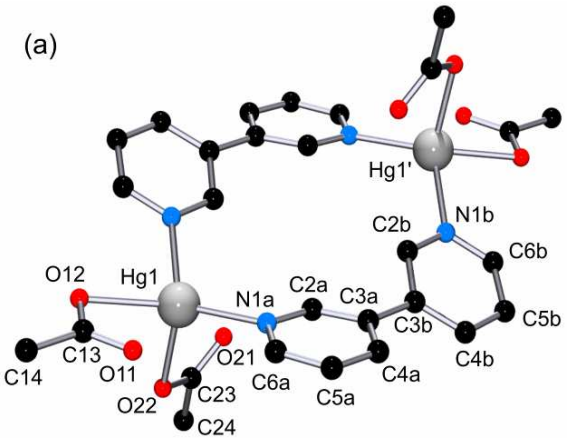

Figure S6: Structure of dinuclear **31**.

German Version

Der Synthese diskreter und polymerer Metallkomplexe wurde aufgrund ihrer verschiedenen Anwendungsmöglichkeiten in den letzten Jahren viel Aufmerksamkeit zuteil. Das erste Kapitel der vorliegenden Arbeit zeigt die Synthese und Charakterisierung durch Röntgenstrukturanalyse verschiedener Pd^{II}- und Pt^{II}- Komplexe mit der unsubstituierten Pyrimidin-Nucleobase Cytosin als Ligand. Die Bestimmung von pK_s-Werten der entsprechenden Verbindungen erfolgte mit pH-abhängiger ^{1}H-NMR-Spektroskopie. Das Kopf-Schwanz-Dimer *cis*-{[Pt$(NH_3)_2$(HC-*N3,N4*)]$_2$}$(NO_3)_2$ (**8**) zeigt ein seltenes Tautomer des Cytosinato-Monoanions (Abbildung S1), stabilisiert durch zweifache Metallkoordination über die N3- und N4-Position des Cytosinanions. Während die Deprotonierung der N1-Position am freien Liganden einen pK_s-Wert von ~ 12.15 aufweist, wird das Anion im vorliegenden Komplex **8** an der exocyclischen Aminogruppe deprotoniert, während die N1-Position weiterhin protoniert vorliegt. Die Kationen der Verbindung **8** agieren als Anionen-Rezeptor über gerichtete Wasserstoffbrückenbindungen der NH_3-Liganden. Zudem wurde in Kapitel 1 die Synthese

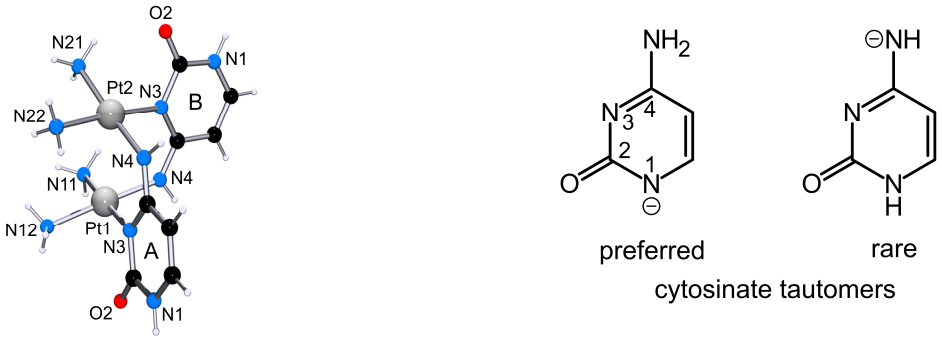

Abbildung S1: Struktur des Kations 8 (links) und der Tautomere des Cytosinato-Monoanions (rechts)

mehrkerniger Metallkomplexe mit Cytosinliganden und variabler Ringgröße vorgestellt. Diese cyclischen Metallkomplexe werden aufgrund ihrer strukturellen Ähnlichkeit zu klassischen Calix[n]arenen als Metallacalix[n]arene bezeichnet. Cytosin führt als Ligand niedriger Symmetrie (C_s) in Kombination mit *cis*-a_2M^{II}-Einheiten (a = Am(m)in, a_2 = Diamin; M = Pt, Pd) zur Bildung von zufälligen Mischungen cyclischer Isomerer und verschiedener Rotamerer. In einem gezielten Ansatz wurden zwei kinetisch inerte Bausteine *cis*-[Pta_2(H_2C-*N3*)$_2$]$^{2+}$ (a = NH_3, **1**; a_2 = en, **2**) und *cis*-[Pta_2(HC-*N1*)$_2$] (a = NH_3, **4**) hergestellt. Die Reaktion dieser Grundbausteine mit kinetisch labilen Metalleinheiten des Typs *cis*-a_2Pd^{II} (a_2 = en; 2,2'-bpy) führt zur Bildung cyclischer Metallacalix[n]arene mit einem einzigen Bindungsisomer. Die intramolekularen Wasserstoffbrückenbindungen zwischen

den exocyclischen O2- und N(4)H_2- Gruppen der Cytosinatoliganden fixieren diese in einer 1,3-alternierenden Anordnung. Als Beispiel dient hier die Reaktion von *cis*-[Pt$(NH_3)_2$(HC-*N1*)$_2$] (**4**) mit [Pd(2,2'-bpy)$(H_2O)_2$]$(NO_3)_2$, die zur Bildung des cyclischen Tetramers *cis*-[{Pt$(NH_3)_2$(*N1*-HC-*N3*)$_2$Pd(2,2'-bpy)}$_2$]$(NO_3)_4\cdot 13H_2O$ (**9**) (Abbildung S2) führt, bei dem die $(NH_3)_2Pt^{II}$-Grundeinheit an die N1-Stickstoffatome von Cytosin gebunden ist, während die (bpy)Pd^{II}-Einheit mit zwei N3-Positionen verbunden ist. Komplex **9** zeigt die Abfolge N1,N3•N3,N1•N1,N3•N3,N1• (wobei • die Metalleinheit repräsentiert) und die 1,3-

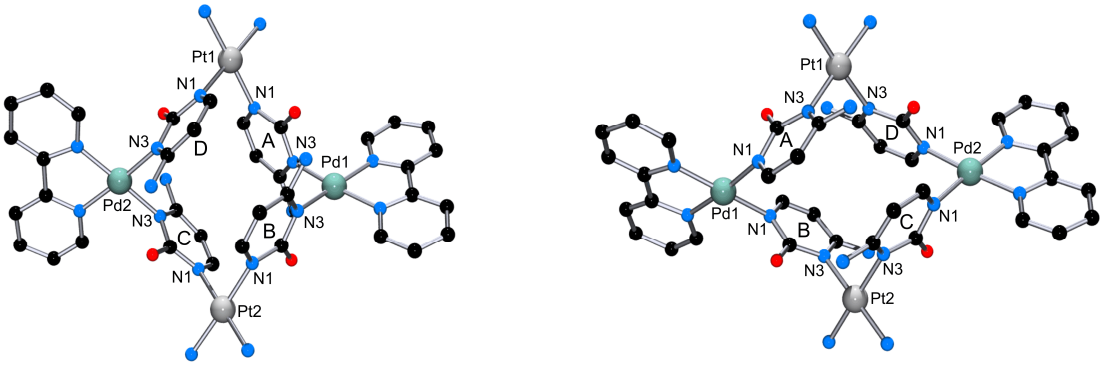

Abbildung S2: Strukturen der Kationen von **9** (links) und **12** (rechts).

alternierende Konformation. Es ist darüber hinaus möglich, Metallacalix[n]arene zu erhalten, mit zwei verschiedenen Metallionen als Ecken und zwei weiteren Am(m)inliganden, die an die Metallionen gebunden sind. Im Isomer von Verbindung **9**, *cis*-[{Pt$(NH_3)_2$(*N3*-HC-*N1*)$_2$Pd(2,2'-bpy)}$_2$]$(NO_3)_4\cdot 9H_2O$ (**12**) (Abbildung S2), sind die beiden Metalleinheiten vertauscht. Weiterhin wurde ein Analogon der Verbindung **12**, [{Pt(en)(*N3*-HC-*N1*)$_2$Pd(2,2'-bpy)}$_2$]$(NO_3)_4\cdot 8.5H_2O$ (**13**) sythetisiert und charakterisiert. Die Inversion

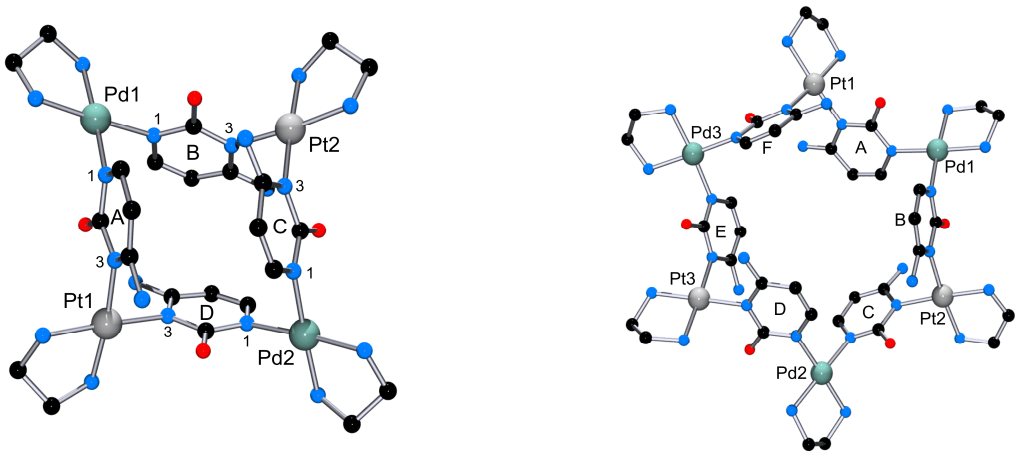

Abbildung S3: Struktur der Kationen des Tetramers **14** (links) und des Hexamers **15** (rechts).

von *cis*-$(NH_3)_2Pt^{II}$ und $(bpy)Pd^{II}$ (Verbindungen **9** und **12**) führt zu Unterschieden in Form und Größe der Strukturen. Unterschiede in der Elektronenverteilung in den Isomeren **9** und **12** spiegeln sich zudem in den ^{1}H-NMR-Spektren der Verbindungen wider. Bei der Reaktion von $[Pt(en)(H_2C\text{-}N3)_2]^{2+}$ (**2**) mit $[Pd(en)(H_2O)_2](NO_3)_2$ bildet sich ein Gemisch des Tetramers $[\{Pt(en)(N3\text{-}HC\text{-}N1)_2Pd(en)\}_2](NO_3)_4\cdot 9.5H_2O$ (**14**) und des Hexamers $[\{Pt(en)(N3\text{-}HC\text{-}N1)_2Pd(en)\}_3](NO_3)_6\cdot 18H_2O$ (**15**) (Abbildung S3). Die gleichzeitige Bildung von Zyklen unterschiedlicher Ringgröße (**14** und **15**) spiegelt das bekannte Verhalten supramolekularer Systeme wider, ein Gleichgewicht zwischen entropisch und thermodynamisch günstigen Zuständen einzustellen. Die exocyclischen O2- und $N(4)H_2$ -Gruppen solcher Komplexe können des weiteren dazu genutzt werden, oktanucleare Verbindungen zu erhalten, die sich durch kurze Metall-Metall-Abstände auszeichnen. Zwei octanucleare Verbindungen (**11** und **16** in Abbildung S4) wurden erhalten, ausgehend von $[Pd(2,2'\text{-}bpy)(H_2O)_2](NO_3)_2$ und Cytosin. Der unterschiedliche Aufbau wird durch die unterschiedliche räumliche Anordnung der exocyclischen O2- und N4-Positionen der Cytosinate verursacht, an die die vier zusätzlichen $(bpy)Pd^{II}$-Einheiten gebunden sind.

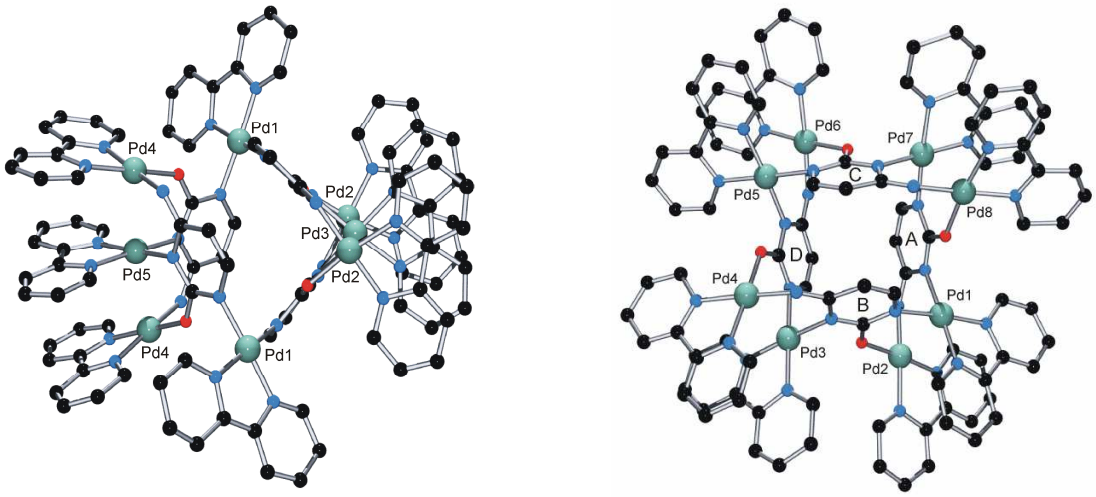

Abbildung S4: Röntgenstruktur der Verbindungen **11** (links) und **16** (rechts)

In Kapitel 2 werden Versuche zur Synthese von Metallacalix[n]arenen mit der unsubstituierten Nucleobase Uracil beschrieben. Insbesondere *cis*-$[Pt(NH_3)_2(HU\text{-}N1)(HU\text{-}N3)]$ (**18**) und *cis*-$[Pt(NH_3)_2(HU\text{-}N1)_2]$ (**19**) wurden mit *cis*-$(NH_3)_2Pt^{II}$ -Einheiten zur Reaktion gebracht. Obwohl sich im NMR-Maßstab die Bildung neuer Spezies nachweisen ließ, war es bisher nicht möglich, einzelne Verbindungen zu isolieren. Das Wesen von sog. Platin-Blau-Verbindungen (“platinum pyrimidine blues”), die mit unsubstituierten Pyrimidinbasen wie Uracil oder Cytosin erhalten werden, ist aufgrund ihres komplexen

Verhaltens noch immer nicht vollständig geklärt. Letztendlich läßt sich jedoch sagen, dass die Ergebnisse der beiden ersten Kapitel der vorliegenden Arbeit zu einem besseren Verständnis dieser Verbindungsklasse beigetragen haben.

In Kapitel 3 wird eine Reihe von Komplexen, die ausgehend von der Reaktion von 1-Methyluracilbasierten Liganden (L1 and L2) mit *cis*-a_2M^{II}-Einheiten erhalten wurden, vorgestellt. Diese Klasse von Metallacyclen wird durch ihren Aufbau mit sowohl verbrückenden Methylen- als auch Metalleinheiten als Hybrid zwischen klassischen Calix[4]arenen und Metallacalix[4]arenen angesehen (Abbildung S5). Die exocyclischen O2- und O4-Positionen des Uracils können zudem dazu genutzt werden, mehrkernige Derivate zu erhalten. Die Reaktion eines Liganden L1 mit *cis*-$[Pt(NH_3)_2(H_2O)_2](NO_3)_2$ ist darüber hinaus von großem Interesse, da durch geeignete Wahl der Reaktionsbedingungen (Konzentration, pH-Wert der Reaktionslösung) cyclische Metallacyclen unterschiedlichen Aufbaus erhalten werden können.

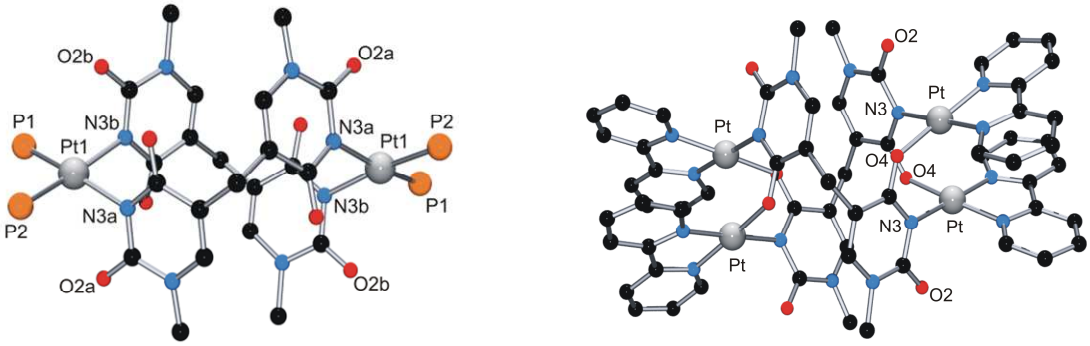

Abbildung S5: Struktur des neutralen *cis*-$[Pt(PPh_3)_2(L1'\text{-}N3)]_2 \cdot 4H_2O$ (**20**) (links) und $\{[Pt(2,2'\text{-bpy})]_2(L1'\text{-}N3,O4)\}_2(NO_3)_4 \cdot 8H_2O$ (**21**) (rechts)

In Kapitel 4 wird das bereits bekannte Gleichgewicht zwischen Keton und geminalem Diol anhand des Di-2-pyridylketons (dpk) (Schema S1) und seiner Metallkomplexe (Pt^{II}, Pd^{II}) *via* ^{1}H-NMR-Spektroskopie in D_2O und DMSO-d_6 untersucht. Für den freien Liganden liegt die Gleichgewichtskonstante für die Umwandlung vom Keton (dpk) zum *gem*-Diol ($dpk \cdot H_2O$) bei einem Wert von 0.04. In Gegenwart von kinetisch labilem Pd^{II} ist die Bildung des *gem*-Diols eindeutig bevorzugt, die Rückreaktion nach $Pd(dpk \cdot H_2O) \rightarrow Pd(dpk) + H_2O$ ist jedoch ebenfalls möglich. Mit Pt^{II} ist es aufgrund der langsameren Kinetik möglich, einen cyclischen dreikernigen Komplex $[Pt_3(\mu\text{-}OH)_3(dpk \cdot H_2O)_2(dpk)](NO_3)_3 \cdot 4.5H_2O$ (**29**) zu erhalten, der sowohl dpk- als auch $dpk \cdot H_2O$-Liganden enthält.

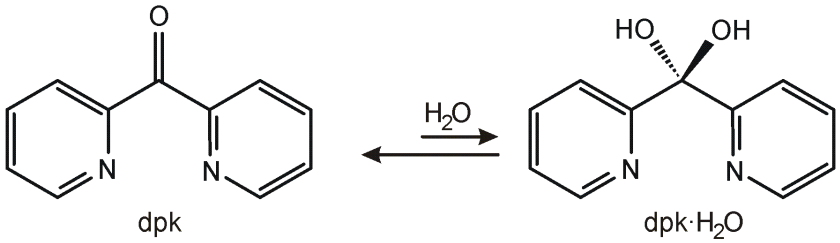

Schema S1: Umwandlung von dpk zu dpk·H_2O

In Kapitel 5 und 6 werden heterocyclische, stickstoffbasierte Liganden (3,3'-bpy, 1,4,5,8-tetra-Azaphenanthren) und ihre Reaktion mit Übergangsmetallionen und Metalleinheiten diskutiert. Die Reaktion von 3,3'-bpy mit $Hg(OAc)_2$ führte zu einem zweikernigen Komplex $[Hg(3,3'\text{-bpy})(CH_3COO)_2]_2 \cdot 3H_2O$ (**31**) (Abbildung S6), der die kleinstmögliche Einheit eines cyclischen Komplexes darstellt. Mit tetra-Azaphenanthren Liganden (L3, L4) ist die Synthese von verschiedenen polymeren Metallkomplexen beschrieben, von denen eine Reihe durch Röntgen-Kristallographie charakterisiert wurde. Eine ungewöhnliche Transmetallierungsreaktion wird bei der Reaktion von $[Pd(en)(L3)](NO_3)_2 \cdot H_2O$ (**34a**) mit $AgNO_3$ beobachtet, bei der der polymere Komplex $\{[Ag(L3)]_2Ag(NO_3)_3 \cdot 3H_2O\}_n$ (**36**) erhalten wird.

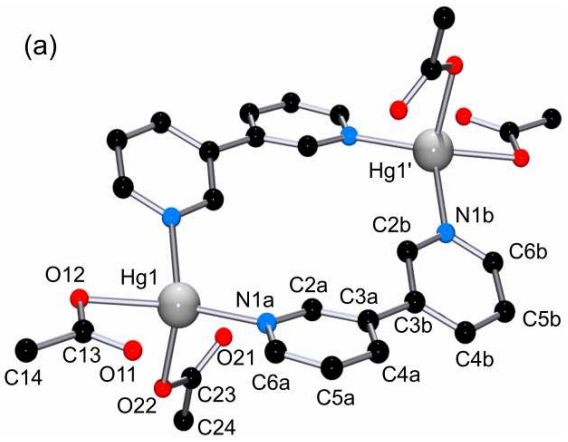

Abbildung S6: Struktur des zweikernigen **31**.

Experimental Section

Materials

The following chemicals were of commercial origin: uracil (H_2U), cytosine (H_2C), $AgNO_3$, $AgClO_4$, CF_3COOAg, $Zn(NO_3)_2 \cdot 6H_2O$, $Zn(ClO_4)_2 \cdot 6H_2O$, $Hg(CH_3COO)_2$, K_2PtCl_4, K_2PdCl_4, $PdCl_2$, di-2-pyridyl ketone (dpk), 3-bromo pyridine, 2,2'-bipyridine. The following starting compounds were prepared as described in the literature: *cis*-$PtCl_2(NH_3)_2$,[1] $PtCl_2$(en),[2] $PtCl_2$(2,2'-bpy),[3] $PtCl_2$(COD),[4] $PdCl_2$(en),[5] $PdCl_2$(2,2'-bpy),[5] sodium cytosinate (Na^+HC^-),[6] 1-methyluracil (1-MeUH),[7] 3,3'-bipyridine (3,3'-bpy),[8] 1,4,5,8-tetra-azaphenanthrene (L3),[9] 2,3,6,7-tetramethyl 1,4,5,8-tetra-azaphenanthrene(L4),[9] *cis*-[$Pt(NH_3)_2$(HU-*N3*)Cl] (**17**),[10] *cis*-[$Pt(NH_3)_2$(HU-*N1*)$_2$] (**19**),[11] [$PtCl_2$(dpk)] (**28**).[12]

***cis*-[$Pt(NH_3)_2(H_2C$-*N3*$)_2](NO_3)_2 \cdot 2H_2O$ (1):** A suspension of *cis*-$PtCl_2(NH_3)_2$ (300 mg, 1 mmol) and $AgNO_3$ (340 mg, 2 mmol) in 15 mL DMF was stirred at room temperature for 1 day with light excluded. The resultant AgCl was filtered off, cytosine (222.2 mg, 2 mmol) was added and the mixture was stirred at 60 °C for 3 days. The solution was evaporated to dryness under vacuum and the precipitate was recrystallized from H_2O (6 mL). After 4 days, colorless crystals were obtained. Yield: 497 mg (81 %); elemental analysis: calcd (%) for $C_8H_{18}N_{10}O_9Pt$ (1-hydrate): C 16.19, H 3.06, N 23.61; found C 16.2, H 3.0, N 23.9. X-ray crystallography revealed the existence of 2 H_2O molecules in the lattice.

[Pt(en)(H_2C-*N3*$)_2](NO_3)_2 \cdot H_2O$ (2): An aqueous suspension (30 mL) of $PtCl_2$(en) (326 mg, 1 mmol) and $AgNO_3$ (340 mg, 2 mmol) was stirred in dark for 3 h at 80 °C. The resultant AgCl precipitate was filtered off and cytosine (222.2 mg, 2 mmol) was added to the filtrate. The solution was stirred at 65 °C for 3 days and then concentrated to a volume of 6 mL. The solution was centrifuged off and kept at room temperature. After 6 days, colorless crystals were obtained. The yield was 531 mg (85 %). Elemental analysis: calcd (%) for $C_{10}H_{20}N_{10}O_9Pt$: C 19.39, H 3.25, N 22.61; found C 19.3, H 3.2, N 22.6.

[Pd(en)(H_2C-*N3*$)_2](NO_3)_2 \cdot 2H_2O$ (3): An aqueous suspension (30 mL) of $PdCl_2$(en) (237.7 mg, 1 mmol) and $AgNO_3$ (340 mg, 2 mmol) was stirred in dark for 12 h at 40 °C. The resultant AgCl precipitate was filtered off and cytosine (222.2 mg, 2 mmol) was added to the filtrate. The solution was stirred at 60 °C for 1 day and then concentrated to a volume of 5 mL. The solution was centrifuged off and kept at room temperature. After 6 days,

colorless crystals were obtained. Yield: 416 mg (76 %); elemental analysis: calcd (%) for $C_{10}H_{22}N_{10}O_{10}Pd$: C 21.89, H 4.04, N 25.52; found C 22.2, H 4.1, N 25.7.

***cis*-Pt(NH$_3$)$_2$(HC-*N1*)$_2$·3.25H$_2$O (4):** A suspension of *cis*-$PtCl_2(NH_3)_2$ (600 mg, 2 mmol) and $AgNO_3$ (665 mg, 3.91 mmol) in 30 mL DMF was stirred at room temperature for 40h with light excluded. The resultant AgCl was filtered off through celite bed, sodium cytosinate (525 mg, 3.95 mmol) was added and the mixture was stirred at RT for 3 days. The white precipitate was then filtered, dried in vacuum and the solid recrystalized from water. Yield: 872 mg (86 %); elemental analysis: calcd (%) for $C_{32}H_{82}N_{32}O_{21}Pt_4$: C 18.92, H 4.07, N 22.06; found C 18.8, H 4.1, N 22.2.

***cis*-[Pt(NH$_3$)$_2$(HC-*N1*)(H$_2$C-*N1*)](NO$_3$)·2H$_2$O (4a):** *cis*-Pt$(NH_3)_2$(HC-*N1*)$_2$·3.25H_2O (**4**) (100 mg, 0.2 mmol) was dissolved in water (4.5 mL) and the pH of the solution was adjusted to 7.1 by using 1M HNO_3. The solution was then centrifuged from some undissolved material and kept at room temperature. After 2 days, a precipitate was obtained. Yield: 82 mg (74 %); elemental analysis: calcd (%) for $C_8H_{19}N_9O_7Pt$: C 17.52, H 3.49, N 22.99; found C 17.4, H 3.3, N 23.1.

***cis*-[Pt(NH$_3$)$_2$(H$_2$C-*N3*)(HC-*N3*)](NO$_3$)·H$_2$O (5):** *cis*-[Pt$(NH_3)_2$(H_2C-*N3*)$_2$]$(NO_3)_2$·2H_2O (**1**; 61.14 mg, 0.1 mmol) was dissolved in water (4 mL) and the pH of the solution was adjusted to 9.6 by using 1M LiOH solution, the sample was kept at 4 ℃. After 2 days, colorless crystals were obtained. Yield: 53 mg (85 %); elemental analysis: calcd (%) for $C_8H_{17}N_9O_6Pt$: C 18.12, H 3.23, N 23.77; found C 18.1, H 3.3, N 23.9.

***cis*-[Pt(NH$_3$)$_2$(HC-*N3*)$_2$]·4H$_2$O (6):** *cis*-[Pt$(NH_3)_2$(H_2C-*N3*)$_2$]$(NO_3)_2$·2H_2O (**1**; 61.14 mg, 0.1 mmol) was dissolved in water (4 mL) and the pH of the solution was adjusted to 12.6 by using 1M NaOH solution. The beaker was covered with parafilm and kept at 4 ℃. After 1 week, colorless crystals were obtained. Yield: 42 mg (80 %); elemental analysis: calcd (%) for $C_8H_{22}N_8O_6Pt$: C 18.43, H 4.25, N 21.49; found C 18.5, H 4.3, N 21.5.

***cis*-[Pt(NH$_3$)$_2$(HC-*N1*)$_2$Ag]Cl·3.5H$_2$O (7b):** A suspension of *cis*-$PtCl_2(NH_3)_2$ (150 mg, 0.5 mmol) and $AgNO_3$ (340 mg, 2 mmol) in 15 mL DMF was stirred at room temperature for 10h with light excluded. The resultant AgCl was filtered off, sodium cytosinate (266 mg, 2 mmol) was added and the mixture was stirred at RT for 3 days. The grey colored precipitate was filtered off and dried in an oven. The precipitate was then dissolved in water (5 mL) and kept at room temperature. After 4 days, colorless crystals of **4b** were

obtained in low yield (10 %). Elemental analysis: calcd (%) for $C_8H_{20}N_8O_5Ag_1Cl_1Pt_1$ (3-hydrate): C 14.89, H 3.11, N 17.33; found C 15.0, H 2.9, N 17.5.

Reaction of *cis*-Pt(NH$_3$)$_2$(HC-*N1*)$_2$·3.25H$_2$O (4) with AgCl: **4** (500 mg, 1 mmol) was added to a freshly prepared suspension of AgCl {prepared *in situ* from $AgNO_3$ (170 mg, 1mmol) and NaCl (58.5 mg, 1 mmol) in water (30 mL)} and the mixture was stirred at room temperature for 16 h. The undissolved AgCl precipitate (80 mg, no peak in IR spectrum) was filtered off and the solution was concentrated to a volume of 4 mL. The solution was kept at room temperature. After 3 days, a mixture of crystalline **4** and a precipitate (**4a** or **4b**) was obtained. Crystals of **4** were separated under microscope and analyzed by X-ray crystallography.

***ht*-{*cis*-[Pt(NH$_3$)$_2$(HC-*N3,N4*)]$_2$}(NO$_3$)$_2$ (8):** An aqueous suspension (30 mL) of *cis*-$PtCl_2(NH_3)_2$ (300 mg, 1 mmol) and $AgNO_3$ (340 mg, 2 mmol) was stirred at 70 °C for 12 h with light excluded. The resultant AgCl was filtered off, cytosine (222.2 mg, 2 mmol) was added and the mixture was stirred at 65 °C for 3 da ys. The solution was concentrated to a volume of 5 mL and kept in a beaker at room temperature. After 4 days, a large amount of colorless microcrystalline **1** along with small amount (6%) of colorless crystals of **8** was obtained. The composition of **1** was confirmed by elemental analysis and comparison of its ^{1}H NMR spectrum (prepared in DMF). Crystals of **8** were separated under a microscope and identified by X-ray analysis and ^{1}H NMR spectroscopy.

***cis*-[{Pt(NH$_3$)$_2$(*N1*-HC-*N3*)$_2$Pd(bpy)}$_2$](NO$_3$)$_4$·13H$_2$O (9):** An aqueous suspension (15 mL) of $PdCl_2$(2,2'-bpy) (66.68 mg, 0.2 mmol) and $AgNO_3$ (68 mg, 0.4 mmol) was stirred in dark for 12 h at 40 °C. The resultant AgCl precipitate w as filtered off and *cis*-Pt(NH$_3$)$_2$(HC-*N1*)$_2$·3.25H$_2$O (**4**) (200 mg, 0.4 mmol) was added to the filtrate. The solution was stirred at RT for 1 day and then concentrated to a volume of 3 mL by means of a rotary evaporator. The solution was centrifuged from some undissolved material and kept at room temperature. After 4 days, yellow crystals were obtained. Yield: 118 mg (62 % based on Pd); elemental analysis: calcd (%) for $C_{36}H_{58}N_{24}O_{23}Pd_2Pt_2$ (7-hydrate): C 24.05, H 3.25, N 18.70; found C 24.2, H 3.2, N 18.6.

***cis*-[{(NH$_3$)$_2$Pt}$_2$(*N1*-C-*N3,02,N4*)$_4${Pd(bpy)}$_6$](NO$_3$)$_8$·xH$_2$O (10):** An aqueous suspension (20 mL) of $PdCl_2$(2,2'-bpy) (66.68 mg, 0.2 mmol) and $AgNO_3$ (68 mg, 0.4 mmol) was stirred in dark for 12 h at 40 °C. The resultant Ag Cl precipitate was filtered off and *cis*-Pt(NH$_3$)$_2$(H$_2$C-*N1*)$_2$·3.25H$_2$O (**4**) (50 mg, 0.1 mmol) was added to the filtrate. The solution

was stirred at 40 °C for 2 days and concentrated to a volume of 4 mL. The solution was centrifuged and kept at room temperature. After 4 days, reddish yellow microcrystals were obtained. Yield: 114 mg (71 %); elemental analysis: calcd (%) for $C_{76}H_{96}N_{36}O_{40}Pd_6Pt_2$ (12 hydrate): C 28.7, H 3.0, N 15.8; found C 28.4, H 3.1, N 16.0.

[{Pd(bpy)}$_8$(C-*N1*,*N3*,*N4*,*O2*)$_4$](NO$_3$)$_8$ (11): An aqueous suspension (25 mL) of $PdCl_2$(2,2'-bpy) (133.36 mg, 0.4 mmol) and $AgNO_3$ (136 mg, 0.8 mmol) was stirred in dark for 12 h at 40 °C. The resultant AgCl precipitate was filtered off and *cis*-$Pt(NH_3)_2(H_2C\text{-}N1)_2 \cdot 3.25H_2O$ (**4**) (50 mg, 0.1 mmol) was added to the filtrate. The solution was stirred at 45 °C for 3 d and then concentrated to a volume of 3 mL and centrifuged. The solution was kept at room temperature and after 6 days, red colored crystals were obtained along with a yellow precipitate. The red crystals (**11**) are separated under a microscope and identified by X-ray analysis. Yield: 33 mg (19 %). The yellow precipitate proved to be **10**, according to ^{1}H NMR spectroscopy.

***cis*-[{Pt(NH$_3$)$_2$(*N3*-HC-*N1*)$_2$Pd(bpy)}$_2$](NO$_3$)$_4$·9H$_2$O (12):** An aqueous suspension (25 mL) of $PdCl_2$(2,2'-bpy) (100.02 mg, 0.3 mmol) and $AgNO_3$ (102 mg, 0.6 mmol) was stirred in dark for 12 h at 40 °C. The resultant AgCl precipitate was filtered off and *cis*-$[Pt(NH_3)_2(H_2C\text{-}N3)_2](NO_3)_2$ (**1**) (172.5 mg, 0.3 mmol) was added to the filtrate. The pH of the solution was adjusted to 7.8 using 1M NaOH solution and the solution was stirred at 50 °C for 1 day. The solution was subsequently concentrated to a volume of 4.5 mL, the solution centrifuged off and kept at room temperature. After 5 days, yellow crystals were obtained. Yield: 209 mg (76 %); elemental analysis: calcd (%) for $C_{36}H_{62}N_{24}O_{25}Pd_2Pt_2$: C 23.58, H 3.41, N 18.33; found C 23.4, H 3.5, N 18.4.

[{Pt(en)(*N3*-HC-*N1*)$_2$Pd(bpy)}$_2$](NO$_3$)$_4$·8.5H$_2$O (13): An aqueous suspension (20 mL) of $PdCl_2$(2,2'-bpy) (66.68 mg, 0.2 mmol) and $AgNO_3$ (68 mg, 0.4 mmol) was stirred in dark for 12 h at 40 °C. The resultant AgCl precipitate was filtered off and $[Pt(en)(H_2C\text{-}N3)_2](NO_3)_2$ (**2**) (120 mg, 0.2 mmol) was added to the filtrate. The pH of the solution was adjusted to 7.4 using 1M NaOH solution and the solution was stirred at 45 °C for 1 day. The solution was concentrated to a volume of 4 mL, centrifuged, and kept at room temperature. Yellow crystals were obtained after 6 days. Yield: 135 mg (72 %); elemental analysis: calcd (%) for $C_{40}H_{58}N_{24}O_{21}Pd_2Pt_2$: C 26.48, H 3.22, N 18.53; found C 26.6, H 3.3, N 18.7.

[{Pt(en)(*N3*-HC-*N1*)$_2$Pd(en)}$_2$](NO$_3$)$_4$·9.5H$_2$O (14) and [{Pt(en)(*N3*-HC-*N1*)$_2$Pd(en)}$_3$](NO$_3$)$_6$·18H$_2$O (15): An aqueous suspension (15 mL) of $PdCl_2$(en) (71.3 mg, 0.3 mmol) and

$AgNO_3$ (102 mg, 0.6 mmol) was stirred in dark for 12 h at 40 ℃. The resultant AgCl precipitate was filtered off and [Pt(en)(H_2C-*N3*)$_2$](NO_3)$_2$·H_2O (**2**) (180 mg, 0.3 mmol) was added to the filtrate. The solution was stirred at RT for 2 days and then concentrated to a volume of 2 mL. The pH of the solution was adjusted to 11.5 using 1M NaOH solution, the solution then centrifuged and kept at 4 ℃. After 6 days, colorless needle-shaped crystals appeared in solution which were collected manually under a microscope and proved to be tetranuclear species **14** by X-ray crystallography. Next day in the same solution, colorless block shaped crystals had formed, which were separated under a microscope and proved to be **15** by X-ray crystallography. According to ^{1}H NMR spectroscopy, **14** and **15** are formed in a ratio of ca 3:1.

[{Pd(2,2'-bpy)}$_8$(C)$_4$](NO_3)$_8$·25H_2O (11) and [{Pd(2,2'-bpy)}$_8$(C)$_4$]$_2$(NO_3)$_{16}$·Pd(2,2'-bpy)(NO_3)$_2$·60H_2O (16): An aqueous suspension (22 mL) of $PdCl_2$(2,2'-bpy) (100 mg, 0.3 mmol) and $AgNO_3$ (102 mg, 0.6 mmol) was stirred overnight at 40 ℃ with light excluded. The mixture was cooled in an ice bath for 1h and then the resultant AgCl precipitate was filtered off. Cytosine (16.67 mg, 0.15 mmol) was added to the solution and stirred at 40 ℃ for 2 days. The solution was concentrated to a volume of 8 mL on a rotary evaporator and was allowed to evaporate slowly at room temperature. After 10 days, a mixture of **11** (red crystals) and **16** (yellow crystals) was obtained. The crystals were separated by hand under a microscope. Isolated yields were: **11**, 15.6 mg (12%) and **16**, 54.8 mg (42%)

***cis*-[Pt(NH_3)$_2$(HU-*N1*)(HU-*N3*)]·H_2O (17):** An aqueous suspension (30 mL) of *cis*-[Pt(NH_3)$_2$(HU-*N3*)Cl] (375 mg, 1 mmol) and uracil (112 mg, 1 mmol) was stirred at 40 ℃. The pH of the solution was always adjusted to 4 – 5 using 1M NaOH solution during the course of the reaction. After 5 days, the solution was evaporated to dryness by a rotavapor. The solid obtained was stirred with 50 mL methanol at room temperature to remove unreacted uracil from this mixture. After 12h, the solid was filtered off and dried. The precipitate was dissolved in water (10 mL) at room temperature, filtered and kept in a beaker. After 3-4 days, a white precipitate was obtained. Yield: 56 mg (12%); elemental analysis: calcd (%) for $C_8H_{14}N_6O_5Pt$: C 20.47, H 3.01, N 17.91; found C 20.3, H 3.1, N 18.0. The composition of **17** was established by ^{1}H NMR spectroscopy.

Synthesis of ligand L1: A mixture of 1-methyluracil (1.5 g, 11.89 mmol) and paraformaldehyde (178 mg, 5.95 mmol) was refluxed in 20 mL conc. HCl for 4 h.[13] The

solution was cooled to room temperature and was poured in ice. The white precipitate was filtered off and dried in an oven (40 ℃). Yield: 1 .51 g (96%).

Synthesis of ligand L2: A mixture of 1-methyluracil (1.5 g, 11.89 mmol) and paraformaldehyde (607 µL, 5.95 mmol) was refluxed in 40 mL conc. HCl for 12 h. The solution was cooled to room temperature and was poured in ice. The white precipitate was filtered off and dried in an oven (40 ℃). Yield: 1 .90 g (94%).

***cis*-[Pt(PPh$_3$)$_2$(L1'-*N3*)]$_2$·4H$_2$O (20):** A mixture of $PtCl_2$(COD) (37.4 mg, 0.1 mmol), triphenylphosphine (52.5 mg, 0.2 mmol), L1·H_2O (84.7 mg, 0.3 mmol) and Ag_2O (69.6 mg, 0.3 mmol) was refluxed in CH_2Cl_2 (25 mL) for 24 h at 40° C. After filtration of the reaction mixture through a bed of celite, the filtrate was evaporated to dryness. The resulting solid (87.2 mg) contained **20** and a small amount of COD, according to ^{1}H NMR spectroscopy ($CDCl_3$). It was dissolved in a minimum amount of CH_2Cl_2 containing a few drops of MeOH and kept at room temperature in an open test tube. Within 3 days, **20** was obtained as a white powder (82.2 mg, 80.8%). Colourless crystals suitable for X-ray crystallography were obtained within 1 day from a solution of **20** in $CHCl_3$ (containing few drops of MeOH) upon slow evaporation in air. Elemental analysis calc. for $C_{94}H_{96}N_8O_{16}P_4Pt_2$ (8-hydrate): C, 53.56; H, 4.59; N, 5.32. Found: C, 53.45; H, 4.6; N, 5.2.

{[Pt(2,2'-bpy)]$_2$(L1'-*N3*,*O4*)}$_2$(NO$_3$)$_4$·8H$_2$O (21): $PtCl_2$(2,2'-bpy) (105.5 mg, 0.25 mmol) was treated with $AgNO_3$ (84.9 mg, 0.5 mmol) in H_2O (30 mL) for 12 h, 80° C in the dark, and AgCl filtered off, following cooling to 4° C for 1 h. L1·H_2O (70.6 mg, 0.25 mmol) was added to the filtrate and the solution stirred for 3 days at 60° C in a stoppered flask. The solution (pH ~ 2.5) was subsequently concentrated to a volume of 6 mL, centrifuged from some precipitate formed, and then kept at room temperature in an open beaker. Red crystals of **21** were collected after 3 days (73.9 mg, 51%). Elemental analysis calc. for $C_{62}H_{68}N_{20}O_{28}Pt_4$: C, 32.07; H, 2.95; N, 12.06. Found: C, 31.8; H, 2.90; N, 12.2.

{[(2,2'-bpy)Pt]$_2$(L2'-*N3*,*O4*)$_2$}(NO$_3$)$_2$·41H$_2$O (22): An aqueous suspension (30 mL) of $PtCl_2$(2,2'-bpy) (84.4 mg, 0.2 mmol) and $AgNO_3$ (68 mg, 0.4 mmol) was stirred for 24 h at 60 ℃. The solution was cooled in ice for 1 h and t he resultant AgCl precipitate was filtered off. L2 (68 mg, 0.2 mmol) was added and the solution was stirred for 3 days at 65 ℃. The resulting solution was concentrated to a volume of 6 mL in a rotary evaporator, centrifuged, and filtered. The clear solution was kept in an open beaker at room temperature. After 4 d, dark red crystals were obtained. Yield: 167 mg (75%). Elemental

analysis: Calcd (%) for $C_{58}H_{66}N_{12}O_{30}Pt_2$ (10-hydrate): C, 38.67; H, 3.69; N, 9.33. Found: C, 38.8; H, 3.5; N, 9.5.

{[*cis*-$(NH_3)_2Pt]_4$(L1'-*N3*,*O4*)$_2$}$(NO_3)_4$ (23): An aqueous suspension (20 mL) of *cis*-$[Pt(NH_3)_2Cl_2]$ (120 mg, 0.4 mmol) and $AgNO_3$ (136 mg, 0.8 mmol) was stirred at 60 ℃ for 12h. The solution was cooled in ice and the AgCl precipitate was filtered off. L1 (52.8 mg, 0.2 mmol) was added to the solution and the mixture was stirred at 40 ℃. The pH of the solution was repeatedly adjusted to 5 using 1M NaOH solution. After one week the solution was concentrated to a volume of 3 mL, filtered and kept at 4 ℃. After 4 days, colorless crystals were obtained. Yield: 131.7 mg (78 %); elemental analysis: calcd (%) for $C_{22}H_{44}N_{20}O_{20}Pt_4$: C 15.65, H 2.63, N 16.59; found C 15.4, H 2.9, N 16.3.

{[*cis*-$(NH_3)_2Pt]_4$(L1'-*N3*,*O4*)(L1'-*N3*,*O4,O2*)}$(NO_3)_4$ (24) and {[*cis*-$(NH_3)_2Pt]_4$(L1'-*N3*,*O4*)$_2$}{[*cis*-$(NH_3)_2Pt]_4$(L1'-*N3*,*O4*)(L1'-*N3*,*O4,O2*)}$(NO_3)_8$ (25): (a) An aqueous suspension (3 mL) of *cis*-$[Pt(NH_3)_2Cl_2]$ (120 mg, 0.4 mmol) and $AgNO_3$ (136 mg, 0.8 mmol) was stirred at 60 ℃ for 12h. The solution was then cooled in ice and the AgCl precipitate was filtered off. L1 (52.8 mg, 0.2 mmol) was added to the solution and the pH of the solution was adjusted to 5 using 1M NaOH solution (one time). The mixture was stirred at 40 ℃ for one week. The solution was centrifuged off and kept at 4 ℃, and it became light blue color after 2 days. Colorless crystals were obtained after 5 days. One crystal was taken from solution for X-ray crystallography and proved to be **24**. (b) The same reaction was carried out in 20 mL aqueous solution under identical conditions as procedure (a). Here also colorless crystals were obtained after 6 days, and one crystal was measured by X-ray crystallography and proved to be complex **25**. The cation of **25** consists of two independent units – cation of **23** and cation of **24**. The ^{1}H NMR spectra of the isolated solids suggest that procedure (a) and (b) are identical, and lead to the simultaneous formation of **23** and **24** (see chapter 3 for details). The crystals of complex **23** and complex **24** have identical shape and can not be separated under a microscope.

[Pd(dpk·$H_2O)_2$]$(NO_3)_2$·$2H_2O$ (26): An aqueous solution (20 mL) of $[PdCl_2$(dpk·$H_2O)]$ (**27**, see below) (75.9 mg, 0.2 mmol) and $AgNO_3$ (68 mg, 0.4 mmol) was stirred for 16 h at 40 ℃ with daylight excluded. The AgCl precipitate was filtered off and the resulting filtrate was concentrated to a volume of 5 mL. The clear solution was kept at room temperature in an open beaker. Colorless crystals of **26** were obtained after 3 d. Yield: 23 mg (35%). Elemental analysis: Calcd (%) for $C_{22}H_{24}N_6O_{12}Pd$: C, 39.4; H, 3.6; N, 12.5. Found: C, 39.5; H, 3.6; N, 12.5.

[$PdCl_2$(dpk·H_2O)] (27): This compound was prepared via the following three routes: (a) An aqueous suspension (15 mL) of K_2PdCl_4 (163 mg, 0.5 mmol) and di-2-pyridylketone (92 mg, 0.5 mmol) was stirred overnight. The yellow precipitate was filtered off, washed with cold water and dried in oven (40 ℃). Yield: 172.7 mg (91%). Elemental analysis: Calcd (%) for $C_{11}H_{10}N_2O_2Cl_2Pd$: C, 34.8; H, 2.7; N, 7.4. Found: C, 34.9; H, 2.8; N, 7.3. (b) Single crystals (6.07 mg, 0.01 mmol) of [Pd(dpk·H_2O)$_2$](NO_3)$_2$·2H_2O (**26)** were dissolved in water (2.5 mL), and K_2PdCl_4 (3.26 mg, 0.01 mmol) was added. The solution was centrifuged off and was kept in an open beaker at room temperature. After 1d, yellow crystals of **27** were recovered in high yield (7.05 mg, 93%). The identity of **27** was confirmed by X-ray analysis and comparison with the reported X-ray structure in the literature.[14] (c) The third route followed the literature report,[14] starting out from $PdCl_2$ and dpk.

[Pt_3(μ-OH)$_3$(dpk·H_2O)$_2$(dpk)](NO_3)$_3$·4.5H_2O (29): An aqueous suspension (30 mL) of [$PtCl_2$(dpk)] (**28**) (90.36 mg, 0.2 mmol) and $AgNO_3$ (68 mg, 0.4 mmol) was stirred for 16 h at 70℃ with light excluded. The resultant AgCl precipitate was filtered off and the clear filtrate was stirred at 60 ℃ for another 2 d (pH = 3.0). The resulting solution was then concentrated to a volume of 6 mL and kept in an open beaker. Yellow crystals were obtained after 5 d. Yield: 52.6 mg (53%). Elemental analysis: Calcd (%) for $C_{66}H_{80}N_{18}O_{43}Pt_6$: C, 26.6; H, 2.7; N, 8.5. Found: C, 26.9; H, 2.6; N, 8.7.

{[Ag(3,3'-bpy)](ClO_4)·H_2O}$_n$ (30): To a solution of 3,3'-bpy (15.6 mg, 0.1 mmol) in water (3mL), an aqueous solution (2mL) of $AgClO_4$ (20.7 mg, 0.1 mmol) was added. The white precipitate which formed immediately was centrifuged off and recrystallized from water (4 mL, 40 ℃). Colorless crystals were obtained after 2 d at room temperature. Yield: 30.5 mg (80%). Elemental analysis: Calcd (%) for $C_{10}H_{10}AgClN_2O_5$: C, 31.5; H, 2.6; N, 7.3. Found: C, 31.4; H, 2.6; N, 7.5.

[Hg(3,3'-bpy)(CH_3COO)$_2$]$_2$·3H_2O (31): An aqueous solution (4 mL) of 3,3'-bpy (15.6 mg, 0.1 mmol) and Hg(CH_3COO)$_2$ (31.9 mg, 0.1 mmol) was stirred at room temperature for 12 h. The solution is filtered and kept at room temperature. After 3 d, colorless crystals were obtained. Yield: 37.1 mg (74%).

[{Pd(en)(3,3'-bpy)}(NO_3)$_2$·H_2O]$_n$ (32): An aqueous suspension (15 mL) of $PdCl_2$(en) (47.4 mg, 0.2 mmol) and $AgNO_3$ (68 mg, 0.4 mmol) was stirred in dark for 12 h. The resultant AgCl precipitate was filtered off and 3,3'-bpy (31.2 mg, 0.2 mmol) was added to the filtrate.

The solution was stirred at 40 ℃ for 1 day and then concentrated to a volume of 4 mL by rotary evaporator. The solution was filtered and kept at room temperature. After 4 d, a light yellow powder was recovered. Yield: 61 mg (66%). Elemental analysis: Calcd (%) for $(C_{12}H_{18}N_6O_7Pd)_n$ (1-hydrate): C, 31.0; H, 3.9; N, 18.1. Found: C, 30.8; H, 4.0; N, 18.0.

***cis*-[{Pt(NH$_3$)$_2$(3,3'-bpy)}(PF$_6$)$_2$·H$_2$O]$_n$ (33):** An aqueous suspension (20 mL) of *cis*-$PtCl_2(NH_3)_2$ (60 mg, 0.2 mmol) and $AgNO_3$ (68 mg, 0.4 mmol) was stirred in dark for 12 h. The resultant AgCl precipitate was filtered off and 3,3'-bpy (31.2 mg, 0.2 mmol) was added to the filtrate. The solution was stirred at 60 ℃ for 3 d, then solid NH_4PF_6 (65.2 mg, 0.4 mmol) was added to it and the solution was stirred at 60 ℃ for another day. The solution was concentrated to a volume of 5 mL (pD = 3.20) and kept in an open beaker at 4 ℃. After 5 d, colorless crystals were obtained. According to MS, **33** represents a cyclic trimer, hence n = 3. Yield: 73 mg (54%). Elemental analysis: Calcd (%) for $C_{30}H_{48}N_{12}O_3P_6F_{36}Pt_3$: C, 17.3; H, 2.3; N, 8.1. Found: C, 17.5; H, 2.6; N, 7.9.

[Pd(en)(L3)](NO$_3$)$_2$·H$_2$O (34a): An aqueous suspension (20 mL) of $PdCl_2$(en) (47.2 mg, 0.2 mmol) and $AgNO_3$ (68 mg, 0.4 mmol) was stirred at 40 ℃ for 12 h. The resultant precipitate is filtered off and L3 (36.4 mg, 0.2 mmol) was added to the filtrate. The mixture was heated to 60 ℃ for 2 days, and then the soution was concentrated to a volume of 4 mL, filtered and kept in an open beaker at room temperature. Yellow crystals were obtained after 3 days. Yield: 72.9 mg (86 %); elemental analysis: calcd (%) for $C_{12}H_{16}N_8O_7Pd$: C 29.37, H 3.29, N 22.83; found C 29.5, H 3.2, N 22.8.

[Pd(en)(L3)](ClO$_4$)$_2$·2H$_2$O (34b): The preparation of **34b** was similar to **34a** with $AgClO_4$ was employed instead of $AgNO_3$. Yield: 95.2 mg (82 %); elemental analysis: calcd (%) for $C_{12}H_{18}Cl_2N_6O_{10}Pd$: C 24.70, H 3.11, N 14.40; found C 24.9, H 3.3, N 14.3.

[Pd(en)(L4)](NO$_3$)$_2$·1.5H$_2$O (35): An aqueous suspension (30 mL) of $PdCl_2$(en) (47.2 mg, 0.2 mmol) and $AgNO_3$ (68 mg, 0.4 mmol) was stirred at 40 ℃ for 12 h. The resultant precipitate was filtered off and L4 (47.6 mg, 0.2 mmol) was added to the filtrate. The mixture was heated to 60 ℃ for 3 days. The solution was subsequently concentrated to a volume of 5 mL, filtered and kept in an open beaker at room temperature. Yellow crystals were obtained after 4 days. Yield: 93.9 mg (85 %); elemental analysis: calcd (%) for $C_{32}H_{50}N_{16}O_{15}Pd_2$: C 34.57, H 4.53, N 20.16; found C 34.8, H 4.7, N 20.4.

{[Ag(L3)]$_2$Ag(NO$_3$)$_3$·3H$_2$O}$_n$ (36): An aqueous suspension (3 mL) of [Pd(en)(L3)](NO$_3$)$_2$·H$_2$O (**34a**) (98 mg, 0.2 mmol) and AgNO$_3$ (34 mg, 0.2 mmol) was stirred at room temperature for 24 h. The solution was centrifuged off and kept in a beaker at 4 ℃. Crystals of **36** were obtained after 3 days. Yield: 20 mg (33 % based on Ag); elemental analysis: calcd (%) for $C_{40}H_{36}N_{22}O_{24}Ag_6$: C 25.89, H 1.96, N 16.6; found C 26.1, H 1.8, N 16.5.

[Pd(L3)(CH$_3$COO)$_2$] (37): Toluene (3 mL) and a solution of Pd(OAc)$_2$ (22.5 mg, 0.1 mmol) in 2 mL THF was layered on a solution of L3 in CHCl$_3$ (3 mL). The solution was allowed to mix slowly at room temperature. After 4 days, crystals of **37** were obtained in good yield. Yield: 40.2 mg (80 %); elemental analysis: calcd (%) for $C_{14}H_{12}N_4O_4Pd$: C 41.35, H 2.97, N 13.78; found C 41.6, H 3.2, N 13.9.

[Hg(L3)(CH$_3$COO)$_2$]$_n$ (38): An aqueous suspension (4 mL) of L3 (18 mg, 0.1 mmol) and Hg(OAc)$_2$ (31.8 mg, 0.1 mmol) was stirred at room temperature for 1 day. The solution was centrifuged off and kept at room temperature. After 5 days, crystals of **38** were obtained. Yield: 37 mg (74 %).

[Ag(CF$_3$COO)(L3)$_2$] (39): A solution of L3 (18 mg, 0.1 mmol) in CHCl$_3$ (2 mL) was overlayered in a test tube first with CH$_2$Cl$_2$ (1 mL) and then with a solution of CF$_3$COOAg (22 mg, 0.1 mmol) in water (2 mL). Crystals of **39** were formed at the phase boundary after 2 days. The crystals were collected and air-dried. Yield: 16 mg (55 %); elemental analysis: calcd (%) for $C_{22}H_{12}F_3N_8O_2Ag$: C 45.15, H 2.07, N 19.15; found C 45.3, H 2.2, N 19.1.

{[Ag$_4$(L3)$_2$(SO$_4$)$_2$]·H$_2$O}$_n$ (40): An aqueous suspension (5 mL) of L3 (18 mg, 0.1 mmol) and Ag$_2$SO$_4$ (31.2 mg, 0.1 mmol) was stirred at room temperature for 1 day. The solution was then centrifuged off and kept at room temperature in an open beaker. After 3 days, single crystals were obtained. Yield: 32 mg (65 %).

{[Ag$_2$(L4)$_2$(H$_2$O)$_2$](ClO$_4$)$_2$·H$_2$O}$_n$ (41): A solution of AgClO$_4$ (20.7 mg, 0.1 mmol) in 3 mL methanol was layered on a solution of L4 (23.8 mg, 0.1 mmol) in 3 mL CHCl$_3$ in a test tube. After 4 days, colorless crystals were appeared in the test tube. Yield: 33.6 mg (71 %); elemental analysis: calcd (%) for $C_{28}H_{34}Cl_2N_8O_{11}Ag_2$: C 35.57, H 3.63, N 11.85; found C 35.7, H 3.5, N 11.7.

$[Ag_3(NO_3)_2(L4)_4][Ag(L4)_2](NO_3)_2 \cdot 8H_2O$ (42): A solution of $AgNO_3$ (17 mg, 0.1 mmol) in 2 mL water was layered on a solution of L4 (23.8 mg, 0.1 mmol) in 3 mL $CHCl_3$ in a test tube. Colorless crystals of **42** were appeared after 3 days. Yield: 25 mg (45 %); elemental analysis: calcd (%) for $C_{84}H_{100}N_{28}O_{20}Ag_4$: C 44.77, H 4.47, N 17.40; found C 44.9, H 4.6, N 17.6.

$[Zn(L3)_2(NO_3)_2]$ (43): A solution of L3 (18 mg, 0.1 mmol) in $CHCl_3$ (4 mL) was overlayered with a solution $Zn(NO_3)_2 \cdot 6H_2O$ (29.74 mg, 0.1 mmol) in methanol (3 mL) in a test tube. The solution was allowed to mix slowly at room temperature. X-ray quality crystals of **43** were obtained after 5 days. Yield: 22 mg (40 %); elemental analysis: calcd (%) for $C_{20}H_{12}N_{10}O_6Zn$: C 43.38, H 2.18, N 25.29; found C 43.6, H 2.3, N 25.4.

$[Zn(L4)_2(H_2O)][Zn(L4)(H_2O)_3](ClO_4)_4 \cdot 5H_2O$ (44): A solution of $Zn(ClO_4)_2 \cdot 6H_2O$ (37.3 mg, 0.1 mmol) in methanol (3 mL) was layered over a solution of L4 (23.8 mg, 0.1 mmol) in 3 mL $CHCl_3$ in a test tube. Crystals of **44** were obtained after 6 days. Yield: 32 mg (45 %); elemental analysis: calcd (%) for $C_{42}H_{60}Cl_4N_{12}O_{25}Zn_2$: C 35.89, H 4.30, N 11.96; found C 36.1, H 4.5, N 12.1.

Instrumentations

Elemental (C, H, N) analysis data were obtained on a Leco CHNS-932 instrument. The ^1H NMR spectra were recorded in D_2O on Bruker AC 300 and Bruker DRX 400 spectrometers. Chemical shifts are referenced to internal tetramethylammonium tetrafluoroborate (TMA) (^1H, δ=3.18 ppm versus TSP). IR spectra (KBr pellets) were recorded on a Bruker Ifs 113v FT spectrometer.

Electrospray Mass Spectrometry: The mass spectrum of **33** was recorded with a LTQ orbitrap (high resolution mass spectrometer) coupled to an Accela HPLC-system (consisting of Accela pump, Accela autosampler and Accela PDA detector), from Thermo Electron. The parameters for HPLC were as follows- i)Eluent A (0.1% formic acid in H_2O) and eluent B (0.1% formic acid in acetonitrile) with mobile phase consisting of 50% A and 50% B; ii) Flow rate 250 µL/min; iii) Injection volume 5 µL; iv) Scan of wavelength range from 200 to 600 nm. The parameters for MS were as follows- i) Ionisation mode ESI (electrospray ionization). ii) Source voltage 3.8 kV. Capillary voltage 41 V, Capillary temperature 275 ℃, tube lens voltage 140 V. iii) Scanned mass range m/z 150 to m/z

2000 with resolution set to 60000. Analysis was done by flow injection (without any column).

Determination of acidity constants: The pK_a value was determined by means of pD dependant ^{1}H NMR measurements in D_2O. pD values of NMR samples were measured by use of a glass electrode and addition of 0.4 units to the uncorrected pH meter reading (pH*). Changes in chemical shifts of protons that result from the change in pD were evaluated with a nonlinear least-squares fit according to Newton-Gauss method.[15] The obtained acidity constants were then converted to the values valid for H_2O, according to literature.[16]

X-ray diffraction studies: X-ray crystal data were recorded at 150 K with an Xcalibur diffractometer equipped with an area detector and graphite monochromated Mo Kα radiation (0.71073 Å). Data reduction was done with the CrysAlisPro software.[17] The structures were solved by direct methods and refined by full-matrix least-squares methods based on F^2 using SHELXL-97.[18] All non-hydrogen atoms were refined anisotropically. All calculations were performed using the SHELXL-97 and WinGX programs.[17,18]

References

[1] S. C. Dhara, *Indian J. Chem*. **1970**, *8*, 193–194.

[2] F. Basalo, J. C. Bailar, B. R. Tarr, *J. Am. Chem. Soc.* **1950**, *72*, 2433–2438.

[3] a) G. T. Morgan and F. H. Burstall, *J. Chem. Soc.*, **1934**, 965–971; b) T. J. Egan, K. R. Koch, P. L. Swan, C. Clarkson, D. A. Van Schalkwyk, P. J. Smith, *J. Med. Chem.* **2004**, 47, 2926–2934.

[4] J. X. McDermott, F. J. White, G. M. Whitesides, *J. Am. Chem. Soc.* **1976**, *98*, 6521–6528.

[5] G. B. Kauffman, D. O. Cowan, *Inorg. Synth.* **1963**, *7*, 239–245.

[6] J. L. Sessler, D. Magda, H. Furuta, *J. Org. Chem.* **1992**, *57*, 818–826.

[7] W. Micklitz, B. Lippert, H. Schöllhorn, U. Thewalt, *J. Heterocyclic Chem.* **1989**, *26*, 1499–1500.

[8] M. Tiecco, L. Testaferri, M. Tingoli, D. Chianelli, M. Montanucci, *Synthesis*, **1984**, 736–738.

[9] R. Nasielski-Hinkens, M. Benedek-Vamos, *J. Chem. Soc. Parkin Trans. 1* **1975**, 1229–1229; b) R. Nasielski-Hinkens, J. Kotel, T. Lecloux, J. Nasielski, *Synth. Commun.* **1989**, *19*, 511–514.

[10] H. Rauter, E. C. Hillgeris, A. Erxleben, B. Lippert, *J. Am. Chem. Soc.* **1994**, *116*, 616–624.

[11] B. Lippert, *Inorg. Chem.* **1981**, *20*, 4326–4343.

[12] M. J. Rauterkus, B. Krebs, Angew. Chem. Int. Ed. 43 (2004), 1300–1303.

[13] S. Kumar, V. Malik, N. Kaur, K. Kaur, *Tetrahedron Lett.* **2006**, *47*, 8483–8487.

[14] G. Annibale, L. Canovese, L. Cattalini, G. Natile, M. Biagini-Cingi, A. -M. Manotti-Lanfredi, A. Tiripicchio, *J. Chem. Soc., Dalton Trans.* **1981**, 2280–2287.

[15] R. Tribolet, H. Sigel, *Eur. J. Biochem.* **1987**, *163*, 353–363.

[16] R. B. Martin, *Science*, **1936**, *139*, 1198–1203.

[17] CrysAlisPro, Oxford Diffraction (Poland), **2009**.

[18] G. M. Sheldrick, SHELXS97 and SHELXL97; University of Göttingen (Germany), **1997**.

List of compounds

(**1**)* *Cis*-[Pt(NH_3)$_2$(H_2C-*N3*)$_2$](NO_3)$_2$·2H_2O

(**2**)* [Pt(en)(H_2C-*N3*)$_2$](NO_3)$_2$·H_2O

(**3**)* [Pd(en)(H_2C-*N3*)$_2$](NO_3)$_2$·2H_2O

(**4**)* *Cis*-[Pt(NH_3)$_2$(HC-*N1*)$_2$]·3.25H_2O

(4a) *cis*-[Pt(NH_3)$_2$(HC-*N1*)(H_2C-*N1*)](NO_3)·2H_2O

(**5**)* *Cis*-[Pt(NH_3)$_2$(H_2C-*N3*)(HC-*N3*)](NO_3)·H_2O

(**6**)* *Cis*-[Pt(NH_3)$_2$(HC-*N3*)$_2$]·4H_2O

(**7a**)* *Cis*-[Pt(NH_3)$_2$(HC-*N1*)$_2$·Ag]Cl·xH_2O

(**7b**)* *Cis*-[Pt(NH_3)$_2$(HC-*N1*)$_2$Ag]Cl·3.5H_2O

(**8**)* *Cis*-{[Pt(NH_3)$_2$(HC-*N3,N4*)]$_2$}(NO_3)$_2$

(**9**)* *Cis*-[{Pt(NH_3)$_2$(*N1*-HC-*N3*)$_2$Pd(2,2'-bpy)}$_2$](NO_3)$_4$·13H_2O

(**10**)* *Cis*-[{(NH_3)$_2$Pt}$_2$(*N1*-C-*N3,O2,N4*)$_4${Pd(2,2'-bpy)}$_6$] (NO_3)$_8$·12H_2O

(**11**)* [{Pd(2,2'-bpy)}$_8$($C)_4$](NO_3)$_8$·25H_2O

(**12**)* *Cis*-[{Pt(NH_3)$_2$(*N3*-HC-*N1*)$_2$Pd(2,2'-bpy)}$_2$](NO_3)$_4$·9H_2O

(**13**)* [{Pt(en)(*N3*-HC-*N1*)$_2$Pd(2,2'-bpy)}$_2$](NO_3)$_4$·8.5H_2O

(**14**)* [{Pt(en)(*N3*-HC-*N1*)$_2$Pd(en)}$_2$](NO_3)$_4$·9.5H_2O

(**15**)* [{Pt(en)(*N3*-HC-*N1*)$_2$Pd(en)}$_3$](NO_3)$_6$·18H_2O

(**16**)* [{Pd(2,2'-bpy)}$_8$($C)_4$]$_2$(NO_3)$_{16}$·Pd(2,2'-bpy)(NO_3)$_2$·60H_2O

(**17**) *cis*-[Pt(NH_3)$_2$(HU-*N3*)Cl]

(**18**) *cis*-[Pt(NH_3)$_2$(HU-*N1*)(HU-*N3*)]·H_2O

(**19**) *cis*-[Pt(NH_3)$_2$(HU-*N1*)$_2$]

(**20**)* *cis*-[Pt(PPh_3)$_2$(L1'-*N3*)]$_2$·4H_2O

(**21**)* {[Pt(2,2'-bpy)]$_2$(L1'-*N3*,*O4*)}$_2$(NO_3)$_4$·8H_2O

(**22**)* {[(2,2'-bpy)Pt]$_2$(L2'-*N3*,*O4*)$_2$}(NO_3)$_2$·41H_2O

(**23**)* {[*cis*-(NH_3)$_2$Pt]$_4$(L1'-*N3*,*O4*)$_2$}(NO_3)$_4$

(**24**)* {[*cis*-(NH_3)$_2$Pt]$_4$(L1'-*N3*,*O4*)(L1'-*N3*,*O4,O2*)}(NO_3)$_4$

(**25**)* {[*cis*-$(NH_3)_2Pt]_4$(L1'-*N3*,*O4*)$_2$} {[*cis*-$(NH_3)_2Pt]_4$(L1'-*N3*,*O4*)(L1'-*N3*,*O4,O2*)} $(NO_3)_8$

(**26**)* $[Pd(dpk\cdot H_2O)_2](NO_3)_2\cdot 2H_2O$

(**27**) $[PdCl_2(dpk\cdot H_2O)]$

(**28**) $[PtCl_2(dpk)]$

(**29**)* $[Pt_3(\mu\text{-}OH)_3(dpk\cdot H_2O)_2(dpk)](NO_3)_3\cdot 4.5H_2O$

(**30**)* $\{[Ag(3,3'\text{-bpy})](ClO_4)\cdot H_2O\}_n$

(**31**)* $[Hg(3,3'\text{-bpy})(CH_3COO)_2]_2\cdot 3H_2O$

(**32**) $[\{Pd(en)(3,3'\text{-bpy})\}(NO_3)_2]_n$

(**33**) *cis*-$[\{Pt(NH_3)_2(3,3'\text{-bpy})\}(PF_6)_2]_3$

(**34a**)* $[Pd(en)(L3)](NO_3)_2\cdot H_2O$

(**34b**)* $[Pd(en)(L3)](ClO_4)_2\cdot 2H_2O$

(**35**)* $[Pd(en)(L4)](NO_3)_2\cdot 1.5H_2O$

(**36**)* $\{[Ag(L3)]_2Ag(NO_3)_3\cdot 3H_2O\}_n$

(**37**)* $[Pd(L3)(CH_3COO)_2]$

(**38**)* $[Hg(L3)(CH_3COO)_2]_n$

(**39**)* $[Ag(CF_3COO)(L3)_2]$

(**40**)* $\{[Ag_4(L3)_2(SO_4)_2]\cdot H_2O\}_n$ (40)

(**41**)* $\{[Ag_2(L4)_2(H_2O)_2](ClO_4)_2\cdot H_2O\}_n$

(**42**)* $[Ag_3(NO_3)_2(L4)_4][Ag(L4)_2](NO_3)_2\cdot 8H_2O$

(**43**)* $[Zn(L3)_2(NO_3)_2]$

(**44**)* $[Zn(L4)_2(H_2O)][Zn(L4)(H_2O)_3](ClO_4)_4\cdot 5H_2O$

Compounds marked with * are crystallographically characterized in this thesis.

Anupam Khutia
Email: anupam.khutia@tu-dortmund.de
Phone: +49 231 755 3839

Faculty of Chemistry
Technical University of Dortmund
44227 Dortmund, Germany

CURRICULUM VITAE

Personal information

Date of Birth: 25th September, 1984 Gender: Male
Marital Status: Single Citizenship: India
Languages: Fluent English, Hindi, Bengali

Highlights:

- **Synthetic inorganic chemistry with background in multi-step organic synthesis**.
- Experience in Schlenk technique for reactions under inert atmosphere.
- Familiar with a wide range of analytical techniques such as FTIR, NMR, ESI-MS, HRMS, UV-Vis, Fluorescence etc.
- Good skills in Separation and purification techniques.
- Experience in various techniques for the growth of single crystal for X-ray diffraction.
- Ability towards independent research with excellent communication and team skills.

Research Experience

September, 2007 – present	**Graduate Fellow**, Technical University of Dortmund, Germany; **Mentor: Prof. Bernhard Lippert** "Supramolecular Chemistry of Metal Ions and Nitrogen Based Ligands including Pyrimidine Nucleobases" • Synthesized a new class of metallacycles with defined shape • Developed a new approach for the synthesis of "metallacalix[n]arene" • Synthesized a new class of cyclic complexes which can be considered as a hybrid between classical calix[n]arene and metallacalix[n]arene.
May, 2006 – April, 2007	**Master thesis (M.Sc.) project**, Indian Institute of Technology Bombay, India; **Mentor: Prof. Chebrolu P. Rao** Thesis Title: "**Calix[4]arene Derivatives: Study of Interaction with Metal Ions and Anions**" • Synthesized lower rim substituted organic calix[4]arene derivatives using multi-step organic synthesis • Studied interaction of transition metal ions with calix[4]arene derivatives using UV-Vis, fluorescence spectroscopy as well as ^{1}H NMR and ESI-MS • Developed a calix[4]arene based receptor which can selectively bind to Hg^{2+} over other transition metal ions in aqueous acetonitrile solution

Publications:

1.	**A. Khutia**, P. J. Sanz Miguel* and B. Lippert*, "„Directed" Assembly of Metallacalix[n]arenes with Pyrimidine Nucleobase Ligands of Low Symmetry. I. Derivatives of *cis*-[a_2M(cytosine-*N3*)$_2$]$^{2+}$ with n = 4 and 6", *Chem. Eur. J.*, **2010**, *in press* (considered as **V**ery **I**mportant **P**aper (**VIP**)).
2.	**A. Khutia**, P. J. Sanz Miguel* and B. Lippert*, "„Directed" Assembly of Metallacalix[4]arenes with Pyrimidine Nucleobase Ligands of Low Symmetry. II. Interchanging Metals in Mixed-Metal Metallacalix[4]arenes and Putting Additional Metals to Exocyclic Groups", *Chem. Eur. J.*, **2010**, *in press* (considered as **V**ery **I**mportant **P**aper (**VIP**)).
3.	**A. Khutia**, P. J. Sanz Miguel* and B. Lippert*, "Isomerism with metallacalix[4]arenes of the non-symmetrical pyrimidine nucleobase cytosine: How connectivity and rotamer state determine the topology of multinuclear derivatives", *Inorg. Chem.*, **2010**, *49*, 7635 – 7637.
4.	**A. Khutia**, P. J. Sanz Miguel* and B. Lippert*, "Molecular Architectures Derived from Metal ions and the Flexible 3,3'-Bipyridine Ligand. Unexpected Dimer with Hg(II)", *Bioinorg. Chem. Appl.*, **2010** (doi: 10.1155/2010/169054)
5.	**A. Khutia**, P. J. Sanz Miguel and B. Lippert*, "Influence of Pt^{II} and Pd^{II} Coordination On the Equilibrium of 2,2'-Dipyridylketone (dpk) with its Hydrated *gem*-Diol Form (dpk·H_2O)", *Inorg. Chim. Acta,* **2010**, *363*, 3048 – 3054.
6.	N. Das, P. J. Sanz Miguel, **A. Khutia**, M. Lazar and B. Lippert*, "Hybrids between classical and metallacalix[4]arenes based on uracil and *cis*-$Pt^{II}L_2$ entities ((L = $P(Ph)_3$ or L_2 = 2,2'-bipyridine)", *Dalton Trans.*, **2009**, 9120 – 9122.
7.	R. Joseph, B. Ramanujam, A. Achariya, **A. Khutia** and C. P. Rao*, "Experimental and Computational Studies of Selective Recognition of Hg^{2+} by amide Linked Lower Rim 1,3-Dibenzimidazole Derivative of Calix[4]arene: Species Characterization in Solution and that in the Isolated Complex, Including the Delineation of the Nanostructures", *J. Org. Chem.*, **2008**, *73*, 5745 – 5758.

Educational Background

September, 2007 – present	Ph.D. student at International Max Planck Research School, Dortmund Technical University of Dortmund, Department of Chemistry, Germany Ph.D. Research Supervisor: **Prof. Bernhard Lippert**
August, 2005 – August, 2007	Master of Science (M.Sc.) in Chemistry at Department of Chemistry, Indian Institute of Technology (I.I.T.) Bombay, India CPI : 8.79/10, 1st Class
August, 2002 – July, 2005	Bachelor of Science (B.Sc.) at Department of Chemistry, Midnapore College, Vidyasagar University, Midnapore, India. Mark obtained: 65%, 1st Class

Awards & Fellowships:

2010	Travel award from **European Journal of Inorganic Chemistry (EURJIC)** to attend a Gordon Research Conference "Metals in Medicine" held at Andover, NH, USA
September, 2007 – November, 2009	Research Scholarship from "**International Max-Planck Research School in Chemical Biology**" (IMPRS-CB); Dortmund, Germany

2007	Qualified **CSIR** in National Eligibility Test (NET), (conducted jointly by UGC-CSIR under Ministry of Human Resources and Development, India for Junior Research Fellowship and eligibility for lectureship held in December 2006)
2007	Qualified, **GATE** (The Graduate Aptitude Test in Engineering) 2007 Exam, India
2005	Received prestigious "**Jai Prakash Book Award**" from Department of Chemistry, I.I.T. Bombay, India
2005 – 2007	Merit cum means scholarship from I.I.T. Bombay, India

Conferences Attended

June 27 – July 2, 2010	Gordon research conference "**Metals in Medicine**" at Andover, New Hampshire, USA Poster with title "How Ligand Connectivity and Rotamer Status Determine the Shape of Octanuclear Calix[4]arenes"
October 14 – 17, 2009	**"7th IMPRS Retreat"** at Ringberg castle, Germany Poster with title "Hybrids between Calix[4]arene and metallacalix[4]arene derived from *cis*-a_2Pt^{II} and uracil based ligands"
September 16 – 19, 2009	**2nd German-Indian Symposium on "Frontiers of Chemistry"** at Leipzig, Germany Poster with title "Hybrids between Calix[4]arene and metallacalix[4]arene derived from *cis*-a_2Pt^{II} and uracil based ligands"
November 10 – 12, 2008	**"6th IMPRS Retreat"** at Witten, Germany Oral presentation with title "Molecular Architecture Based on N-ligands (Pyrimidine Nucleobases, 4,4´Bipyrimidine) and Metal Ions"
September 2 – 6, 2008	"**9th European Biological Inorganic Chemistry Conference**" (EUROBIC 9) at Wroclaw, Poland Poster with title "Linkage Isomerism in complexes of Uracil with *cis*- $(NH_3)_2Pt^{2+}$"
August 24 – 28, 2008	**"4th EuCheMS Conference on NITROGEN LIGANDS in Coordination Chemistry, Metal Organic Chemistry, Bioinorganic chemistry & Homogeneous catalysis"** at Garmisch-Partenkirchen (Germany) Poster with title "Linkage Isomerism in Complexes of Uracil with *cis*- $(NH_3)_2Pt^{2+}$"